Design of a Steady State pH Sensor for Chronic Wound Monitoring

Anna McLister

BSc

Faculty of Computing and Engineering

of Ulster University

Thesis submitted for the degree of

Doctor of Philosophy

June 2018

I confirm that the word count of this thesis is less than 100,000 words

Contents

List of Figures x

List of Tables xvii

List of Schemes xviii

Acknowledgements xix

Abstract xx

Abbreviations xxi

Copyright / Credit Notices xxiii

Notes on Access to Contents xxvi

Chapter 1 Introduction and Project Aims

1.1 Introduction 2

1.2 Wound Infection 3

1.3 Health Costs 5

1.4 Summary and Project Aims 8

Chapter 2 Literature Review

2.1 Chronic Wounds 11

2.1.2 Diabetic Ulceration and Impaired Healing 11

2.2 Normal Wound Healing 14

2.2.1 Stage 1: Inflammation Phase 14

2.2.2 Stage 2: Proliferative Phase 15

2.2.3 Stage 3: Tissue Remodeling Phase 16

2.3 Wound Treatment Approaches and Technologies 16

2.4 Wound Management Strategies 18

2.5 Wound Diagnostics 18

2.6 Conventional Diagnostics 21

2.7 Core Methodologies 22

2.8 Moving Towards Smart Dressings 23

2.9 Wound Fluid 24

2.10 Potential Biomarkers 26

2.11 Wound pH 29

2.12 Approaches to Measure pH 31

2.12.1 Visual pH Devices 31

2.12.2 Quantitative Wound pH Imaging 33

2.12.3 Radiofrequency Identification (RFID) Optical Sensors 35

2.13 Electrochemical pH Systems 37

2.13.1 Screen printed potentiometric smart dressings 38

2.13.2 Carbon Fibre pH Sensors 40

2.13.3 Screen Printed Voltammetric Sensors 42

2.13.4 Carbon Fibre Weave Dressings 45

2.13.5 Carbon Composite Film Dressings 46

2.13.6 Signal Aquistion 48

2.14 Conclusion 50

Chapter 3 Experimental Details and Methodologies

3.1 Materials and Instrumentation 52

3.2 Electrochemical Instrumentation 52

3.3 Electrochemical Cells 53

3.3.1 Reference Electrodes 54

3.3.2 Working Electrodes 56

3.3.3 Counter Electrodes 58

3.4 Mass Transport 58

3.4.1 Diffusion 58

3.4.2 Migration 59

3.4.3 Convection 59

3.5 Voltammetry 60

3.5.1 Cyclic Voltammetry 60

3.5.2 Over Potential 65

3.5.3 Amperometry 66

3.5.4 Chronopotentiometry 69

3.5.5 Square wave voltammetry 70

3.6 Variation of Peak Potential with Solution pH 72

3.7 Surface Modification /Modification Methods 73

3.7.1 X-Ray Photoelectron Spectroscopy 73

3.7.2 Electrochemical Anodisation 76

Chapter 4 Development of Functionalized Palladium electrodes for Smart Bandage applications for monitoring wound pH

4.1 Introduction 79

4.2 Experimental Details 82

4.2.1 Materials 82

4.2.2 Electrochemical Configuration 82

4.2.3 Sensor Design and modification 82

4.3 Results and Discussion 83

4.3.1 Electrochemistry of Palladium Electrodes 83

4.3.2 Potentiometric Response of Palladium to pH 85

4.3.3 Surface Modifications 86

4.3.4 Electrochemical Investigation 86

4.3.5 L-Cysteine Modified Palladium Film 93

4.4 Conclusion 95

Chapter 5 Voltammetric pH Sensing Based on Poly-L-tryptophan Modified Carbon Fibre Mesh

5.1 Introduction 98

5.2 Experimental Details 102

5.2.1 Materials 102

5.2.2 Electrochemical Configuration 102

5.2.3 Sensor Design and Modification 103

5.3 Results and Discussion 103

5.3.1 Anodisation of the Carbon Fibre Mesh 109

5.3.2 Anodised Carbon-Poly-L-Tryptophan Composite 113

5.3.3 Response to pH 115

5.3.4 Simulated wound environments 116

5.4 Conclusion 117

Chapter 6 Investigating the Use of Electrogenerated Quinone Dimers Entrapped onto the Surface of a Carbon Screen Printed Electrode for Wound Monitoring Technologies

6.1 Introduction 120

6.2 Experimental Details 123

6.2.1 Materials 123

6.2.2 Electrochemical Configuration 123

6.2.3 Sensor Design and Modification 124

6.3 Results and Discussion 124

6.3.1 Voltammetric Techniques 128

6.3.2 Interferences 130

6.3.3 Screen Printed Electrodes (SPEs) 133

6.3.4 Nafion® Modification 135

6.3.5 Stability of the Salicylic Acid Electrodes 139

6.3.6 Defibrinated Horse blood 141

6.4 Conclusion 143

Chapter 7 Investigating the Use of an Engineered Poly Flavin on Carbon Screen Printed electrodes as the Foundation of a pH Sensor for Wound Monitoring

7.1 Introduction 146

7.2 Experimental Details 149

7.2.1 Materials 149

7.2.2 Sensor Design and Modification 150

7.2.3 Flavin Electro – Polymerisation 150

7.3 Results and Discussion 151

7.3.1 Flavin Phenol Electrochemical Properties 151

7.3.2 Carbon-Polyethylene Mesh Fabrication 154

7.3.3 Carbon-Polyethylene Mesh Electrochemistry 156

7.3.4 Screen Printed Electrodes 160

7.3.5 Analytical Applicability in Defibrinated Horse Blood 163

7.4 Conclusions 166

Chapter 8 Conclusions and Recommendations for Future Work

8.1 Conclusions 169

8.2 Recommendations for future work 172

References 175

Publications Resulting from this Research Work 192

List of Figures

Figure 1.1 Research growth in wound dressings. Reproduced with permission (Davis, *et al.*, 2016).

Figure 2.1.1 Mechanism of wound healing in healthy people compared to those with diabetes. Reproduced with permission (Brem, *et al.*, 2007)

Figure 2.2.1 The various stages of healing in acute and chronic wounds. Reproduced with permission (Davis, *et al.*, 2016)

Figure 2.5.1 Diagnostic tests and their impact. Adapted from(Practice, 2008)

Figure 2.6.1 Central lab vs Point of Care Analysis. Reproduced with permission (Davis, *et al.*, 2016)

Figure 2.7.1 Assay / Device Development Methodology. Reproduced with permission (Davis, *et al.*, 2016)

Figure 2.11.1 Typical pH profiles observed for acute and chronic wounds. Adapted from (Schneider *et al.*, 2007).

Figure 2.12.2 A) Proposed implementation of the "traffic light" pH swab B) Proposed pH-sensitive bandage by Trupp and coworkers. Adapted from (Trupp, *et al.*, 2010).

Figure 2.12.3 Modified dressing for measuring pH and Po_2. Reproduced with permission (Schreml, *et al.*, 2014).

Figure 2.12.4 Silicon Nitride CCD pH Imaging. Reproduced with permission (Hizawa, *et al.*, 2006).

Figure 2.12.5 RFID pH detection methodology. Reproduced with permission (Steinberg, *et al.*, 2009).

Figure 2.13.1 Smart bandage based on screen printed sensors with a polyaniline (PANI) sensing layer. Reproduced with permission (Guinovart, *et al.*, 2014)

Figure 2.13.2 pH transition of the emeraldine salt and bases within polyaniline. Reproduced with permission (Davis, *et al.*, 2016).

Figure 2.13.3 Redox transition of endogenous quinone groups on carbon. Reproduced with permission (Anderson, *et al.*, 2014).

Figure 2.13.4 Probe design specifications. Reproduced with permission (Anderson, *et al.*, 2014).

Figure 2.13.5 Fabrication of the screen printed urate pH sensor. Reproduced with permission (Phair, *et al.*, 2011).

Figure 2.13.6 A)Electrochemical oxidation of urate B) Influence of pH on the voltammetric response to urate at a screen printed sensor. Reproduced with permission (Phair, *et al.*, 2011).

Figure 2.13.7 A) Structure of the carbon fiber weave and B) proposed implementation. Adapted from (McLister, Lowry, *et al.*, 2015).

Figure 2.13.8 A) Schematic highlighting the composite nature of the carbon loaded films B) Carbon loaded polyethylene before and after laser treatment. Reproduced with permission (J Phair, Joshi, *et al.*, 2014)

Figure 2.13.9 Fabrication of the urate biosensor and its mode of operation. Reproduced with permission (Kassal, *et al.*, 2015).

Figure 3.3.1 A schematic of a typical electrochemical system of a three-electrode set up. Adapted from (Fisher, 1996)

Figure 3.3.2 Assembly of a typical silver-silver chloride reference electrode. Adapted from (Fisher, 1996)

Figure 3.4.1 A) A general schematic electrochemical reactions occurring at the working electrode during a cyclic voltammogram B) Triangular waveform characteristic of cyclic voltammetry.

Figure 3.4.2 Cyclic voltammogram detailing the reversible, quasi-reversible and irreversible system involved in electron kinetics. Adapted from (Compton, *et al.*, 2011)

Figure 3.4.3. Cyclic voltammograms detailing the relationship between the different sizes of electrodes (with respect to the diffusion layer thickness) and the contribution of convergent diffusion. Adapted from (Compton, *et al.*, 2011).

Figure 3.4.4 Schematic examples of the four different diffusion profiles which a microelectrode array may experience. Reproduced with permission (Compton, *et al.*, 2011).

Figure 3.5.1 Potential step procedure used in amperometry.

Figure 3.5.2 Typical amperometric response to current.

Figure 3.5.3 Impact of varying times on the concentration of a typical amperometric profile.

Figure 3.5.4 Example of potentiometry, in which the potential of the working electrode is a measured in relation to the potential of the reference electrode against the function of time.

Figure 3.5.5 A) Outline of the waveform and parameters used in square wave voltammetryB) A staircase profile of a square wave scan. Adapted from (Compton, *et al.*, 2011)

Figure 3.5.6 An example of the different current displayed in a typical

square wave voltammogram.

Figure 3.7.1 An example of an X-Ray Photoelectron Spectroscopy system. Adapted from (Fisher, 1996)

Figure 3.7.2 A typical XPS spectrum of carbon, detailing the different energies of different chemical states.

Figure 3.7.3 The impact of electrochemical anodization of the surface of a graphite particle.

Figure 4.1.1 Pallidum and L-cysteine reaction scheme.

Figure 4.1.2 Schematic detailing the impact of pH on the structure of L-cysteine.

Figure 4.3.1 Cyclic voltammograms detailing the response of a palladium electrode cycled 10 times in sulphuric acid (0.1 M H_2SO_4, 50 mV/s). N_s=10

Figure 4.3.2 A) Potentiometric response of an unmodified palladium electrode towards various pH regimes. B) A plot of the average potential over a period of 20s as a function of pH. N_s=7, N_{pH}=7

Figure 4.3.3 A) Cyclic voltammograms detailing the response of a palladium electrode dip coated in L-cysteine (0.1 M) for varying periods of time (30 – 900 seconds), towards ferrocyanide (2 mM, 0.1 M KCl, 50 mV/s) N_s=5 B) Influence of L-cysteine immersion time on ferrocyanide peak separation.

Figure 4.3.4 Cyclic voltammograms detailing the response of a bare palladium electrode towardsferrocyanide (2 mM, 0.1 M KCl, 50 mV/s) as well as in the presence of ascorbic acid, compared against a L-cysteine modified palladium electrode response towards ferrocyanide. N_s=3.

Figure 4.3.5 XPS profiles for the S 2_p peak obtained from a L-cysteine modified and unmodified Pd electrode.

Figure 4.3.6 Cyclic voltammogram detailing the response of the L-cysteine modified palladium electrode towards 10 consecutive scans towards ferrocyanide (2 mM, 0.1 M KCl, 50 mV/s). N_s=10.

Figure 4.3.7 Cyclic voltammogram comparing the response of a bare palladium electrode and a L-cysteine modified palladium electrode towards ferrocyanide (2 mM, 0.1 M KCl, 50 mV/s) after a 24-hour delay. N_s=2.

Figure 4.3.8 Potentiometric response of a L-cysteine modified palladium electrode response under various pH regimes. N_s=7, N_{pH}=7

Figure 4.3.9 Potentiometric response of the L-cysteine modified palladium electrode towards A) three consecutive pH regimes.

Figure 5.1.1 Schematic representation of the effect of pH on the voltammetric peak position.

Figure 5.1.2 Schematic of the proposed poly-L-tryptophan composite structure.

Figure 5.3.1 Cyclic voltammogram detailing the initial response of a poly-L-tryptophan modified carbon fibre electrode in pH 7 buffer. Conversion of the indole units to the corresponding quinoid forms Scan rate: 50 mV/s. N_s= 1.

Figure 5.3.2 Consecutive cyclic voltammograms detailing the response of a poly-L-tryptophan carbon fibre electrode: redox cycling between the reduced and oxidised forms of the electrogenerated indole-quinone polymer. N_s=2

Figure 5.3.3 Cyclic voltammograms detailing the influence of scan rate on the response of the electrogenerated indole-quinone polymer in fresh pH 7 buffer.

Figure 5.3.4 Influence of scan rate on the peak height – confirming behaviour characteristic of an immobilised species.

Figure 5.3.5. Square wave voltammograms of an unanodised poly-L-tryptophan modified carbon fibre electrode in pH 3 buffer. N_s=2.

Figure 5.3.6 Generic representation of the electron transfer sites at carbon based electrodes.

Figure 5.3.7 Scanning electron micrograph of a section of unmodified carbon fibre mesh used in this work (McLister, Lowry, *et al.*, 2015).

Figure 5.3.8 Cyclic voltammograms detailing the effect of varying anodisation times on the response of the carbon fibre electrode towards 2 mM ferrocyanide in 0.1 M KCl (Scan rate: 50 mV/s). N_s=4

Figure 5.3.9 XPS spectra obtained before (A); and after (b) electrochemical anodisation. Reproduced with permission from (Anderson, *et al.*, 2014).

Figure 5.3.10 Schematic representation of the redox transitions associated with quinoid groups endogenous to the carbon fibre substrate. Reproduced with permission (Anderson, *et al.*, 2014)

Figure 5.3.11 Square wave voltammograms detailing the response of an anodised carbon fibre electrode to pH 3 buffer before (Blank scan) and after the addition of poly-L-tryptophan, N_s=3. Reproduced with permission from (McLister, Lowry, *et al.*, 2015).

Figure 5.3.12 Square wave voltammograms detailing the response of a modified poly-L-tryptophan redox wire in Britton Robinson buffer solutions covering the range pH 3 - pH 10. N_s=24, N_{pH}=8

Figure 5.3.13 Square wave voltammograms detailing the poly-L-tryptophan modified mat carbon fibre electrode response to defibrinated horse blood (A) and consecutive scans (B). N_s=1; N_s=4.

Figure 6.1.1 Chemical structure of Tyramine, Resorcinol and Salicylic Acid (SA).

Figure 6.3.1 Cyclic voltammograms detailing the response of an anodised carbon fibre electrode towards the oxidation of salicylic acid (10 mM, 0.1 M NaOH, 50 mV/s). N_s=10

Figure 6.3.2 Cyclic voltammograms detailing the response of an anodised carbon fibre electrode towards the oxidation of tyramine (10 mM, 0.1 M NaOH, 50 mV/s). N_s=10

Figure 6.3.3 Cyclic voltammograms of a dimer modified anodised CF electrode response towards two consecutive scans in pH 7 BR buffer solution. N_s=2

Figure 6.3.4 Plot detailing the linear response of the peak positions of the oxidation of the dimer towards varying scan rates (5 – 250 mV/s) in pH 7 BR buffer solution.

Figure 6.3.5. Square voltammogram detailing the response of an anodised CF electrode towards a pH 3 BR buffer solution and the subsequent peaks formed due to the oxidation of the surface bound quinone and electrochemically generated salicylate dimer species.

Figure 6.3.6 Square wave voltammogram detailing the response of the dimer modified anodised CF electrode towards a pH range in an a) Oxidation scan and b) Reduction scan. Both including a plot detailing the linear response (including mean standard deviation error bars) found between the dimer peak position and pH. N_s=32, N_{pH}=6

Figure 6.3.7 Square wave voltammograms detailing the response of the dimer modified anodised carbon fibre electrode towards 99 μM UA and 228 μM AA (pH 7 BR solution). N_s=3

Figure 6.3.8 Square wave voltammograms detailing the response of the anodised SPE response towards the oxidation of salicylic acid (10 mM, 0.1 M NaOH). N_s=3,

Figure 6.3.9 A) Square wave voltammogram detailing the response of the dimer modified anodised SPE towards a pH range (pH 3 - 8). B) Quantitative calibration data revealing the Nernstian response and mean standard deviation error bars. N_s=18, N_{pH}=6

Figure 6.3.10 Peak position response of a Nafion® coated anodised SPE with adsorbed dimer towards pH 7 buffer solution over a period of 20 minutes.

Figure 6.3.11 A) Square wave voltammograms detailing the response of the Nafion® coated dimer modified anodised SPE towards a pH range B) Plot detailing the linear response and error bars of the mean standard deviation of the peak position of the Nafion® coated anodised SPE towards a single pH range (pH 3 – pH 8). N_s=18, N_{pH}=6

Figure 6.3.12 Plot detailing the linear response of the average peak position and error bars of three separate Nafion® coated anodised SPEs towards a single pH range (pH 3 – pH 8). Including mean standard deviation error bars. N_s=12, N_{pH}=4

Figure 6.3.13 Stability graphs detailing the response of Nafion® coated dimer modified SPE towards four consecutive pH ranges. N_s=48, N_{pH}=4

Figure 6.3.14 Square wave voltammogram detailing the response of the Nafion® coated SPE response towards a sample of defibrinated horse blood and pH 7 BR buffer solution.

Figure 7.1.1 Laser processing procedure for the preparation of a conductive polyethylene mesh film.

Figure 7.1.2 Redox transition of the flavin unit (**I->II**) and the electro-oxidation of the phenolic substituent leading to the production of a polyphenylene oxide polymer (**I->III**) on exposed carbon surfaces at the film interface.

Figure 7.3.1 Five consecutive cyclic voltammograms detailing the response of a glassy carbon electrode towards the Flavin-phenol derivative in pH 7 buffer. Scan rate: 50 mV/s. N_s=5

Figure 7.3.2. Cyclic voltammograms detailing the response of a poly Flavin modified glassy carbon electrode in buffers of varying pH. Scan rate: 50 mV/s. N_s=3, N_{pH}=6

Figure 7.3.3 DekTak surface profile of the lasered film highlighting the typical depth profile of areas receiving a single and double pass. Insert: photograph of the C-PE film after laser treatment.

Figure 7.3.4 Scanning electron micrographs of the carbon-polyethylene mesh after laser processing. A) low magnification highlighting the direction of the laser raster and creation of holes within the film. B) Comparison of the laser etched track and unmodified film. C) Removal of the polyethylene at the pore edge as a consequence of laser double pass

Figure 7.3.5 Five consecutive cyclic voltammograms detailing the response of the carbon-polyethylene mesh electrode towards the Flavin-phenol derivative in pH 7 buffer. Scan rate: 50 mV/s. N_s=5

Figure 7.3.6 Square wave voltammograms detailing the response of a poly Flavin modified carbon-polyethylene mesh electrode in buffers of varying pH. N_s=3, N_{pH}=7

Figure 7.3.7 A) Variation of peak potential with pH over three consecutive pH series recorded at the Flavin modified carbon-polyethylene mesh. B) Influence of repetitive cycling and pH on the peak magnitude of the Flavin modified carbon-polyethylene mesh. N_s=63, N_{pH}=7

Figure 7.3.8 Five consecutive cyclic voltammograms detailing the response of a SPE towards the flavin-phenol derivative in pH 7 buffer. Scan rate: 50 mV/s. N_s=5

Figure 7.3.9 Square wave voltammograms detailing the response of a poly Flavin modified SPE electrode in buffers of varying pH. N_s=3, N_{pH}=7

Figure 7.3.10 Peak potential response of Flavin modified SPE to a pH range over a period of five consecutive days. N_s=3, N_{pH}=4

Figure 7.3.11 Square wave voltammogram detailing the response of a poly flavin modified SPE electrode in defibrinated horse blood.

List of Tables

Table 2.1 Wound Technologies and Healing Aids. Adapted from (Frykberg and Banks, 2015)

Table 2.2 General Diagnostic Tests. Adapted from World Union of Wound Healing Societies 2008 (World Union of Wound Healing Societies, 2008)

Table 2.3 Potential Wound Biomarkers. Adapted from (Broadbent, *et al.*, 2010)

Table 2.4 Common wound diagnostic markers Reproduced with permission (Davis, *et al.*, 2016)

Table 2.5 Comparison of electrochemical pH sensors. Reproduced with permission (Davis, *et al.*, 2016)

Table 6.1 A detailed breakdown of results of three separate Nafion® coated dimer modified anodised SPEs towards a single pH range. E= Electrode

Table 6.2 Recorded peak position values towards four consecutive pH ranges for a Nafion® and dimer modified SPE

Table 6.3 Peak positions obtained from the Nafion® coated dimer modified SPE response towards defibrinated horse blood and their calculated pH. E= Electrode

Table 6.4 Peak positions obtained from the Nafion® coated SPE response towards defibrinated horse blood over a 2 day period and their calculated pH. DHB = Defibrinated Horse blood

Table 7.1 Flavin modified SPE average peak position response over duration of up to 5 days .E= Electrode

Table 7.2. Analysis of the peaks obtained from the poly Flavin modified SPE electrode response in defibrinated horse blood. E= Electrode

Table 7.3. Variation of the peak position from respectively scanning (10 scans) three Flavin modified SPE electrodes in defibrinated horse blood. E= Electrode

List of Schemes

Scheme 4.1 EC' mechanism involving a L-cysteine modified Pd electrode and ferrocyanide.

Scheme 5.1 Electro-oxidation of L-tryptophan leading to the generation of 1,4 and 1,2 indole quinones. Adapted from (Enache, *et al.*, 2011).

Scheme 6.1 ECE reaction and polymerisation pathway of substituted phenols. Reproduced with permission (Dai, *et al.*, 2015).

Scheme 6.2 Potential product spread as postulated by Park (2016) from the electro-oxidation of salicylate (Park, *et al.*, 2016).

Scheme 6.3 Redox transition between Hydroquinone-quinone species from the electrogenerated dimer resulting from the oxidation of salicylic acid. Reproduced with permission (Rawlinson, *et al.*, 2017).

Scheme 7.1. Preparation of the phenolic flavin derivative.

Acknowledgements

First and foremost, I would like to express my sincere gratitude and appreciation to my supervisor Prof James Davis, who has provided an abundance of support and guidance throughout the entirety of my PhD and university life. His patience, encouragement and enthusiasm have been intrinsic to the completion of this research project. His mentoring in both my academic and career development have been next to none, I could not imagine having a better supervisor.

My gratitude also extends to the other staff and academics who have contributed to my PhD either through collaboration or technical assistance including: Prof Dewar Finlay, Dr Jill Cundell, Dr Stephen Badger, Dr Karl McCready, Prof Jim Mc Laughlin, Mrs Ann Blair, Mr Damian McDonald and Miss Christine McDonald.

I would also like to thank all the members of Team Biomole, especially Dr Jolene McHugh and Dr Jordan Atchison for their support and wisdom. To Aaron, Catherine, and Charente, thank you for all the laughs, it has been a pleasure to work with you in the lab. A special thanks to Ashleigh and Sean who have journeyed with me every step of the way, and without their encouragement and support I would not have survived this thesis. To Dr Ashleigh Anderson, thank you for your endless support and friendship.

Last but certainly not least, I would like to thank my friends and family who have supported me throughout my PhD, especially to my parents and my brothers, Zack and Robbie.

Abstract

Infection is a major concern for those with chronic wounds, without appropriate and early interventions this can lead to limb threating events. At present, there is a clear requirement for the development of an *in-situ* sensor for point of care management of chronic wounds. The availability of such a sensor could significantly improve the clinical outcome by providing the clinician with a more detailed picture of the healing status of the wound, as well as identifying the early onset of infection.

The methodology employed here focuses on the development of a novel electrochemical sensor to monitor pH, a key biomarker used to help determine the healing status of a wound. Ultimately, it is envisioned that the proposed pH sensor could be incorporated into a conventional wound dressing to allow for periodical monitoring. A variety of carbon-based composite materials were assessed as a potential base sensing substrate. Ultimately, a carbon-based screen printed electrode was selected as the most suitable substrate due to its ability to be manufactured in bulk at a relatively low cost, which is essential considering the frequency of which wound dressings are replaced.

The novel aspects of this research are based upon a variety of surface modification techniques to improve the ability of the electrode to confer pH. The surface modification techniques that were investigated, and critically assessed, included the electroxidation of a pH sensitive redox wire onto a carbon fibre electrode and, both the electrogeneration of a pH sensitive dimer and the electropolymerisation of a custom poly flavin derivative onto carbon screen printed electrodes.The electrode performance was then assessed against a clinically relevant pH range for wound monitoring (pH 3 – 8), and the viability of the modified electrode response in a simulated wound environment using a more complex media, such as defibrinated horse blood, was investigated.

Abbreviations

AA	Ascorbic Acid
ADP	Adenosine Diphosphate
Ag	Silver
AgCl	Silver Chloride
ATP	Adenosine Triphosphate
BR	Britton - Robinson
CE	Counter Electrode
CF	Carbon Fibre
CPE	Carbon Polyethelene
CPS	Counts Per Second
CSH	Cysteine
CV	Cyclic voltammogram
DFU	Diabetic Foot Ulcer
DHB	Defibrinated Horse Blood
E	Electrode Potential
ECE	Electrochemical – Chemical – Electrochemical reaction
EC'	Electrochemical – Chemical Prime reaction
EGF	Epithelial Growth Factors
EMF	Electromotive Force
EPS	Extracellular Polymeric Substances
ECM	Extracellular Matrix
FGF	Fibroblast growth factors
GC	Glassy Carbon
HER	Hydrogen Evolution Reaction
IGIF-I	Insulin-like Growth Factor I
IL	Interleukin
KCl	Potassium Chloride
KGF	Keratinocyte Growth Factor
MMPs	Matrix Metalloproteinases

mV	Millivolts
NHS	National Health Service
NaOH	Sodium Hydroxide
NO	Nitric Oxide
N_S	Number of scans
N_{pH}	Number of pH buffer solutions
PANI	Polyaniline
Pd	Palladium
PVB	Polyvinyl Butyral
PVD	Peripheral Vascular Disease
PDGF	Plated Derived Growth Factors
RFID	Radio Frequency Identification
ROS	Reactive Oxygen Species
SA	Salicylic Acid
SEM	Scanning Electron Microscope
SPE	Screen Printed Electrode
SQW	Square Wave Voltammogram
TIMPs	Tissue Inhibitors of Metalloproteinase
TGF	Transforming Growth Factors
TGF-α	Transforming Growth Factors alpha
TGF-β	Transforming Growth Factors beta
UA	Uric Acid
V	Volts
VEGF	Vascular Endothelial Growth Factors
VICC	Vicinity Integrated Circuit Card
WE	Working Electrode
XPS	X-Ray Photoelectron Spectroscopy

Copyright / Credit Notices

Within this thesis material (like text, figures, or tables) from the author's publications is reprinted. The copyright / credit notices are listed at this place in common for all the related chapters, paragraphs or sections. The material might have been modified slightly, however these copyright / credit notices still apply.

Acknowledgement is given to the original source of publication for:

McLister A, Davis J. Molecular Wiring in Smart Dressings: Opening a New Route to Monitoring Wound pH. *Healthcare* 2015;3(3):466-477.

The final publication is available at Mdpi via
doi:10.3390/healthcare3030466.

Acknowledgement is given to the original source of publication for:

McLister A, McHugh J, Cundell J, Davis J. New Developments in Smart Bandage Technologies for Wound Diagnostics. *Adv. Mater.* 2016.

The final publication is available at Wiley via
doi:10.1002/adma.201504829.

Acknowledgement is given to the original source of publication for:

Book: *Smart Bandage Technologies : Design and Application*. Editor: Maria Convey, July, 2016. Elsevier, ISBN 978-0-12-803762-1.

The final publication is available at Elsevier via
eBook ISBN 9780128038468

Acknowledgement is given to the original source of publication for:

Rawlinson S, **McLister A**, Kanyong P, Davis J. Rapid determination of salicylic acid at screen printed electrodes. *Microchem. J.* 2018. 137

The final publication is available at Science Direct via
doi:10.1016/j.microc.2018.09.019.

Acknowledgement is given to the original source of publication for:

Morelli F, Anderson A, **McLister A**, Fearon J-J, Davis J. *Electrochemically Driven Reagent Release from an Electronic Suture*.; 2017;81.

The final publication is available at Science Direct via
doi:10.1016/j.elecom.2017.05.020.

Acknowledgement is given to the original source of publication for:

Martin A, McConville A, Anderson A, **McLister A**, Davis J. Microneedle Manufacture: Assessing Hazards and Control Measures. *Safety* 2017;3(4):25.

The final publication is available at MDPI via
doi:10.3390/safety3040025

Acknowledgement is given to the original source of publication for:

McLister A, Mathur A, Davis J. Wound diagnostics: Deploying electroanalytical strategies for point of care sensors and smart dressings. Curr Opin Electrochem. Elsevier; 2017 Jun 1;3(1):40–5.

The final publication is available at Science Direct via
doi: 10.1016/J.COELEC.2017.05.002

Notes on Access to Contents

“I hereby declare that with effect from the date on which the thesis is deposited in Research Student Administration of Ulster University, I permit

1. the Librarian of the University to allow the thesis to be copied in whole or in part without reference to me on the understanding that such authority applies to the provision of single copies made for study purposes or for inclusion within the stock of another library.

2. the thesis to be made available through the Ulster Institutional Repository and/or EThOS under the terms of the Ulster eThesis Deposit Agreement which I have signed.

IT IS A CONDITION OF USE OF THIS THESIS THAT ANYONE WHO CONSULTS IT MUST RECOGNISE THAT THE COPYRIGHT RESTS WITH THE AUTHOR AND THAT NO QUOTATION FROM THE THESIS AND NO INFORMATION DERIVED FROM IT MAY BE PUBLISHED UNLESS THE SOURCE IS PROPERLY ACKNOWLEDGED".

Chapter 1

Introduction and Project Aims

Overview

Chronic wounds are a pressing concern for the modern healthcare system, due to the economic burden associated with the treatment and management of the wound. As such, there is a clear demand for the development of *in situ* sensors that could continuously monitor the healing process of the wound. This would provide the clinician with valuable information on the wound status, and could alert them to the early onset of infection. In turn, this could enable more effective and timely treatments, that could result in an enhanced outcome for the patient. This chapter provides a concise overview of the factors that underpin the healing processes involved in wound healing and highlights the aims and objectives of this research project.

Part of this literature has been published in the following:

Davis J, McLister A, Cundell J, Finlay D. *Smart Bandage Technologies : Design and Application*. 1st ed. Academic Press; 2016.

McLister A, McHugh J, Cundell J, Davis J. (2016) New Developments in Smart Bandage Technologies for Wound Diagnostics. *Advanced. Materials.* 28(27), pp. 5732 – 5737.

1.0 Introduction

Cuts and grazes are a feature of everyday life and if the trauma to the skin is relatively minor, the process of repairing the wound will depend upon the myriad of biochemical processes that govern wound healing. Typically, beyond the simple act of cleansing the wound, the body is expected to re-establish the integrity of the skin barrier on its own accord without the slightest oversight from the patient. However, this is not always the case, in some instances the healing processes that regulate tissue regeneration can slow down and even stall (Falanga, 2005; Posnett, *et al.*, 2010; Siddiqui, *et al.*, 2010; Holman, *et al.*, 2012; Moura, *et al.*, 2013). The latter can develop because of numerous factors such as, infection, poor circulatory supply and compromised nutritional/and or immune status. The development of chronic wounds is a perennial concern for healthcare clinicians, especially those in the field of diabetes where ulceration is a common and increasingly problematic complication (Posnett, *et al.*, 2010; Siddiqui, *et al.*, 2010; Holman, *et al.*, 2012). While there have been numerous advances in sensing technologies for the daily management of diabetes via patient own monitoring of blood glucose levels, there is an emerging opportunity for these same methods to provide diagnostic insights into the healing process of chronic wounds.

The ability to extract quantitative data on the dynamics of key molecular players rather than relying on gross physical symptoms and visual clues could enable more informed decisions and optimise treatment (World Union of Wound Healing Societies, 2008). Currently there are a range of standard tests which can be conducted as part of a routine assessment: measuring systemic inflammatory markers, temperature or blood pressure. These tests are not specific to the wound and, although they may help to inform the clinician, they do not, by themselves, indicate a diagnosis (Practice, 2008). The development of tests that could provide detailed information on the activity of cellular and molecular species within the wound, would clearly be of major benefit in appropriate treatment selection. However, such tests are seldom available to the attending clinician and, where they

are, it is invariably through a central laboratory (Practice, 2008; Dargaville, *et al.*, 2013; McLister, *et al.*, 2014). The time delay in receiving and analysing the results means that the wound condition may have changed in the intervening days, therefore negating these initial results.

This issue corresponds with one of the key findings reported in a recent World Union of Wound Healing Societies' report, that "diagnostic tools need to be moved into the clinic or the patient's home to ensure optimal care is provided for patients with wounds" (Practice, 2008). At the time of writing, there are currently no available technologies to address this recommendation.

Advances in the development of diagnostic technology has created a clear opportunity for those in the field of biomedical science and engineering to develop systems suitable for use not only in the clinic but within the community using remote autonomous sensing (Matzeu, *et al.*, 2015). The development of a 'smart' dressing would effectively remove many of the variables and potential error associated with the user (patient or clinician), and could, at least in principle, provide more accurate analytical data. However, before a robust system can be implemented there are a substantial number of hurdles to overcome (Practice, 2008; Dargaville, *et al.*, 2013; McLister, *et al.*, 2014; Mehmood, *et al.*, 2014). The science behind the measurement is not the only aspect that needs to be considered: the direct integration of the sensor within a conventional dressing is necessary, as is the production of a cost effective and disposable sensor.

1.2 Wound Infection

One of the key concerns of any patient's management of a chronic wound or ulceration is their susceptibility towards to infection (Practice, 2014). The longer the wound remains unhealed and untreated, the greater the chance of infection taking hold. Bacterial contamination of an open wound is inevitable and, in most cases, exerts little influence on the healing dynamics and doesn't unduly impair wound closure. However, some bacterial strains such as Staphylococcus aureus,

Pseudomonas, aeruginosa, Streptococcus pyogenes, when present in significant amounts, can pose as a life threating risk to the patient (Brook, 1996; Bowler, *et al.*, 2001). These species can be present on skin and, while normally benign, are generally recognised as adventitious agents and can cause infection where the normal barriers are removed and inadequate control measures have been employed. Once infection takes hold, it not only impedes the healing process but can also lead to cellulitis and if not treated, bacteremia and septicemia.

The main approach to combat infection is to reduce the bioburden via topical and /or systemic administration of antimicrobial compounds (Lipsky, *et al.*, 2009; Barnea, *et al.*, 2010; Moura, *et al.*, 2013). During routine clinical assessment, if there is any suspicion of infection, a swab or tissue sample of the wound would be sent for microbiological testing to identify possible candidates to select the appropriate antimicrobial. After the sample, has been sent for testing, the clinician would then have debrided the wound to remove compromised tissue and any biofilms that could harbor microbes and which could also act as a barrier to the selected microbial (MacMillan, 1980; Hunt, 1981).

Over the past few decades, there has been a rapid surge of interest surrounding wound dressings, as highlighted in **Figure 1.1**. This has ultimately led to the gradual evolution of dressings from purely passive absorbent polymers to more functional materials that actively encourage the wound to heal and minimise the risk of infection. Examples of the components incorporated within these new materials include of metalloproteinase inhibitors and/or antimicrobial agents such as iodine or silver (Moura, *et al.*, 2013).

The debate about the use of silver within dressings can be quite polarized at times and, while there are studies to indicate some cytotoxicity (Poon, *et al.*, 2004; Cortese-Krott, *et al.*, 2009; Boonkaew, *et al.*, 2014), there is also substantial evidence indicating that it does improve the healing process (Barillo, *et al.*, 2014; Zhong, 2015). The increasing prevalence of resistant bacteria is of course a major

concern for healthcare providers, as such there is a need for continuing research into new approaches that shall be discussed further in Chapter 2.

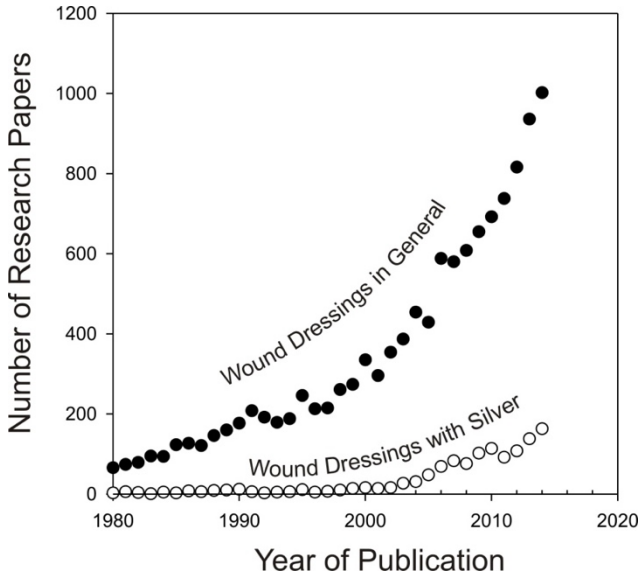

Figure 1.1 Research growth in wound dressings. Reproduced with permission (Davis, *et al.*, 2016).

1.3 Health Costs

Chronic wounds are a tremendous economic burden on the healthcare services irrespective of geographical location. When a spotlight is trained on the estimated cost of treatment associated with wounds, results frequently lie in the multibillion region (Thomas, 2006; Nations, 2010). In the UK alone, it has been estimated that some 650,000 patients suffer from some form of wound that requires clinical intervention with published reports suggesting that the combined cost to the National Health Service for their treatment reaches approximately £3 billion per year (Posnett, *et al.*, 2010). In regards to the US, with a greater population and an atypical medical care system, it is reported their estimated costs are at a heftier $25 billion (Sen, *et al.*, 2009).

Upon further inspection of these estimates, it has been speculated that only 5% of these costs are down to the material costs for dressings, while 80% are said to be attributed to the high staff overhead associated with the nurse / consultant time

(Posnett, *et al.*, 2010). Chronic wounds can arise from numerous conditions but for this research project, the principal focus is on those arising as a consequence of diabetic complications. The global figure for diabetes worldwide is expected to rise from 370 million at present, to some 552 million people by 2030 (Bakker, *et al.*, 2011). It is widely recognised that some 5-7% of diabetic patients in the UK have had, or presently manage, a foot ulcer (Diabetes UK, 2011; Kerr, 2012) but, more worrying, are the predictions that the lifetime probability of a diabetic patient developing a chronic foot ulcer lies in the region of 10-25% (Singh, *et al.*, 2005). In addition, in the US it has been reported that the cost associated with the treatment of a single DFU incident over a two year period equates to $28,000 (Ramsey, *et al.*, 1999), and that the inpatient costs for major amputations is in a region of $31,000 (Assal, *et al.*, 2002; Rathur, *et al.*, 2007).

The current austere financial climate is not only limited to healthcare providers but will also have an impact on the patient employment where there will be clear issues (financial and logistical) with staff days lost of illness and recovery. This can mean that many are denied employment (O'Donnell, *et al.*, 1977). The psychological impact of daily management of the disability will inevitably impact on wound healing (Phillips, *et al.*, 1994; Lanzafame, 2007; Ghanassia, *et al.*, 2008). From the literature a number of surveys have been identified (Phillips, *et al.*, 1994; Herber, *et al.*, 2007; Augustin, *et al.*, 2014) which have assessed and reported how such conditions can affect the patient's quality of life, however few address the daily inconveniences incurred. Irrespective of age, a chronic wound will mean lost working hours, potential job loss and financial insecurity. Philips et al. reported extensively on the correlation of the effects of managing leg ulceration and how this condition can impact the patient's daily routine, where, not surprisingly the survey concluded that there was a strong correlation between the time taken to manage the treatment and the impact on patient mental health where issues of anger, isolation and resentment can present themselves. These emotions can undoubtedly escalate and lead to depression which will do little to improve patient recuperation (Da Silva, *et al.*, 1992; Margolisa, *et al.*, 2002; Patel, *et al.*, 2006).

Bearing these factors in mind, there is no doubt that timely management of infection is a critical issue in chronic wounds. However, deciding how to re-stimulate healing processes in a wound that has been in a chronic phase for many months or years requires a knowledge of the cellular and molecular processes and the cause of the inhibition. This calls for a “smart” system that can proactively deal with critical colonisation – offering either a means of alerting the patient or, ultimately, enabling autonomous treatment. The key factor in both scenarios is the reduction in time between diagnosis and treatment.

The next chapter will critically review the literature and research currently being conducted in the field of novel wound monitoring technologies. In addition, a summary of the underpinning factors involved in the healing process is also discussed to highlight the significance of the role a variety of biochemical protagonists in wound management.

Chapter 3 will provide details on the fundamental principles of the experimental methods and techniques employed throughout this research project in terms of electrode modification, analysis and characterisation.

In Chapter 4, a palladium film will be investigated to determine its ability to effectively act as a conductive substrate to confer pH. The film will be modified using self-assembling monolayers, in order to maximise the electrode potentiometric response towards pH. The potentiometric technique shall be employed during these investigations in determining pH. The relatively simplistic electronics associated with the potentiometric techniques makes it attractive to the field of wearable biosensors, therefore this shall be taken into consideration when critical assessing and validating this approach.

Chapter 5 sees the transition from potentiometric approaches to voltammetric techniques. The sensing capability of a Poly-L-tryptophan modified carbon fibre mesh towards pH is assessed. In addition, the analytical performance of the

composite electrode was challenged in a biological relevant environment, namely horse blood.

In Chapter 6, a carbon-based screen printed electrode was employed to monitor pH, by exploiting the quinone dimer that was generated from the electrochemical oxidation of salicylate and adsorbed onto the electrode surface. The electrode surface was then coated with a layer of Nafion® to entrap the electrogenerated dimer. This modification resulted in the electro-oxidation of the dimer bound at the electrode surface providing a pH dependent response that exhibited a sub Nernstian response (51 mV/pH) over a pH range (pH 3 – pH 8). The analytical performance and stability of the dimer modified screen-printed electrode was assessed using horse blood as a simulated wound environment.

The final result chapter, chapter 7, will again look at the response of a modified screen printed electrode. This time however a custom Flavin derivative bearing a phenol substituent was electropolymerised onto the electrode surface. The stability of the composite will be evaluated and the analytical applicability towards the voltammetric measurement of pH in horse blood is critically assessed.

1.4 Summary and Project Aims

The present investigation focuses on the research surrounding the development of an electrically conductive sensor that could eventually be incorporated within a conventional dressing to identify changes in the chemical composition of wound fluid, and to provide the clinician with a simple and effective means of understanding the true condition and health of the wound. This could potentially lead to more efficient and effective treatments, and thereby resulting in a more positive outcome for the patient. Therefore, the project objectives are:

1. To design and develop a new functional material that is capable of monitoring pH within a clinically relevant range for chronic wounds (pH 3 – 8);

2. To characterise the sensing performance of the functional material and optimise their electroanalytical properties to confer pH;
3. To demonstrate the robustness of the steady state pH sensor towards repetitive scanning in a clinically relevant pH range;
4. To demonstrate that the sensor is capable of monitoring the pH within a more complex matrix, such as defibrinated horse blood that mimics a wound environment, without losing selectivity and sensitivity towards pH sensing;

Ultimately, the core remit of the project will focus on the development and characterisation of the sensing film to provide a steady state pH sensor that could potentially be used in the future as a disposable sensor to indicate the healing status of the wound and allow for the early detection of infection within the wound exudate to the attend.

Chapter 2

Literature Review

Overview

The pH of wound fluid has long been accepted as one of the key diagnostic indicators for assessing the health of a wound, but there are currently few technological options available to the clinician. The advent of a sensor that could measure wound pH, whether in a clinic or home setting, could significantly improve the clinical outcome, especially in the early identification of complications such as infection. This literature review explores new material designs and electrochemical research currently being conducted that is focused on the development of wound diagnostics. In turn, this review also provides a critical overview of emerging research that could be pivotal change for future devices.

Aspects of the work described in this chapter has been in previously published:

McLister A, McHugh J, Cundell J, Davis J. New Developments in Smart Bandage Technologies for Wound Diagnostics. *Adv. Mater.* 2016;28(27):5732-5737.

Davis J, McLister A, Cundell J, Finlay D. *Smart Bandage Technologies : Design and Application*. 1st ed. Academic Press; 2016.

McLister A, Mathur A, Davis J. Wound diagnostics: Deploying electroanalytical strategies for point of care sensors and smart dressings. *Curr. Opin. Electrochem.* 2017;40:96-99.

2.1 Chronic Wounds

Chronic wounds are defined as the failure to produce an adequate and functional result in an orderly process (Lazarus, *et al.*, 1994). They are commonly associated with diabetic complications, peripheral vascular disease and pressure ulcers and can affect all ages but tend to be more prevalent in older patients (Siddiqui, *et al.*, 2010). A delay in the healing response makes the patient more susceptible to complications such as infection and limb threating events that would inevitably increase costs for healthcare providers. The treatment of chronic wounds is a worldwide issue, in the US alone, chronic wounds are said to affect 6.5 million people, costing the USA health service $25 billion annually to treat (Huang, *et al.*, 2009). In the UK it is estimated that by 2035, 17% of the overall National Health Service budget will be spent on diabetes, roughly equating to £13.5 billion, of which 79% is reported to be spent on complications – many of which are preventable (Consortium, 2011). This further highlights the demand for a more proactive approach to wound management in response to infection, which will ultimately improve the quality of life of patients as well as reducing the burden and economic cost to the National Health Service.

2.1.2 Diabetic Ulceration and Impaired Healing

Throughout the USA and the UK, it has been previously reported that 25% of all diabetes related hospital submissions are related to ulceration of the diabetic foot and the subsequent limb threating infection (Pecoraro, *et al.*, 1990; Bouter, *et al.*, 1993; Levin, *et al.*, 1993; Gibbons, *et al.*, 1995; Lavery, *et al.*, 2003; Armstrong, *et al.*, 2004). Approximately 12% of individuals with a chronic foot ulcer will require amputation as a result of infection (Greer, *et al.*, 2012). The decision to conduct an amputation is not arrived at lightly, but only becomes a necessity when the diabetic foot experiences physical trauma and ulceration due to a combination of intrinsic factors such as peripheral neuropathy and vascular insufficiency, as well as external factors such as callus formation and excessive pressure, that ultimately leads to

infections and gangrene (Most, *et al.*, 1983; Fylling, *et al.*, 1989; Larsson, *et al.*, 1995; Edmonds, 2005). These figures highlight the importance of preventing complications such as infection, which can have a substantial impact on the healing time of a wound as well as causing further discomfort to the patient.

Diabetes and impaired wound healing is a commonly accepted phenomenon (Lipsky, *et al.*, 1990; Hehenberger, *et al.*, 1998; Moulin, *et al.*, 1998), yet the exact mechanism in which impaired healing occurs is not yet fully understood. This lack of understanding adds ambiguity to the clinician's decision making process of determining the most appropriate and effective treatment for each individual patient. To shine some light on this phenomenon, numerous studies have been conducted to determine the exact mechanism of healing. An example of which includes the work of Lipsky and colleagues, who reported that several specific mechanisms are responsible for chronic wound healing, some of which include: increased glycation of protein, a defective inflammatory response and an inadequate production of polypeptide growth factors at the local site (Consortium, 2011). In addition to this, a myriad of factors have been reported to impair the healing rate of the wound, some of which include fibroblast dysfunction, hypoxia, high levels of MMPs and impaired angiogenesis. A simplified schematic of how these factors interplay and impair healing is detailed figuratively by Brem (2007) in **Figure 2.1.1**. It is evident from this simplified schematic that the healing process of a diabetic foot wound is complex and the process of healing can fail due to several factors. However, a key factor that contributes to insufficient healing that is not included in this schematic, is infection. Irrespective of the exact cause of the diabetic foot wound, the first step in its management is to treat any bacterial infection (Jeffcoate, *et al.*, 2003), followed by the appropriate treatment for the management of neuropathy and ischemia (McNeely, *et al.*, 1995)

Figure 2.1.1 Mechanism of wound healing in healthy people compared to those with diabetes. Reproduced with permission (Brem, *et al.*, 2007)

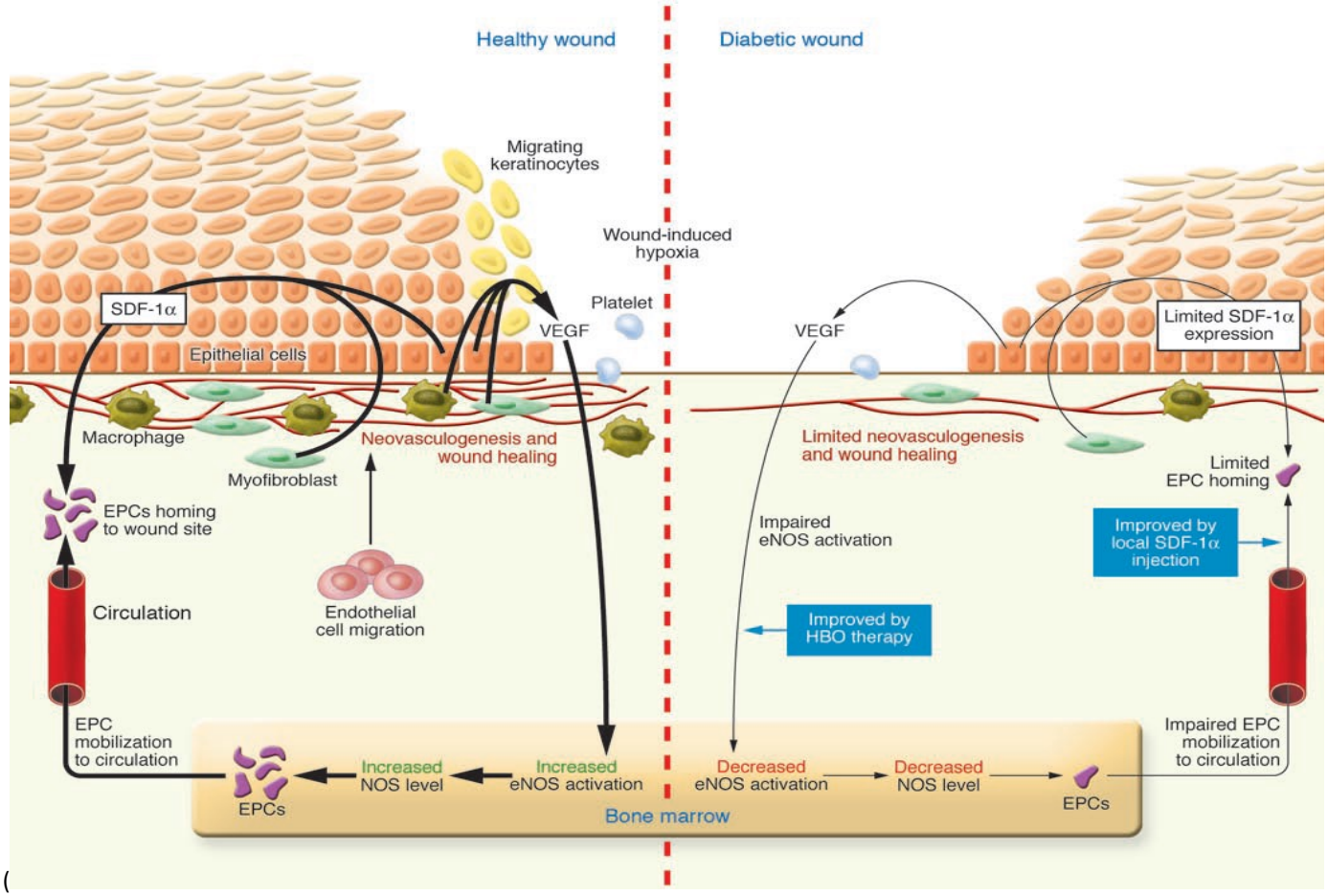

(

2.2 Normal Wound Healing

Wound healing can be defined as the physiology by which the body replaces and restores function to damaged tissues (Tortora, *et al.*, 2008). It is a dynamic process that involves complex mechanisms mediated by a range of growth factors (Ma, *et al.*, 2007), and entails a complex interplay between connective tissue formation, cellular activity and growth factor activation. The process of wound healing primarily involves three activities: inflammation, proliferation and remodeling, as indicated in **Figure 2.2.1** . Although there is a considerable overlap between these phases, they occur in an orderly and predictable manner during the normal wound healing process (Clark, 1998). Comprehension of the effects of diabetes on wound healing, and the fact that most diabetic foot wounds have impaired healing involving many complex pathophysiological mechanisms, requires an understanding of the normal wound healing processes.

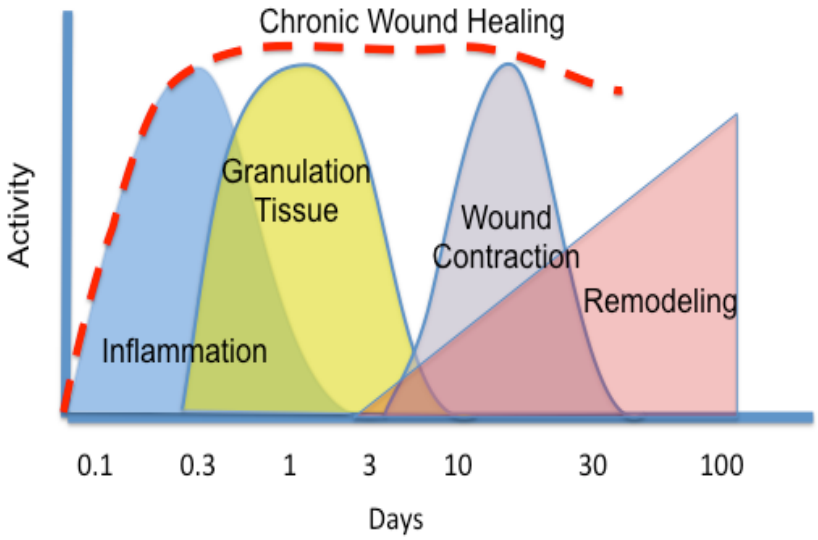

Figure 2.2.1 The various stages of healing in acute and chronic wounds. Reproduced with permission (Davis, *et al.*, 2016).

2.2.1 Stage 1: Inflammation Phase

Inflammation occurs immediately after injury and generally lasts between two to four days, as highlighted in **Figure 2.2.1**. Upon injury bleeding occurs followed by the enzymatic activation of a number of processes that include the clotting cascade,

the complement cascade and the kinin cascade. In addition, platelet aggregation and activation occurs and the cumulative effect of all of these factors results in inflammatory cells invading the wound tissue within a couple of hours of injury (Weyrich, *et al.*, 2004)**.** The first to arrive at the site of the wound is the neutrophils, followed by the monocytes and the lymphocytes. Their primary role is to provide a defense against contaminating microorganisms via the production of a variety of proteinases and reactive oxygen species (ROS), as well as helping the phagocytosis of cell debris (Werner, *et al.*, 2003; Dovi, *et al.*, 2004). These inflammatory cells also play a vital role in initiating the proliferative phase by providing an important source of growth factors and cytokines. The release of these growth factors helps to stimulate the influx of a variety of cells that include: white cells, fibroblasts and cells that aid in angiogenesis. A similar pattern is expressed by the lymphocytes (McGrath, 1990), while the macrophages continue to secrete growth factors which attract fibroblasts that leads on to the subsequent phase of healing and proliferation.

2.2.2 Stage 2: Proliferative Phase

The secondary overlapping phase of wound healing is the proliferative phase where tissue granulation occurs. Both epithelial proliferation and re-epithelialisation of the epithelia cells occur at this stage via the migration of cells over the provisional matrix formed succeeding wounding (Moulin, 1995). Granulation tissue contains a dense population of fibroblasts and macrophages characterised by an extensive network of new blood vessels surrounded by loosely structured collagen, elastin and proteoglycans (Clark, *et al.*, 1998; Slavin, 1999). The role of the fibroblasts is to bind the growth factors and secrete additional growth factors and extracellular molecules. The influx of growth factors induces both the autocrine and paracrine stimulation of fibroblasts and ingrowing capillaries. At the same time, epithelial cells begin to grow inwards from the wound edges to cover the wound. Parallel to the stress lines of the wound, strands of collagen will grow to strengthen the site of the wound (Witte, *et al.*, 1997).

2.2.3 Stage 3: Tissue Remodeling Phase

The remodeling phase is often referred to as maturation and during this period the amount of water present within the wound reduces, while the collagen laid down during proliferations stage is replaced with type III collagen which provides a more stable structure. As the wound contracts and the scar begins to form, the amount of connective tissue and number of capillaries begin to reduce. A variety of growth factors, such as TGF- ß, PDGF and FGF, that are stimulated during tissue injury are responsible for the regulation of the remodeling phase (Steenfos, 1994; Amjad, *et al.*, 2007)**.** For the next two years after the injury has occurred, a continuous process of fibroblast induced collagen synthesis occurs coupled with the breakdown of collagenases and the regression of inflammatory cells which helps to gradually remodel the wound into a mature scar (Thorn, *et al.*, 2004). The three phases described above are atypical of the process of wound repair in an acute wound, however in instances where the timely healing of the wound is stalled and it remains in the inflammatory stage for a prolonged period, as highlighted in **Figure 2.2.1**, it is often referred to as a chronic wound.

2.3 Wound Treatment Approaches and Technologies

The primary aim of wound management is to heal the wound and restore full function in a timely manner, while not causing undue pain to the patient. Up to now, the main approach for managing wounds has been to cleanse the wound site and then protect it from external contaminants. Recent developments in scientific research has led to the discovery of key insights into the relationships that exist between the cellular and molecular components within the wound and how they can be utilised for the benefit of the patient. One of these advances, that was only recognised and accepted in the past 50 years, was that maintaining a moist wound environment encourages the wound healing process (Winter, 1962). Early medical methodologies, that at times are in sharp contrast to the experimental systematic approaches employed today, essentially paved the way for the development of new functional materials designed to specifically interact with the wound (Moura, *et al.*, 2013; Mayet,

et al., 2014; Boateng, *et al.*, 2015). At one point, a cotton gauze / cotton wool pad, would have been the primary wound dressing available to the clinician, whereas now a multitude of different products, each possessing a variety of materials, additives and functions are readily available at your local pharmacy (Boateng, *et al.*, 2015). Examples of the range of wound management technologies currently available (Boateng, *et al.*, 2015; Frykberg, *et al.*, 2015) are summarised in **Table 2.1.**

Table 2.1 Wound Technologies and Healing Aids. Adapted from (Frykberg, *et al.*, 2015).

Negative pressure wound therapy
Hyperbaric oxygen therapy
Topical oxygen therapy
Electrical stimulation, diathermy, pulsed electromagnetic fields
Pulsed radiofrequency energy
Low-frequency noncontact ultrasound—MIST
Extracorporeal shock wave therapy–DermaPACE
Growth factors
Acellular matrix tissues
Xenograft dermis
Xenograft acellular matrices
Human dermis
Human pericardium
Placental tissues
Bioengineered allogeneic cellular therapies

The skin is capable of repairing itself naturally, however when the injury is sufficiently severe, it is sometimes necessary to introduce wound aids, such as dressings or tissue scaffolds. Different wounds require different treatments, therefore there is a plethora of commercially available dressings, that will conform to the core criteria of an

idealised dressing. However, selecting the most appropriate aid to accelerate healing for a given patient is a considerable challenge as there is certainly no universal bandage or dressing to accomplish this (Moura, *et al.*, 2013; Mayet, *et al.*, 2014; Boateng, *et al.*, 2015; Frykberg, *et al.*, 2015)**.**

2.4 Wound Management Strategies

Chronic wounds are typically examined by employing classic clinical assessments, such as recording a patient's medical history combined with a preliminary physical examination. The latter typically involves consideration of wound location, exudates, pain, oedema, lipodermosclerosis and hyperpigmentation and will almost inevitably be followed by several tests to determine the aetiology, comorbidities and to gauge the status of the wound.

2.5. Wound Diagnostics

Classification systems are predominately the first diagnostic tool the clinician will use to help classify the type of wound and subsequently help determine the most appropriate follow up procedure, whether that be further lab tests or imaging. Currently, there are a variety of tests available to aid in the clinician's wound diagnosis, that can be categorised into three distinct categories: nonspecific, diagnostic and theranostic (Zhou, *et al.*, 2011). These reflect the degree to which they indicate an appropriate intervention as indicated in **Figure 2.5.1**.

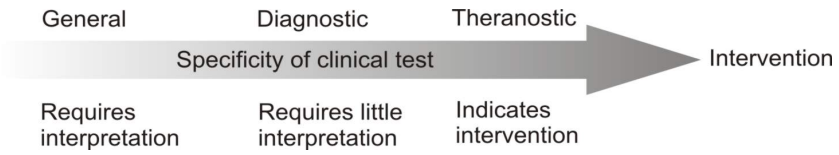

Figure 2.5.1 Diagnostic tests and their impact. Adapted from (Practice, 2008) .

General testing entails testing for systemic inflammatory markers, temperature and or blood pressure. Although these tests may not be specific to the wound and cannot confirm a diagnosis, they do however inform the clinician of the general health of the patient (Zhou, *et al.*, 2011). More specific diagnostic tests however, can remove some of the ambiguities and provide direct insights into the physiological or biochemical processes at play within the wound. As such they could provide more meaningful guidance to the clinician and positively influence subsequent interventions. The final category, theranostic testing, is different to the previous two categories in that it does not directly lead to diagnosis, rather it provides confirmation for a specific intervention. An example of this would include the identification a haemolytic streptoccoi within the wound that would then lead to the prescription of a specific antibiotic (Practice, 2008). With the advent of personalised medicine, theranostics is gaining considerable research interest due to its potential to accurately direct treatment with the promise of more favorable outcomes and this will also have an important beneficial impact in terms of health economics (Practice, 2008).

Currently a range of diagnostic tests are employed for wound assessment, as it is unlikely that one single test will fit all diagnosis of chronic wounds. Typical tests considered for the assessment of chronic wounds (Angel, *et al.*, 2011) are listed in **Table 2.2**. The tests denoted as (C) are those that can be conducted within the clinic at the time of consultation, while those labelled with an (L) require either biological or biochemical analysis which will almost invariably require the wound/blood sample being sent to the central clinical laboratory. With the latter type of testing, there will be inevitable delays in processing and reporting the results which can in turn impede the treatment outcomes. It is important to note that the tests highlighted in **Table 2.2** have seldom changed in recent years, demonstrating the pressing need for either new point of care diagnostics that could be employed during clinical assessment, or the development of smart technologies that could be incorporated into conventional dressings that could then conduct analysis autonomously.

Table 2.2 General Diagnostic Tests. Adapted from World Union of Wound Healing Societies 2008 (Practice, 2008)

Type	Description	
Wound specific	Dimensions	C
	Odema	C
	Erythema/heat	C
	Wound bed condition	C
	Wound margin	C
	Location	C
	Exudate colour, odour, quantity	C
	Pain	C
General tests	Temperature	C
	Pressure	C
	Reflexes and sensation	C
	Arterial pulses	C
	Monofilament sensitivity	C
Biological tests	Microbial culture	L
	Wound histology	L
	White cell count	L
	Erythrocyte sedimentation	L
Biochemical tests	Glucose	C/L
	Haemoglobin	L
	Plasma albumin	L
	Lipids	L
	Urea and electrolytes	L
	HbA1C	L
	Rheumatoid factor	L
	CRP	L
Miscellaneous	Oxygen	C
	Ankle brachial pressure index	C
	X-rays / CT / MRI	C
	High frequency ultrasound	C
	Duplex scanning	C

Where C = Clinic/Point of Care; L = Laboratory Test

2.6 Conventional Diagnostics

There has been a marked effort to step away from the traditional laboratory based diagnostics in recent years and step towards the design and development of decentralised tests and sensors for biomedical applications (Dargaville, *et al.*, 2013; McLister, *et al.*, 2014; Mehmood, *et al.*, 2014; Matzeu, *et al.*, 2015). The reason this form of diagnostic has gained such interest is attributed to the promise of rapid analysis providing the user (or clinician) with immediate feedback on a physical parameter (i.e. temperature), a chemical concentration (i.e. glucose) or an enzyme activity (i.e. proteases). The term decentralised refers to a device that can be used outside a laboratory environment and still be used by people with limited scientific experience. Therefore, the intention would be that the device could be used within a clinic, by a community healthcare provider or even by the patients themselves. In order to achieve this the device would need to be robust and portable and require little sample preparation to allow for a quick and simple measurement. These requirements embody the guidelines proposed by Harding and colleagues (Practice, 2008). One of the main benefits associated with approach is that it minimises the time delay often associated with conventional lab-based analysis as indicated in **Figure 2.6.1**. In regards to wound management, rapid analysis and reporting would result in a quicker intervention and help inform the clinician on the correct selection of dressing that would hopefully aid the healing process and improve patient outcomes (Practice, 2014).

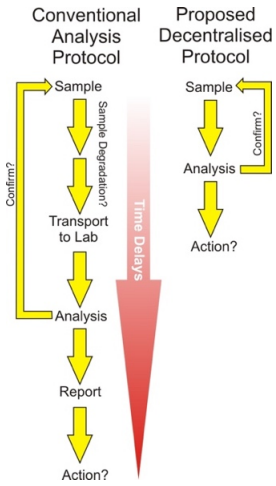

Figure 2.6.1 Central lab vs Point of Care Analysis. Reproduced with permission (Davis, *et al.*, 2016)

2.7 Core Methodologies

The main hurdle to overcome in developing a point of care diagnostic device, lies in attempting to make a device sensitive and selective enough to detect an analyte, without the need for extensive sample manipulation. Realistically, it would be unrealistic to expect the user, whether it be the clinician or patient, to perform a series of chemical manipulations before results could be obtained. The issue here does not simply relate to the time additional steps would require, rather the introduction of possible errors that could be introduced with each step. Therefore, any test should be as simplistic as possible and require the minimum amount of manipulation and, in a practical sense, should only involve the sampling of wound fluid (Practice, 2008). This places a considerable amount of responsibility on the underlying technology to process the sample and detect the target analyte, especially when dealing with the complex matrix that is wound fluid (Broadbent, *et al.*, 2010; Loffler, *et al.*, 2013)**.** An example of a basic rationale behind a simplistic test system, is shown in **Figure 2.7.1.** It must be noted the nature of the wound condition will impact on the sampling considerations - a wound that has lots of slough will present a radically different challenge than a wound that has been freshly debrided. Therefore, depending on the condition of the wound, it may be necessary to add additional steps to the procedure (such as debridement) or instrumentational sophistication (i.e. permselective barriers) to address the demands of a sample.

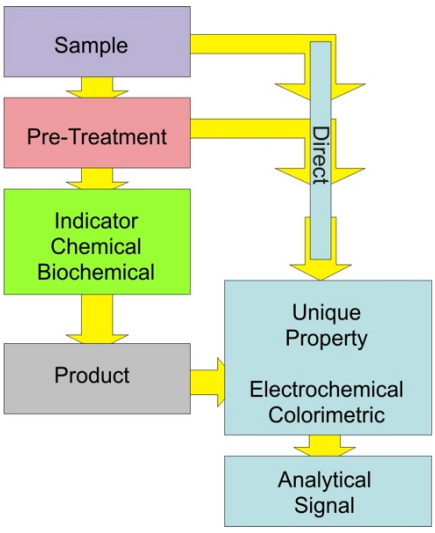

Figure 2.7.1 Assay / Device Development Methodology. Reproduced with permission (Davis, *et al.*, 2016)

A crucial factor in the development of a testing sensor is its ability to correctly identify the correct analyte from a sample containing a multitude of different species, without this ability the sensor would be useless (Menendez-Botet, 2003). Much research has been focused on developing the chemistry to not only directly measure the quantity of the target analyte, but to selectively transform the target analyte into an "unique and measurable' property that has little or no interference from other components as indicated in **Figure 2.7.1.** Often this requires the design of a chemical indicator that will readily and selectively react with the target analyte, or use a biological agent, such as an enzyme or antibody, that could selectively act upon a substrate. It is important to reiterate that the process is completed with minimal sample preparation so that this reduces the number of steps required by the user to simply supplying the sample. A classic example is the use of glucose test strips whereby a simple finger prick will result in a few microliters of blood being delivered to a test strip. The strips are designed with an enzyme (typically glucose oxidase) which will selectively react with glucose in the sample whilst ignoring a plethora of other sugar molecules. As the analysis is conducted in whole blood, no sample manipulation is required.

It is possible to design a test or device that acts directly upon the analyte and thereby removes the need for any other additional reactions. However, this approach is far less commonly used as it is normally only reserved for very simple samples and to exploit the inherent difference in the electrochemical or spectroscopic properties of the molecules present within the sample. The characterisation of the device sensing surface chemistry and the enhancement of the detection properties is another key interest for both the bioanalytical and materials science communities (Dargaville, *et al.*, 2013; McLister, *et al.*, 2014).

2.8 Moving Towards Smart Dressings

Moving towards a smart dressing that provides a digital analysis 'readout' of the result, removes the ambiguity of trying to assign the appropriate colour based on a given chart (Menendez-Botet, 2003). A numerical readout value provided by an electronic system would certainly help to remove the uncertainty of the measurement

reading that could be considered as a significant step forward in wound management. Although there are numerous systems that could be applied to wound monitoring (Dargaville, *et al.*, 2013; McLister, *et al.*, 2014; Mehmood, *et al.*, 2014; Matzeu, *et al.*, 2015), the present overview has focused predominantly on those targeting: pH and endogenous wound biomarkers. Many of these approaches have been investigated with regards to the likelihood of being implemented within a clinic setting, but the major challenge is still acquiring sufficient selectivity with minimal sample preparation, especially when considering the limited time available during a patient consultation.

2.9 Wound Fluid

Prior to the development of a sensor for measuring chemical species, whether for a point of care application or for the incorporation within a dressing, some indication as what needs to be detected has to be determined. Before this can be achieved it is necessary to consider the issue of samples and sampling (Broadbent, *et al.*, 2010; Angel, *et al.*, 2011; Thomas, 2012; Loffler, *et al.*, 2013). The latter is significant for any diagnostic as the sensor will ultimately work in a discrete portion of the wound sample, and therefore it is important to determine whether the sensor will be immersed within the sample or placed in direct contact with it. The two most common types of sample will be either tissue biopsy or the fluid which bathes the actual wound site (Broadbent, *et al.*, 2010; Loffler, *et al.*, 2013). Currently there is no consensus as to which approach provides a better insight into the healing status of the wound. The nature of the device, the wound type and its intended operation will also impact on the method selected.

It can be extremely difficult to obtain meaningful data due to the highly variable nature of both the wound and the sample itself. Considering that wound fluid is the chosen sample for the majority of studies tackling the characterisation of chronic wounds, it may be considered as being the more accessible sample. However, concerns have been raised over the reliability/reproducibility and it's representative nature due the inherent variability of the sample collection and subsequent standardisation (Broadbent, *et al.*, 2010; Angel, *et al.*, 2011; Thomas, 2012; Loffler, *et*

al., 2013). Another issue to address is the short or long term storage of the sample. Considering that wound fluid is a dynamic matrix where even minor manipulation or a short time delay between collection and analysis can affect composition (Broadbent, *et al.*, 2010; Loffler, *et al.*, 2013), it is therefore imperative that the sample is correctly stored.

Wound fluid is a highly heterogeneous mixture that originates from a variety of sources, therefore its composition is believed to reflect the clinical condition of the wound at the time of sampling (Broadbent, *et al.*, 2010; Loffler, *et al.*, 2013). Depending on the healing stage of the wound, the composition of the fluid will vary considerably because of changes in the microenvironment as cell migration and tissue remodeling occurs. Currently the main driving force behind the development of wound monitoring technologies today, is to equip the clinician with vital information on the healing status of the wound, so that they can select the most effective treatment plan for their patient. Underlying factors such as diabetes and neuropathy, can also impact the nature of the wound fluid (Broadbent, *et al.*, 2010; Loffler, *et al.*, 2013). Exogenous factors such as bacterial load, treatments applied whether systemic or topical, as well as the type of wound dressing used will also affect the milieu (Broadbent, *et al.*, 2010).The ability to correctly assess the changes in the wound environment through simple diagnostic tests could revolutionise treatment (Loffler, *et al.*, 2013).

There are a variety of methods for collection of wound fluid but the selection of the most appropriate technique will depend upon the nature of wound, the volume available and the purpose for which the sample is requested. Irrespective of the end-use, obtaining reproducible samples, however is regarded as a considerable challenge in that the sampling procedure is likely to induce alterations in the sample itself. The standard approach, pioneered by Varghese (1986) has been to use occlusive dressings in which the wound fluid accumulates and therefore be easily sampled by aspiration with a micropipette, syringe, needles or vacutainers (Varghese, *et al.*, 1986). Since then a number of modifications to the general approach have been applied, but the basic methodology has effectively remained the same. The most common issue regarding this approach however is the time in which the dressing is applied, and the degree of

wound bed preparation and local treatments applied prior to placement (Loffler, *et al.*, 2013). Another significant issue that needs to be taken into consideration is the heterogeneous nature of the wound itself which will inevitably influence the amount and nature of the fluid obtained.

If there is little wound fluid available for direct extraction by pipetting, this could prove to be problematic, in which case, the only viable option that remains, would be to take an occlusive dressing and try to absorb the available fluid (Loffler, *et al.*, 2013). The variability of wound fluid sampling has led to a highly contentious debate about the appropriateness of the use of alternative control biofluids such as serum (Rao, *et al.*, 1995; Trengove, *et al.*, 1996; Wagner, *et al.*, 2003), plasma (Schmidtchen, 2000; James, *et al.*, 2003), acute wound fluid (Schmidtchen, 2000; James, *et al.*, 2003) and surgical fluid (Schmidtchen, 2000; James, *et al.*, 2003). Broadbent and co-workers have suggested the use of patient matched serum/plasma to be taken at the time of the wound fluid collection (Broadbent, *et al.*, 2010). It would be assumed that the tissue sample would be rich in the wound related molecule as with their corresponding wound fluid sample. The tissue sample would be obtained by either surgical removal or by a punch biopsy preformed under local anesthetic, and then immediately preserved for analysis. Typically, the sampling sites for the controls are selected from around the wound margins, or they may also include intact epidermis (Broadbent, *et al.*, 2010).

2.10 Potential Biomarkers

Present within wound fluid are a multitude of biochemical species that in some way have a role in the wound dynamics and healing process. As previously discussed, there is no ideal sample for biomarker discovery, however, it could be agreed that a non-invasive approach may be best. This would limit the pain level for the patient and reduce the likelihood that artefacts would arrive through the sampling process. One issue that may still be a concern, relates to the sensitivity of the technique when dealing with a high volume of wound fluid which could unduly dilute the target and impact the result. In these cases, an argument could be justified for tissue sampling,

however it creates a predicament in that a matched control sample from healthy tissue would be necessary, which could initiate a secondary wound. Another concern would be that the concentration of protein biomarker could vary significantly from one tissue sample to the next (Broadbent, *et al.*, 2010).

Currently, research is ongoing to elucidate the significance of each of these biochemical species, to identify which would be the most diagnostically useful in the clinical management of chronic wounds (Muller, *et al.*, 2008; Ciani, *et al.*, 2012; Ferreira, *et al.*, 2016; Yagati, *et al.*, 2016; McLister, *et al.*, 2017). Monitoring key markers that could act as an early warning system towards the onset of complications, especially infection, is the key challenge in the development of smart dressings. Clinical investigations of wound fluids, exudates and tissues have provided substantial insights and with that there have been several attempts to classify the main protagonists involved in the healing progression of the wound. Broadbent and co-workers have detailed over 150 proteins (highlighted in **Table 2.3**) whose concentrations are influenced by the cellular/tissue remodeling and associated inflammatory responses (Broadbent, *et al.*, 2010). The dysregulation of growth factors and the up regulation of proteases have been identified as valuable therapeutic and prognostic indicators (Liu, *et al.*, 2009; Cao, *et al.*, 2011). The ability to control the activation of such species has been shown to aid the healing process but, such interventions clearly require the aid of analytical tools that can monitor the species concentration within the time frame of the consultation (Practice, 2008). Despite the extensive list indicated in **Table 2.3** the diagnostic community have tended to focus on a more limited selection and an overview of the chemical components which are presently being investigated (Practice, 2008) as highlighted in **Table 2.4**

Table 2.3 Potential Wound Biomarkers. Adapted from (Broadbent, *et al.*, 2010)

α-1-antitrypsin	Haemopexin
α-1-acid glycoprotein	Hepatocyte growth factor
α-1-globulin	Haptoglobin
α-2-macroglobulin	Heparin binding protein
Alanine aminotransferase	IgA
Albumin	IgG
Alkaline phosphatase	Insulin-like growth factor -1
Angiostatin	Insulin-like growth factor binding protein-2
Antichymotrypsin	Insulin-like growth factor binding protein-3
Apolipoprotein A-1	Inter-α-inhibitor
Asparate	Interferon-inducible protein-10
aminotransferase	Interleukin-1 , 1a, 1b, 6, 8 , 10
β-1-globulin	Interleukin-1 receptor antagonist protein
β-globulin	Keratin 6
β-2-glycoprotein-1	H, L-Kininogens
Basic fibroblast growth factor	Lactate Dehydrogenase
Calgranulin A and B	Macrophage inflammatory protein 1a, 1b
Cathepsin G	Matrix metalloproteinases -1, 2, 8, 9
Ceruloplasmin	Monocyte chemoattractant protein 1
Collagen I and III	Nucleosome assembly protein 2
Complement C3 and C4	Neutrophil cathepsin-D
C-reactive protein	Orosomucoid 1
Cytokeratin-1	Plasmin
Elafin	Plasminogen
Elastase	Plasminogen activator
Elastase (Neutrophil)	Plasminogen activator inhibitor
Endostatin	Platelet derived growth factor – AA, AB
Epithelial growth factor	Platelet factor-4
Epithelial neutrophil activating peptide – 78	Tenascin-C
Factor B	Tetranectin
Fibrinogen-α, b gA chains	Tissue inhibitor of metal proteinases-1 and 2
Fibronectin	Tumor necrosis factor-α
Ferritin	Transferrin
γ-globulin	Transforming growth factor-β, B1
γ-glutamyltranspeptidase	Urokinase plasminogen activator

Table 2.4 Common wound diagnostic markers .Reproduced with permission (Davis, *et al.*, 2016)

Bacterial metabolites	**Inflammatory mediators**
Pyocanin*	Cytokines
Nitrite*	Interleukins
Hydrogen sulfide*	Nitric oxide
Enzymes	Reactive oxygen species
Matrix metalloproteinases	**Nutritional factors**
Plasmin	Zinc
Collagenase	Glutamine
Growth factors/hormones	Glucose
Platelet-derived growth factor (PDGF)	Ascorbic acid
Sex steroids (andmgens/oestrogens)	Glutathione
Thyroid hormones	**Physico-chemical parameters**
Immunohistochemical markers	Wound fluid pH*
Integrins	Water loss*
Chemokine receptors	Temperature*
Transforming growth factor Beta II receptors	Oxyegen
	Carbon dioxide

The list of markers indicated in **Table 2.4**, follows the same pattern as that outlined by Harding (2007) and can be separated into two groups that reflect the size of the target biomarker (Harding, 2007). However, it is important to note that although significant discoveries have been made to characterise the biochemical fluxes that occur within a chronic wound, the focus within the diagnostic community has been on more niche groups, as such, there is still no set of definitive markers. In regards to this research project, the primary focus will be monitoring wound pH as an indicator of the healing status of the wound.

2.11 Wound pH

Wound exudate is known to vary depending on the stage of healing, as highlighted in **Figure 2.11.1**, it is also widely accepted that pH plays a vital role in a multitude of biochemical reactions (Schneider, *et al.*, 2007). Numerous studies have been held to evaluate monitoring the wound surface pH as a potential method for wound assessment (Shukla, *et al.*, 2007; Musa, *et al.*, 2011; Gethin, *et al.*, 2018). One study in particular by Dissemond and co-workers, found that the pH chronic wounds of varying aetiologies broadly ranged from pH 5.45 to 8.65, with a mean pH of 7.42

(Dissemond, *et al.*, 2003). These findings provide an explanation as to why there is currently no defined pH threshold to class a wound as a healing or non-healing wound. However, the typical pH of undamaged skin is reported to lie between a narrow acidic region from pH 5.4 – 5.9 (Dissemond, *et al.*, 2003; Greener, *et al.*, 2005). A benefit to maintaining the surface pH at this slightly acidic level is because it helps impede bacterial proliferation and helps to minimise infection. However, when a cutaneous wound occurs and the underlying skin is exposed which is homeostatically regulated at a pH of 7.4, it can result in bacterial proliferation and increases the risk of infection. Acute wounds tend to follow a predictable trajectory whereby the pH returns to the normal acidic skin regime as the wound heals (Schneider *et al.*, 2007), as highlighted in **Figure 2.11.1.**

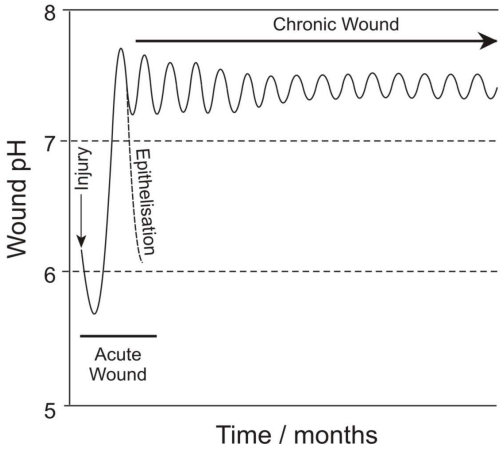

Figure 2.11.1 Typical pH profiles observed for acute and chronic wounds. Adapted from (Schneider *et al.*, 2007).

Previous research has indicated that chronic wounds tend to oscillate in a narrow, weakly alkaline range, as highlighted in **Figure 2.11.1**, which can increase the susceptibility of the patient to infection. It has also been postulated that an increase in pH of local wound fluid could be attributed to the presence of bacteria which creates an environment that is more accommodating for continued bacterial growth (Gethin, 2007; Schneider, *et al.*, 2007)**.** Therefore, monitoring fluctuations in pH could be exploited as a simplistic diagnostic tool to identify the onset of infection (Ono, *et al.*, 2014) or, at the very least, raise an alarm for vigilance. It is important to note however, that this is still a simplistic model and there have yet to be conclusive studies demonstrating that a definitive change in pH occurs upon infections, or that confirmation of the presence of bacteria influences the wound in the same manner.

Therefore, it may be more beneficial to use the oscillation of pH as a baseline in which a significant or sustained deviation from the regular pattern may be sufficient to raise concern. Considerable effort has been dedicated to developing disposable sensors and modified dressings to monitor wound pH using a range of analytical methodologies (Davis, *et al.*, 2016). The following sections shall delve into the current research avenues being explored for pH monitoring and discuss in turn, the applicability for monitoring chronic wounds such as in diabetic foot ulcers.

2.12 Approaches to Measure pH

2.12.1 Visual pH Devices

The use of chromophore and fluorophore modified textiles have been utilised by Mohr and co-workers to pioneer smart fabrics that can respond to pH changes (Mohr, *et al.*, 2008). Their research has significant implications for a wide range of medical applications and their indicator system employs an innovative use of the universally acknowledged “traffic light’ warning sequence to alert healthcare workers to possible issues (Evans, *et al.*, 2006; Wang, *et al.*, 2008). The discovery that makes this research truly innovative is the successful incorporation of a specific combination of dyes directly onto the polymer backbone which transitions from green to red when the pH increases, that is in accordance with the universally associated change from ‘good’ to ‘bad’. The significance of this work relates to the fact that there is currently no single indicator capable of providing the desired colour change and thus the need for a specific formulation. This traffic light approach was implemented in the design of a smart textile to monitor the pH of the skin but, the technology was also proposed as a smart swab through which to assess the pH of chronic wounds (**Figure 2.12.2**).

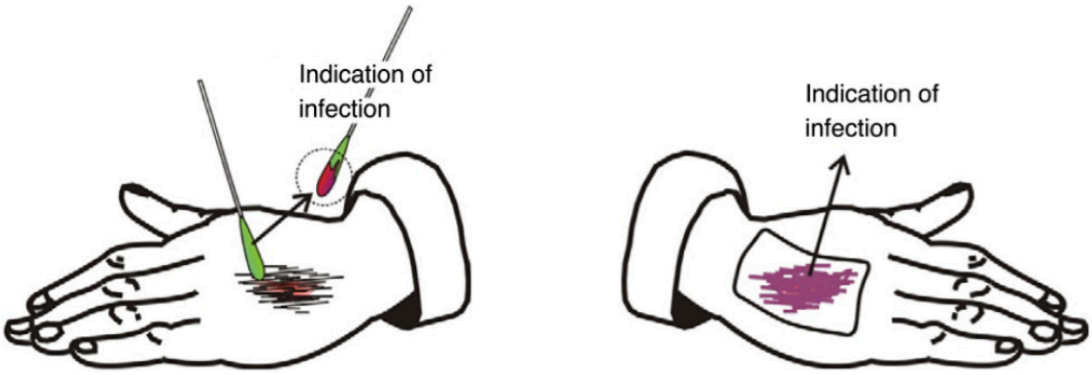

Figure 2.12.2 A) Proposed implementation of the "traffic light" pH swab B) Proposed pH-sensitive bandage by Trupp and coworkers. Adapted from (Trupp, *et al.*, 2010).

Due to the covalent immobilisation of the dye onto the cotton fibre of the swab, it would be expected that the possibility of leaching would be minimised (Mohr, *et al.*, 2015). However, there are still issues surrounding this system, as noted, considerable debate is ongoing as to the added value of swabbing (Angel, *et al.*, 2011; Thomas, 2012; Loffler, *et al.*, 2013) . Also, the assumption that there will be sufficient wound fluid available for the sample may be unrealistic. While the green-red transition provides a very clear visual indicator, the possibility exists that it will provide a false negative reading when dealing with complex matrices where there is substantial slough.

An alternative to the swab system was proposed by Trupp and his colleagues in which they implement a colorimetric indicator that is loaded onto an actual dressing complete with transparent protective film as indicated in **Figure 2.12.2**. The rationale behind this approach is similar to that demonstrated by Mohr, albeit without the traffic light sequence, but it can be anticipated that it will encounter much the same issues. Both these approaches by Mohr and Trupp rely on visual inspection, which has the advantage of ease of manufacturing and a minimised cost but, none the less they are dependent upon the subjective colour perception of the person conducting the test/inspection (Mohr, *et al.*, 2008; Trupp, *et al.*, 2010; Davis, *et al.*, 2016).

2.12.2 Quantitative Wound pH Imaging

In contrast to the previous approach, Schreml and coworkers employed a more quantitative approach using luminescent detection technique to obtain two dimensional images of oxygen and pH distributions across the wound bed (Schreml, *et al.*, 2014). Palladium(II)-meso-tetraphenyltetrabenzoporphyrin was deployed within poly(styrene-co-acrylonitrile) microparticles as the oxygen probe (Schreml, *et al.*, 2011) with fluorescein-isothiocyanate covalently immobilised on aminoethylcellulose microparticles as the pH dependent system. The microparticles sensing elements were then embedded in a polyurethane hydrogel layer with a transparent poly(vinylidenechloride) (PVdC) interface layer to provide mechanical support and prevent leaching of the components into the wound bed itself. The basic structure of the approach is highlighted in **Figure 2.12.3.**

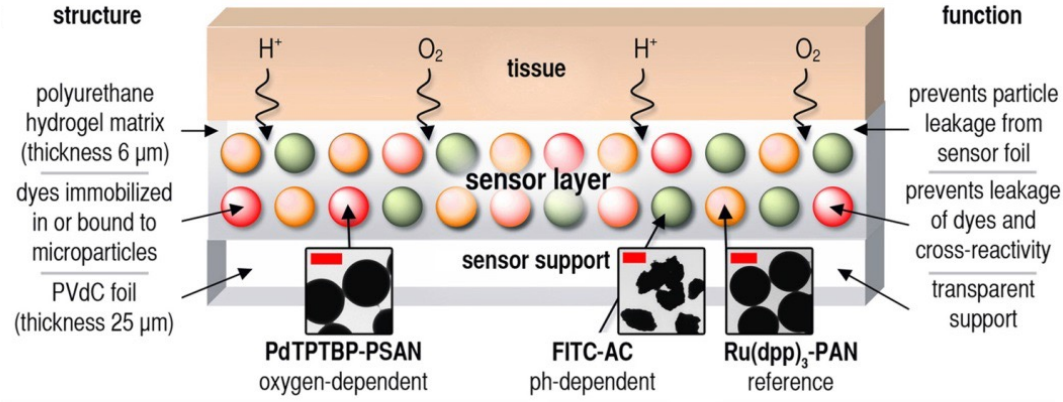

Figure 2.12.3 Modified dressing for measuring pH and Po_2. Reproduced with permission (Schreml, *et al.*, 2014).

The luminescence was detected using a charge-coupled device (CCD)-camera and the signal separated by optical filters. A degree of caution is needed when applying the sensing layer, to minimise the entrapment of air bubbles which could compromise the oxygen and proton measurement. The polymeric membrane however, was found to be sufficiently flexible to conform to the wound enabling surface wetting and subsequent adherence to the wound contours (Schreml, *et al.*, 2014). The sensing foil is photoexcited with an appropriate LED and the time gated luminescence signals acquired and pseudo-colour maps of the respective oxygen and pH levels rendered.

Schreml and co-workers demonstrated the presence of extracellular pH gradients that were found to negatively influence keratinocyte viability, proliferation and migration at the wound periphery (Schreml, *et al.*, 2014).

This discovery marks significant implications for wound closure where decreasing pH within the wound centre inhibits keratinocyte recruitment. The procurement of such information would be diagnostically beneficial in offering the possibility of targeted therapeutic interventions. A limitation however, lies in the need for considerable expertise as the system is highly sophisticated when considering its use and would certainly require the user to be trained prior to application. Therefore, it may be more applicable to investigate wound dynamics rather than routine diagnostics. The high equipment overhead cost ultimately makes it more suitable for a clinical setting rather than a home health care device.

Sawada, Hizaqa and colleagues proposed an alternative approach to the use of the charge coupled devices (Sawada, *et al.*, 2005; Hizawa, *et al.*, 2006). Rather than employing a luminescent indicator system, their strategy employed a solid-state membrane based on silicon nitride (Si_3N_4) to serve as a pH sensitive layer. The latter is scanned by an integrated analysis system to provide a two-dimensional pH image of the wound. The system is built on a CMOS fabrication system as outlined in **Figure 2.12.4**. The prototype system is based on a 10 by 10 pixel array covering a size of 5.1x5.1 mm (Hizawa, *et al.*, 2006). The system has been shown to provide a sensitivity (50.9mv/pH) which, is consistent with most ion selective electrochemical systems. The underlying engineering of this device heralds a considerable achievement; however, it is faced with considerable limitations to its implementation. Considering that the system would ultimately need to be disposable, the overall cost of the device would be considered a major impediment. Furthermore, problems surrounding the limited resolution, positioning within irregular wound and, conformity to the wound are all issues that would still need to be addressed (Davis, *et al.*, 2016).

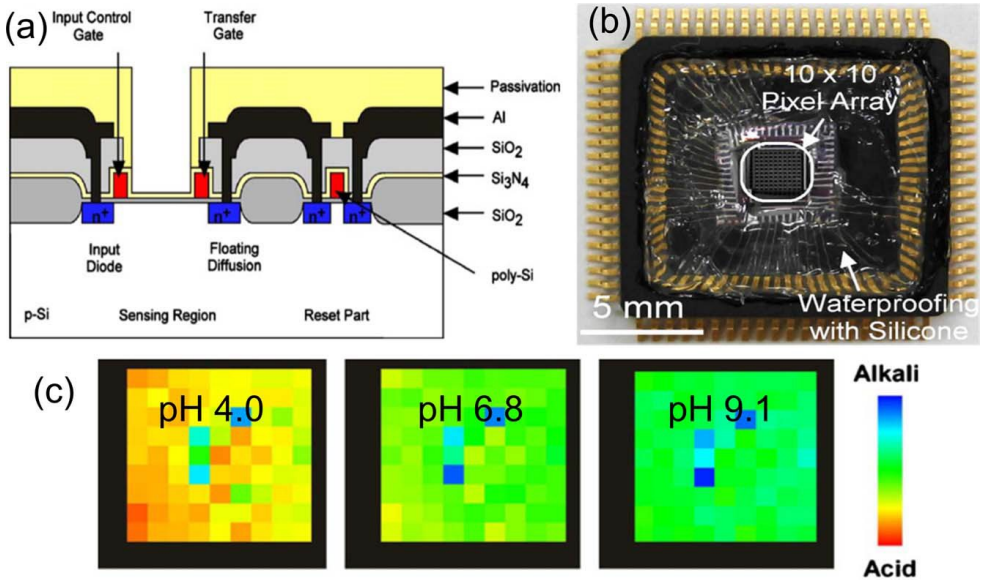

Figure 2.12.4 Silicon Nitride CCD pH Imaging. Reproduced with permission (Hizawa, *et al.*, 2006).

2.12.3 Radiofrequency Identification (RFID) Optical Sensors

In recent years there has been great advancement in the development of wireless protocols (Bluetooth, Zigbee etc) for sensing applications (Byrne, *et al.*, 2006; Zampolli, *et al.*, 2008). Originally, Radiofrequency identification (RFID) was intended for applications to identify products over a very short range, typically less than 2m (Byrne, *et al.*, 2006; Steinberg, *et al.*, 2009). However, this approach gained considerable interest as a potential addition to chemical sensors (Byrne, *et al.*, 2006; Steinberg, *et al.*, 2009), and could potentially be adapted for wound monitoring. The fact that this approach is already widely used for consumer goods, demonstrates that this sensor can be produced economically and therefore, in principle, it could be incorporated into a disposable smart dressing.

Based on a RFID protocol, Steinberg developed a battery free, contactless optical sensor (Steinberg, *et al.*, 2009). The sensing component of this approach involved the incorporation of a pH sensitive dye (Bromocresol Green) within a sol-gel film. Although the so-gel approach to chemical sensors is well established (Jerónimo, *et al.*, 2007; Matzeu, *et al.*, 2015), it is yet to translate to a wound monitoring context because of the potential for the dye to leach and the relative inflexibility of the sensor.

A schematic outlining the basis of the approach is highlighted in **Figure 2.12.5**. The RFID based sensor does not possess a battery but is powered by a vicinity integrated circuit card (VICC) that passively harvests energy from an electromagnetic field generated by a suitable reader (Steinberg, *et al.*, 2009). The prototype sensor consists of the antenna, the RFID processor, the optoelectronic interface and sol-gel/indicator interface.

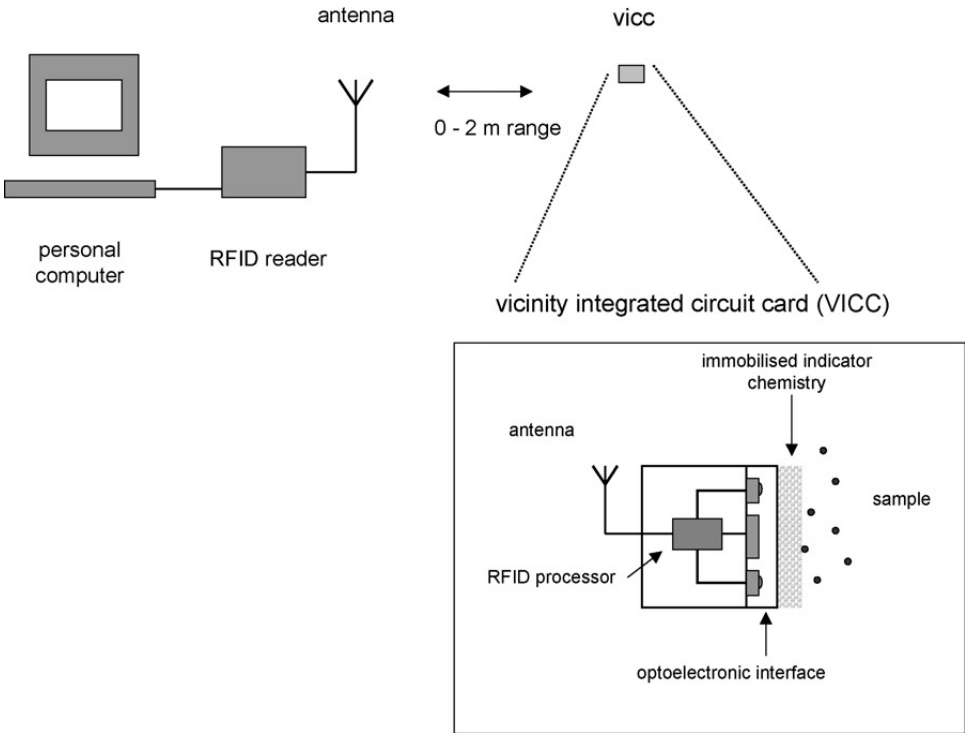

Figure 2.12.5 RFID pH detection methodology. Reproduced with permission (Steinberg, *et al.*, 2009).

The detection methodology is based on the differential absorbance of light measured at two wavelengths: 435 nm and 619 nm capturing λ_{max} for the protonated and deprotonated forms of bromocresol green respectively (Steinberg, *et al.*, 2009). The two LEDs on the VICC tag were tuned to 505 nm (the isobestic point used as a reference) and 619 nm with the intensity from each measured by a photodiode and allowed a measurement range of pH 5.2 – pH 8.3 which covers the majority of pH transitions expected within a chronic wound (Schneider, *et al.*, 2007). However, it is important to note that this sensor has yet to be tested in complex biological matrices and given the wavelength that it operates in, it is likely to encounter substantial interference. Although these issues may question the applicability of this sensor for

wound monitoring, the underlying technology certainly holds considerable promise (Davis, *et al.*, 2016).

2.13 Electrochemical pH Systems

Commercially there are numerous electrochemical pH probes available, however, traditionally they employ a glass bulb and are predominately designed for use within a bioanalytical laboratory. The fragile nature of the glass membrane and its mechanical rigidity renders the conventional systems unsuitable for the direct monitoring of wounds given the variation in surface morphologies. However, in response to the limitation of the traditional glass pH probe, there have been significant advances in the detection methodologies employed in recent years (Dargaville, *et al.*, 2013; McLister, *et al.*, 2014). It must be noted however that few have been designed specifically for biomedical contexts.

The development and introduction of an electrochemical sensor system for wound monitoring has been plagued with numerous concerns that include, probe size, disposability, and limited sample volume issues (i.e. dry wounds or those with low exudate). In an effort to address these issues several approaches have been pursed, including the investigation into both potentiometric (Hemmink, *et al.*, 2010; Herlem, *et al.*, 2010; Taouil, *et al.*, 2010) and voltammetric (Streeter, *et al.*, 2004; Lafitte, *et al.*, 2008; Xiong, Batchelor-Mcauley, *et al.*, 2011; Davis, *et al.*, 2013; Park, *et al.*, 2013; Li, *et al.*, 2014) methodologies. In order to confer selectivity, a functional material containing a pH sensitive component is normally applied to the surface of the sensor substrate. Typically, to enhance the sensors response, a variety of modification methods and designs have been assessed that include: adsorption of monolayers (Lee, *et al.*, 2012; Park, *et al.*, 2013), polymer films (Zampolli, *et al.*, 2008; Zhao, *et al.*, 2010), printed inks (Byrne, *et al.*, 2006; Hizawa, *et al.*, 2006; Jerónimo, *et al.*, 2007; Li, *et al.*, 2011), covalent binding (Inoue, *et al.*, 2011; Li, *et al.*, 2011) or the use of electrodeposited layers (Herlem, *et al.*, 2010; Taouil, *et al.*, 2010; Cherchour, *et al.*, 2011). A summary of the surface modification and associated sensitivities is presented in **Table 2.5.**

The process of modifying the surface of a sensor is considered acceptable when designing a point of care sensor, however certain issues remain such as electrode fouling, biocompatibility and the potential of the pH sensitive component to leaching into the biological matrix. As such, several of these approaches detailed in T**able 2.5** would be limited when considered for the integration of the sensor within a conventional dressing (Davis, *et al.*, 2016).

Table 2.5 Comparison of electrochemical pH sensors. Reproduced with permission (Davis, *et al.*, 2016)

Electrode Modifier	Method	mV / pH	Error /mV
Iridium Oxide	P	69	1
Polyglycine	P	52	NS
Ion Selective Membrane	P	61	1.7
Metalloprophyrins	P	54	NS
CeO2	P	51	NS
Carbon nanotubes	P	43	NS
TiO2 nanontubes	P	54	NS
Co/Al Hydroxides	P	76	0.6
Palladium	P	60	NS
Nitroso-Phenyl/Ferrocene	V	60	2
Ferrocene / Dyad	V	52	NS
Anthraquinone / Diphenylphenylenediamine	V	114	NS
Polyplumbagin	V	51	3
Nafion / Benzoquinone	V	59	NS
Uric Acid	V	62	NS
Ferrocene/Phenathraquinone	V	97	NS

Where: P = potentiometric; V=voltammetric; NS = not specified

2.13.1 Screen Printed Potentiometric Smart Dressings

Wang and co-workers exploited the use of a polyaniline modified screen printed sensor to monitor changes in wound pH (Guinovart, *et al.*, 2014). Their approach included the incorporation of the sensor into the gauze dressing of a conventional adhesive polymer bandage, as highlighted in **Figure 2.13.1**

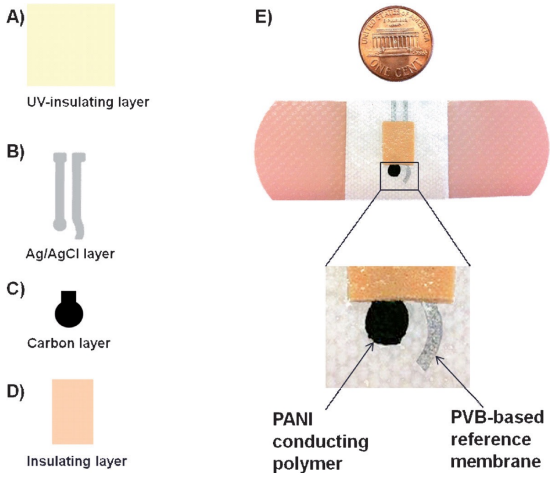

Figure 2.13.1 Smart bandage based on screen printed sensors with a polyaniline (PANI) sensing layer. Reproduced with permission (Guinovart, *et al.*, 2014).

The potential difference between the working (sensing) electrode and the polyvinyl butyral (PVB)/silver-silver chloride reference is measured to obtain the analytical signal. The carbon layer is modified with polyaniline (PANI) and the system exploits the transition between the emeraldine salt and emeraldine base moieties within the polymer backbone (Lindfors, *et al.*, 2003; Kaempgen, *et al.*, 2006) as indicated in **Figure 2.13.2**. The strategy effectively combines the manufacturing simplicity/reproducibility of screen printing with solid state potentiometry to produce a device that has been shown to exhibit a conventional Nernstian behaviour over pH 4 - pH 8**.** Overall, this system offers advantages in terms of it's simplistic operation however, there are a number of limitations – particularly the need to modify the surface with an exogenous component.

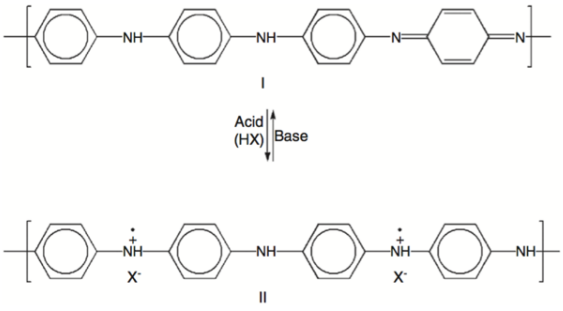

Figure 2.13.2 pH transition of the emeraldine salt and bases within polyaniline. Reproduced with permission (Davis, *et al.*, 2016)

2.13.2 Carbon Fibre pH Sensors

Anderson and co-workers proposed an innovative approach that did not require the additional manufacturing step of modifying the electrode surface with an exogenous component. Instead, they created a pH probe by utilising the endogenous redox components already present on carbon fibre (Anderson, *et al.*, 2014). Although carbon fibre is traditionally associated with structural engineering applications, in the present context its mechanical flexibility, conductivity and its relative inexpensive makes it of particular interest. However, the unmodified form of the fibre has a relatively poor electroanalytical response, initial studies demonstrated there was a distinct lack of selectivity towards changes in pH from either potentiometric or voltammetric methodologies . Instead of using Wang's approach of adding exogenous groups onto the surface (Guinovart, *et al.*, 2014), Anderson's team exploited the quinone redox chemistry present on the carbon surface as a means of enhancing the pH response through a voltammetric approach.

Essentially, the voltammetric approach examines the oxidation-reduction characteristics of a target analyte such that upon applying a sufficient potential at the electrode surface, a transfer of electrons occurs (discussed in detail in Chapter 3) and, can give rise to a peak value. The position of the peak on the applied potential scale can give some indication as to the identity of the analyte whereas the magnitude of the current is, in principle, proportional to the concentration within the sample. The principal issue with voltammetry of complex matrices (particularly biofluids) relates to the fact there will be many molecules that can be oxidised or reduced which can lead to over-lapping signals that obscure the response of the target biomarker. The difficulty of this approach lies in obtaining an unambiguous signal from one particular target without interference from another electroactive species. Voltammetry has been extensively employed for electroanalytical purposes and, generally the surface of the electrode is modified in a way to confer selectivity towards a particular analyte (Lawrence, *et al.*, 2002), but only until recently has this approach been exploited for pH measuring.

The approach taken by Anderson and co-workers was to exploit the pH dependence of a redox couple – typically quinone-hydroquinone (Q/H_2Q) systems. The analytical signal is extracted by measuring the peak position of the oxidation processes associated with the hydroquinone moiety. As the system involves a transfer of protons, there is an inherent pH dependence and thus, the position of the oxidation peak can be related to the pH of the sample in accordance with the well established Nernst relationship of 0.059 m/n V/pH (m/n is the ratio of protons to electrons). In this case, the quinoid forms are present as an integral component of the carbon surface as indicated in **Figure 2.13.3***.*

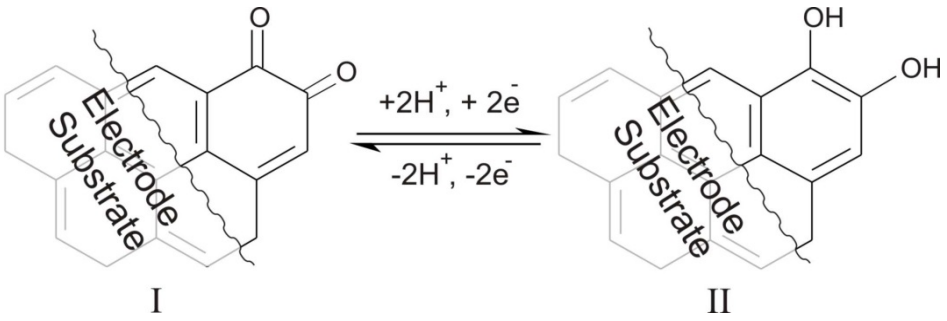

Figure 2.13.3 Redox transition of endogenous quinone groups on carbon. Reproduced with permission (Anderson, *et al.*, 2014).

The endogenous populations of the quinone groups present on an un-modified carbon fibre is typically low, which results in a poor electrode response towards pH. However, the surface of the carbon can be modified to increase the proportion of the redox groups present, via several processes such as: laser ablation(J Phair, Joshi, *et al.*, 2014), plasma treatment (Phair, *et al.*, 2013) or electrochemical oxidation (Phair, *et al.*, 2011; Anderson, *et al.*, 2014). Anderson and colleagues employed a novel laminate manufacturing process, summarised in **Figure 2.13.5**, to encapsulate the carbon fibre as a means to integrate it as a working, standalone sensor. In comparison to conventional approaches, such as colorimetric swabs, this approach offers several advantages such as: quantitative analysis, disposability and the relative inexpensive fabrication associated with carbon fibre. The main advantage of this approach lies in the small dimensions associated with the assembled probe, which could allow for the rapid analysis of ultra low volumes of wound fluid samples.

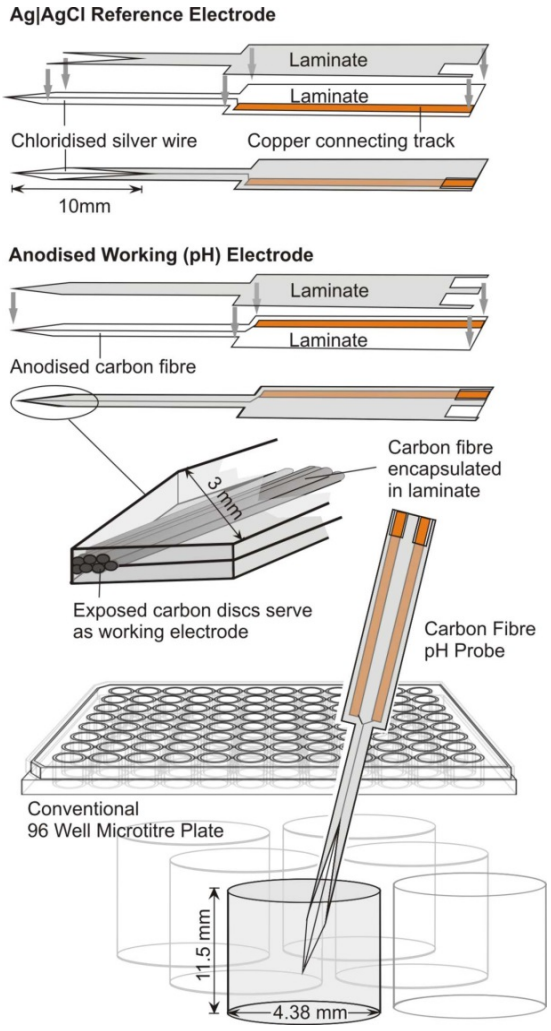

Figure 2.13.4. Probe design specifications. Reproduced with permission (Anderson, *et al.*, 2014).

2.13.3 Screen Printed Voltammetric Sensors

The techniques previously listed in **Table 2.5** have some potential to be transferred to a wound context, however, they are more focused on the underpinning science rather than providing a critical examination of their clinical accessibility. There are however a number of exceptions, an example of this includes Phair *et al.* (2011) who proposed a screen-printed sensor specifically designed for assessing wound pH based on the voltammetric determination of uric acid and the various components used in its construction are shown in **Figure 2.13.5** (Phair, *et al.*, 2011).

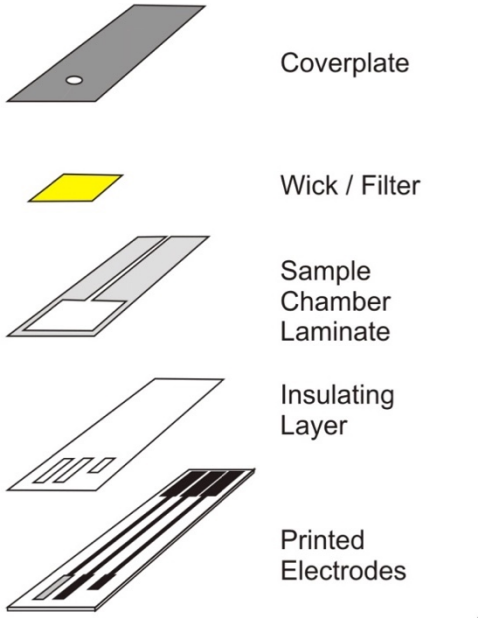

Figure 2.13.5 Fabrication of the screen printed urate pH sensor. Reproduced with permission (Phair, *et al.*, 2011).

What is particularly interesting about this sensor is its alternative approach compared to ones listed in **Table 2.5**, mainly that the sensor does not rely on the modification of the electrode substrate with an exogenous pH sensitive indicator. Instead, it relies on the oxidation of urate, which is present within wound fluid, to provide an indirect measure of the pH. Due to purine catabolism, uric acid is ubiquitous within biofluids and therefore it is relatively easy to detect at a conventional, unmodified, electrode (Dutt, *et al.*, 2005). In most electroanalytical applications, uric acid is considered to be a rather pernicious interference precisely due to these characteristics (Lawrence, *et al.*, 2002; Dutt, *et al.*, 2005)'. The oxidation of urate involves protons (**Figure 2.13.6**) and thus the peak position of the associated electrode process will be dependent upon the prevailing pH within the solution (or wound fluid). This approach is analogous to the work of Anderson and co-workers, however in this case the oxidation peak is due to a diffusing, solution based, species rather than quinone groups anchored within the carbon substrate (Phair, *et al.*, 2011). Square wave voltammograms detailing the response to urate under different pH regimes are compared in **Figure 2.13.6** where it can be seen that there is a distinct shift in the peak position.

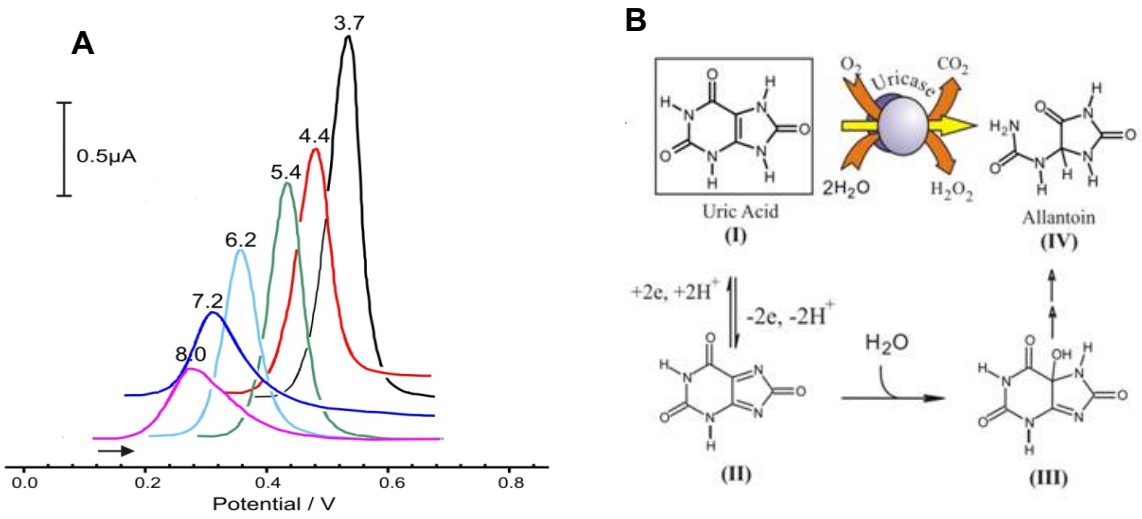

Figure 2.13.6 A)Electrochemical oxidation of urate B) Influence of pH on the voltammetric response to urate at a screen printed sensor. Reproduced with permission (Phair, *et al.*, 2011).

The shift in the position of the oxidation peak can be used as the basis of a calibration graph from which the pH of an unknown sample could be determined. As per the Harding Consensus document, the single disposability of the system doesn't adequately meet the set objectives as it still requires the use of the device by the healthcare provider (Practice, 2008). It does however offer a more direct manufacturing route in comparison to the laminate system proffered by Anderson and it could be envisioned that the process of printing the sensors could be similar to the large scale manufacturing processes.

It could be suggested that this approach could be exploited in the same way as glucose meters and effectively be used by patients themselves to monitor the condition of the wound. However, a crucial issue surrounding this approach would be patient compliance (Cerkoney, *et al.*, 1980; Lin, *et al.*, 2008). The development of a system that would periodically monitor the pH of the wound, would be ideal, especially if it could also provide telemetry of its condition so that it could easily be seen by healthcare professionals. This of course would require the integration of the device within the dressing itself.

2.13.4 Carbon Fibre Weave Dressings

A survey to elucidate the key factors involved in the treatment of wounds within the UK was conducted by Dowsett and coworkers (2014). One of the key issues recorded was the number of dressing changes per week, the average was reported as 2.5 per week (Dowsett, *et al.*, 2014). These findings further reiterate the significant ramifications for the development of technology for a smart dressing to be inherently disposable and of a low cost. The ability to mass produce the sensors through the screen printing technique is one approach to addressing such concerns. However, one issue to consider when using a single, discrete probe would relate to the positioning within the dressing to ensure that the sensing element was active. Therefore, in order to obtain a measurement, the sensor would need to be in contact with the wound fluid. In addition, it also assumes that the measurement is representative of the wound fluid in general rather than an isolated pocket of fluid, disconnected from the main wound bed.

Phair and co-workers suggested one innovative approach to overcome this issue by combining aspects of both carbon fibre and urate analysis as the core detection rationale. The carbon fibre weave is sufficiently flexible which allows it to follow the highly variable surface morphology of the wound. In addition, it can be manufactured in the volumes necessary to enable the mass production of wound dressings at a relatively low cost (Phair, *et al.*, 2013). It was proposed that the carbon component of the weave would provide the backbone of the electrochemical transduction enabling quantitative information of key biomarkers associated with wound healing to be obtained through a connected electronic monitor that was worn either by the patient or connected at the time of consultation. As previously indicated in the work by Anderson and co workers, the structure of the carbon can be readily modified to enhance the electrochemical performance – using either endogenous quinone groups (Anderson, *et al.*, 2014) or exploiting the presence of uric acid (Phair, *et al.*, 2011). It could therefore be envisaged that the carbon fibre weave (**Figure 2.13.7A**) could then be directly incorporated as an additional layers of a conventional dressing as indicated in **Figure 2.13.7B.**

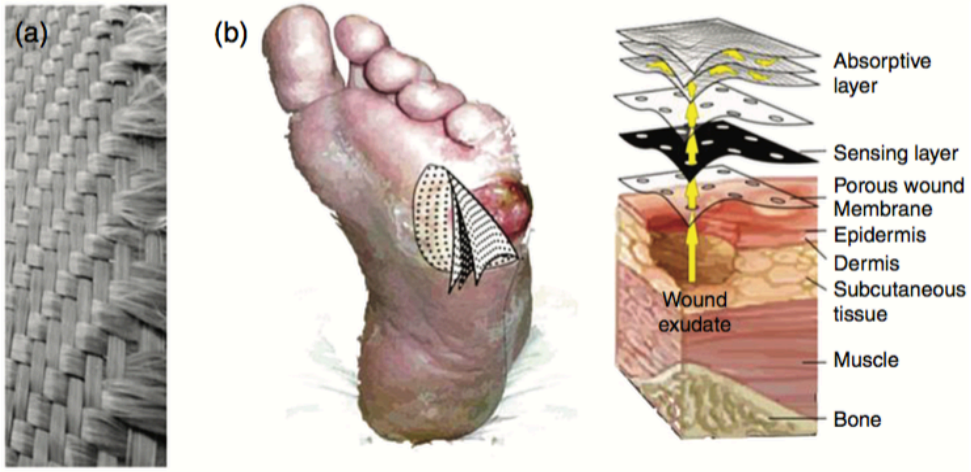

Figure 2.13.7 A**)** Structure of the carbon fiber weave and B) proposed implementation. Adapted from (McLister, Lowry, *et al.*, 2015).

2.13.5 Carbon Composite Film Dressings

It is important to highlight that carbon fibre can present some additional issues in that, although generally flexible, the fracturing of individual fibres could contaminate the wound with fragments that could initiate irritation that could prolong the state of inflammation. An alternative has been proposed in which a carbon composite polymer based on polyethylene doped with carbon particles could be integrated within a conventional wound dressing (J Phair, Benson, *et al.*, 2014). The core rationale is similar to that outlined in **Figure 2.13.7** but with a polymer film replacing the carbon fibre weave. This would provide an inherently more viable solution to the greater mechanical flexibility offered by the composite film – a prerequisite given the high degree of morphological variability encountered with chronic wounds. This polymer flexibility stands in marked contrast to the brittleness typically associated with the carbon fibre matting (Phair, *et al.*, 2013) previously investigated. In addition, it also offers the critical advantage of component simplicity (requiring only carbon and polyethylene) which could be manufactured using conventional polymer processing techniques(J Phair, Joshi, *et al.*, 2014)

Although the carbon-polymer approach has clear advantages, it also has some significant limitations in that the effective electrode area required to analyse the sample is relatively small. Despite the film being large, the composite effectively consists of carbon particles (nm-micron diameter) encapsulated within a sea of polymer as highlighted in **Figure 2.13.8**.

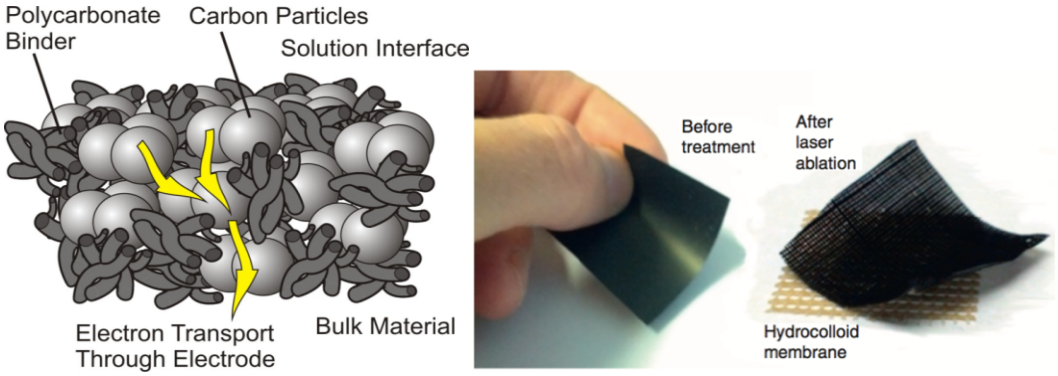

Figure 2.13.8 A) Schematic highlighting the composite nature of the carbon loaded films B) Carbon loaded polyethylene before and after laser treatment. Reproduced with permission (J Phair, Joshi, *et al.*, 2014)

The electroanalytical performance of the film was found to be relatively poor and can be attributed to the fact that the predominant form of the carbon encapsulated within the polymer is basal plane. It has long been recognised that faster electron transfer and hence improved analytical performance can be obtained at edge plane carbon sites. The latter can be created *in situ* through the use of electrochemical anodisation (as discussed previously in the case of Anderson's carbon fibre probe) (Anderson, *et al.*, 2014).

The polymer film indicated in **Figure 2.13.8** is impermeable to gases and moisture and therefore would form an occlusive membrane which would be less than ideal. A key advantage of the film approach lies in the fact that the substrate can be easily manipulated through a variety of processing techniques (laser or plasma etching) and patterned to suit a given application. Therefore, it is possible to create pores (from the nano-to the milli scale) that can enable the transport of gases and exudate (J Phair, Joshi, *et al.*, 2014)

The patterned film can be utilised as an additional layer within a conventional dressing assembly, as highlighted in **Figure 2.13.7**. The mesh like structure allows for the wound exudate to be transported through the film to an overlying gauze. When the wound exudate encounters the sensing surface this completes the circuit and a pH measurement can be made on the basis of uric acid oxidation – similar to the methodology employed in the screen print sensor as shown in **Figure 2.13.6.a**. An advantage of this approach is that it avoids the errors associated with spatial positioning with the mesh covering the entire wound surface.

2.13.6 Signal Aquistion

An issue that is quite often overlooked in the case of electrochemical sensors is the extraction of a signal from the wound. Normally a greal deal of effort is spent on the material science aspect of the sensor, while the actual signal acquistion is usually achieved via the use of expensive and cumbersome laboratory based equipment. Joshi's team developed a small foot print potentiostat that could be used as an alternative to expensive laboratory equipment, to send the signal to a smart device(J Phair, Joshi, *et al.*, 2014). One of the major limitations of this approach lies with the requirment of the sensor, controller and data recording system to be hardwired, and although there have been significant steps forwards in the development of a discrete sensor, signal aquistaion still requires further development. With the advancement in battery and circuitry minitaurisation, it could be envisioned that a smaller footprint could be attained and this highlights the fact that a simple amperometric system could be employed to relay chemical information, which could be useful in wound diagnostics (Davis, *et al.*, 2016).

Wang and coworkers took an alternative approach to the measurement of urate through using the enzyme uricase as indicated in **Figure 2.13.9**. (Kassal, *et al.*, 2015). This converts the urate to allantoin and in doing so hydrogen peroxide is produced as a by-product. The team exploited the ability of Prussian Blue particles to catalyse the reduction of the enzymatically produced peroxide and thus the operating potential can be moved to a potential where there is less likelihood of interference (Kassal, *et al.*,

2015). Although this arrangement is more complex, Wang and his colleagues have successfully demonstrated the manufacture of screen printed systems that could open an avenue towards the production of the system. The innovative nature of the approach was further illustrated through the use of wireless signal transduction to a smart device, as highlighted in **Figure 2.13.9**.

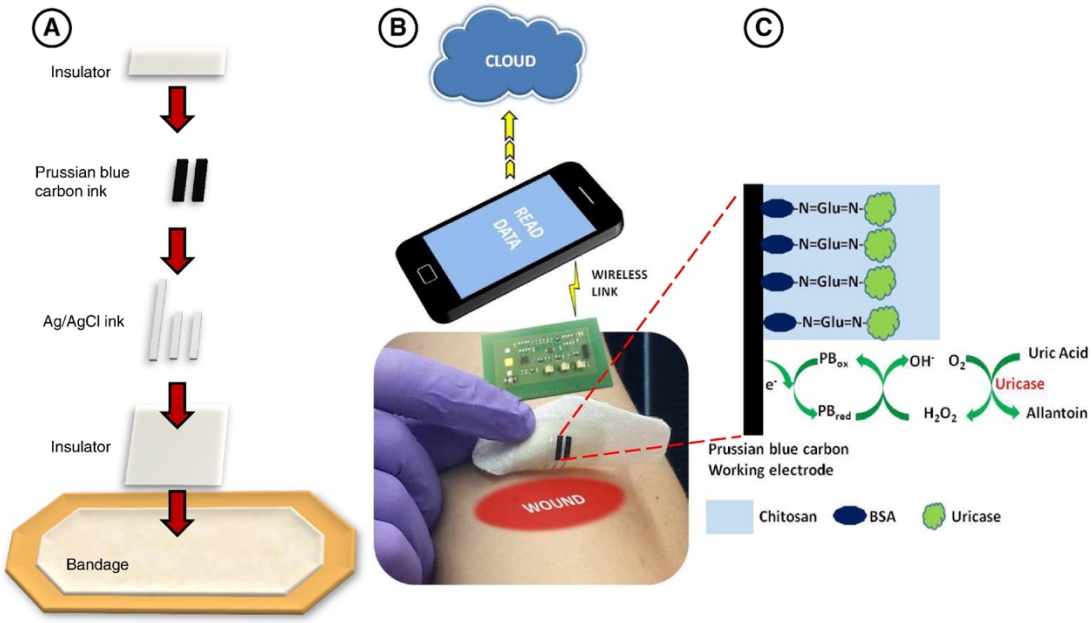

Figure 2.13.9 Fabrication of the urate biosensor and its mode of operation. Reproduced with permission (Kassal, *et al.*, 2015).

The translation of the bionsesnsing system from a point of care diagnostic to a smart dressing would be relatively easy to imagine. Manufacturing the actual sensor using conventional screen printing techniques lends itself to simple processes and low manufacturing costs thus making it disposable. Although the electronic component of the system is not disposable, it could be further miniaturised and adapted for remote/telemonitoring. What is interesting about this system is that it does not solely rest on the measurement of urate but rather on the generic nature of the methodology itself: uricase is an oxidase enzyme and thus it could be substituted for a range of other enzyme systems and therefore open up the possibility of other analytes being analysed or multiparametric analysis (Davis, *et al.*, 2016).

2.14 Conclusion

Based on the presented literature, it is evident that there is an abundance of research surrounding wound pH which has ultimately led to the advent of technological advancements in recent years. However, the propensity in which these novel techniques are incorporated within standard clinical practice are greatly hindered by perennial problems that surround the translation of the technology itself. Examples of these issues include: device usability, portability, associated costs, and sample preparation. The latter contains a myriad of issues itself, in terms of sample volume, composition, and viscosity that could dampen the effectiveness of the more accessible methods of monitoring pH such as indicator sticks or pH probes. Therefore, if the clinician was equipped with a robust and quantifiable means of measuring wound pH within the clinical environment, this would provide them with vital information to aid their decision making process in selecting the most appropriate treatment plan (Davis, *et al.*, 2016).

Chapter 3

Experimental Details and Methodologies

Overview

The following chapter details the materials, methods, and instruments used throughout the duration of this research project. A concise overview of the key underpinning principles of the implemented techniques and the presentation and analysis of the results are described. Individual results chapters will provide more specific experimental details for individual experiments under the Experimental Details section within each chapter.

3.1 Materials and Instrumentation

All reagents used throughout the various experiments were purchased at the highest grade possible from Sigma-Aldrich (Dorset, UK) unless specified otherwise. Stock solutions of uric acid and salicylic acid, typically 10 mM, were prepared in 0.1 M NaOH. Unless specified, all other solutions were prepared using Britton-Robinson buffer (acetic, boric and phosphoric acid, all at 0.04 M) with the pH adjusted by additions of concentrated NaOH. To define the reference potential of pseudo references and provide supporting electrolytes, 0.1M KCl was added to all buffer solutions. Solutions were prepared in deionised water from an Elgastat (Elga, UK) water system. To challenge the electrode response towards more complex matrices, defibrinated horse blood purchased from TSC Bioscience (Buckingham, UK), was employed.

Electrochemical measurements were conducted at room temperature (22^{o}C ±2^{o}C) using either a μAutolab type III computer controlled potentiostat (Eco-Chemie, Utrecht, The Netherlands), a BioLogic SP-300 single potentiostat (Bio-Logic Instrument, Seyssinet-Pariset, France), or DropSens potentiostat (DropSens, Asturias, Spain).

The majority of experiments were carried out in a three-electrode configuration, while others experiments employed a two-electrode system where a silver/silver chloride coated wire acted as both a counter and reference electrode. In regards to the working electrode, a variety of different materials were utilised, including carbon fibre, glassy carbon and a number of carbon composites. In most cases, a platinum wire was utilised as a counter electrode, while a 3M KCl Ag | AgCl half-cell (BAS Technical, UK) was used as the reference electrode. Further specific electrochemical experimental detail is listed accordingly in the subsequent chapters.

3.2 Electrochemical Instrumentation

Electrochemistry can be described as the study of chemical species and reactions that occur between the working electrode (electron conductor) and the

electrolyte solution (ion conductor) in which electron transfer occurs between the two. Based on the resulting electrochemical measurements, it is possible to gain both qualitative and quantitative information that can provide an insight to the kinetics and thermodynamics of the chemical reaction under study. In the present context, analytical electrochemistry is largely employed to identify and/or quantify several key biomarkers via the process of oxidation/reduction and to elucidate the electron transfer processes occurring at the electrode substrates being investigated as potential wound fluid sensors.

The rise in popularity of electrochemistry over other analytical methods, such as spectroscopy, can be attributed in part to the relatively low-cost instrumentation, and the variety of electrode materials that can be manipulated in a multitude of ways to confer selectivity and sensitivity towards particular applications. Complex biofluids such as blood, urine and wound fluid, all contain a myriad of electrochemically active species that can, in principle, interfere with the response of the species that are of direct interest. Therefore, it is common for physical or chemical modifications to be employed at the working electrode in order to minimise their influence. Several of these processes were used in this project but are described in greater detail in the appropriate chapter.

3.3 Electrochemical Cells

In most amperometric or voltammetric electrochemical experiments, the system is set up as a three-electrode arrangement, as highlighted in **Figure 3.3.1**, and consists of a working electrode (WE), a reference electrode (RE), and a counter electrode (CE). In a three-electrode system, the WE is the electrode of interest in terms of electrode response, as this is where the reaction occurs. The potential of the WE is measured relative to the RE and thus the latter must provide a stable and constant potential. Under amperometric or voltammetric control, the principal analytical signal is the electron transfer at the WE induced by the application of a potential. This gives rise to a measureable current and it is necessary to have the CE in place to complete the circuit and avoid the perturbation of the RE potential. On occasions, a two-electrode

system is implemented, whereby the RE is combined with the CE into one electrode with two functions, all while the potentiostat maintains the potential of the WE in relation to the RE. There is an implicit assumption in such instances that the current being measured is small that the influence on the RE electrochemistry is minimal and that the reference potential is relatively unaffected.

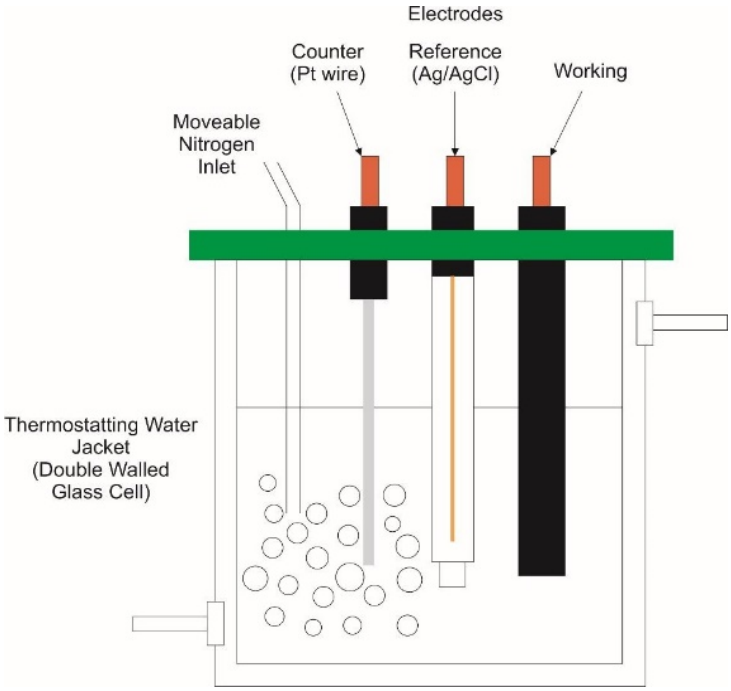

Figure 3.3.1 A schematic of a typical electrochemical system of a three-electrode set up. Adapted from (Fisher, 1996)

3.3.1 Reference Electrodes

As noted, the role of the reference electrode is to provide a fixed and stable potential to allow for the control of the magnitude of the potential of the working electrode. The potential of the reference electrode should be unaffected by the composition of the sample solution and, ideally, should be independent of the current density. The majority of electrochemical measurements, and unless otherwise stated, utilised a silver-silver chloride (Ag | AgCl) half-cell reference electrode. The construction of the latter is highlighted in **Figure 3.3.2**. and consists of silver wire (Ag) that is coated with its porous halide salt (AgCl). A critical element is that the electrode itself is placed within a glass sheath filled with 3M KCl solution which is employed to maintain the constant potential. To ensure that there is an electrical conduction

between the test solution and the electrode, a porous frit is located at the bottom of the glass electrode allowing for a slow outflow of KCl.

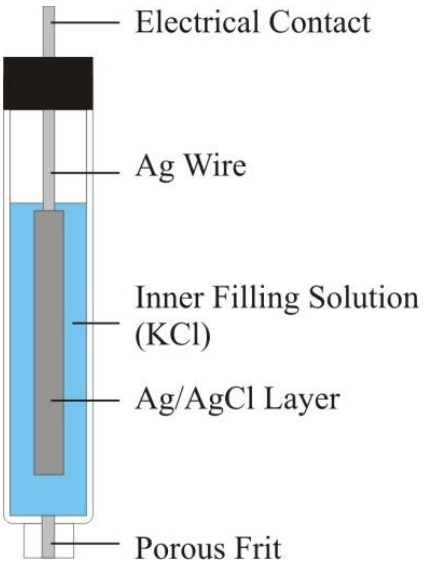

Figure 3.3.2 Assembly of a typical silver-silver chloride reference electrode. Adapted from (Fisher, 1996)

Two chemical reactions occur within the cell – oxidation and reduction. The difference between these two potentials is called the electromotive force (emf) of the cell. The Nernst equation, as detailed in Equation 3.1, describes the electrochemical processes taking place in the cell.

$$Cl^-_{(aq)} | AgCl_{(s)}, Ag_{(s)}$$

$$AgCl_{(s)} + e^- \leftrightarrow Ag_{(s)} + Cl^-_{(aq)} \qquad E^o = 0.222 \text{ v}$$

$$A + ne^- \leftrightarrow B$$

Substituted into the Nernst equation:

$$E = E^{O} - \frac{RT}{nF}\ln\frac{[B]}{[A]} \qquad E = 0.222 - \frac{0.0591}{1}\, log\, \frac{[Cl^{-}]}{1}$$

…Eq 3.1

where: (Fisher, 1996)

E is an electrode potential (volts);

E^{o} is a standard electrode potential (volts);

R is the gas constant 8.314 $JK^{-1}mol^{-1}$;

T is temperature in Kelvin (Typically 298.15 K);

n is the number of electrons transferred to the electrode during the reaction;

F is Faraday constant 96485 C mol^{-1}

[*A*] and [*B*] are activities of the oxidised and reduced species

When the values corresponding to the Ag|AgCl reaction that is occurring at the reference electrode is substituted into the Nernst equation, the electrode potential is established as being directly proportional to the concentration of the chloride ion. Therefore, it is imperative to maintain a constant KCl concentration, typically 3 M, to obtain a stable microenvironment, which enables a constant reference potential.

3.3.2 Working Electrodes

Electrochemically, the working electrode is the greatest point of interest in terms of being the site of the electrochemical reaction under study. A computer controlled potentiostat enables the user to apply a potential between the working and reference electrode. The latter electrode provides a fixed and stable potential, therefore any changes in E could be reflective of changes occurring at the working electrode.

$$E = (\emptyset_M - \emptyset_S)_{working} - (\emptyset_M - \emptyset_S)_{reference}$$

…Eq 3.2

(Compton, *et al.*, 2011)

where:

E = Electrode Potential

$\emptyset_M$ = Electrical

$\emptyset_S$ = Solution

Conventionally, a three-electrode electrochemical setup is implemented, however, in instances where a two-electrode system is implemented, the above equation is no longer valid as it is now possible that the current may pass through the reference and ultimately alter $-(\emptyset_M - \emptyset_S)_{reference}$. Therefore, the equation is adjusted to:

$$E = (\emptyset_M - \emptyset_S)_{working} + IR - (\emptyset_M - \emptyset_S)_{reference}$$

…Eq 3.3

(Compton, *et al.*, 2011)

where:

IR = Electrical resistance of the bulk solution between RE and CE

In a two-electrode setup, any changes would result in an unknown change in IR as well as $= (\emptyset_M - \emptyset_S)_{working}$, which means that current through the working electrode is no longer being controlled. There is one exception where this may not ring true, and that is when we are dealing with microelectrodes. Due to the meniscal low currents that are passed in microelectrodes, they tend to have a negligible effect on the electrolytic change within the reference electrode and therefore the IR will be small enough to neglect (Compton, *et al.*, 2011)

In regards to the substrate used for a working electrode for an application, there is an abundance of materials to choose from. Gold, platinum, palladium, and carbon are commonly chosen due to relative chemical inertness. When choosing a suitable substrate for a working electrode, it should ideally exhibit fast electron transfer kinetics and also reproducible results. Another crucial factor to consider is the ability to effectively determine the electrode surface area as the response is dependent on the latter.

3.3.3 Counter Electrodes

The role of a counter electrode is to ensure that a current of equal magnitude but opposite sign, is passed through itself rather than passing through the reference electrode. Typically, an inert metal is chosen as a counter electrode to ensure that it will conduct relatively easily and will not interfere with the reaction at hand or be influenced by the sample constituents. When selecting an appropriate counter electrode whether it be carbon, nickel, steel or platinum, it is important to factor in the type of reaction taking place as well as the economic implications. To minimise the current density drawn at the counter electrode, Pletcher (2009) has suggested that the size of the counter electrode should be as large as possible. A platinum wire was selected as the counter electrode for all experiments, due to its high conductivity and inert nature (Pletcher, 2009).

3.4 Mass Transport

When dealing with electrochemical analytical measurements it is important to take into consideration the mode of molecular transport when dealing with an electrode-solution interface in which molecules are chemically altered in the measurement process.

3.4.1 Diffusion

The imposition of a potential that leads to a chemical change (because of oxidation or reduction) at the electrode surface invariably leads to the generation of a diffusion gradient. At the surface of the electrode, the concentration of the starting material is lower than that which is contained in the bulk of the solution, and vice versa for the product produced. As the electrode process continues, fresh starting material will diffuse to the electrode surface, while the product will diffuse away from the electrode surface (Pletcher, 1982). This process can be described quantitatively by Fick's first law of diffusion (Equation 3.4) that states that the flux ie. Rate of diffusion from a place of high concentration to low concentration is proportional to the concentration gradient

$$\text{Flux} = -D\frac{dc}{dx} \quad \text{...Eq 3.4}$$

where: (Compton, *et al.*, 2011)

D = diffusion coefficient in cm^2/s

dc/dc = the concentration gradient at distance x

In addition to the first law, there is also Fick's second law, which explains the changes in the concentration gradient with time with respect to the diffusion process, as highlighted in Equation 3.5. Ultimately, this results in the concentration being a function of both time and distance (Pletcher, 2009).

$$\frac{\delta c}{\delta t} = D\frac{\delta^2 c}{\delta x^2} \quad \text{...Eq 3.5}$$

(Pletcher, 2009)

3.4.2 Migration

Migration is the movement of charged molecules because of electrostatic-attraction and electrostatic-repulsion. A charged species will move through a potential gradient via an electrolyte solution (Pletcher, 1982). During an experiment, the mass transport of electroactive species is carried out in a large quantity of inert electrolyte that carries the majority of the charge. Therefore, migration has very little impact on the transport of electroactive species (Pletcher, 1982).

3.4.3 Convection

The physical movement of molecules within a solution is brought about by the process of convection which can be initiated naturally by density gradients or can be mechanically induced by stirring or flowing apparatus. If convection is brought about by mechanical force either by using a rotating disc electrode or even by stirring the solution, this becomes the dominant mode of mass transport (Pletcher, 1982).

3.5 Voltammetry

Voltammetry is a common electrochemical technique, whereby the potential (voltage) between the working and the reference electrode is varied and the current flow (amps) is measured and displayed in relation to the potential, resulting in a voltammogram. In the upcoming section, various techniques implemented during the project will be discussed in greater detail.

3.5.1 Cyclic Voltammetry

Cyclic voltammetry (CV) is a widely-used electroanalytical technique which can provide a wealth of diagnostic information. Typically, it is the first technique employed to understand the underlying electrochemical processes as it allows for the rapid and qualitative interpretation of the data. This technique provides information about the diffusion / adsorptive nature of the electrode process, as well the kinetic and thermodynamic parameters of the species being tested. It also provides a useful indicator to evaluate of the magnitude of undesirable effects derived from ohmic drop or double layer capacitance (Compton, *et al.*, 2011).

Typically, the potential is applied to the working electrode at (E_1) at which no chemical reaction occurs and then swept to a more positive potential (E_2), as highlighted in **Figure 3.4.1.A**. The potential E2 is typically greater than the potential required for the oxidation or reduction process of interest so as to record the reaction (Pletcher, 2009). Throughout a CV, a potential waveform is carried out as highlighted in **Figure 3.4.1.B**. The first half of the triangular waveform is identical to that used in Linear Sweep Voltammetry, however, at E_2, the direction of the sweep is reversed and the electrode potential is scanned back to its original value (E_1). The current recorded, I, is proportional to the rate of the electron transfer, is plotted against the potential as described in **Figure 3.5.1.A.**

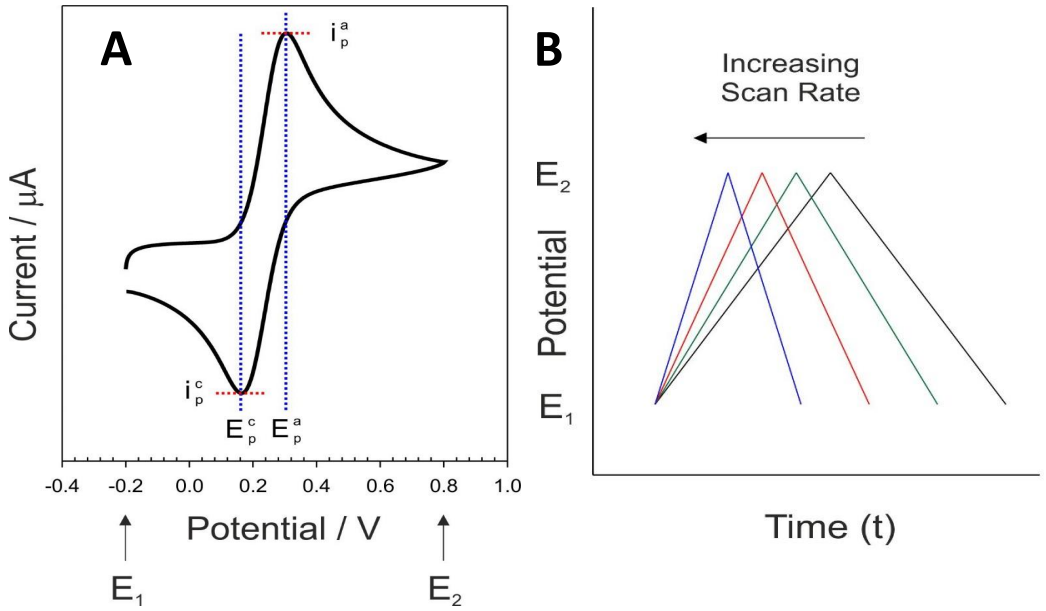

Figure 3.4.1 A) A general schematic electrochemical reactions occurring at the working electrode during a cyclic voltammogram B) Triangular waveform characteristic of cyclic voltammetry.

The scan rate, *v*, (V/s) is the constant rate at which the voltage sweeps from the initial potential, E_1, to the vertex potential, E_2, and back again. The scan rate can be determined by the rate of change of the potential.

The benefit of using this technique is that the results provide the user with specific information on the electrochemical fingerprint of both species undergoing oxidation and reduction reactions. Upon further analysis of the position and shape of the peak, this can provide important information on the electrochemical process as well as giving an insight into the chemical species themselves.

An electrochemical reaction is said to be reversible when it demonstrates fast electron kinetics and maintains the concentration of both the oxidised and reduced species in equilibrium. However, if equilibrium is not met due to the insufficient electron kinetics then the reaction is described as irreversible. A standard cyclic voltammogram can provide an insight into the nature of a reaction by analysing the positioning of the oxidation and reduction peak, as highlighted in **Figure 3.4.2.**

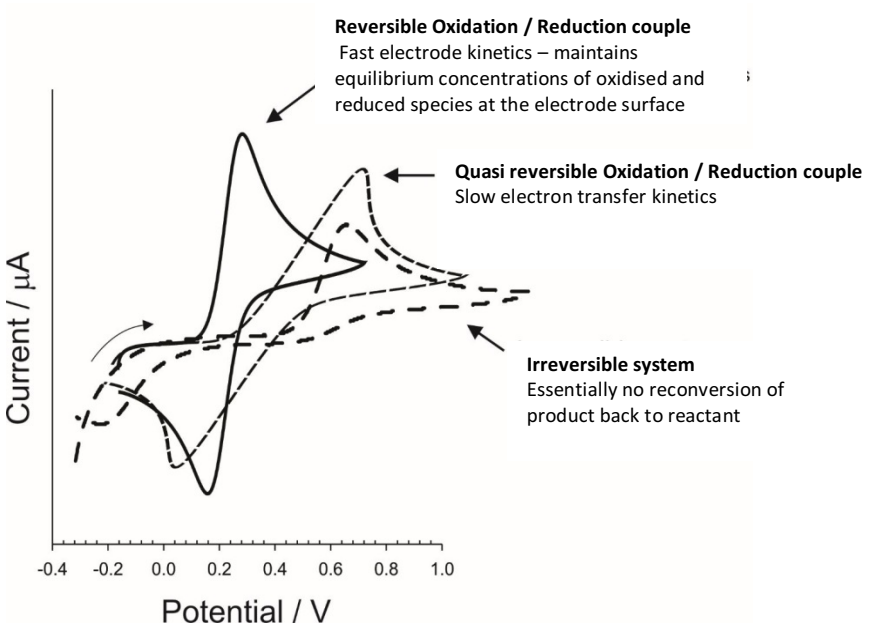

Figure 3.4.2 Cyclic voltammogram detailing the reversible, quasi-reversible and irreversible system involved in electron kinetics. Adapted from (Compton, *et al.*, 2011)

The following relationships can be used to elucidate the nature of the electrode process under investigation (Compton, *et al.*, 2011):

- The voltage separation between the oxidation and reduction peak potentials are described below and are independent of the scan rate

$$\Delta E = E_p^a - E_p^c = \frac{59}{n}\, mV \qquad \text{…Eq 3.6}$$

- The ratio of the peak current is equal to one

$$\frac{i_p^a}{i_p^c} = 1 \qquad \text{…Eq 3.7}$$

- Lastly, the peak currents ($i\frac{a}{p}/i\frac{c}{p}$) are proportional to the square root of the scan rate.

Theoretically, a truly reversible couple expresses a peak separation of 59/n mV that is also independent of the scan rate. The further apart the peaks produced by the reduction and oxidation reaction are, the slower the electrode kinetics become. As the overpotential required to oxidise the species becomes higher with increasing current density, the oxidation peak will shift to a more positive potential and appear more drawn out compared to the sharper peaks of a reversible couple. This same effect can

be seen with the reduction peak, where the peak will shift to a more negative potential and in doing so this can be then described as a quasi-reversible couple.

In regards to an irreversible system, the separation between oxidation peak and, if present, reduction peaks are at its maximum. The peaks for an irreversible system are also noticeably smaller than that of a reversible system. In addition, the time taken for the concentration of the reactant at the surface to dwindle is far longer, which will therefore mean that the impact of the reactant flux at the peak potential will be decreased (Pletcher, 2009).

Another distinct difference between a reversible and irreversible system lies in the dependency of the scan rate. In the case of a reversible couple, much of the current vs the square root of the scan rate will result in a linear relationship for a reversible couple. The diffusion coefficient of the electroactive species can be calculated by using the Randles-Sevcik equation (Equation 3.8) when incorporated into the scan rate, which is square rooted and plotted against the current, it should provide a linear relationship.

$$j_p = 2.69x10^5 n^{3/2} D^{1/2} c v^{1/2}$$ …Eq 3.8

where: (Compton, *et al.*, 2011)

j_p= maximum peak current density in A/cm^2

n= number of electrons

D=diffusion coefficient in cm^2/s

c=concentration in mol/cm^3

v=scan rate V/s

However, for an irreversible couple this is not true, and ultimately the current density now becomes:

$$jp = 3\ x\ 10^5 n(n\alpha)^{1/2} D^{1/2} C V^{1/2}$$ Eq 3.9

(Compton, *et al.*, 2011)

The response described above in terms of cyclic voltammetry is characteristic of linear diffusion for a macroelectrode. A macroelectrode is described as an electrode which has a diameter equal or greater than one millimeter. As the exposed electrode area in respect to the diffusion layer thickness decreases, the diffusion layer becomes hemispherical, which of course will impact the shape of the cyclic voltammogram. A steady-state behaviour is now experienced which results in the characteristic peak disappearing as shown in **Figure 3.5.5**.

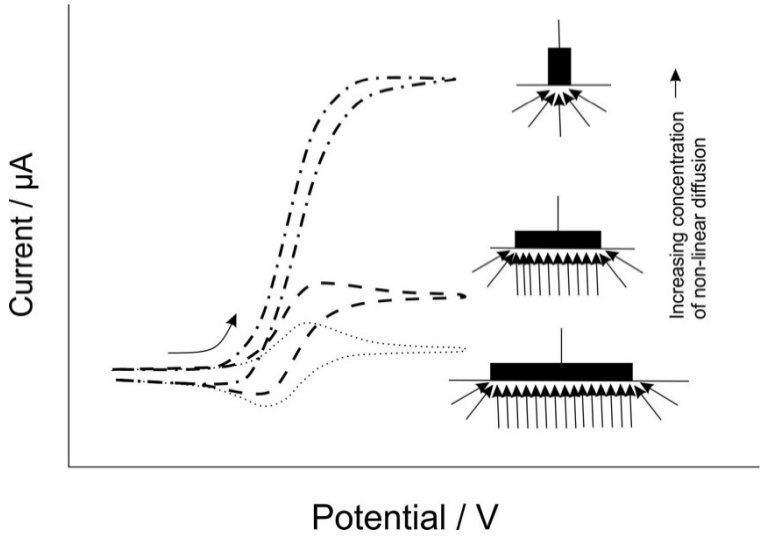

Figure 3.4.3. Cyclic voltammograms detailing the relationship between the different sizes of electrodes (with respect to the diffusion layer thickness) and the contribution of convergent diffusion. Adapted from (Compton, *et al.*, 2011).

If a macroelectrode is described as having a diameter of equal or greater than a millimeter, then a microelectrode describes an electrode that works at the micrometer scale. Unsurprisingly, macro and microelectrodes behave differently in regards to planar diffusion, in which microelectrodes express faster rates of mass transport. Another distinction between the two kinds of electrodes are that microelectrodes have a reduced capacitance in comparison to macroelectrode. This effect is due to the fact a directly reduced area of electrode also directly reduces the capacitance (Compton, *et al.*, 2011).

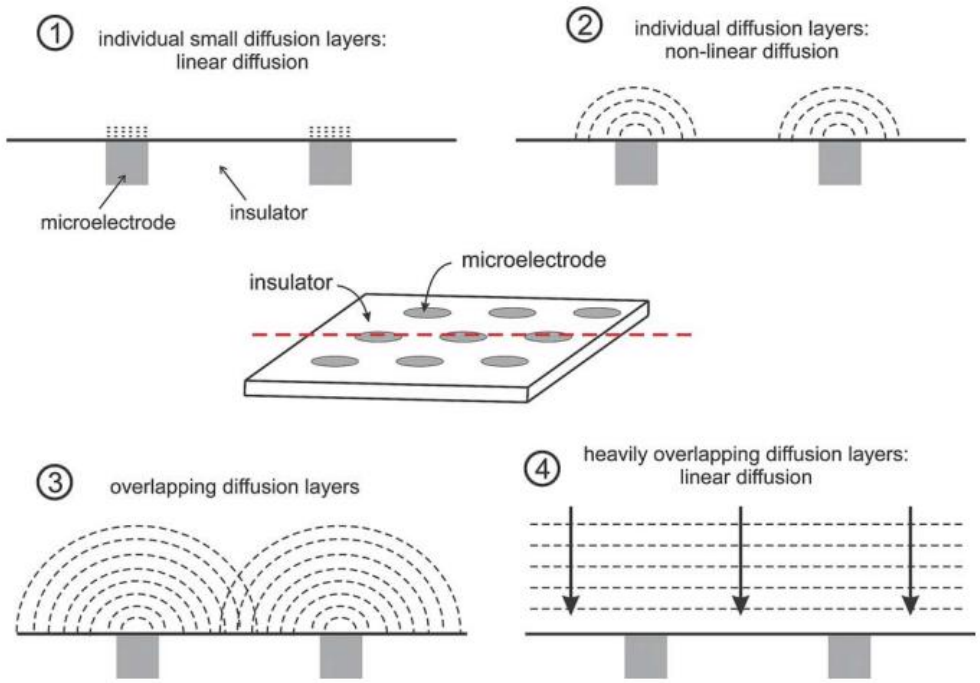

Figure 3.4.4 Schematic examples of the four different diffusion profiles which a microelectrode array may experience. Reproduced with permission (Compton, *et al.*, 2011).

3.5.2 Over Potential

An over-potential can be described as the additional potential, (beyond the thermodynamic requirement) needed to drive a reaction at a certain rate (Bard, *et al.*, 2001). As previously discussed in Section 3.5, when the applied potential (E) and the equilibrium potential (Ee) are equal, no current shall pass through the cell. Therefore, any other value of E would mean that the rate of electron transfer (Equation 3.7) would no longer be in equilibrium, and therefore the electrode reaction under investigation will be dependent on kinetic energy for the current to flow (Fisher, 1996). For electrolysis to occur a value other than Ee must be applied to the working electrode to 'drive' the reaction. This alternative value of E from the equilibrium potential is denoted by the term 'over potential', as highlighted in Equation 3.10.

$$N = E - Ee \qquad \ldots \text{Eq } 3.10$$

where: (Fisher, 1996)

N = Over potential

E = Resultant potential

Ee = Equilibrium potential

The purpose of defining the overpotential relative to Ee, is that the resulting value now has a directly comparable meaning with over equilibria and therefore comparisons can be made between the different overpotentials of varying systems (Fisher, 1996).

3.5.3 Amperometry

Amperometry is a step procedure in which the potential at the working electrode is stepped from one potential where no electrode is present (E1) to another (E2) and held at that potential for a specified period of time as indicated in **Figure 3.5.1**. Typically, this step procedure is applied to the electrode to induce oxidation or reduction.

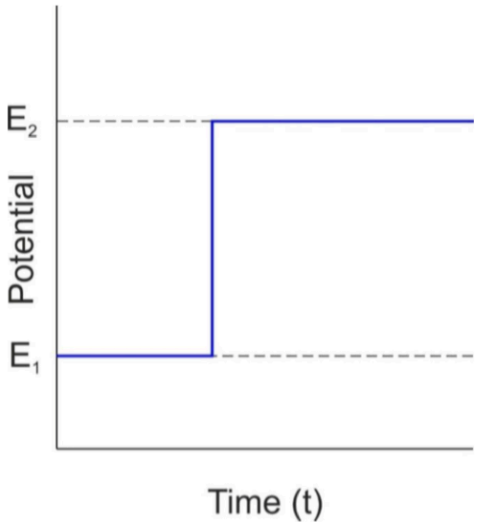

Figure 3.5.1 Potential step procedure used in amperometry.

The instant after the step the concentration of the electroactive species is high, as is current, as there has been little time for any depletion of the electroactive material.

However, gradually over time, the concentration of the electroactive species will begin to deplete and the diffusion layer thickness increases resulting in the decrease of current, eventually to zero as highlighted in **Figure 3.5.2** (Fisher, 1996).

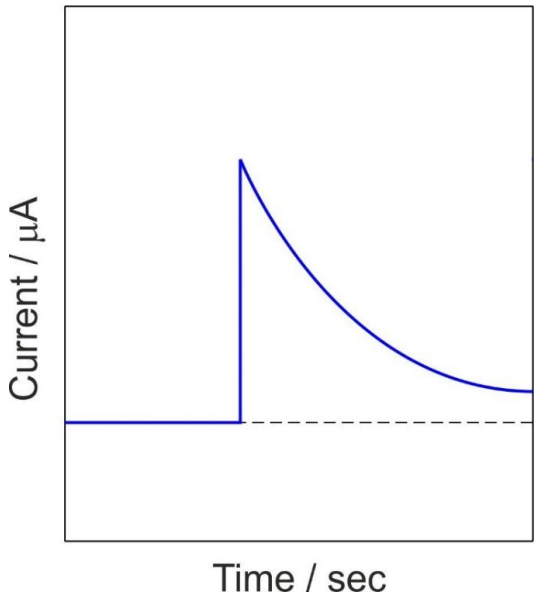

Figure 3.5.2 Typical amperometric response to current**.**

The current can be measured as a function of time, and the behaviour of the current with time when applying a potential step can be described by the Equation 3.11.

$$i = \frac{E}{R_S} e^{-t/RsCd}$$

…Eq 3.11

(Compton, *et al.*, 2011)

where:

I = current in amps

E = electrode potential in V

e= electronic charge in C

t = time in s

R_s = solution resistance in ohms

C_d = differential capacitance of the double layer in F

The current-time response reflects the change in the concentration gradient in the electrode vicinity as highlighted in **Figure 3.5.3**. Therefore, key physical parameters, such as electron transfer, the diffusion coefficient, effective electrode area etc., can be extracted from the system under investigation.

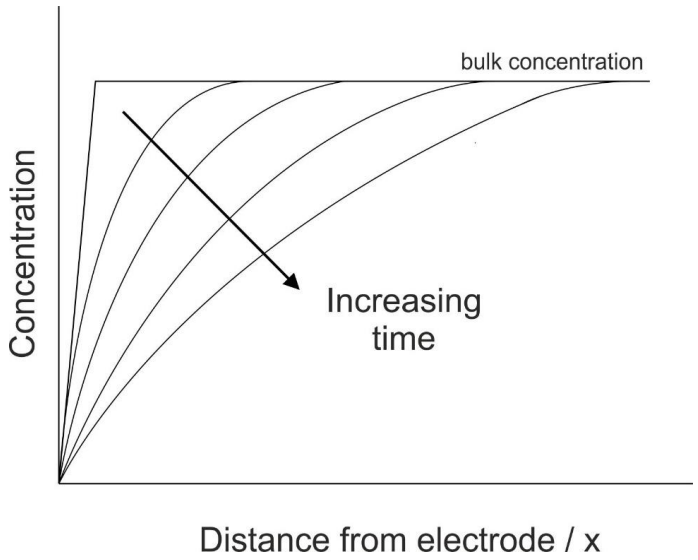

Figure 3.5.3 Impact of varying times on the concentration of a typical amperometric profile.

This change in potential leads to a change in the concentration of the reactant at the surface of the electrode, resulting in differences in the reactant concentration nearby the electrode surface. This results in the diffusion of the reactant towards the electrode, thereby creating concentration differences away from the electrode leading to the expansion of the diffusion layer into the bulk solution (Pletcher, 2009). As the diffusion layer and concentration gradient increases with time, the flux of reactant to the electrode surface decreases with time, which results in a falling current density versus time (**Figure 3.5.3**). The current response, as a function of time, can be described by the Cottrell equation (Equation 3.12), which suggests that the potential step experiment can be used to measure diffusion coefficients.

$$i = \frac{nFAc_j^0\sqrt{D_J}}{\sqrt{\pi t}} \quad \text{...Eq 3.12}$$

where: (Compton, *et al.*, 2011)

i = current, in unit A

n = number of electrons (to reduce/oxidize one molecule of analyte j, for example)

F= Faraday constant, 96,485 C/mol

A = area of the (planar) electrode in cm^2

c_j^0 = initial concentration of the reducible analyte j in mol/cm^3

D= diffusion coefficient for species j in cm^2/s

t = time in s.

3.5.4 Chronopotentiometry

Chronopotentiometry is the measure of the potential difference between the working electrode and the reference electrode under "zero current" over a set period of time, an example of which is highlighted in **Figure 3.5.4**. As effectively very little current is being passed through the cell, the composition of the cell should remain unchanged therefore it should provide quantitative measurements of the solution's composition.

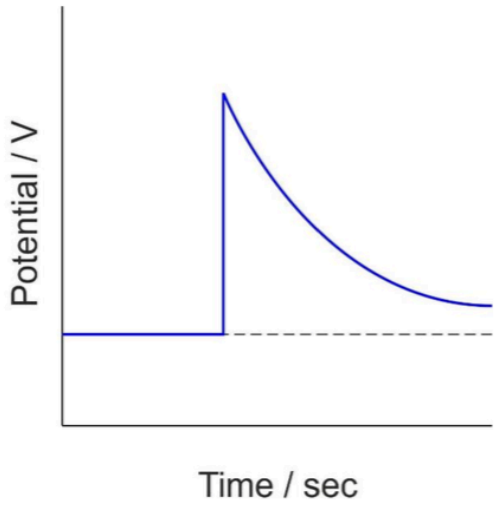

Figure 3.5.4 Example of potentiometry, in which the potential of the working electrode is a measured in relation to the potential of the reference electrode against the function of time.

In this research project, the last twenty seconds of data points for each pH unit were taken, averaged and used to form a calibration graph. This was typically employed in the characterisation of the pseudo reference electrodes involving silver electrodes or for the potentiometric analysis of the solution pH.

3.5.5 Square Wave Voltammetry

Square wave voltammetry records the current as the potential of the working electrode sweeps linearly in time in a staircase fashion, as highlighted in **Figure 3.5.5**. It is the staircase fashion that makes this technique different from cyclic voltammetry. Another key distinction between cyclic voltammetry and square wave voltammetry is that CVs are used to provide largely qualitative analysis, while square wave voltammetry is used for more sensitive quantification of the chosen species.

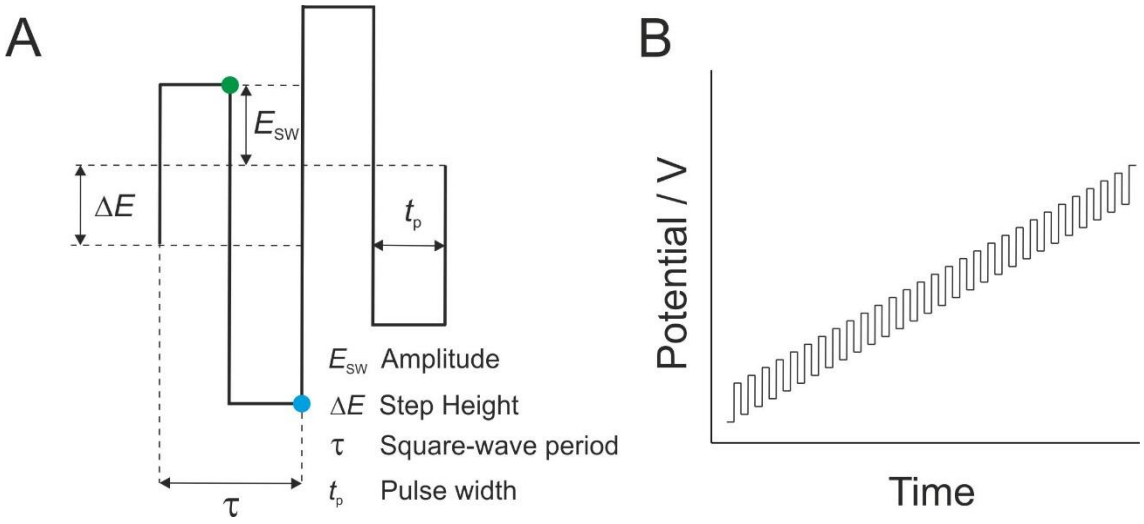

Figure 3.5.5 A) Outline of the waveform and parameters used in square wave voltammetry B) A staircase profile of a square wave scan. Adapted from (Compton, *et al.*, 2011)

The fundamental principles of SQW are highlighted in **Figure 3.5.5,** where the time taken to complete one square wave cycle/staircase is referred to as square-wave period (*T*). The characterisation of the square is based on two factors: the amplitude (E_{sw}) and the pulse width (t_p). The latter can also be expressed in terms of frequency defined as f=1/t or f=1/2tp. When determining the scan rate of an experiment, the value for the step height, E, is used in the following equation:

$$Scan\ Rate\ (mV/sec) = \frac{\Delta\ \mathrm{E}\ (\mathrm{m}V)}{\tau\ (\mathrm{sec})} \qquad \text{…Eq 3.13}$$

(Bard, *et al.*, 2001)

During a square wave voltammogram experiment, the current is recorded twice per square-wave period, as highlighted previously in **Figure 3.5.5**, once at the forward scan (green dot) and once in the reverse sample (blue dot). When both the forward and reverse currents are combined, and plotted, they resemble that of a linear sweep voltammogram with similar diagnostic values (Bard, 2001), as demonstrated in **Figure 3.5.6.**

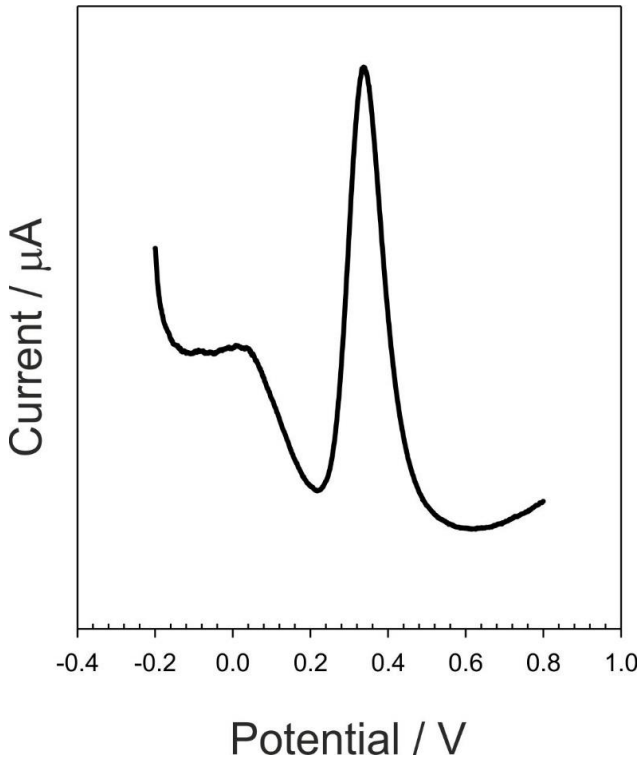

Figure 3.5.6 An example of the different current displayed in a typical square wave voltammogram.

In terms of the present project, the predominant advantage of using SQW over cyclic voltammetry lies in the background suppression and the high sensitivity of the SQW response due to the different timings in which the current is recorded. With a SQW scan, the current is recorded twice within each square wave period, at the end of each pulse which results in a delay of several milliseconds in the current. Whereas, with the CV the current is measured immediately after the change in step potential. The

significance of the short delay in the SQW is that when the potential at electrode surface changes, there is instantaneous re-arrangement of ions at the surface of the interface which results in a capacitance current (Bard, *et al.*, 2001). In regards to sensing biomarkers, it is of interest to monitor the current from the transfer of electrons to or from the target biomarker, which is known as Faradaic current. Thus, SQW voltammetry can measure much lower concentrations of the species being investigated compared to the CV, where the small faradaic current can oftentimes be obscured by the large capacitance effects. Therefore, by creating a pause before the current is recorded, this allows for the capacitance to dissipate yielding a greater signal to noise ratio which ultimately leads to improved detection limits (Bard, *et al.*, 2001).

3.6 Variation of Peak Potential with Solution pH

The main premise of this body of research was focused on the devolvement of a steady state pH sensor for monitoring chronic wounds. As previously discussed in Chapter 2, there are currently a multitude of techniques available for monitoring pH, however not all of which are practical or suitable for the complex environment of a chronic wound. Therefore, this research focused on the development of a sensor that could detect variations of peak potentials towards varying pH solutions, by utilising square wave voltammetry and cyclic voltammetry. It was envisioned that based on the resultant peaks from these two techniques, the pH could be indirectly measured in accordance with the Nernst equation.

The Nernst equation can be taken and further manipulated to allow us to calculate the electrochemical shift (E) due to a log change in Hydrogen ion concentration (i.e. 1 pH unit). Therefore, it could be expected that in a Nernstian relationship, a potential shift by the change of 1 pH unit would result in a 59.1mV shift at 25^{O}C where n=1. Based on this fundamental relationship between the pH sensing capabilities of a variety of working electrode shall be investigated (Compton, *et al.*, 2011).

$$E = E^O + \frac{2.303RT}{nF}\log[H^+] + log\frac{[B]}{[A]}$$

$$E = E^O + \frac{RT}{nF}2.303\,pH$$

$$E = E^O + \frac{8.314 \times 298.15}{96485}2.303\,pH$$

$$E = E^O + 0.0591\ \mathrm{V}\,pH$$

...Eq 3.14

(Compton, *et al.*, 2011)

3.7 Surface Characterisation / Modification Methods

The following sections describes the different techniques employed to gather information on the electrode surface chemical composition and surface morphology. In addition to this, a detailed description of the main method of modifying the electrode surface throughout the research presented here is described.

3.7.1 X-Ray Photoelectron Spectroscopy

X-Ray Photoelectron Spectroscopy (XPS) is a quantitative spectroscopic technique that is used to collect key information on the composition of a sample, such as the elemental composition, empirical formula, chemical and electronic state. It is a highly sensitive technique that can extract information from the top 10nm of the surface of the sample. The sample is placed into a ultra-high vacuum (UHV), and exposed to a low-energy, monochromatic x-ray source (15Kv and 10Ma). The incident x rays cause the core level electrons to be ejected from the sample atoms. The energy from the photoemitted core electrons is a function of the samples binding energy and also provides characteristics of the element from which it is emitted. The primary data generated from the XPS is the energy analysis of the emitted photoelectrons. In accordance with the work of Ernest Rutherford (1914), if the energy of an X-ray with a particular wavelength is known then the electron binding energy of each of the emitted electrons can be calculated using Rutherford following equation:

$$E_{binding} = E_{photon} - E_{Kinrtic} + \emptyset$$

where:

$E_{binding}$= the binding energy (BE) of the electron

E_{photon} = the energy of the X-RAY photons being used

$E_{kinetic}$ = the kinetic energy of the electron

Ø = the work function of the spectrometer Eq 3.15

(Fisher, 1996)

When an incident x-ray ejecting a core electron, an outer electron will fill the hole left by the ejected core electron. The transition of energy caused by this is balanced by the emission of an Auger electron or by a characteristic X-ray. Therefore, in addition to analyzing the emitted photoelectrons in XPS data, Auger electrons can also be analysed.

To detect both the Auger electrons and the photoelectrons emitted from the sample, a detector known as an electron energy analyzer is implemented, as highlighted in **Figure 3.7.1.** An electron energy analyser is composed of two hemispherical electrodes which allows for selection of the energy of the photoelectrons. The potential difference between these two electrodes determines the path of the energy of the electrons. The only kind of electrons to arrive at the detector, are those what have kinetic energy included in an interval of energy created on this path energy.

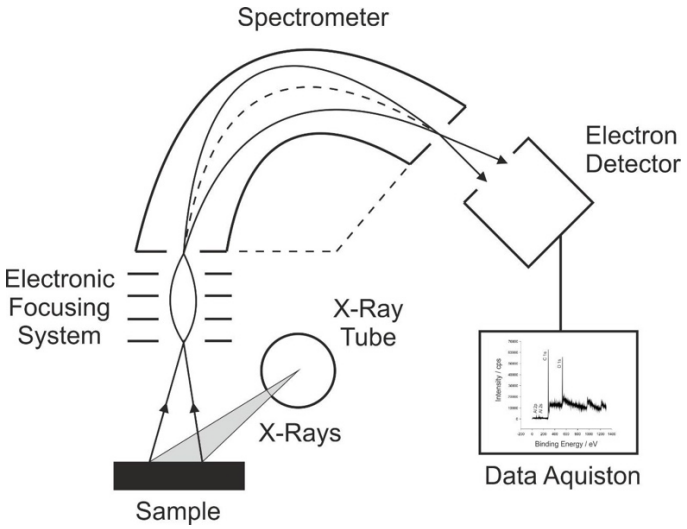

Figure 3.7.1 An example of an X-Ray Photoelectron Spectroscopy system. Adapted from (Fisher, 1996)

By taking the number of Auger electrons and photoelectrons emitted as a function of their energy, a spectrum can be created which represents the samples surface characterisation. Below in **Figure 3.7.2,** provides a typical spectrum of carbon. The energy corresponding to each peak is characteristic of an element present in the sample volume. The relative amount of that element can be determined by the area underneath the corresponding peak. While the peak position and shape indicates the chemical state of the element.

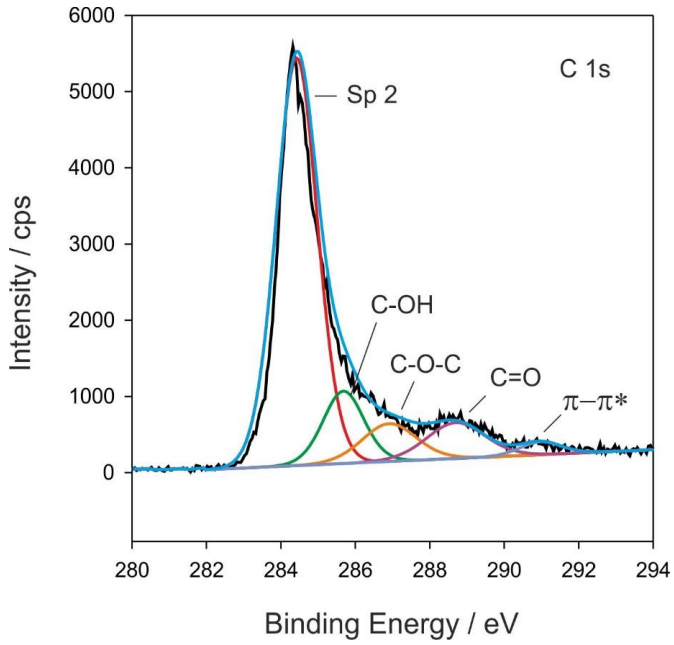

Figure 3.7.2 A typical XPS spectrum of carbon, detailing the different energies of different chemical states.

This research project conducted X-ray Photoelectron Spectroscopy (XPS) using an Axis Ultra DLD spectrometer (Kratos Analytical, Japan), with an operating pressure lower than $6x10^{-8}$ Pa, using monochromated Al Ja X-rays (15 kV and 10 mA). The analysis was carried out in a hybrid lens mode, and to achieve charge neutralization an immersion lens was selected with a film current between 1.7 and 2.1 mA at a charge balance voltage between 3.0 and 3.6V. Three spots on each sample were analysed as well as a wider energy survey scan (binding energy, 0–1300 eV), with a pass energy of 160 eV and a high resolution for C_{1s} (272.5–297.5 eV) and O_{1s} (519.5–544.5 eV) with a pass energy of 20 eV. Using the data from the high-resolution spectra, the quantification of the atomic percentage of oxygen on the surface was analyzed by subtracting the linear background and calculating the area under the peaks on the 01s and C 1s spectra using Vision 2.2.8 software (Kratos Analytical, Japan).

3.7.2 Electrochemical Anodisation

To improve upon the electrode response, a variety of surface modification methods were implemented. Electrochemical anodisation was commonly used to increase edge plane populations on graphite based electrodes and therein enhance the electron transfer kinetics. The anodisation process was essentially an adaptation of chronoamperometry (Section 3.5.3) and follows on from the work of Dutt and colleagues (Dutt, *et al.*, 2005).

Electrochemical anodisation of carbon electrodes was achieved by applying a direct current (+2V) through an electrolytic solution, 0.1M NaOH, in which the working electrode (typically carbon) serves as the anode (the positive electrode). The current passing through generates oxygen at the working electrode and releases hydrogen at the cathode (the negative electrode). The oxidation process also facilitates nucleophilic attack at the carbon interface leading to an increase in oxygen functionality (carbonyl, hydroxyl, and quinol) at the carbon surface (Banks, *et al.*, 2005). There will also be microscopic changes in the texture of the surface as well as the crystal structure of the

electrode near the surface leading to more exfoliation of the layers and an increase in edge plane sites (Banks, *et al.*, 2005), as highlighted in **Figure 3.7.3**.

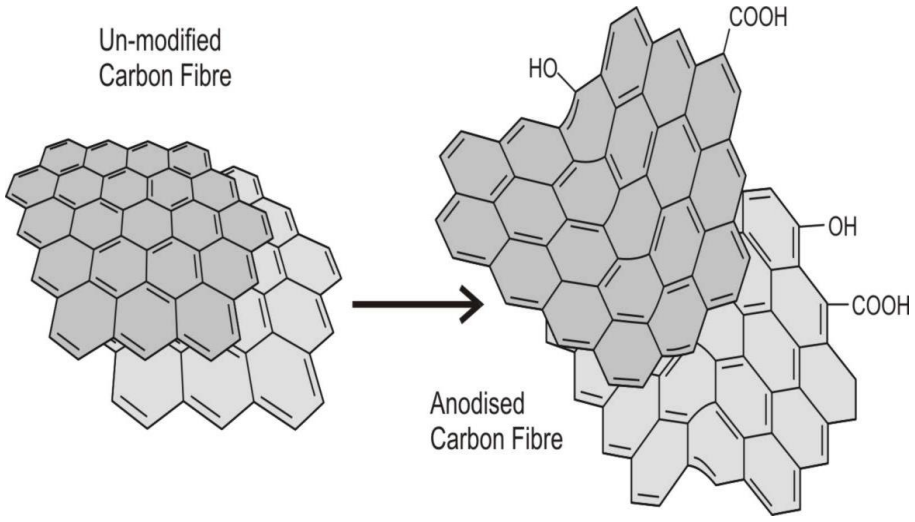

Figure 3.7.3 The impact of electrochemical anodization of the surface of a graphite particle.

These changes have been shown to significantly improve electrode performance with increased electron transfer kinetics often cited as the main contributing factor and ultimately improves voltammetric peak resolution and detection sensitivity.

Chapter 4

Development of Functionalized Palladium Electrodes for Smart Bandage Applications for Monitoring Wound pH

Abstract

A palladium film electrode was used as a conductive substrate for conferring pH over a biologically relevant pH range for chronic wounds. The electrode surface was modified with a self-assembly monolayer (SAM), L-cysteine, that enhanced the standardisation of the electrode potentiometric response towards pH. The presence of the L-cysteine layer on the modified palladium film was confirmed using XPS analysis. The self-assembly monolayer (SAM) was found not to impact the electrode kinetics of the electrode, which exhibited a sub Nernstian response (33 mV/pH) over a pH regime (pH 3 – 9). The performance of the modified electrode and the applicability of the potentiometric approach for continuous wound monitoring was demonstrated through repetitive scanning in relevant pH regimes.

Aspects of this work were included in a poster presentation for Materials Today at 'New Scientist Live' 2016, where it was awarded Best Materials Development Poster.

4.1 Introduction

The significance of pH sensing for *in vivo* monitoring within biomedical applications has garnered tremendous interest in recent years (Korostynska, *et al.*, 2008; McLister, *et al.*, 2016). Conventional glass pH probes are typically employed within a clinical environment to monitor wound pH. However, the fragile nature of the glass probe and its robust dimension, coupled with the frequent and necessary need for maintenance and calibration has prevented its translation into a sensor for continuous wound monitoring. One of the most commonly employed electrochemical techniques to monitor pH is potentiometry. The simplistic circuitry and ease of fabrication of this technique lends itself to miniaturisation, that could potentially be translated into a compact wearable device (Qin, *et al.*, 2016). In recent years, the use of metal oxides as a means of pH sensing have been studied for use as potentiometric sensors. In particular, the following have been used as pH sensors; iridium oxide (IrOx) (Kim, *et al.*, 2014; Nguyen, *et al.*, 2014; Chu, *et al.*, 2015), cobalt oxide (Hussain, *et al.*, 2014), ruthenium oxide (Sardarinejad, *et al.*, 2014) and palladium oxide (PdO) (Kreider, *et al.*, 1995).

Palladium exhibits high catalytic activity towards several electrochemical processes which include: hydrogen evolution reactions (HER) (Naga Mahesh, *et al.*, 2016; Zhang, *et al.*, 2016; Yin, *et al.*, 2018), hydrogen absorption (Konda, *et al.*, 2016; Kong, *et al.*, 2016) and the reduction of simple organic compounds (Mirza-Aghayan, *et al.*, 2015). The unique expedient quality of palladium is its ability to absorb hydrogen (Lewis, 1967), under both gas phase and electrochemical conditions (Grdeń, *et al.*, 2008; Metters, *et al.*, 2013). A recent publication by Qin and coworkers (2016), reported that palladium oxide yielded a super Nernstian response towards pH in comparison to other materials. The current method of fabricating Pd/PdO films include: electrochemical deposition (Grubb, *et al.*, 1980), physical vapour deposition (Horwat, *et al.*, 2011) and thermal oxidation (Kinoshita, *et al.*, 1986).

However, certain limiting factors associated with the majority of these processes can include the requirement of high electrical energy, a vacuum environment and high temperatures. Although these fabrication requirements are not conducive to the

development of a low cost and low volume sensing applications – given the potential scale for chronic wound problems and the frequency of which the dressings (and hence the sensors) will need to be replaced – the production of Pd electrodes could become more economically viable. Therefore, the aim of this chapter is to investigate the well known properties of Pd towards protons and report on the potentiometric response of a surface modified Pd film electrode to confer pH.

The approach taken in this methodology was to modify the Pd electrode surface with a self-assembled monolayer (SAM). SAMs can form a single layer on a surface either by spontaneous physical or chemical adsorption of organic molecules, due to the attractive forces between specific functional groups in the moiety and the surface of the substrate (Pedrosa, *et al.*, 2007; Feliciano-Ramos, *et al.*, 2010). The benefit of this approach includes the ability to introduce a variety of different chemical functionalities with a high level of order at a molecular dimension (Pedrosa, *et al.*, 2007). This approach facilitates the development of specific electrochemical surfaces that could be employed for selective interactions or act as a catalysis for electron transfer reactions (Morrin, *et al.*, 2004; Park, *et al.*, 2004; Pedrosa, *et al.*, 2007). Previous studies have suggested that palladium would be a suitable substrate for SAMs due to its physical properties, that includes its high reactivity towards sulphur and its relatively small lattice (2.75 A) in comparison with silver and gold (Wolfe, *et al.*, 2002; Love, *et al.*, 2003; Feliciano-Ramos, *et al.*, 2010).

L-cysteine is one of the two sulphur containing amino acids that contain thiol functional groups that can be absorbed very strongly onto metallic surfaces (Qingwen, *et al.*, 2001; Feliciano-Ramos, *et al.*, 2010). Another aspect of L-cysteine that makes it attractive to the field of biosensors, is that it contains both carboxylic acid and amino functional groups, as detailed in **Figure 4.1.1**, that could be used for the conjugation of biomolecules such as antibodies and enzymes (Feliciano-Ramos, *et al.*, 2010).

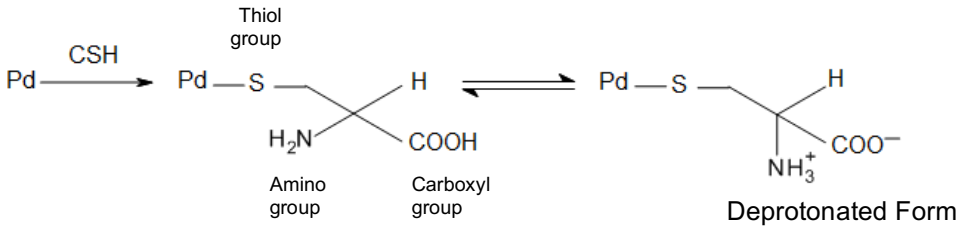

Figure 4.1.1 Pallidum and L-cysteine reaction scheme.

L-cysteine, contains a carboxyl group (COOH) and an amino group (NH_2) that have acidic and basic qualities respectively and can exist in a zwitterion form as indicated in **Figure 4.1.2**.

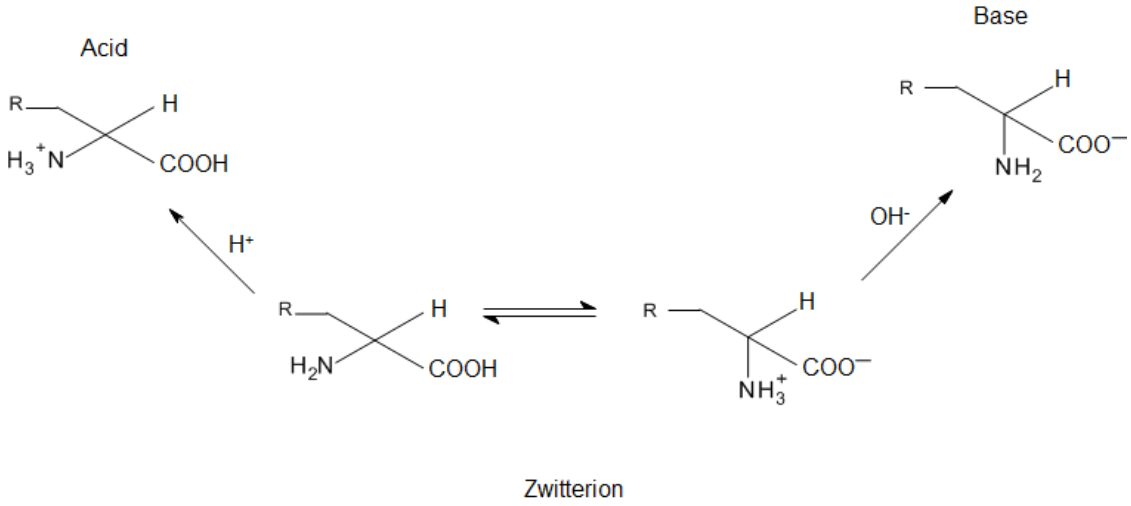

Figure 4.1.2 Schematic detailing the impact of pH on the structure of L-cysteine.

The palladium and the thiol group of the L-cysteine will preferentially bind together due to the formation of soft acid-soft base interaction. Therefore, as the carboxylic acid and amine are not involved in the binding of the palladium they are still susceptible to protonation/deprotonation and as such could confer pH sensitivity to the electrode surface as highlighted in **Figure 4.1.2**. The intention here was to investigate the fundamental interaction between a L-cysteine modified palladium electrode towards a potentiometric pH range, in order to assess its applicability as a point of care sensor for measuring wound pH.

4.2 Experimental Details

4.2.1 Materials

All lab reagents were purchased at the highest grade and required no further purification. All experiments were carried out at room temperature (+22 ^{o}C ±2 ^{o}C) in Britton Robinson (BR) Buffer in a range from pH 3 to pH 9, unless stated otherwise. Stock solutions of L-cysteine (CSH) typically 10 mM, were prepared in deionized water. Single sided palladium film used for the working electrode was purchased from Sigma Aldrich, (Dorset, UK).

4.2.2 Electrochemical Configuration

Electrochemical measurements were conducted on either an μAuto lab type III computer controlled potentiostat (Eco-Chemie, Utrecht, and The Netherlands) or Biologic VSP-300 Multichannel Potentiostat / Galvanostat / EIS (Bio-Logic Science Instruments, EC-Lab Ltd). A three-electrode system consisting of a platinum wire counter electrode, a standard Ag/AgCl reference electrode (3 M NaCl, BAS Technicol UK) and a working electrode was utilised for cyclic voltammogram and square wave voltammogram technique. Cyclic voltammograms were recorded with a scan rate of 50 mV/s unless stated otherwise.

A two-electrode system was employed for potentiometric measurements, which consisted of a working electrode and a reference electrode. The potential was recorded over a 2-minute period and the average potential over the last 20 seconds was calculated and plotted against the corresponding pH.

4.2.3 Sensor Design and Modification

The palladium electrodes were prepared by sandwiching the single sided palladium film between a resin-polyester lamination pouch with a film thickness of 75 μm (Rexel, UK) using commercially available office laminator. The resin-polymer

laminate was pre-etched with the sensing window (16 mm^2 diameter) using a 25 W CO_2 Computer Controlled Laser Cutter (CadCam Technology Ltd, UK). The palladium film was encased in the laminate in order to provide a defined electrode area (16 mm^2). The electrical connection for the palladium film was created by adhering strips of adhesive backed, copper shielding tape (100 μm thick), which was purchased from RS Electronics, UK.

Prior to any experiment the palladium electrodes were degreased by sonication in methanol for five minutes and then rinsed with distilled water before use. The palladium electrodes were then cycled 10 times in 1 M H_2SO_4 via the process of cyclic voltammetry conducted in a potential range from – 0.2 V to +1.2 V. Following the cyclic cleaning, the electrodes were rinsed in distilled water and placed directly into a 10 mM L-cysteine solution for varying amounts of time (30 – 900 seconds).

4.3. Results and Discussion

4.3.1 Electrochemistry of Palladium Electrodes

The peak current in cyclic voltammetry is dependent on the composition of the Pd surface, therefore the ambient conditions present within the laboratory could potentially impact the binding kinetics of thiols in addition to the electrochemistry (Fischer, *et al.*, 2009). Therefore, it is imperative that the Pd surface is cleaned prior to experiments. A common electrochemical cleaning technique typically employed to clean electrodes, involves cycling the electrode potential in 1 M sulphuric acid until a stable cyclic voltammogram is obtained (Fischer, *et al.*, 2009). Cyclic voltammograms detailing the response of repetitive scanning of Pd film electrodes in 1 M H_2SO_4 are highlighted in **Figure 4.3.1.**

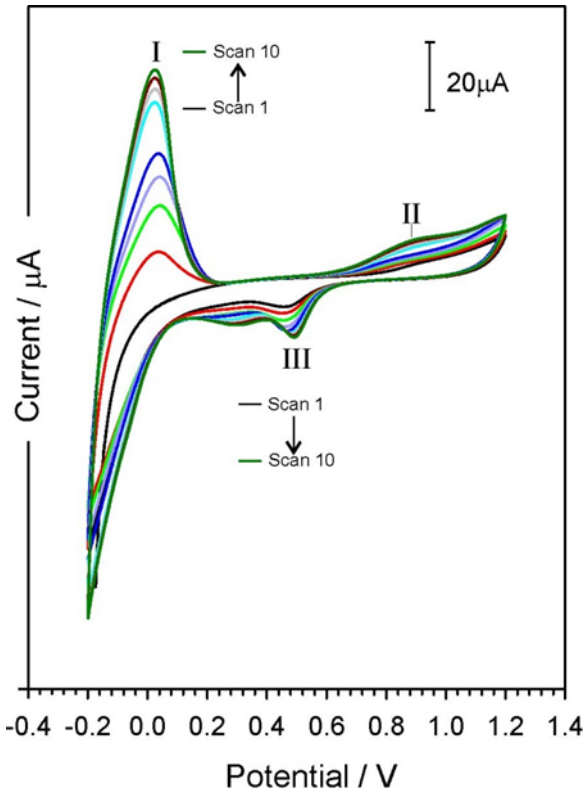

Figure 4.3.1 Cyclic voltammograms detailing the response of a palladium electrode cycled 10 times in sulphuric acid (0.1 M H_2SO_4, 50 mV/s). N_s=10

The Pd film electrode does not display a well separated process of hydrogen adsorption, desorption and evolution normally expected of polycrystalline Pd electrodes. In the anodic scan, the current increases rapidly around 0 V and this peak (**I**) corresponds to the oxidation of absorbed hydrogen as per Equation 4.1

$$H_{(ads)} \rightarrow H^{+}_{(aq)} + e \qquad \text{…Eq 4.1}$$

The onset of the formation of the palladium oxide/ hydrous oxide layer (**II**) can be seen at +0.85V with the corresponding reduction (**III**) process observed at +0.5V on the reverse sweep, which is in accoradance with previous work by (Sun, *et al.*, 2012). The general process is summarised in Eq 4.2

$$Pd^{0}_{(s)} \leftrightarrow PdO_{(s)} / Pd(OH)_{2(s)} + ne \qquad \text{…Eq 4.2}$$

With each subsequent cycle – the definition of the various processes was found to improve indicating that the “working” of the electrode surface was effectively cleaned

4.3.2 Potentiometric response of Palladium to pH

The relatively minimal nature of the potentiometric technique allows for a less complicated system for data acquisition. Therefore, it was of particular interest to determine the applicability of the potentiometric response of the Pd towards monitoring pH. The influence of pH on the potentiometric response of the cleaned Pd film electrode is reported in **Figure 4.3.2**. The electrode was immersed in a buffer of defined pH and the potentiometric response (measured relative to a conventional 3M Cl^- Ag/AgCl half cell reference) was recorded over a period of 120 seconds. The data presented in **Figure 4.3.2A** was derived by taking the last 20 seconds of the potentiometric scan for each pH buffer. A more quantitative comparison of the average potential (over the 20s) as a function of pH is detailed in **Figure 4.3.2B.**

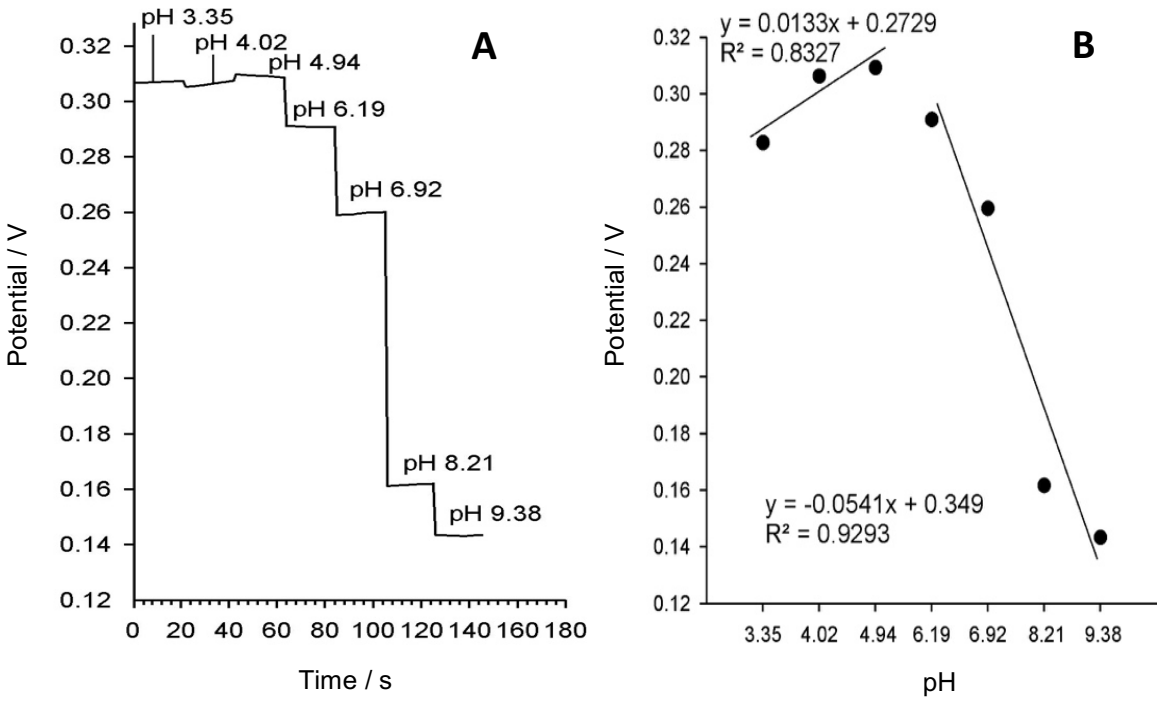

Figure 4.3.2 A) Potentiometric response of an unmodified palladium electrode towards various pH regimes. B) A plot of the average potential over a period of 20s as a function of pH. N_s=7, N_{pH}=7

The potentiometric response of the Pd film electrode consists of two distinct phases. An insensitivity towards pH was observed at a pH lower than pH 6. As the pH moves toward a more neutral/alkaline state – a near Nernstian response was observed (54mV/pH unit). Considering that the clinically relevant pH range for monitoring

wounds lies in a region between pH 5 and pH 9, the bare Pd film electrode could potentially be suitable for this application. However, it was envisaged that the electrode sensitivity toward pH could be further enhanced by modifying the electrode surface.

4.3.3 Surface Modifications

The electrochemistry of palladium is dictated by its surface chemistry, therefore leaving the electrode out over a period of time can introduce variations in its response due the formation of an oxide or hydroxide layer. The formation of this layer could inhibit the electrode reproducibility; therefore, it was envisaged that modification of the electrode surface with a monolayer coating of L-cysteine, would aid the acquisition of a standardised / more reproducible response.

4.3.4 Electrochemical Investigation

In order to determine the impact that leaving the Pd film electrode in L-cysteine, has on the electrochemical response, a time study was conducted. The Pd film electrode was degreased prior to the study via sonication in methanol, it was then rinsed and directly placed into the 10 mM L-cysteine solution for various amounts of time ranging from 5 minutes to 4 hours. In order to evaluate the electrochemical performance of the Pd film with varying time intervals of L-cysteine modification, it was necessary to test the electrode response in the presence of a model redox probe such as ferrocyanide. Cyclic voltammograms detailing the electrode response towards ferrocyanide (2 mM in 0.1 M KCl) at each time interval is reported in **Figure 4.3.3**

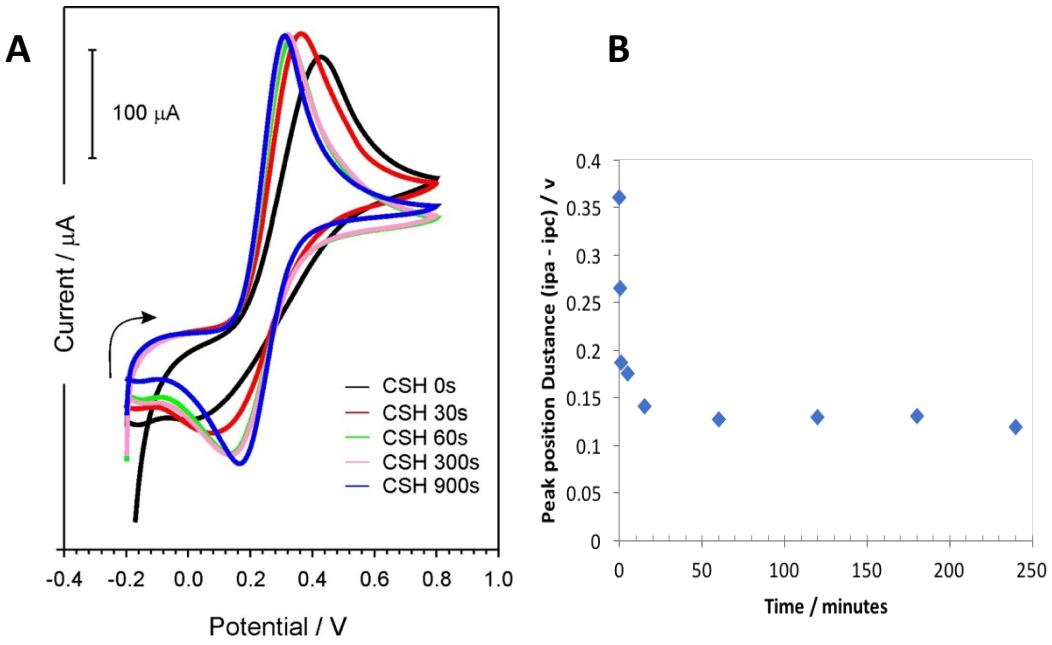

Figure 4.3.3. A) Cyclic voltammograms detailing the response of a palladium electrode dip coated in L-cysteine (0.1 M) for varying periods of time (30 – 900 seconds), towards ferrocyanide (2 mM, 0.1 M KCl, 50 mV/s) N_s=5 B) Influence of L-cysteine immersion time on ferrocyanide peak separation.

Taking the peak-to-peak separation of the voltammograms detailed in **Figure 4.3.3**, a qualitative assessment of the electron transfer between the redox couple and the monolayer on the Pd surface can be determined. A difference of 240 mV peak separation was noted between the voltammogram of the bare Pd and an electrode treated with L-cysteine (3 hour immersion). This decrease in peak separation indicates that the L-cysteine monolayer coating on the palladium electrode improved the electron transfer of the redox couple in solution (Feliciano-Ramos, *et al.*, 2010). To ensure that the electrodes were completely coated in the L-cysteine, it was decided that from this point forward, all electrodes would be dip coated for a period of 3 hours.

However, while the peak to peak separation decreased, there was an increase in electron transfer kinetics. Santos and coworkers suggested that this may occur due to the electrostatic attraction of the L-cysteine monolayer and the negative charge of the redox couple (Santos, *et al.*, 2007), due to the isoelectric point of L-cysteine is 5.02 and the functional groups that are affected by the pH of the redox solution (Feliciano-Ramos, *et al.*, 2010).

Under the neutral / mildly acidic conditions expected of a solution containing 2 mM ferrocyanide in 0.1 M KCl, the positively charged nitrogen would be considered as a zwitterion. Therefore, it would be expected that the overall positive and negative charges would cancel out to leave no net charge at the electrode interface. Qingwen and colleagues reported similar electrochemical behavior with gold electrodes. They suggested that the presence of the amine group, which may carry a positive charge in phosphate buffer, allows for the electron transfer of the redox couple by the electrostatic attraction of the L-cysteine monolayer (Qingwen, *et al.*, 2001).

An alternative mechanism for the enhanced response could be attributed to simple redox exchange between the adsorbed L-cysteine and ferrocyanide. One is a reducing agent (Cys) and the other an oxidiser (ferro) and therefore could it be possible that a direct chemical reaction occurs between them? Moreover, could any reducing agent mimic the behaviour? These were critical questions that needed to be addressed. The response of the L-cysteine modified electrode towards ferrocyanide is shown in **Figure 4.3.4** and compared against the response obtained with a Pd electrode without any L-cysteine modification. It is clear that the presence of the L-cysteine dramatically improves the reversibility of the electrode process. A third scan is also included in **Figure 4.3.4** whereby the response of an unmodified electrode towards ferrocyanide is recorded in the presence of ascorbic acid. The latter was introduced to serve as an alternative reducing agent. From **Figure 4.3.4**, it is clear that the addition of ascorbate has no influence on the reversibility as the voltammetric profile was similar in shape to that of the unmodified response to ferrocyanide alone. Therefore, the enhanced electrode response of the L-cysteine modified electrode must be attributed to the direct binding of the sulphur on the electrode surface.

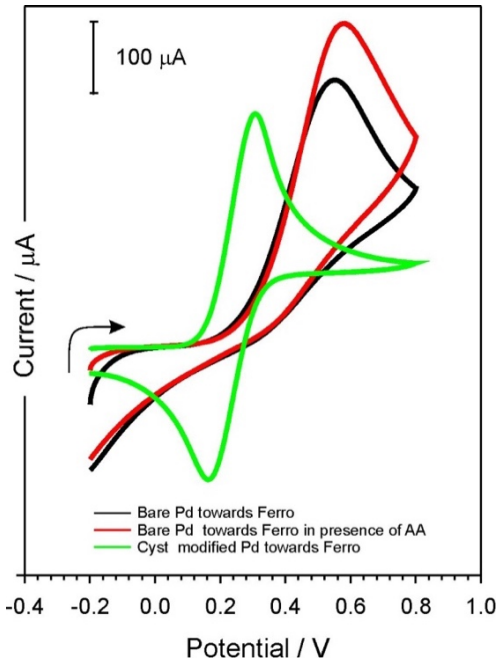

Figure 4.3.4 Cyclic voltammograms detailing the response of a bare palladium electrode towards ferrocyanide (2 mM, 0.1 M KCl, 50 mV/s) as well as in the presence of ascorbic acid, compared against a L-cysteine modified palladium electrode response towards ferrocyanide. N_s=3.

To confirm that CSH adheres to / combines with the Pd chemically, XPS analysis was conducted ,as previously described in section 3.7.1, on a sample of both unmodified Pd film and a L-cysteine modified Pd film. The results of which are presented below in **Figure 4.3.5**

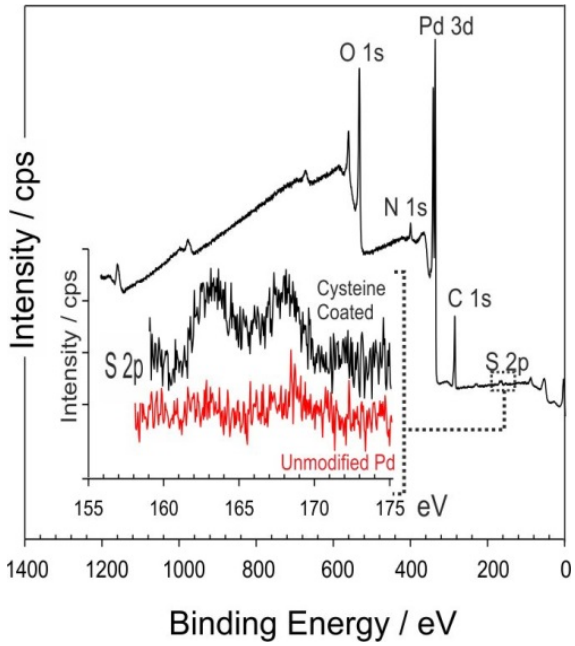

Figure 4.3.5 XPS profiles for the S 2_p peak obtained from a L-cysteine modified and unmodified Pd electrode.

The presence of two new additional S 2p peaks that were not previously present for the unmodified Pd sample confirms the presence of L-cysteine on the surface of the electrode and given that the electrode was repeatedly rinsed, it is assumed that the L-cysteine molecules are absorbed onto the Pd surface. This assumption is confirmed by previous work by Feliciano-Ramos, which indicated that the L-cysteine molecules were absorbed onto the Pd surface through the sulphur atom, while leaving the carboxylic acid and amino groups free on the surface (Feliciano-Ramos, *et al.*, 2010).

In order to determine the stability of the L-cysteine modified Pd film, the catalytic performance of the electrode was then assessed through repetitive scanning in ferrocyanide. Cyclic voltammograms detailing the impact of repetitive scanning on the L-cysteine modified Pd film electrode towards ferrocyanide is highlighted in **Figure 4.3.6.**

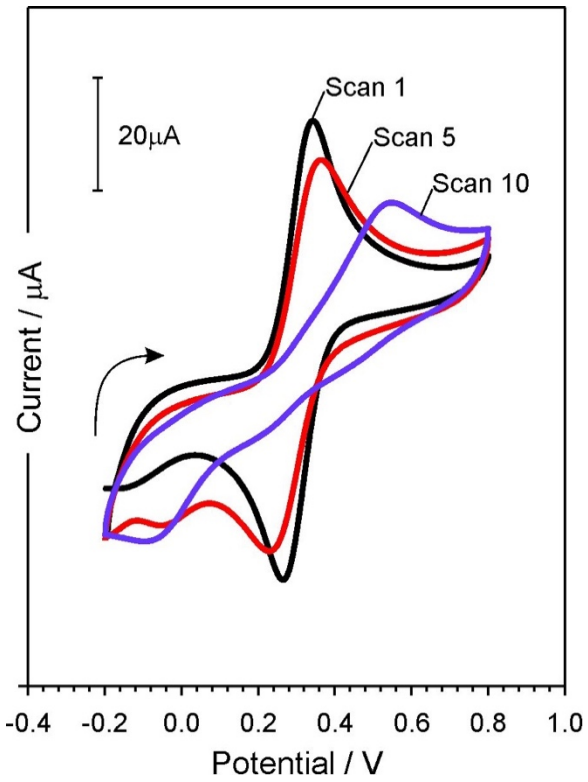

Figure 4.3.6 Cyclic voltammogram detailing the response of the L-cysteine modified palladium electrode towards 10 consecutive scans towards ferrocyanide (2 mM, 0.1 M KCl, 50 mV/s). N_s=10.

Based on the response detailed in **Figure 4.3.6**, the initial scan yields a definite redox couple response with a peak separation of 78 mV, peak current ratio of 1.14, which are

very close to the theoretical; values of 59 mV peak separation and a peak current ratio of 1. However, by the tenth scan the reduction peak of the redox couple has significantly diminished resulting in a quite large peak separation of 327 mV and a peak current ratio is 2.78. Therefore, it is believed that the repetitive scanning of the L-cysteine modified electrode leads to destruction of catalytic performance in the presence of ferrocyanide. It is postulated that the degradation of the electrode response may be due to an electroanalytical effect such as the oxidation of the CSH monolayer as a consequence of the actual scanning process through an EC' process. An exploration into the EC' reaction mechanism is detailed in **scheme 4.1**.

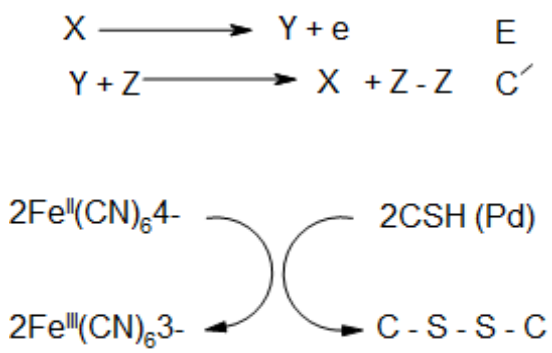

Scheme 4.1 EC' mechanism involving a L-cysteine modified Pd electrode and ferrocyanide.

The reactant (X) is regenerated during the reaction and therefore can react again at the electrode surface, and as the quantity of (Z) is increased the current will also increase as more chemical reactions can occur. As such, there should be a disparity in the relative peak heights of the oxidation and reduction processes with the latter diminishing. In the CV's shown in **Figure 4.3.6** – the ratio of the peak heights for the L-cysteine functionalised electrode is 1 which would negate the possibility of the EC' being central to the enhance performance.

It is clear however that the L-cysteine layer is being gradually degraded and while an EC' mechanism is not the main driver, oxidation of the adsorbed species must be occurring. An alternative explanation could be attributed to air oxidation directly impacting on the immobilised L-cysteine – generating the disulphide and thereby removing it from the electrode. To determine the impact of air oxidation on the

electrode response, the L-cysteine modified Pd film electrode was left uncovered for a period of 24 hours and its response towards ferrocyanide recorded, as detailed in **Figure 4.3.7**.

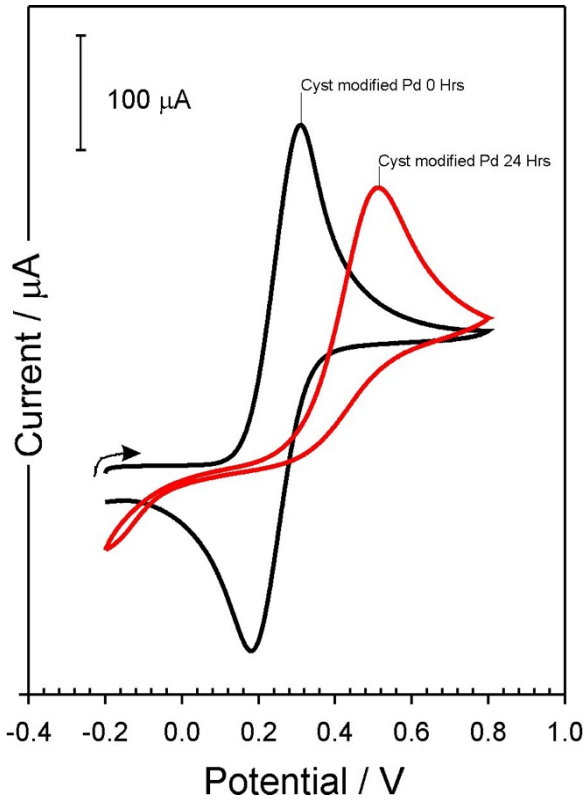

Figure 4.3.7 Cyclic voltammogram comparing the response of a bare palladium electrode and a L-cysteine modified palladium electrode towards ferrocyanide (2 mM, 0.1 M KCl, 50 mV/s) after a 24-hour delay. N_s=2.

It is clear from the cyclic voltammogram presented in **Figure 4.3.7.** that after a period of 24 hours the reduction peak at 0.246 V has dramatically diminished. Therefore, it is believed that exposure to the air has resulted in the generation of disulphide bonds that thereby remove the L-cysteine from the electrode surface, resulting in poor electron transfer. One approach to counter air oxidation would be to degas the solution under nitrogen in a sealed container. However, considering the end application of this sensor is in an aerobic wound environment, this solution would not be applicable.

4.3.5 L-Cysteine Modified Palladium Film

The potentiometric response of the L-cysteine modified Pd electrode in buffer solutions of varying pH are detailed in **Figure 4.3.8**. In contrast to the response observed with the unmodified Pd electrode (**Figure 4.3.2**), the L-cysteine modification provides a distinct and linear response towards the defined pH range.

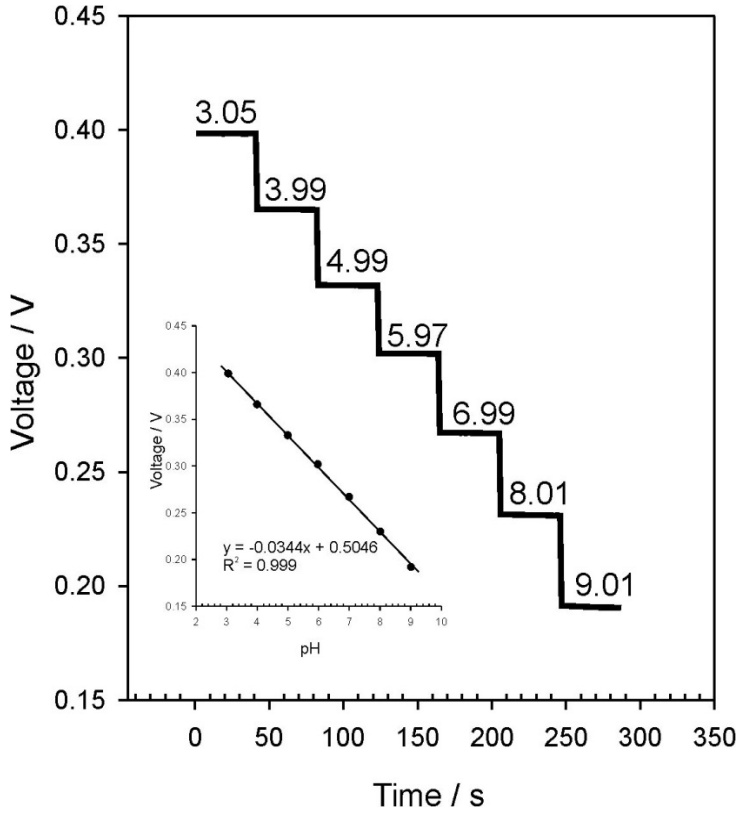

Figure 4.3.8 Potentiometric response of a L-cysteine modified palladium electrode response under various pH regimes. N_s=7, N_{pH}=7

A calibration graph detailing the peak average voltage against pH is shown in the inset of **Figure 4.3.8**. A linear response is observed and the electrode expresses a sub-Nernstian response with a shift of 34 mV per pH unit. The equation of the line was Ep (V/s) = -0.0344 [pH] + 0.5046; R^2 = 0.999; N_{pH} = 7.

To determine the feasibility of this electrode modification in terms of shelf life and reproducibility, the electrode was dipped in L-cysteine then left out for a period of two days before three consecutive pH ranges were conducted. In addition, the pH range

was extended from pH 3 to 10 and scanned at increments of 0.5 pH units. The results of which are detailed in **Figure 4.3.9.**

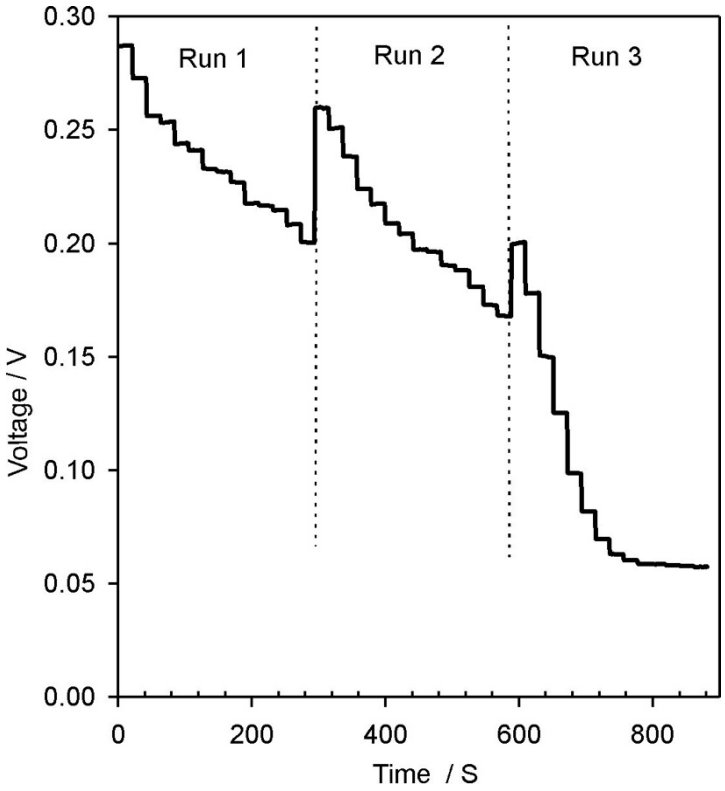

Figure 4.3.9 Potentiometric response of the L-cysteine modified palladium electrode towards A) three consecutive pH regimes.

In terms of variation between each consecutive run, it is evident from **Figure 4.3.9**, that there is a considerable drift between the first and second run recording of pH 3. The responses yielded – **Run 1** ($y = -0.0096x + 0.299$ $R^2 = 0.985$), **Run 2** ($y = -0.0209x + 0.2357$ $R^2 = 0.7853$) and **Run 3** experience significant deterioration in the electrode response ($y= -0.023x + 0.2441$ $R^2 =0.862$).

Examining the potential position of pH 3 over the three consecutive scans indicates there was a drift of 56 mV between the first two pH ranges and a 126 mV difference between the first and the third pH range. This drift could be attributed to the palladium surface being poisoned by the formation of an oxide layer, which could inhibit the reproducibility of the pH range. Considering that the experiment, conducted over a period of less than 15 minutes resulted in such a significant drift, suggests this

system is unsuitable for further investigation as the reproducibility of results was clearly problematic.

4.4 Conclusion

A sputtered thin Pd film was initially selected as a conductive sensing material to potentiometrically confer pH for wound monitoring technologies, due to its well-known properties towards protons. Prior to any experiments the film was initially cycled in 0.1 M H_2SO_4 to clean the surface of the electrode and improve the electron transfer kinetics. The cleaned electrode potentiometric response towards a typical pH range (pH 3 - 9) resulted in two distinct phases (**Figure 4.3.2**). The first phase, pH 3 – pH 5 proved to be insensitive to pH, while the second phase (pH 6 to pH 9), reported a sub Nernstian response (54 mV) with a R^2 value of 0.929. However, considering that the typical pH of skin lies in the region of pH 4.5 - 5.5, this limited range would not be applicable or sensitive enough for wound monitoring.

In order to improve the electrode sensitivity towards pH, the electrode was further modified with a self-assembly monolayer. This modification process was conducted by dip coating the electrode into a solution containing the thiol functional group, L-cysteine. The response of the L-cysteine modified electrode towards ferrocyanide demonstrated a marked improvement in the electron transfer kinetics in comparison to the bare palladium film. Based on XPS analysis (**Figure 4.3.5**), it is believed the L-cysteine molecules are absorbed onto the Pd surface through the sulphur atom, leaving the carbocyclic acid and amino groups free on the surface to conjugate with biomolecules. The stability of the L-cysteine bond was assessed through repetitive scanning (**Figure 4.3.6**), which resulted in a diminished response by the tenth scan. In addition, upon exposure to air for a period of 24 hours, the L-cysteine modified Pd electrode proved to be susceptible to air oxidation (**Figure 4.3.7**).

The L-cysteine modified Pd electrode potentiometric response towards a pH range of 3 to 9 expressed a sub Nernstian response (34 mV/ pH, **Figure 4.3.8**). The stability of this response after a two day delay was investigated by assessing the response after three

consecutive potentiometric pH ranges (**Figure 4.3.9**). A drift of 126 mV was reported by the third consecutive pH range, highlighting the significant impact that repetitive scanning and surface oxidation has on the reproducibility of the electrode response.

The significant degradation of the L-cysteine modified electrode response towards repetitive scanning and air oxidation would prove to be problematic for continuous monitoring of pH within a wound environment. While there is clearly an extensive literature on the use of Pd as an attractive substrate for a variety of sensing applications, it is clear that it only functions well under controlled conditions. The variable conditions of the wound environment and the application demands of the final dressing (ie shelf life, handling etc) appears to critically compromise the selection of Pd in this instance.

Chapter 5

Voltammetric pH Sensing Based on Poly-L-tryptophan Modified Carbon Fibre Mesh

Abstract

The sensing capability of a pH responsive redox wire prepared from a polypeptide homopolymer of L-tryptophan is described. The novel aspect of this research focuses on the electroxidation of the L-tryptophan indole substituents that leads to the production of quinoid functionalities that provide a pH dependent redox signature. The oxidation peak position of the polymer locked quinone components exhibit a Nernstian response (59 mV/pH) over pH 3 – pH 8. The analytical performance of the composite electrode was assessed using defibrinated horse blood as more relevant complex media that could act as a simulated wound environment.

Aspects of the work described in this chapter has been in previously published:

McLister A, Davis J. Molecular Wiring in Smart Dressings: Opening a New Route to Monitoring Wound pH. *Healthcare* 2015;3(3):466-477.

McLister A, Lowry N, Anderson A, McHugh J, Davis J. Novel pH sensing redox wire based on a polyamide homopolymer of L-tryptophan. *Fibers Polym.* 2015;16(10):2294-2297.

5.1 Introduction

It is clear from the previous chapter that attempting to exploit potentiometric techniques with Pd thin films for use in wound monitoring applications can be complicated by drift in the electrode potential used to determine the pH. The use of voltammetric methods as an indirect measure of pH have come to the fore in recent years as an alternative to the more traditional potentiometric systems. These exploit the pH dependence of the electrode potentials associated with the redox transitions of marker compounds. The relationship between pH and electrode potential for compounds possessing acid base functionality has long been recognised and enshrined in the Nernst equation.

The Nernst equation can be manipulated (as previously described in Section 3.6) to calculate the electrochemical shift (E) due to a log change in Hydrogen ion concentration (i.e. 1 pH unit). Therefore, provided the temperature remains constant, a potential shift by the change of 1 pH unit would result in a 59.1 mV shift at 25^{o}C where n=1.

$$E = E^{O} + \frac{2.303RT}{nF}\log[H^{+}] + log\frac{[B]}{[A]}$$

…Eq 5.1

The Nernstian equation is effectively the equation of a straight line;

$$Y = mx + c$$

where

Y = E = the measured electrode response in mV

M = 2.303RT/nF = the gradient of the line

X = Log(b)

C= E^{0} = the intercept on the y axis …Eq 5.2

Therefore, an electrode is said to express a Nernstian response over a given concentration range if a plot of the potential difference versus the logarithm of the ionic activity of the species present in the solution, is linear with a gradient of 59.1 mV.

In principle, the marker compound can be any species capable of being oxidised or reduced at the electrode and whose electrode processes involves the transfer of protons. As the pH changes, it can be expected that the position of redox peaks will also change in accordance with the predictions of the Nernst equation (Eq 5.1). A schematic representation of the shift in potential with pH is highlighted in **Figure 5.1.1**. Determining the peak potential can therefore enable an indirect measure of the solution pH.

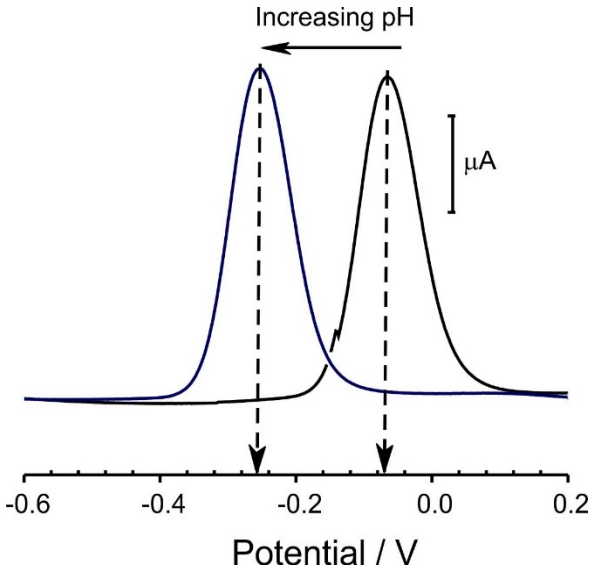

Figure 5.1.1 Schematic representation of the effect of pH on the voltammetric peak position.

The marker compound can be a diffusing solution based species (Phair, *et al.*, 2011), immobilised as a single layer (Lee, *et al.*, 2012; Park, *et al.*, 2013)**,** polymer bound (Mcister and Davis, 2015) or generated directly as an intrinsic species at the electrode surface (McLister, Lowry, *et al.*, 2015). Irrespective of the nature of the material, the principal advantage over potentiometric systems should be a relative insensitivity towards drift and, therefore, should be a more robust approach for periodic or continuous monitoring applications associated with wound diagnostics.

Quinone/hydroquinone redox couples are typically employed in voltammetric sensing applications and there have been numerous approaches to immobilising such species onto electrodes in the pursuit of reagentless pH sensors. These have been designed with environmental sensing as the intended application and thus could encounter issues of biocompatibility when considering their direct translation

to biomedical contexts. In this work, quinone systems are again used as the principal components in the indirect measurement of pH but the intention was to encase these within a polypeptide layer composed of L-tryptophan. It was envisaged that the outer layer, composed of the amino acid, would minimise biocompatibility issues as indicated in **Figure 5.1.2**.

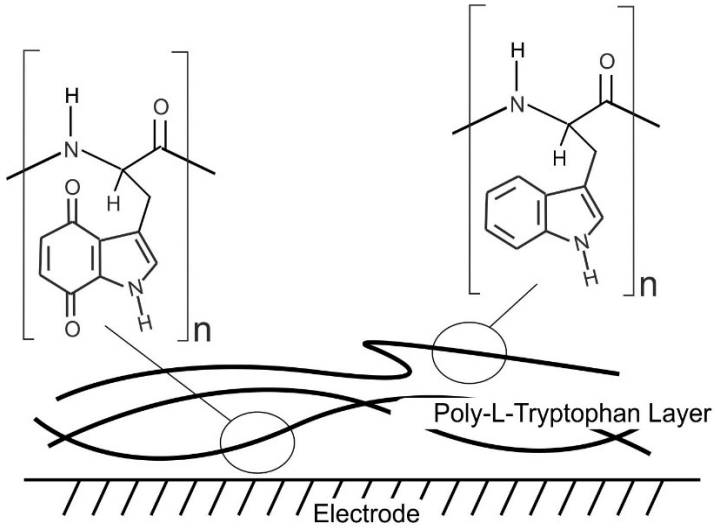

Figure 5.1.2 Schematic of the proposed poly-L-tryptophan composite structure.

Ordinarily, the inclusion of quinone systems within the polymer network would require elaborate synthesis but in this instance, a novel approach to the electrogeneration of the quinone groups within the polypeptide backbone was investigated. The electrochemical characteristics of L-tryptophan are well established and, given the amino acid's role in serotonin biosynthesis (Murc, *et al.*, 2000)**,** there has been considerable research effort directed towards the development of electroanalytical methods for its detection (Szunerits, *et al.*, 2010; Beitollahi, *et al.*, 2014; Dehdashtian, *et al.*, 2016; Chen, *et al.*, 2017; Liu, *et al.*, 2017)**.** In contrast, peptide polymers consisting of amide linked L-tryptophan have remained unexplored.

from an electrochemical perspective and thus its deployment as the foundation of a sensor is entirely novel. The work builds on previous studies of monomeric L-tryptophan where it has been demonstrated by Enache and colleagues that oxidation of the indole substituent can lead to the production of indole-quinone hybrid species as indicated in **Scheme 5.1** (Enache, *et al.*, 2011).

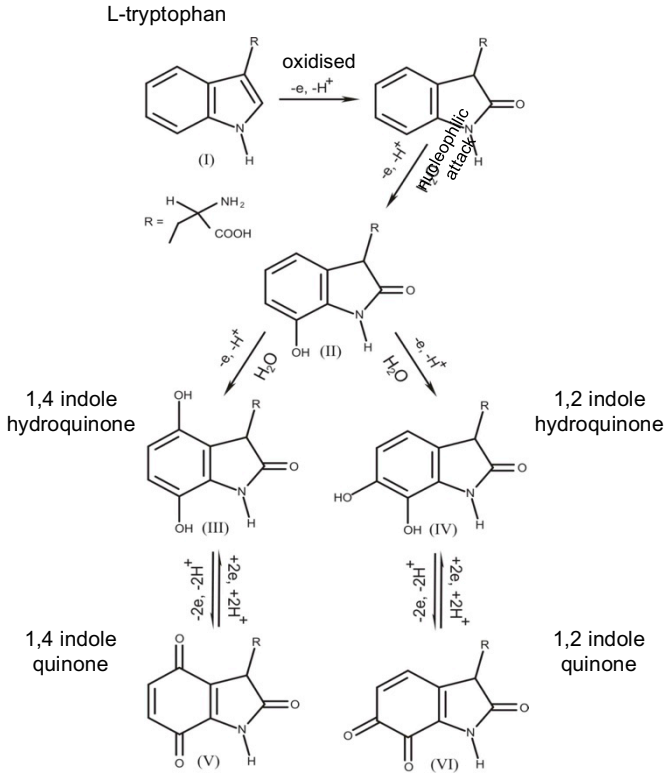

Scheme 5.1 Electro-oxidation of L-tryptophan leading to the generation of 1,4 and 1,2 indole quinones. Adapted from (Enache, *et al.*, 2011).

It was therefore anticipated that the oxidation of a polymer confined L-tryptophan would lead to similar 1,4 and 1,2 products (**Scheme 5.1** structures V and VI respectively) being generated at the electrode interface. The implication being that the deposition of the polymer onto a suitable disposable substrate (i.e. carbon fibre) could enable the production of the quinone pH receptors *in situ* at the electrode but with the outer layers remaining essentially unmodified and thereby maintaining a degree of biocompatibility.

Carbon fibre has proven to be a versatile electrode material that poses little inherent toxicological issues for sensor development and is extensively used in the construction of *in vivo* microelectrodes (Wightman, 1988; Gerhardt, *et al.*, 2001). It was therefore selected as the base substrate upon which to immobilise the poly-L-tryptophan layer. The fibre itself is relatively inexpensive and thus could be useful from the perspective of creating a disposable sensor (Phair, *et al.*, 2013; Li, *et al.*, 2014) and could be ideal in the context of wound monitoring where dressings are

replaced with a relatively high frequency. The intention here was to investigate the construction of a composite system employing carbon fibre/poly-L-tryptophan and critically assess its potential applicability as the basis of a point of care sensor for measuring pH.

5.2 Experimental Details

5.2.1 Materials

All experiments were conducted at 22^{o}C ±2^{o}C in Britton Robinson buffer in a range from pH3 to pH 10 (acetic, boric and phosphoric acids – each with a concentration of 0.4 M and adjusted to the appropriate pH through the addition of concentrated sodium hydroxide). The carbon fibre mesh and single carbon fibre filament (10 μm diameter), employed as the working electrodes, were both supplied by Goodfellow Research Materials Ltd (Cambridge, UK). The blood used for the measurements was defibrinated Horses Blood (DHB) and was purchased from TSC Biosciences (Buckingham, UK)

5.2.2 Electrochemical Configuration

Unless stated otherwise, all electrochemical measurements were conducted using a μAutolab type III computer controlled potentiostat (Eco-Chemie, Utrecht, and The Netherlands). A three-electrode configuration consisting of a single carbon fibre filament as detailed in subsequent section (5.2.3), a commercial Ag|AgCl (3 M KCl) half-cell reference electrode (Alvatek, Hampshire, UK) and a platinum wire counter electrode. Cyclic voltammograms were recorded at a scan rate of 50 mV/s, while square wave voltammograms were recorded using a frequency of 25 Hz, a step potential of 2 mV and an amplitude of 20 mV.

5.2.3 Sensor Design and Modification

A section of the mat carbon fibre mesh was cut to size and sandwiched between two laminate sheets with a 16 mm^2 square window. A similar process was employed for the single 10-micron carbon fibre filament – in this instance the single fibre length (4 mm) traversed the window. The carbon fibre working electrode was modified via the process of anodisation in 0.1 M NaOH using a fixed potential of +2 V with varying time periods ranging from 0 to 300 seconds. The small diameter of the single filament fibre meant that the anodisation time was truncated to 10 - 60 s to prevent critical erosion of the fibre through exfoliation which can lead to breakage of the fibre over prolonged durations.

Poly-L-tryptophan (MW: 5000-15,000, Sigma-Aldrich, Dorset, UK) was dissolved in DMF/acetonitrile (5 mg/mL) and an aliquot, typically 25 μL was applied to the electrode. The polymer was deposited through the process of drop casting onto the surface of the window of the working electrode and left overnight to allow for the evaporation of the solvent.

5.3 Results and Discussion

The carbon fibre electrode was modified with poly-L-tryptophan through drop casting a solution (5 mg/mL) of the polyamide on to the electrode surface and allowing the solvent to evaporate. Initial investigations of the polymer modified electrode response in pH 7 buffer solutions were conducted using cyclic voltammetry. Representative voltammograms are shown in **Figure 5.3.1** where a well-defined oxidative peak process can be observed at +0.91 V on the first forward scan. It is important to note that there is no corresponding reduction process and therefore it is clear that this initial oxidation is irreversible.

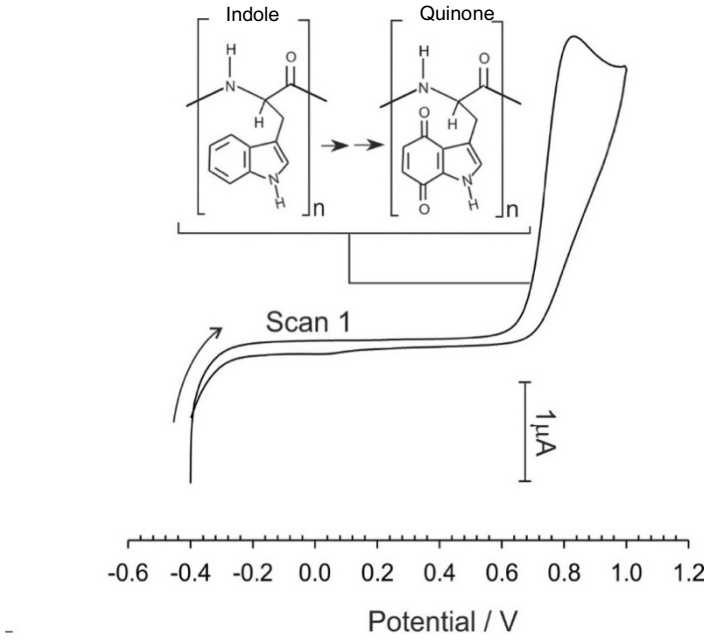

Figure 5.3.1 Cyclic voltammogram detailing the initial response of a poly-L-tryptophan modified carbon fibre electrode in pH 7 buffer. Conversion of the indole units to the corresponding quinoid forms Scan rate: 50 mV/s. N_s= 1.

A separate peak process can however be observed on the reverse scan at +0.05V and is attributed to the reduction of quinoid species arising from the initial oxidation process as previously suggested by Enache and co-workers (Enache, *et al.*, 2011). The basic mechanism, with regards to the polyamide L-tryptophan, occurring in the first scan is abridged in **Figure 5.3.2** and it is anticipated that it will follow the same pathways as the oxidation of monomeric L-tryptophan outlined previously in **Figure 5.3.1**. The hypothesis that electrogenerated quinone groups are produced was corroborated through inspecting the voltammetric profile of the second scan whereby the corresponding quinoid oxidation peak (absent on the first scan) can be observed at +0.12 V as indicated in **Figure 5.3.2.**

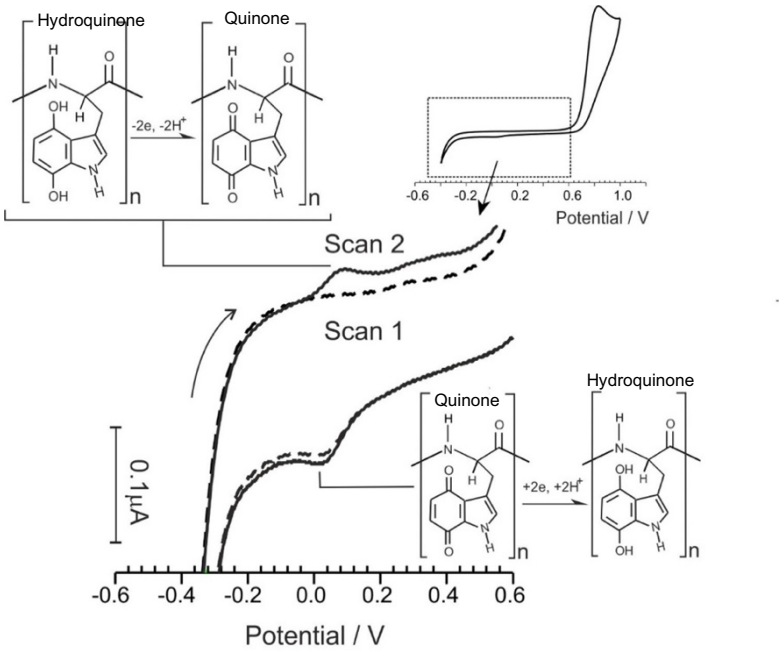

Figure 5.3.2. Consecutive cyclic voltammograms detailing the response of a poly-L-tryptophan carbon fibre electrode: redox cycling between the reduced and oxidised forms of the electrogenerated indole-quinone polymer. N_s=2

It is important to note that these new peak processes only occur after the oxidation of the L-tryptophan-indole component and that repetitive scanning over a narrower potential region (-0.2 V to +0.6 V for example) does not change the voltammetric profile. It was also necessary to ensure that the quinone generated is still directly attached to the polymer backbone and that the various transitions have not lead to chain scission. Thus, the electrode was removed after these initial scans, rinsed and then placed within fresh buffer – the assumption being that if the quinone groups are cleaved from the polymer backbone upon their formation they would be free to diffuse away. Cyclic voltammetry was again applied to investigate the electrode response post modification and rinse and representative scans are highlighted in **Figure 5.3.3**. The redox peaks were retained confirming that the electrogenerated quinone systems are retained within the film. Further evidence, that the quinone groups are locked in to the polymer network was obtained through examining the peak response with scan rate - a standard diagnostic for confirming the immobilised redox behaviour (Compton, *et al.*, 2011)**.** A linear relationship was found, indicated in **Figure 5.3.4.**

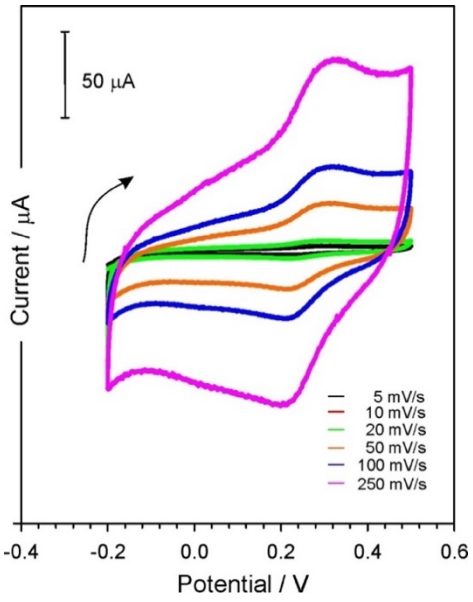

Figure 5.3.3. Cyclic voltammograms detailing the influence of scan rate on the response of the electrogenerated indole-quinone polymer in fresh pH 7 buffer.

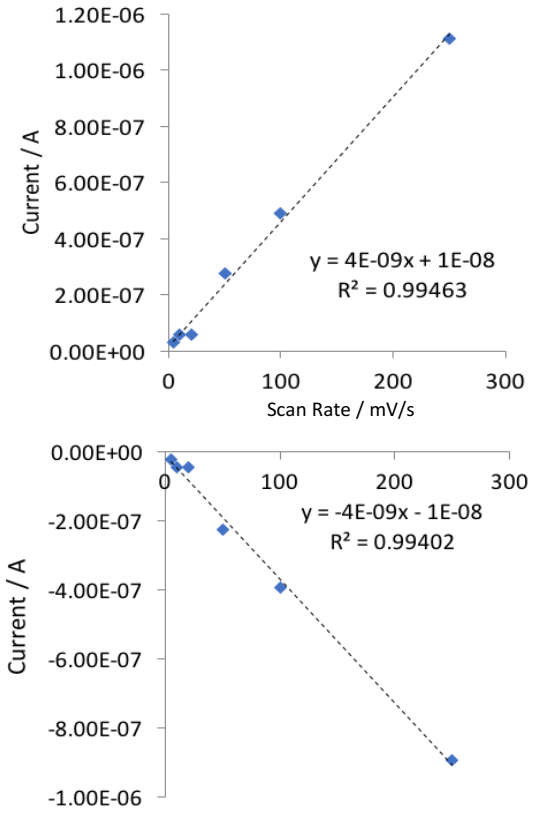

Figure 5.3.4 Influence of scan rate on the peak height – confirming behaviour characteristic of an immobilised species.

The core rationale was to exploit the variation of peak position with pH as a means of indirectly measuring the latter but it is clear from the voltammograms in **Figure 5.3.3** that the broad peak shapes would create a degree of ambiguity. It has been previously described (Section 5.1) that the peak potential is expected to shift by 59 mV/pH unit (on the assumption of a $2H^+$, 2e process) and thus even small errors in ascribing the peak position could create considerable error. There is a need for the acquisition of sharp voltammetric peaks that would improve the accuracy of recording peak potentials.

Square wave voltammetry was selected as a more appropriate technique in this instance as the differential step method, previously described in **Section 3.5.5** provides a means of reducing the capacitance background (common to cyclic voltammetry) resulting in a much sharper voltammetric signature. Square wave voltammograms detailing the first two scans of a freshly prepared but unanodised poly-L-tryptophan modified electrode are detailed in **Figure 5.3.5**. The initial features are analogous to those observed during the cyclic voltammetry experiments (**Figure 5.3.1**) with a large oxidation peak (+1.0 V) on the first scan. This is again attributed to the oxidation of the indole substituent of the L-tryptophan monomer resulting in the production of the quinoid moieties (**Figure 5.3.2**, **I→V**).

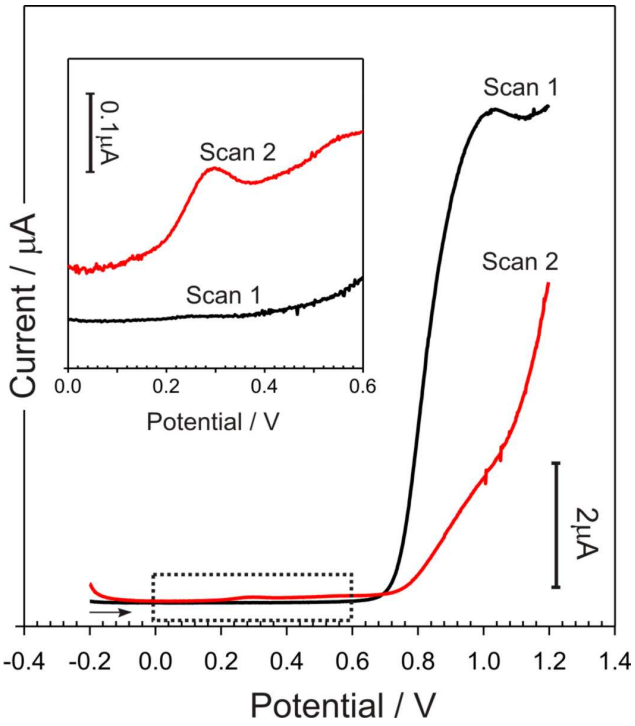

Figure 5.3.5. Square wave voltammograms of an unanodised poly-L-tryptophan modified carbon fibre electrode in pH 3 buffer. N_s=2.

Closer inspection of **Figure 5.3.5** reveals that on the second scan, the initial oxidation observed at +1.0 V on the first scan) is absent and suggests that the electrochemically accessible indole groups within the polymer network are oxidised on the first sweep. Examination of the second scan reveals the presence of a new oxidation peak (+0.3 V) corresponding to the quinone product. The latter is analogous to the process observed earlier with the cyclic voltammograms (**Figure 5.3.3**). Initiating the second scan at -0.3 V will lead to the immediate reduction of the quinoid species (**II**) generated in the first scan to the hydroquinone form and then, as the scan progresses towards more positive potentials, will be re-oxidised leading to the peak process observed at +0.3 V. It is important to note that while the overall processes is analogous to that observed with the cyclic voltammetry, the peak definition obtained with the square wave methodology is superior and this is highlighted when examining the voltammetric profile in more detail in the Inset within **Figure 5.3.5**.

Qualitatively, the quinone peak is better resolved than that obtainable through cyclic voltammetry but, the peak current magnitude remains poor and there is a

possibility that the peak could be swamped when considering the application of the electrode within complex media where there could be competing electrode processes. This could be attributed to poor electron transfer from the base substrate to the redox groups distributed along the polymer backbone. It was anticipated that the electrode response could be further improved through pre-anodisation of the substrate prior to the immobilisation of the poly-L-tryptophan. It has long been established that edge plane sites rather than the more common basal plane (**Figure 5.3.6**) are known to enhance electron transfer kinetics (Banks, *et al.*, 2005) and therefore it was envisaged that exfoliating the carbon surface would increase the population of edge sites within the carbon fibre framework and thereby improve the electrode response to the L-tryptophan polymer and the electrogenerated quinones.

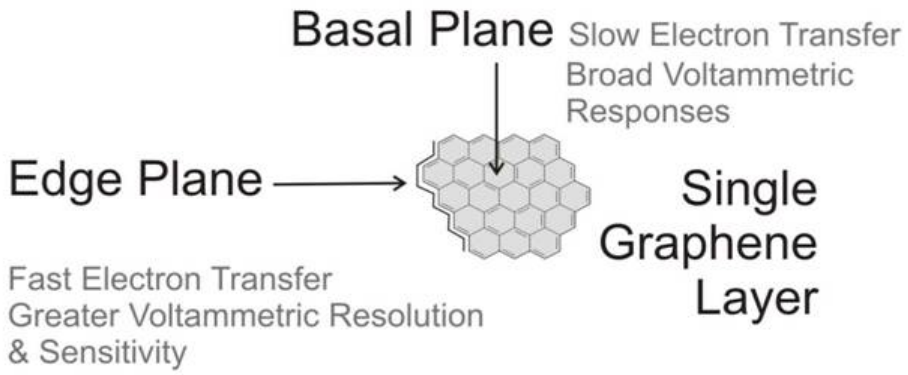

Figure 5.3.6 Generic representation of the electron transfer sites at carbon based electrodes.

5.3.1 Anodisation of the Carbon Fibre Mesh

The carbon fibre mesh used in this work is composed of a relatively open network of fibres that typically have diameters around 10 microns and expected to consist for predominately basal plane morphology (Moore, *et al.*, 2004; Banks, *et al.*, 2005, 2006; Lawrence, *et al.*, 2007). A representative sample of the fibre mesh is highlighted in the electron micrograph detailed in **Figure 5.3.7** (McLister, Lowry, *et al.*, 2015)**.** Various strategies can be applied to exfoliate carbon and include

plasma (Phair, *et al.*, 2013), chemical (Paixão, *et al.*, 2002; Di, *et al.*, 2003) and electrochemical (Wang, *et al.*, 2000; Li, *et al.*, 2004; Lin, *et al.*, 2005; Chen, *et al.*, 2007; Kotkar, *et al.*, 2007; Tao, *et al.*, 2007) methodologies. The latter was employed in this instance as a relatively simple method through which to manipulate the structure of the fibres and thereby, hopefully improve their electroanalytical performance (Wang, *et al.*, 2000b; Paixão, *et al.*, 2002). Ferrocyanide was used as a standard redox model through which to assess changes in electrode behaviour and determine the optimal conditions.

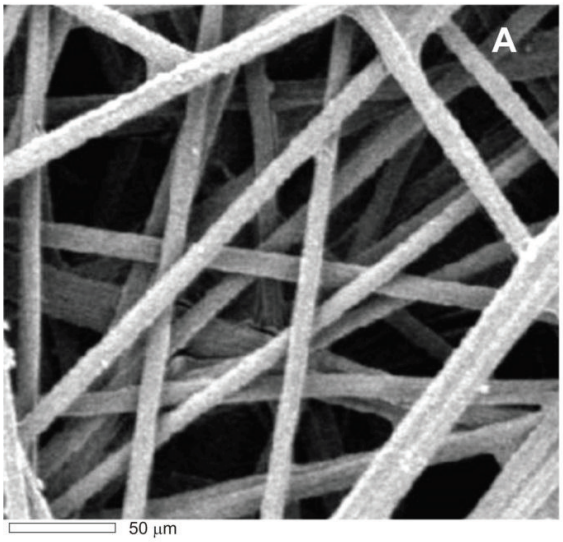

Figure 5.3.7 Scanning electron micrograph of a section of unmodified carbon fibre mesh used in this work (McLister, Lowry, *et al.*, 2015).

Although the fibres are conductive (electrical resistivity; through plane 80 mΩcm, in plane 5.8 mΩcm), the electrode performance can be relatively poor (Toray, 2017). Cyclic voltammograms detailing the response of the carbon fibre electrode towards ferrocyanide (2 mM, 0.1 M KCl, 50 mV/s) before and after electrochemical anodisation are compared in **Figure 5.3.8**.

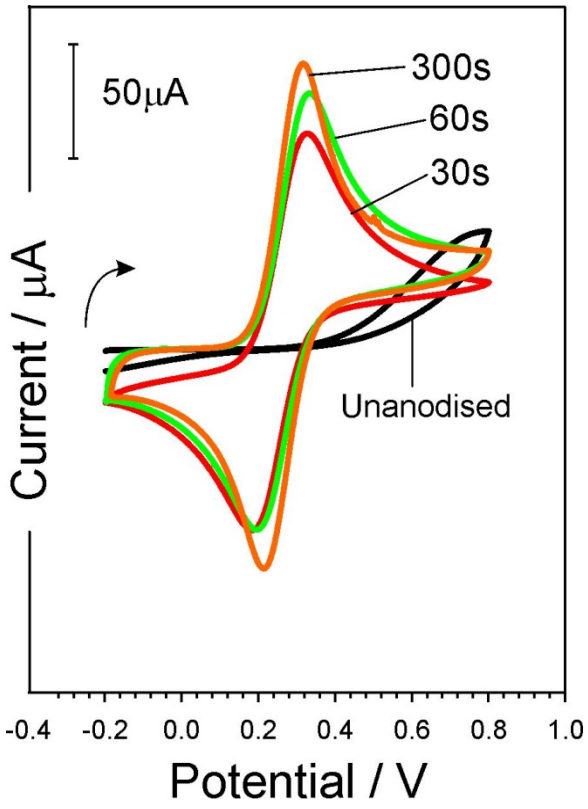

Figure 5.3.8 Cyclic voltammograms detailing the effect of varying anodisation times on the response of the carbon fibre electrode towards 2 mM ferrocyanide in 0.1 M KCl (Scan rate: 50 mV/s). N_s=4

The response of the unanodised fibre exhibits a very poor response to the ferrocyanide redox probe with poor peak definition (*cf.* the L-tryptophan system) and large peak separation greater than 800 mV, suggesting irreversible behaviour. Electrochemical pre-treatment of the fibre however was found to dramatically change the response with both oxidation and reduction processes clearly identifiable and consistent with the theoretical predictions. The ratio of the peak heights is equal to 1 and the peak separation is close to the ideal 59 mV predicted by Nernst (Compton, *et al.*, 2011).

While the improvement in the electrode response is attributed to the exfoliation of the carbon surface it must be acknowledged that this is accompanied by significant changes in the chemistry of the carbon (and hence electrode) interface. These changes have been previously studied using X-ray Photoelectron Spectroscopy (XPS). It can be expected that in the basal structure – the predominate form of the carbon will be sp^2 but, upon oxidation in alkali, the aromaticity of the graphite ring

structure will diminish and more oxygen functionalities will arise. This is seen in the spectra before and after anodisation (**Figure 5.3.9**) where there is a significant increase in C=O and COOH groups and it is likely that these will aid electron transfer (Anderson, *et al.*, 2014)**.** This is supported by the work of Tao and colleagues who observed similar changes when dealing with immobilised multiwalled carbon nanotubes (MWNTs) on organically modified silicate films (Tao, *et al.*, 2007)**.**

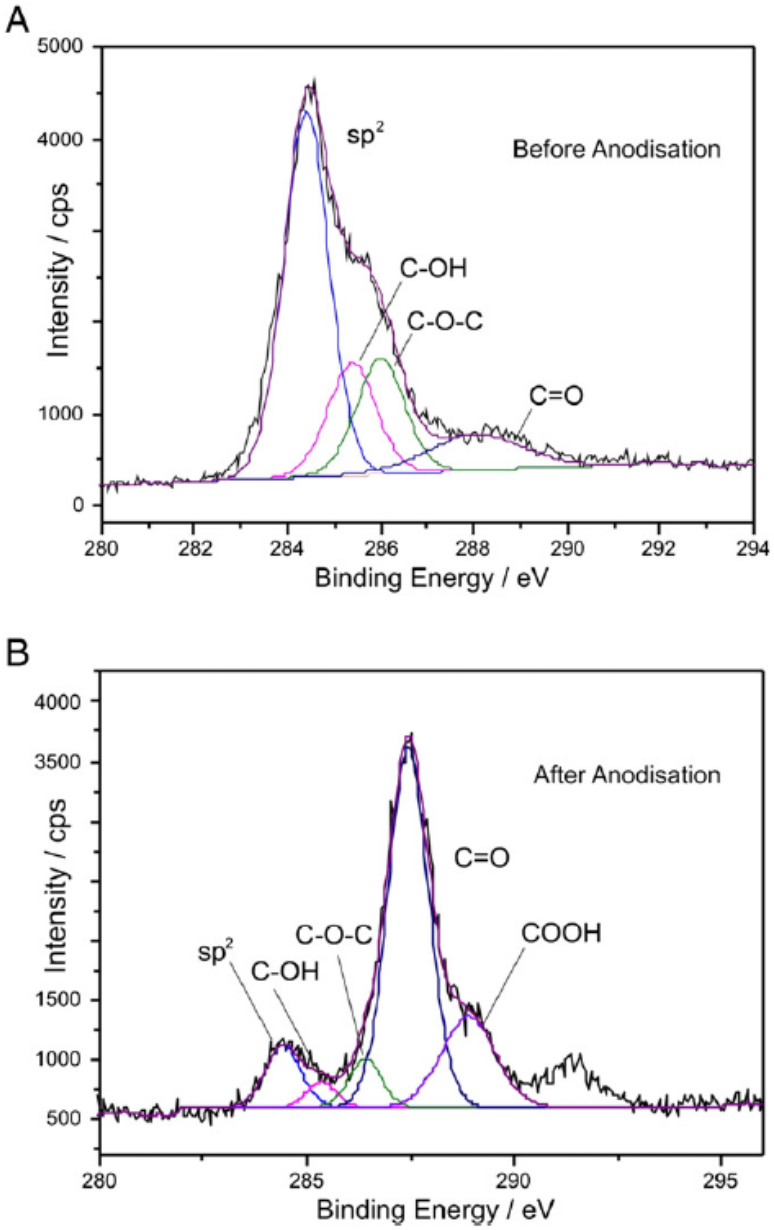

Figure 5.3.9 XPS spectra obtained before (A); and after (b) electrochemical anodisation. Reproduced with permission from (Anderson, *et al.*, 2014).

Based on the electrode response in **Figure 5.3.8**, it is evident that the process of anodisation has a significant impact on the voltammetric profile, in that, as the

anodisation time is increased, the current also increases. This response can be attributed to the exfoliation of the carbon fibre, which ultimately results in a greater surface area and an analytically significant distinct peak position. Increasing the anodisation time leads to an increase in the peak magnitude as the surface is progressively modified. Therefore, the optimal anodisation period was determined as 300 s.

5.3.2 Anodised Carbon-Poly-L-Tryptophan Composite

The process of anodic exfoliation of the fibre will inevitably result in the incorporation of oxygen functional groups at the electrode interfaces as highlighted by the XPS results. It must be acknowledged that quinoid species will also arise as indicated in **Figure 5.3.10** and again this is suggested through the increase in the C=O signatures (accounting for 55% of surface carbon moieties) in the XPS profile post anodisation.

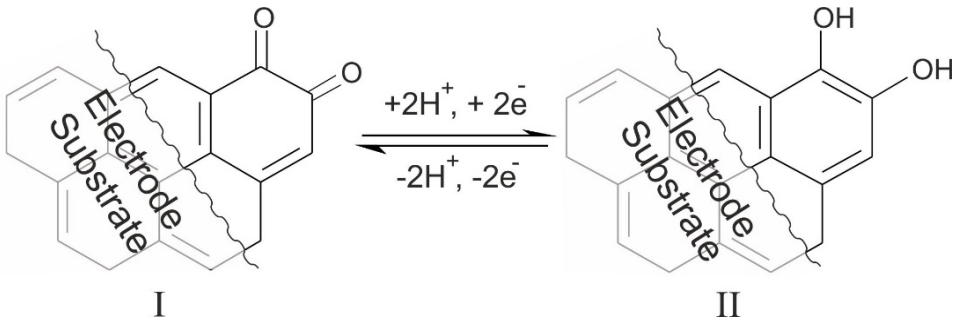

Figure 5.3.10 Schematic representation of the redox transitions associated with quinoid groups endogenous to the carbon fibre substrate. Reproduced with permission (Anderson, *et al.*, 2014)

These quinoid species will possess their own particular redox characteristics and it could be envisaged that through increasing the population of such species at the electrode interface that their close proximity to the electrogenerated quinones within the L-tryptophan polymer would further facilitate electron transfer.

Square wave voltammograms detailing the response of the anodised carbon electrodes with and without the L-tryptophan polymer in pH 3 buffer are compared in **Figure 5.3.11**. Considering the bare, anodised electrode first (the blank scan), a broad oxidation processes can be observed on the first scan. Given that there are

no oxidisable species within the solution, then the oxidation peak can only be attributed to the formation of quinones endogenous to the carbon structure. Note that there were no similar processes on the unanodised system and therefore the peak arising here is due to quinones created as a consequence of the anodisation.

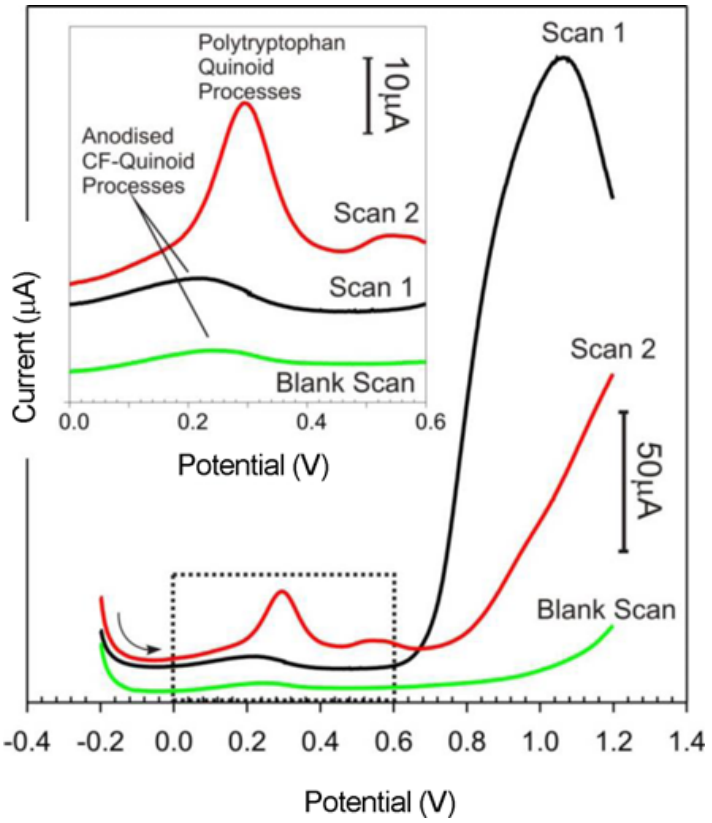

Figure 5.3.11 Square wave voltammograms detailing the response of an anodised carbon fibre electrode to pH 3 buffer before (Blank scan) and after the addition of poly-L-tryptophan, N_s=3. Reproduced with permission from (McLister, Lowry, *et al.*, 2015).

Examination of the voltammetric response to the poly-L-tryptophan modified anodised carbon fibre electrode reveals behaviour which largely mirrors that observed previously with the unanodised system. There is however a significant increase in the current (20 fold) and the peak definition of the electrogenerated quinone systems. It could be postulated that the endogenous quinones on the carbon, acting in concert with the increased edge plane structuring, have created a more favourable nanostructured interface through which to connect to the indole-quinone groups within the polyL-tryptophan redox wire.

5.3.3 Response to pH

Given the improved resolution of the indole-quinone peak as a consequence of pre-anodising the carbon interface, the next phase is to investigate whether the system could be utilised as a viable pH sensor. The response of the poly-L-tryptophan electrode after oxidation and conversion of the indole substituent to the quinone form towards buffers of varying pH are shown in **Figure 5.3.12**.

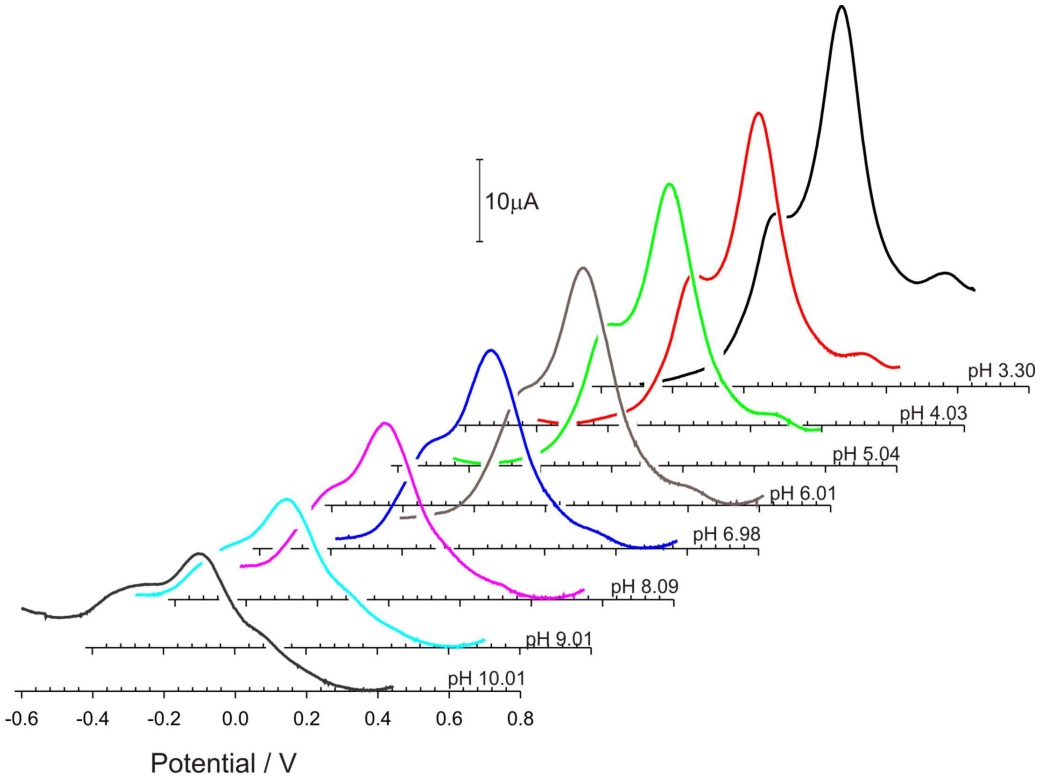

Figure 5.3.12. Square wave voltammograms detailing the response of a modified poly-L-tryptophan redox wire in Britton Robinson buffer solutions covering the range pH 3 - pH 10. N_s=24, N_{pH}=8

The oxidation of the electrogenerated indole-quinoid substituents provides a distinct peak process which can be ascribed without ambiguity. The magnitude of the peak does however reduce as the pH is increased and can be attributed in part to the electrochemical processes involved where there are fewer protons available. Nevertheless, the response over pH 3 to pH 8 was found to exhibit ideal Nernstian behaviour (pH 3-8; E_{pa} /V = -0.059 pH + 0.4673; N = 7; R^2 = 0.999). Testing the probe above pH 8 however leads to a deviation in the response with peak separation between pH 9 and pH 10 falling to 40 mV. This can be attributed to the system moving towards a 2 electron, 1 proton regime brought about by the lack of

proton availability under alkaline conditions. It should be noted that the measurements for the data presented in **Figure 5.3.12** were repeated in triplicate and that the standard error is in the range of +/- 2 mV which corresponds to a measurement error of 0.04 pH units.

5.3.4 Simulated Wound Environments

The typical wound environment is complex and comprised of a huge number of different molecules and, it is inevitable that many will be electroactive. To assess the viability of the proposed sensor response, explorative testing in defibrinated horse blood was undertaken. This will contain both mono and macromolecular species and cellular components that could ultimately interact or obscure the signal arising from the poly-L-tryptophan modified electrode. Square wave voltammograms detailing the response of the modified electrode in defibrinated horse blood are shown in **Figure 5.3.13**. The oxidation peak attributed to the quinoid component within the poly-L-tryptophan film is easily identifiable. A blank scan run using an anodised carbon fibre without the presence of the poly-L-tryptophan did not reveal any peak process within the potential region highlighted in **Figure 5.3.13.** This served to confirm that the peak formed wasn't the result of the oxidation of other components already present such as ascorbate.

The pH of the defibrinated horse blood was extrapolated by examining the peak position of the quinoid oxidation and plotting it against the calibration equation previously noted in **Figure 5.3.12**. Four consecutives square wave voltammograms were conducted, as detailed in **Figure 5.13B**, which resulted in an average peak position of + 0.082 V, and a standard error of the peak measurements of ± 2 mV, based on N = 4.

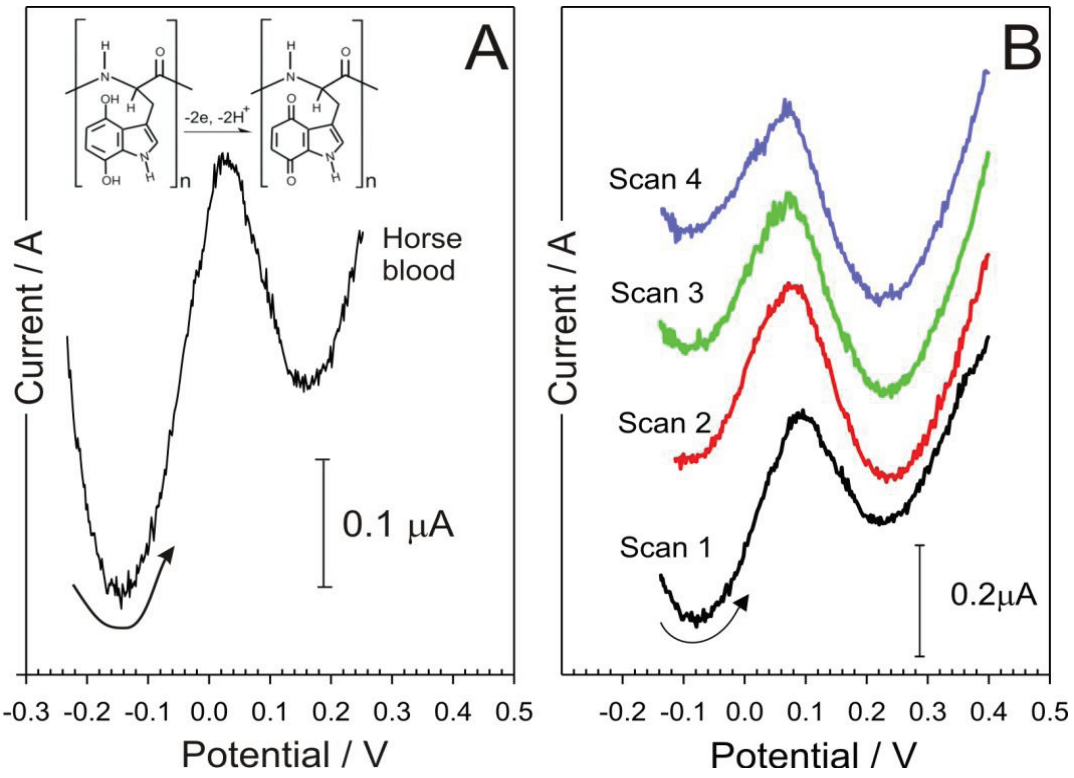

Figure 5.3.13 Square wave voltammograms detailing the poly-L-tryptophan modified mat carbon fibre electrode response to defibrinated horse blood (A) and consecutive scans (B). N_s=1; N_s=4.

It should be noted that this methodologically similar procedure used conventional pH probe measurements whereby the potential of the unknown samples is used in conjunction with a preset calibration equation. Based on the similar process, the defibrinated horse blood solution was found to be pH 7.41, while the conventional pH probe reported a value of pH 7.31. Although this result does not lie in the region of accuracy (± 0.05 pH units) reported by Schneider et al. to monitor chronic wounds fluctuations (Schneider, *et al.*, 2007) it does however lie within the typical region of blood pH. Therefore, it could be envisioned that it could be used to monitor changes within the wound environment associated with infection – i.e. bacterial growth/colonisation.

5.4 Conclusion

The novel aspect of this research is based on the electrochemical oxidation of the polymer bound L-tryptophan to create a quinoid functionality that provides a

simple means of generating pH responsive centres which are locked onto the electrode substrate. It avoids much of the complexities of chemical synthesis and surface modifications that have been used in previous pH sensing designs. The quinone centres themselves demonstrate Nernstian behaviour (**Figure 5.3.12**) and the oxidation peak used to extract the analytical signal has been shown to lie in a potential region where there are no interfering compounds when challenged in defibrinated horsed blood **(Figure 5.3.13**). The response of the electrochemically functionalised L-tryptophan polymer provides a clear and unambiguous signal over a wide pH range of biomedical relevance.

Moreover, it has been shown that the redox interaction between the polyamide groups and the electrode surface is facilitated by the presence of endogenous quinoid functionalities. That latter has important ramifications for bioelectronic wiring of peptide/proteinaceous components at carbon electrodes. The use of the L-tryptophan homopolymer is but a model system and it could be envisioned that other peptides, containing a defined sequence of L-tryptophan units, could be used as reporter molecules and may go some way to creating tailored sensing interfaces.

Chapter 6

Investigating the Use of Electrogenerated Quinone Dimers entrapped onto the Surface of a Carbon Screen Printed Electrode for Wound Monitoring Technologies

Abstract

A carbon-based screen printed electrode was employed to monitor pH, by exploiting the quinone dimer that was generated from the electrochemical oxidation of salicylate and adsorbed onto the electrode surface. The electrode surface was then coated with a layer of Nafion® to entrap the electrogenerated dimer. This modification resulted in the electro-oxidation of the dimer bound at the electrode surface providing a novel pH dependent response that exhibited a sub Nernstian response (51 mV/pH) over a pH range (pH 3 – pH 8). The analytical performance and stability of the dimer modified screen-printed electrode was assessed using defibrinated horse blood as a simulated wound environment.

Aspects of the work described in this chapter have been in previously published:

Rawlinson S, McLister A, Kanyong P, Davis J. Rapid determination of salicylic acid at screen printed electrodes. *Microchem. J.* 2018, 137: 71 - 77.

6.1 Introduction

The previous chapter looked at exploiting the electrogenerated quinoid functionalities to create a polymer bound redox signature that was pH dependent. However, the brittle nature of the carbon fibre substrate does not lend itself towards the high degree of flexibility required to conform to the morphological variability encountered with diabetic foot ulcers. Carbon screen printed electrodes (SPEs) were investigated as an alternative substrate for the sensing layer due to the versatility inherent in the manufacturing technique. It was envisaged that direct printing onto conventional wound dressings could be achieved in the future. As such, this approach would stand in marked contrast to the brittleness associated with mat carbon fibre (Sharp, *et al.*, 2008). The use of screen printed electrodes have been extensively exploited as a sensing substrate for various biomedical applications: glucose sensors (Raza, *et al.*, 2018), wound monitoring (Kassal, *et al.*, 2015) and biomarker detection (Kanyong, *et al.*, 2016). Although the unmodified form of the screen-printed electrode has been reported to exhibit poor electron transfer kinetics at the substrate-solution interface, it was anticipated that surface modifications using electrochemical anodisation, as per the processes discussed previously in Chapter 5, could enhance the performance at the SPE.

The main rationale behind this body of research was to examine the response of electrodeposited films with a variety of different acid/base functionalities, and determine whether it was possible to confer pH sensitivity to the underlying substrate. The main approach adopted in this chapter was focused on the response of the quinone by-products arising from the electrochemical oxidation of substituted phenols, towards a clinically relevant pH range (pH 3 – pH 9).

In recent years, there has also been a steady interest in the use of voltammetric approaches to measure local pH. Recent work by Lawrence and co-workers, investigated a range of substituted phenols, including salicylic acid, for use as a voltammetric pH sensor. This work primarily focused on the development of a voltammetric pH sensor for environmental monitoring applications (Dai, *et al.*,

2015). However, it also provided the foundation for this investigation into an alternative approach to monitoring pH using salicylic acid and adapting it for biomedical applications.

The electrochemical oxidation of phenols typically occurs via a 1- electron 1 proton oxidation, resulting in the formation of a passive layer on the electrode surface (Comninellis, *et al.*, 1991; Stradins, *et al.*, 1993). However, Enache and co-workers have suggested that the substituted phenols follow an electrochemical – chemical – electrochemical (ECE) reaction, in which the phenol is initially oxidised by a 1 electron 1 proton transfer which generates a radical species. This radical species could then react with water molecules to be further oxidised and electropolymerised as indicated in **Scheme 6.1** (Enache, *et al.*, 2011). It is believed that the radical species generated through the 1 electron 1 proton step and its tautomers could alternatively produce a self electropolymerisation, that could potentially result in a pH sensitive redox compound.

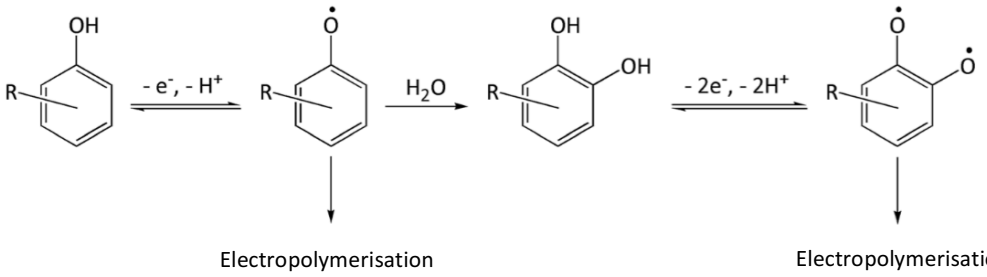

Scheme 6.1 ECE reaction and polymerisation pathway of substituted phenols. Reproduced with permission (Dai, *et al.*, 2015).

The selected substrates for this investigation include, tyramine, resorcinol and salicylic acid as detailed in **Figure 6.1.1** Each of these substrates were investigated in terms of their electrochemical applicability to monitor pH, however, a particular focus shall be trained on salicylic acid.

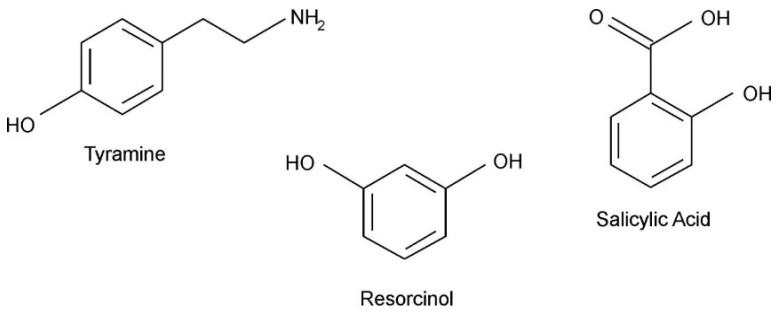

Figure 6.1.1 Chemical structure of Tyramine, Resorcinol and Salicylic Acid (SA).

Typically, the application of electrochemical techniques employed to detect salicylic acid are normally hindered by several issues, mainly involving the large anodic potential required for oxidation and the subsequent electrode fouling by polymeric and oligomeric oxidation products. To minimise these effects, a variety of approaches have been tested which include the use of the following: glassy carbon electrodes (Supalkova, *et al.*, 2006), gold electrodes coated with copper nanoparticles (Wang, Wei, *et al.*, 2010), platinum electrodes (Wang, Ai, *et al.*, 2010; Chrzescijanska, *et al.*, 2014), screen printed (González-Sánchez, *et al.*, 2015) and graphene based systems (Kruanetr, *et al.*, 2014; Patil, *et al.*, 2014). Recent work by Park and Eun (2016) has suggested that although passivated polymeric films may arise, several additional products will also be formed (Park, *et al.*, 2016) as highlighted in **Scheme 6.2**.

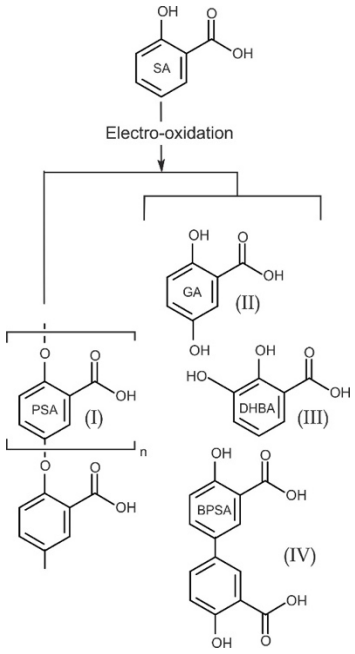

Scheme 6.2 Potential product spread as postulated by Park and Eun (2016) from the electro-oxidation of salicylate(Park, *et al.*, 2016).

The direct oxidation of salicylate under acidic or neutral pH conditions would require a large anodic potential, that could result in the oxidation of other simple components present and thereby compromise the voltammetric accuracy (Park, *et al.*, 2016)**.** Therefore, the approach adopted in this chapter focuses on oxidising certain by-products (**II-IV**) at much lower potentials, in order to eliminate the possibility of interferences from another electroactive specie at higher potentials

6.2 Experimental Details

6.2.1 Materials

All chemicals were purchased from Sigma-Aldrich at the highest grade available without any further modification in terms of purification. All measurements were carried out at room temperature ($22^{o}C \pm 2^{o}C$) in Britton Robinson (BR) solution ranging from pH 3 to 10. Stock solutions of 10 mM salicylic acid, uric acid, resorcinol and tyramine was prepared in 0.1 M NaOH, while the ferrocyanide (2 mM) and ascorbic acid (10 mM) was prepared in 0.1 M KCl. The mat carbon fibre was supplied by Goodfellow Research Materials (Cambridge, UK).

6.2.2 Electrochemical Configuration

Electrochemical measurements were conducted on a μAutolab type III computer controlled potentiostat (Eco-Chemie, Utrecht, and The Netherlands). A three-electrode system consisting of a platinum wire counter electrode, a standard Ag/AgCl half-cell reference electrode (3 M NaCl, BAS Technicol UK) and a working electrode (either a mat carbon fibre or SPE) was utilised. Cyclic voltammetry measurements were typically conducted at 50 mV/s, while square wave voltammograms were conducted with the following parameter; scan rate = 50 mV/s; frequency = 25 Hz; step potential = 2 mV; amplitude = 20 mV.

6.2.3 Sensor Design and Modification

Screen printed electrodes (SPE) were manufactured in house using a DEK 240 Manual Screen Printing Machine, with a stainless-steel screen mesh and graphite ink (Gwent Electronic Materials (GEM), product code: C205010697). The SPE base was printed onto a Valox substrate that was cured for ninety minutes at 70^{o}C. To define the exact working area of the electrode, an additional layer consisting of a polymeric dielectric material (GEM Product code: D2071120P1) was also screen printed on top and left to cure. To determine the surface morphology of the carbon-based sensors, a JEOL jsm-6010 Plus scanning electron microscope (SEM) was employed.

It has become relatively common to electrochemically anodise carbon based electrodes in order to improve their electrochemical behavior (Phair, *et al.*, 2011; Anderson, *et al.*, 2014). In this investigation, the electrodes were electrochemically anodised in a solution of 0.1 M Salicylic Acid (SA) prepared in 0.1 M NaOH, at a fixed potential of +2 V for 5 minutes, followed by three SQW scans (-0.4 - 0.6 V) in the same solution in order to generate the salicylic dimer. The final step in this process was to drop cast 1 μL of Nafion onto the electrode surface to create an electrostatic border to encapsulate the SA.

6.3 Results and Discussion

Carbon fibre was used as the initial substrate to examine the responses of the various phenol derivatives in order to identify the best candidates to take forward to the screen-printed system. The electro-polymerisation of the given phenol monomer (10 mM, 0.1 M NaOH) onto an anodised carbon fibre electrodes was investigated using cyclic voltammetry. Cyclic voltammetry was employed to investigate the electrode process resulting from the oxidation of salicylic acid and to also provide a diagnostic insight into the electrogenerated by-products. The response of the anodised carbon fibre electrode towards the oxidation of salicylic acid (10 mM) in 0.1 M NaOH are detailed in **Figure 6.3.1**. Based on the previous

work by Park and Eun (2016), NaOH was selected as the electrolyte as it was believed to help to minimise the build-up of polymeric material (**I**) and it favours the production of the electrogenerated hydroquinones (Park, *et al.*, 2016). On the first scan, a single large oxidation peak is observed at +0.6 V resulting in the generation of radical cations that undergo further reaction to form the various products highlighted in **Scheme 6.2**. Considering the potential required to oxidise the salicylate, it can be anticipated that the resulting hydroquinones will be immediately oxidised and converted to the corresponding quinone forms (i.e. **IV ->V**). Therefore, on the reverse sweep, a reduction processes (+0.102 V) can be observed leading to the reduction of the electrogenerated quinones back to the hydroquinone (**V-> IV**). The subsequent scans catch the hydroquinone-quinone redox transitions indicated in **Scheme 6.3.**

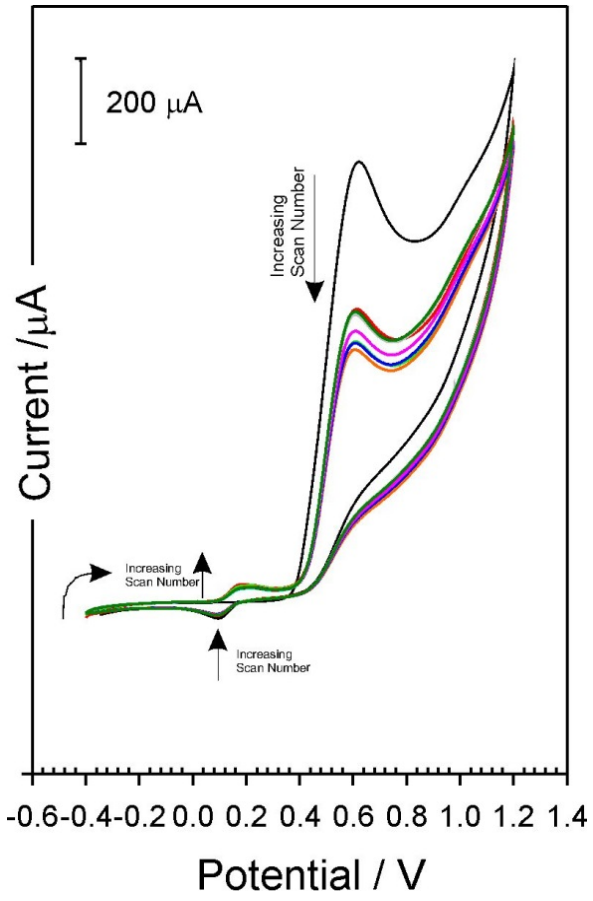

Figure 6.3.1 Cyclic voltammograms detailing the response of an anodised carbon fibre electrode towards the oxidation of salicylic acid (10 mM, 0.1 M NaOH, 50 mV/s). N_s=10

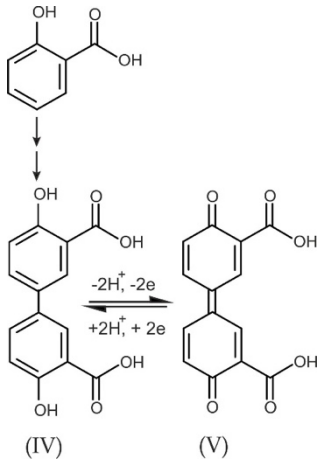

Scheme 6.3 Redox transition between Hydroquinone-quinone species from the electrogenerated dimer resulting from the oxidation of salicylic acid. Reproduced with permission (Rawlinson, *et al.*, 2017).

The voltammogram presented in **Figure 6.3.1** highlights that the peak magnitude relating to the dimer by-product (**IV**) was relatively small in comparison to the direct oxidation of the salicylic acid, which was believed to contribute to the product spread, as detailed in **Scheme 6.2**. The investigation was extended to tyramine and resorcinol and similar experimental parameters were employed. Cyclic voltammograms detailing the response of an anodised carbon fibre electrode towards 10 mM tyramine in 0.1 M NaOH are detailed in **Figure 6.3.2.**

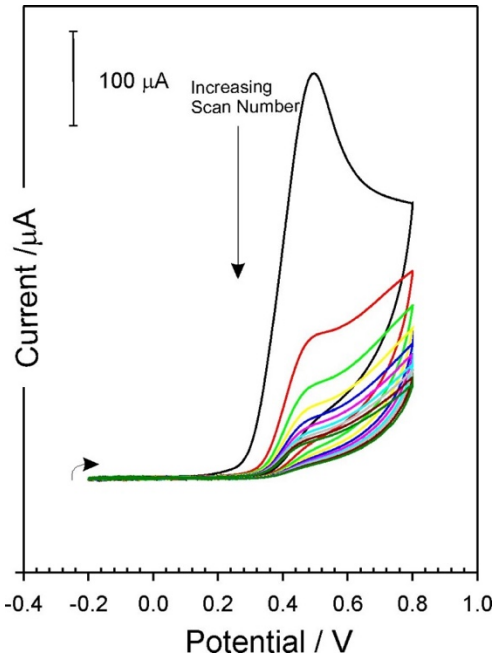

Figure 6.3.2 Cyclic voltammograms detailing the response of an anodised carbon fibre electrode towards the oxidation of tyramine (10 mM, 0.1 M NaOH, 50 mV/s). N_s=10

The oxidation of the tyramine monomer can be clearly seen at +0.48 V, which decreases with each successive scan. This behavior was similar to that observed with the salicylate but, in contrast, there were no additional redox processes arising on the second and subsequent scans. A similar voltammogram profile was observed for the resorcinol and therefore, given the absence of any electrogenerated redox probe, any further investigation of these systems was terminated. The remainder of the chapter therefore focuses on the responses of the salicylic acid system. To further confirm whether the biphenol (IV – V) was adsorbed onto the electrode surface and that this newly formed redox species wasn't only present in very basic conditions, i.e. NaOH, the anodised carbon fibre electrode was cycled ten times in the SA solution (10 mM, 0.1 M NaOH, 50 mV/s), rinsed and then immediately placed in a pH 7 buffer solution. The cyclic voltammograms detailing the electrode response towards the pH 7 buffer is presented in **Figure 6.3.3.**

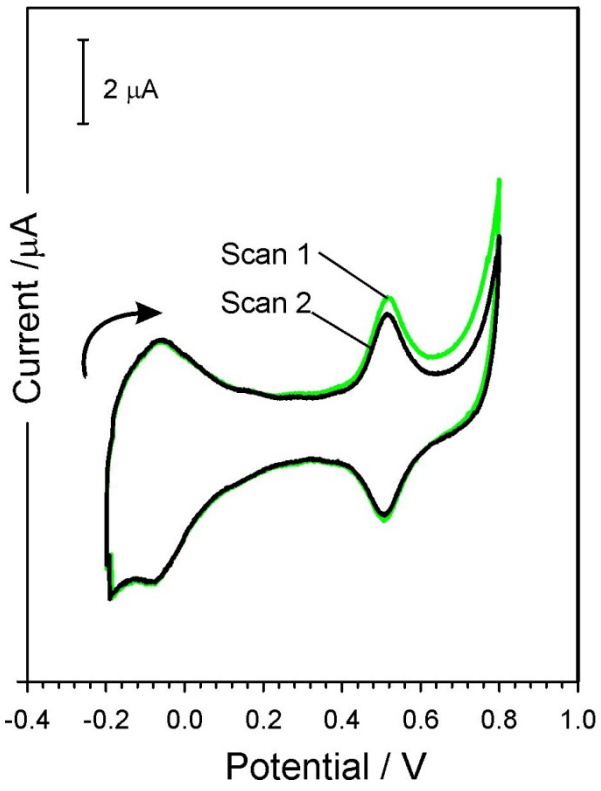

Figure 6.3.3 Cyclic voltammograms of a dimer modified anodised CF electrode response towards two consecutive scans in pH 7 BR buffer solution. N_s=2

The redox couple observed at +0.515 V was attributed to the formation of the dimer with the peak separation of ~10mV consistent with an adsorbed species. The

magnitude of the dimer peak process was found to decrease with each consecutive scan and could be attributed to its gradual loss from the surface of the electrode into the solution bulk. It was envisaged that upon reduction to the hydroquinone, the hydrophilicity (and hence solubility) of the molecule is increased and therefore leaches from the surface.

In order to confirm the adsorptive behaviour of the dimer, whether it was experiencing adsorption or diffusion, the electrode response towards varying scan rates in pH 7 buffer solution was recorded, as highlighted in **Figure 6.3.4**.

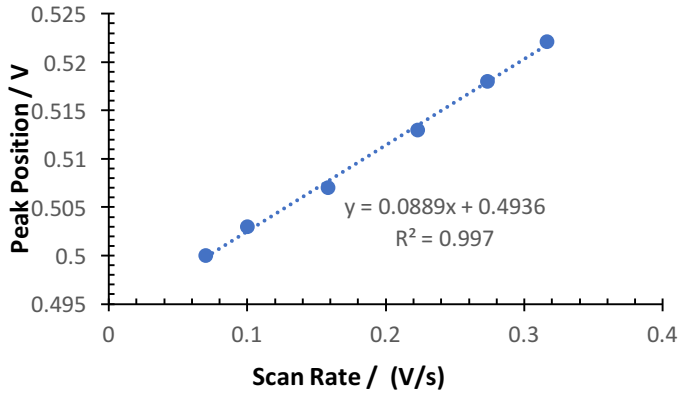

Figure 6.3.4 Plot detailing the linear response of the peak positions of the oxidation of the dimer towards varying scan rates (5 – 250 mV/s) in pH 7 BR buffer solution.

A plot of the peak current against the scan rate can provide useful diagnostic information regarding whether the electrode reaction is controlled by the mass transport of the electroactive species to the electrode surface, via a concentration gradient. The linear response (R^2=0.997) towards various scan rates in the pH 7 BR buffer solution highlighted in **Figure 6.3.4**, indicated that the dimer was adsorbed onto the electrode surface.

6.3.1 Voltammetric Techniques

In a similar approach previously described in **Chapter 5**, the core rationale of this investigation will be dependent on the variation of the peak position of the dimer in relation to pH. Based on the assumption of a 2 H^+, 2e process, the peak potential is expected to shift by 59 mV/pH unit. Therefore, it is imperative that the

peak position is reported accurately, as a considerable inaccuracy could be introduced from the slightest error in reporting the peak potential. In order to minimise the risk of incorrectly ascribing the peak potential, square wave voltammetry was employed as it provides a sharper voltammetric peak in comparison to cyclic voltammetry.

Previous work by Anderson et al. (2014), demonstrated that anodising carbon fibre filaments resulted in the formation of quinone species (Anderson, *et al.*, 2014). Square wave voltammogram detailing the response of an anodised carbon fibre electrode towards pH 3 BR buffer is detailed in **Figure 6.3.5.** Previous XPS analysis, **Figure 5.3.9**, confirmed that the anodisation process increased the number of oxygen functional group resulting in peaks towards a lower potential region. Therefore, it is believed that the peak formed at +0.211 V is due to the oxidation of the carbon quinone species that were created by anodising the electrode. The remaining peak present at +0.710 V in the pH 3 BR buffer solution is due to the oxidation of the dimer, as highlighted in **Figure 6.3.5**.

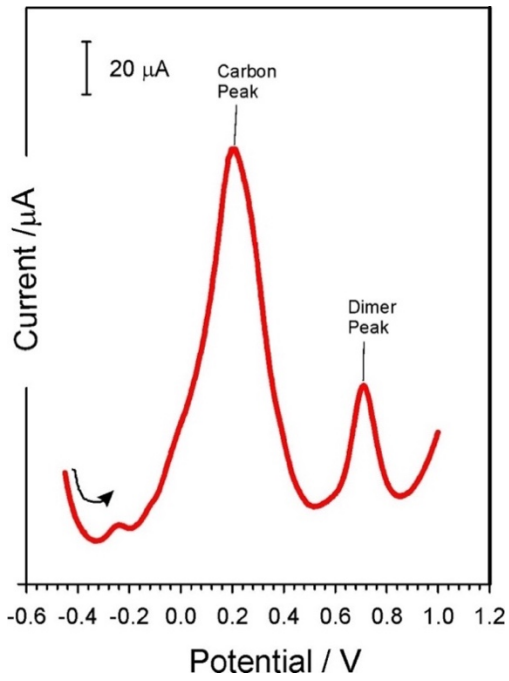

Figure 6.3.5. Square voltammogram detailing the response of an anodised CF electrode towards a pH 3 BR buffer solution and the subsequent peaks formed due to the oxidation of the surface bound quinone and electrochemically generated salicylate dimer species.

Square wave voltammograms detailing the responses of the dimer species response to three consecutive scans in buffer solutions of varying pH, in both and oxidative and reductive range, are highlighted in **Figure 6.3.6.**

Based on the previous square wave voltammogram reported in **Figure 6.3.5**, the two peaks present in the reduction scan pH range in **Figure 6.3.6.b**, corresponds to the reduction of the carbon quinone and the absorb dimer, indicating that they are a redox species. It is evident from **Figure 6.3.6** that a sharp and distinct dimer peak is formed and remains visible and distinguishable at the higher pH in both the oxidative and reductive scan. A total of three scans were conducted for each pH buffer solution and upon inspection of the gradient of both the oxidation and reduction scans of the absorbed dimer expressed near ideal Nernstian responses were obtained (59.5 mV and 52.4 mV, respectively).

6.3.2 Interferences

The core detection rationale behind this research project depends on the ability of the pH sensitive probe to unambiguously detect the SA dimer peak position amongst potential interferences, such as ascorbic acid (AA) and uric acid (UA) which are typically present within the wound environment. The response of the anodised CF electrode towards 100 μM UA and 228 μM AA (pH 7 BR buffer solution) is presented in **Figure 6.3.7**. The additions of UA and AA lie within relevant concentration regions reported by previous published studies. A study conducted by James et al. (2003), reported the concentration range of UA present in chronic venous ulcers wound fluid ranged from 46 – 368 μM (James et al 2003). While Long et al. (2003) reported that the normal region of AA found in plasma samples of patients with pressure ulcers lies in the region of 25.56 to 68.13 μM (Long, *et al.*, 2003).

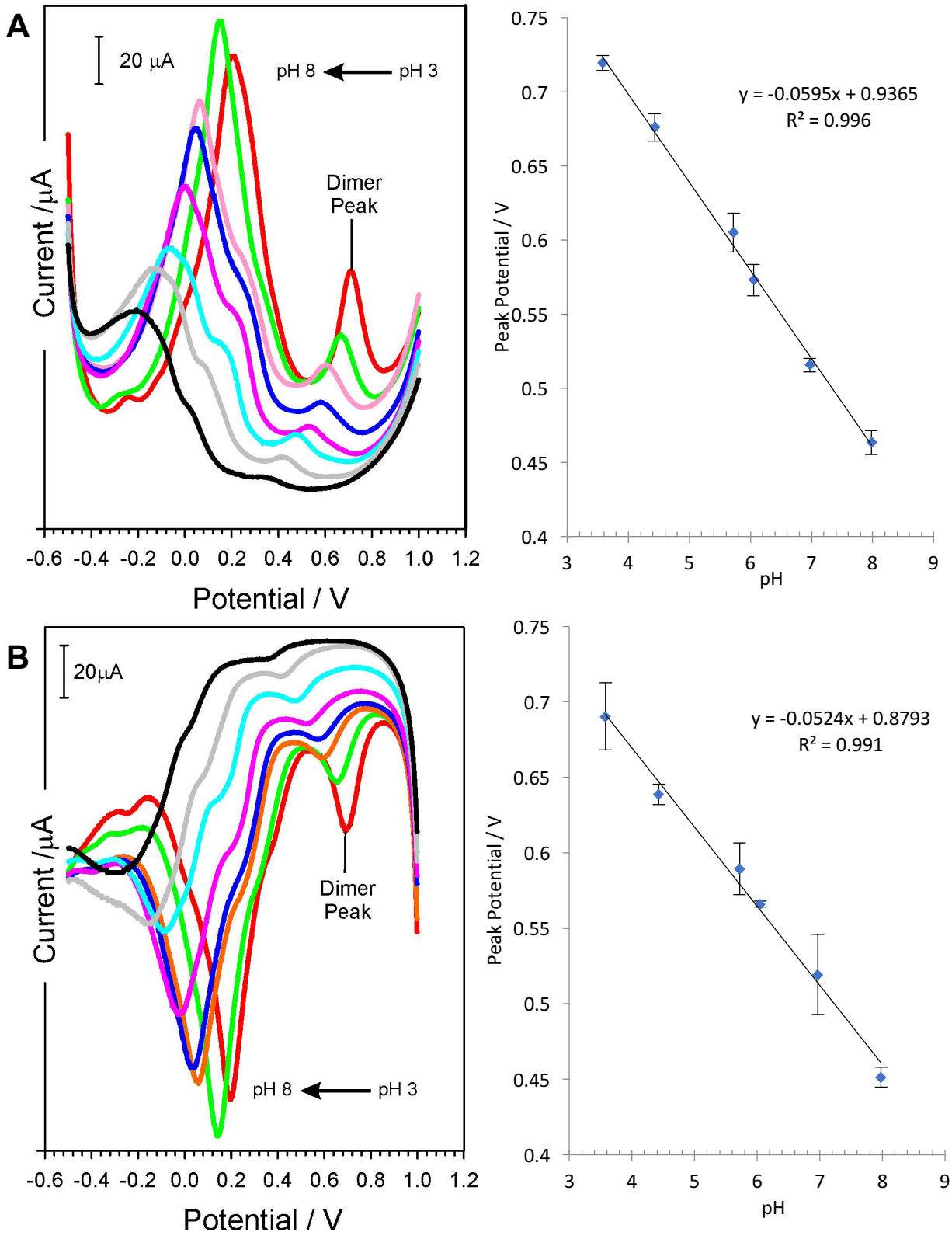

Figure 6.3.6 Square wave voltammogram detailing the response of the dimer modified anodised CF electrode towards a pH range in an a) Oxidation scan and b) Reduction scan. Both including a plot detailing the linear response (including mean standard deviation error bars) found between the dimer peak position and pH. N_s=32, N_{pH}=6

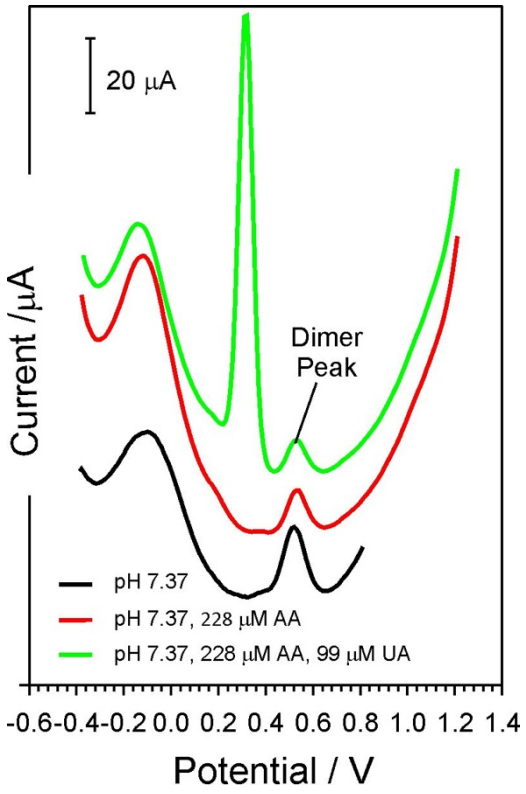

Figure 6.3.7 Square wave voltammograms detailing the response of the dimer modified anodised carbon fibre electrode towards 99 μM UA and 228 μM AA (pH 7 BR solution). N_s=3

The anodised CF electrode displayed two defined oxidation peaks at -0.109 V and +0.521 V. Based on previous results (**Figure 6.3.5**), the latter peak is associated with the presence of the dimer, while the first peak is the quinone peak associated with the underlying carbon fibre. It has been previously reported that AA does not give rise to a visible peak in anodised carbon materials (Phair, *et al.*, 2011). However, upon the addition of the AA, there was a minor shift in the peak position, which would translate to an error of 0.16 pH units. No further shift in the peak position occurred when UA was added. The addition of the UA resulted in a sharp peak at +0.3 V, that had a peak separation of 200 mV from the SA dimer peak. Although the slight shift in the peak position due to the addition of AA is not ideal, it is important to note that the oxidation of both the AA and UA is an irreversible reaction. Therefore, if the scan was to be reversed i.e. start at a positive potential, this would result in the immediate oxidation of the AA and UA present in the solution. Consequently, as the scan is swept towards a more negative potential the only thing that remains to be reduced would be the SA dimer. This would ultimately prevent the presence of the AA and UA from interfering with the peak position of

the SA dimer. Therefore, it was decided that when testing the electrode in more complex biological solutions, such as defibrinated horse blood, the reduction peak process of the SA dimer will be selected to determine pH.

6.3.3 Screen Printed Electrodes (SPEs)

The use of SPEs for decentralised sensing applications has become commonplace, however, it was of interest to determine how the electrode would respond towards the salicylic acid and the subsequent detection of the dimer. Initially, the SPEs were anodised in 0.1 M NaOH, +2 V for 5 minutes – effectively following the standard procedure used in previous carbon electrodes. Following anodisation, the SPE was then placed in SA (10 mM, 0.1 M NaOH) and scanned between -0.4 V and +0.9 V, as detailed in **Figure 6.3.8.**

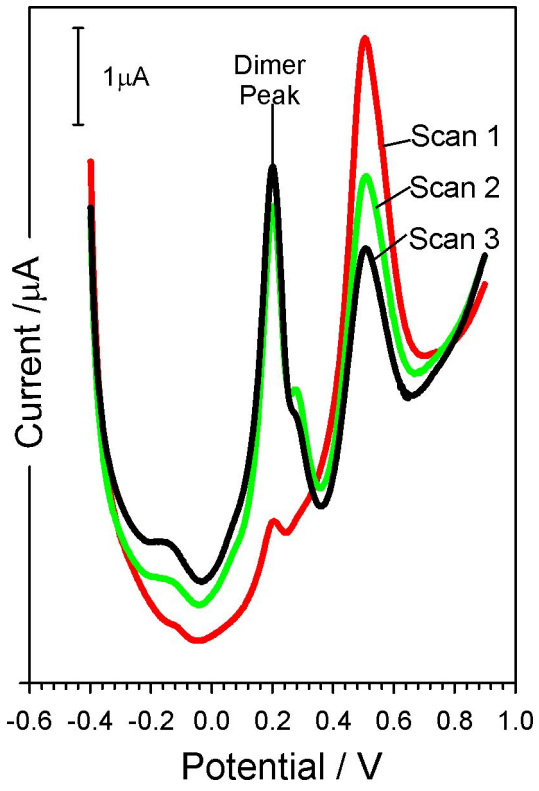

Figure 6.3.8 Square wave voltammograms detailing the response of the anodised SPE response towards the oxidation of salicylic acid (10 mM, 0.1 M NaOH). N_s=3,

As highlighted in **Figure 6.3.8,** the oxidation of SA occurs at +0.512 V and is broadly consistent with the oxidation peak position observed with the anodised carbon

fibre detailed previously in **Figure 6.3.5.** The second and third scans resulted in the formation of a new electrode process at +0.2 V and again this is believed to be attributed to the oxidation of the dimer resulting from the initial oxidation of SA. In each case the behaviour is consistent with the responses observed with carbon fibre.

Given the emergence of the new electrode process at +0.2 V and the assumption that this is attributed to the dimer, then it could be expected that it would adsorb onto the SPE carbon surface as it had done previously with the CF electrodes. This was confirmed by removing the electrode, rinsing with deionised water and placing in fresh buffer solution. Square wave voltammograms detailing the response of dimer adsorbed SPE in various buffer solutions are detailed in **Figure 6.3.9** along with the quantitative calibration data.

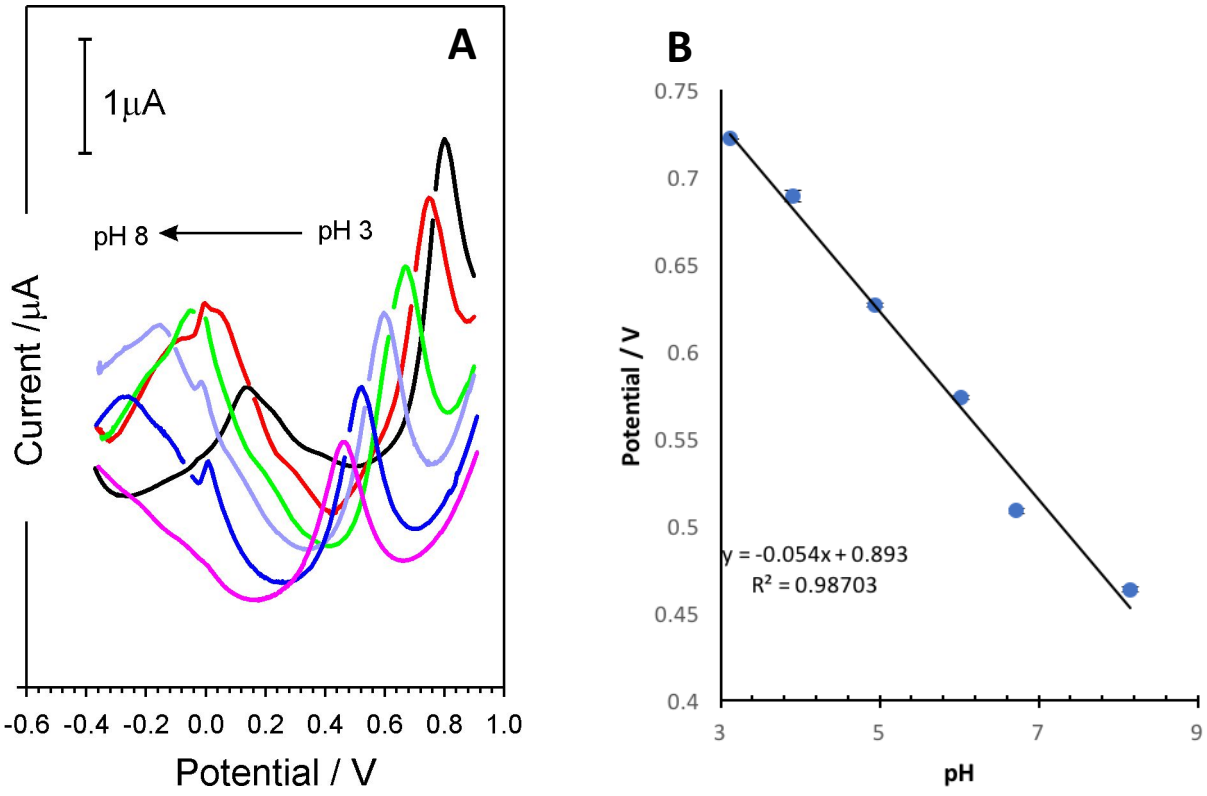

Figure 6.3.9 A) Square wave voltammogram detailing the response of the dimer modified anodised SPE towards a pH range (pH 3 - 8). B) Quantitative calibration data revealing the Nernstian response and mean standard deviation error bars. N_s=18, N_{pH}=6

6.3.4 Nafion® Modification

As previously demonstrated in **Figure 6.3.9**, the anodised SPE response towards increasing pH, resulted in deviations from the line of best fit (R^2= 0.987). This response could possibly be attributed to either nucleophilic attack at alkaline conditions or by the dimer leaching back into the solution. It was thought that the latter was the predominant issue and, in order to counter the loss, a membrane system was employed in an attempt to entrap the dimer.

Nafion® is classed as an ionomer as it contains a tetrafluroethylene backbone with a perfluorovinyl ether group terminated with sulphonate group (Heitner-Wirguin, 1996). It is a cation exchanger that allows the movement of positively charged molecules or cations through the porous film (Nagy, *et al.*, 1985; Kreuer, *et al.*, 2000) while excluding the movement of negatively charged molecules (anions) (Zhang, *et al.*, 2005).

In relation to this experiment, the pKa of the carboxyl group on the dimer is approximately around pKa 3-4 – as such, except for a pH lower than 4, it will deprotonate (COO^-) and have a net negative charge. Thus, if it is adsorbed onto the electrode surface and a top coating of Nafion® is applied – the net negative charge of the Nafion®, will retard the movement of the negatively charge dimer through the film. This exclusion effect has been shown to enhance the electrode's sensitivity towards biological molecules (Frith, *et al.*, 2010). A concern surrounding the use of Nafion® is that, due to the diffusional constraints, this may potentially diminish the sensitivity of the electrode towards pH (Gogol, *et al.*, 2000). A previous study conducted by Frith et al. looked at the electrochemical behaviour of L-tryptophan at a Nafion® modified electrode and based on this, further investigations were conducted to determine if it could be used to entrap the electrochemically generated dimer at the surface of the electrode and in turn improve the electrode sensing capabilities to pH (Frith, *et al.*, 2010).

The SPE were modified by drop casting, 1 μL of Nafion® solution (5 wt %) onto the surface and allowing it to dry overnight. Prior to the addition of the Nafion®, the SPE were anodised in a salicylic acid solution (10 mM, 0.1 M NaOH) via ten cyclic voltammogram scans in a potential range of -0.4 V to 0.8 V. The electrodes were then placed directly into pH 3 buffer solution and three square wave voltammograms were recorded to confirm that the dimer had been formed and had adhered to the electrode surface.

The optimal volume of the Nafion® solution of 1 μL for drop casting onto the electrode surface was determined by investigating the electrode response of a number of SPE, each having different volumes of Nafion® ranging from 0 μL to 3 μL. A volume of 2 μL of Nafion® was found to substantially decrease the height (i_{pa} = 0.99 μA) of the peak associated with the dimer oxidation, in comparison to the peak height of the 1 μL volume (i_{pa}= 5.73 μA). This could be attributed to the reduction of the number and size of pores as more of the polymeric Nafion® molecule was overlaid.

The next phase was to investigate the reproducibility of the Nafion® modification step. This involved comparing the peak position of a number of different modified electrodes to determine if all the responses were consistent. The preliminary responses indicated variability in the reported dimer peak positions which were suspected to be as a result of the Nafion® layer. Therefore, a time study was conducted, as highlighted in **Figure 6.3.10**, to determine whether the typical time delay of two minutes for electrode calibration was sufficient for the electrodes coated with the Nafion® layer.

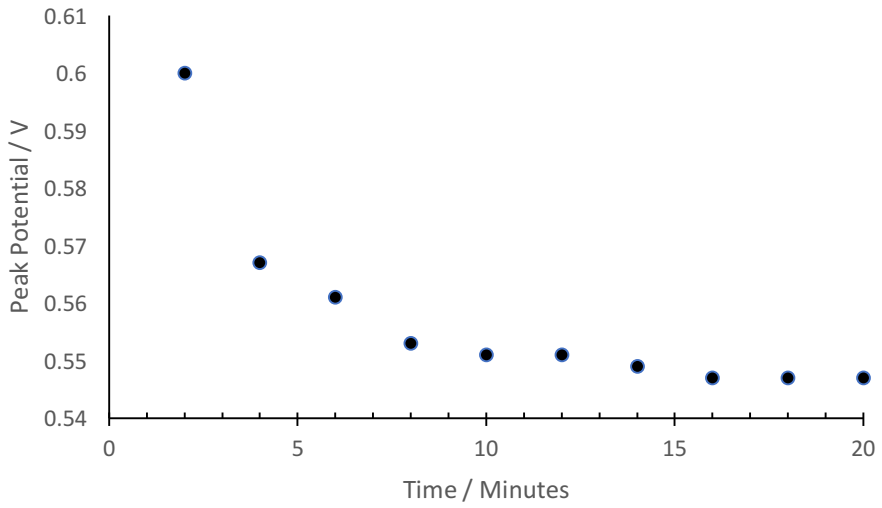

Figure 6.3.10 Peak position response of a Nafion® coated anodised SPE with adsorbed dimer towards pH 7 buffer solution over a period of 20 minutes.

Based on these results, it was postulated that the difference in the peak position was attributed to the Nafion® layer acting as a buffering layer and thereby creating a delay in which the buffer solution reached the electrode surface. It can be clearly deduced from **Figure 6.3.10** that not leaving enough time for the electrode to equilibrate in the solution, (at least ten minutes) could potentially lead to a peak potential error of 49 mV. In accordance with the Nernst equation, this would equate to an error of nearly 1 full pH unit. Therefore, it was deemed necessary to implement a ten-minute calibration period prior to recording a scan, to ensure that the electrode had time to equilibrate to the new solution.

Square wave voltammograms detailing the response of the anodised SPE with a Nafion® coating towards BR buffer solutions from pH 3 – pH 8 are detailed in **Figure 6.3.11.** The plotted graph of the peak potential for the Nafion® coated SA SPE electrodes demonstrates a linear relationship with a gradient of 51 mV per pH unit, within a working range of pH up to 8. Standard error bars are included in the graph below, however, they are so minute that they are obscured by the marker.

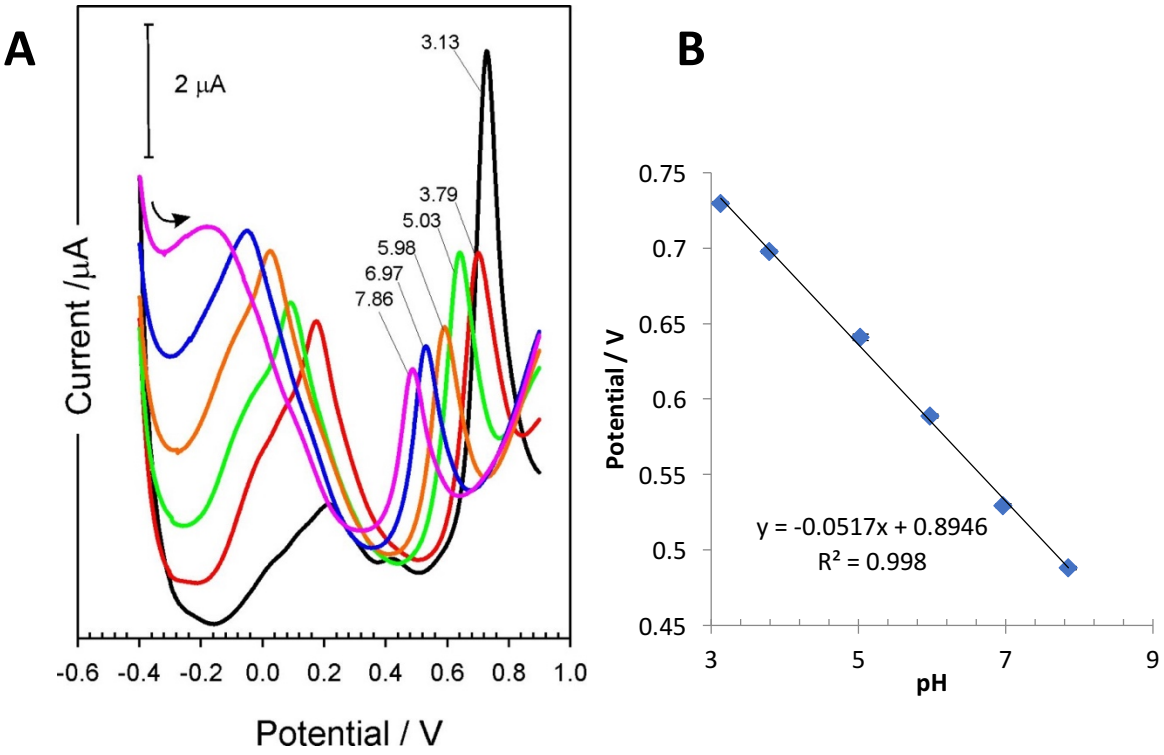

Figure 6.3.11 A) Square wave voltammograms detailing the response of the Nafion® coated dimer modified anodised SPE towards a pH range B) Plot detailing the linear response and error bars of the mean standard deviation of the peak position of the Nafion® coated anodised SPE towards a single pH range (pH 3 – pH 8). N_s=18, N_{pH}=6

In comparison to the previous pH range reported in **Figure 6.3.9,** the addition of the Nafion® layer onto the electrode surface, was found to greatly improve the definition of each peak process. In order to determine the reproducibility of the system, three electrodes were selected to determine the inter electrode response. Each measurement was recorded 3 times for each electrode and the average peak position was plotted, along with error bars of the mean standard deviation as highlighted in **Figure 6.3.12**. The full analysis of the peaks can be found in **Table 6.1,** in which the standard error is relatively low, indicating the reproducibility of the system.

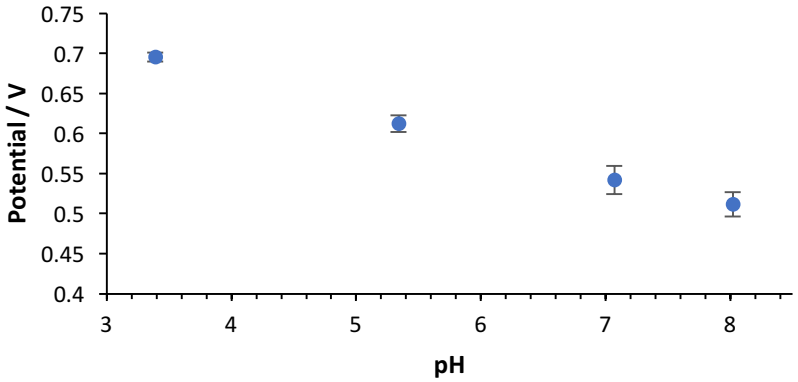

Figure 6.3.12 Plot detailing the linear response of the average peak position and error bars of three separate Nafion® coated anodised SPEs towards a single pH range (pH 3 – pH 8). Including mean standard deviation error bars. N_s=12, N_{pH}=4

Table 6.1 A detailed breakdown of results of three separate Nafion® coated dimer modified anodised SPEs towards a single pH range. E= Electrode

pH	Potential / (V)			Mean Inter (V)	Standard Deviation
	E1	E2	E3		
3.39	0.695	0.701	0.690	0.695	0.006
5.34	0.614	0.621	0.601	0.612	0.010
7.07	0.562	0.532	0.532	0.542	0.017
8.02	0.529	0.503	0.502	0.511	0.015

6.3.5 Stability of the Salicylic Acid Electrodes

The next step in characterising the Nafion coated SPE was to test its repeatability in various pH buffers in order to determine its repeatability. To examine the electrode stability, the peak potential of a single Nafion® coated SPE response against the pH to a select range of pH buffer solutions (3, 5, 7 and 8) with a 10 minute delay, was recorded over a period of four consecutive pH ranges. The average peak potential (N_s=3) for each pH, was plotted in a stability graph, as shown in **Figure 6.3.13**.

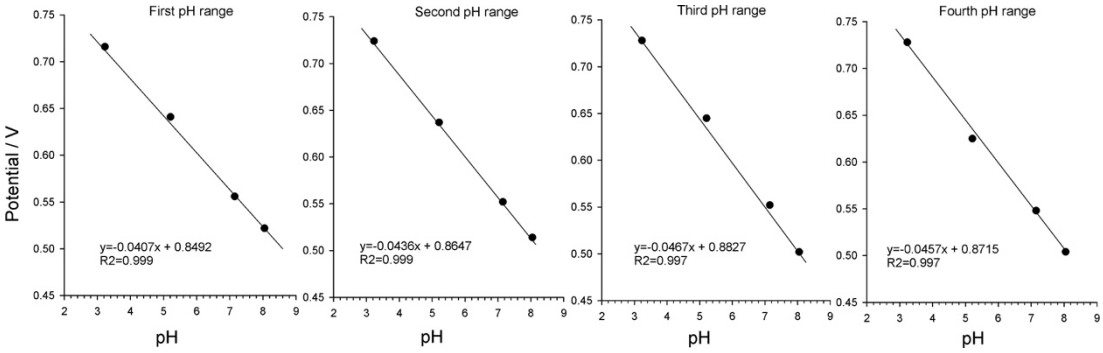

Figure 6.3.13 Stability graphs detailing the response of Nafion® coated dimer modified SPE towards four consecutive pH ranges. N_s=48, N_{pH}=4

The stability graph detailed in **Figure 6.3.13** demonstrates that the Nafion® coated SPE response to a range of pH buffers (3, 5, 7 and 8) produced a linear response over the four consecutive pH ranges. Each individual response was recorded and documented in **Table 6.2**. Based on these results it was then possible to calculate both the intra electrode mean for each individual electrode (the mean of the three scans conducted for each pH), as well as the overall mean between the three electrodes at each individual pH (inter electrode mean).

Table 6.2 Recorded peak position values towards four consecutive pH ranges for a Nafion® and dimer modified SPE.

pH	Peak position / V Intra Mean				Inter Mean / V	Standard Deviation
	Run 1	Run 2	Run 3	Run 4		
3.23	0.716	0.724	0.728	0.728	0.724	0.006
5.21	0.641	0.637	0.645	0.625	0.637	0.009
7.15	0.556	0.552	0.552	0.548	0.552	0.003
8.05	0.522	0.514	0.502	0.504	0.5105	0.009

The intra variation of the peak position for each pH over the average four pH ranges resulted in, at most, a minor standard deviation of 0.009 which would equate to a variation of 0.002 pH units.

6.3.6 Defibrinated Horse blood

The next step in characterising the response of the adsorbed dimer species onto the Nafion® coated SPE, was to determine how effective it is sensing pH in a much more complex matrix, i.e. defibrinated horse blood. In line with previous work by Kaimori et al. (2006), commercially available defibrinated horse blood was selected as a substitute to human blood (Kaimori, *et al.*, 2006). In order to maximise the viable working time of the defibrinated horse blood sample, it was essential to select defibrinated horse blood to help prevent the formation of blood clots, which could significantly impede an electrode reading.

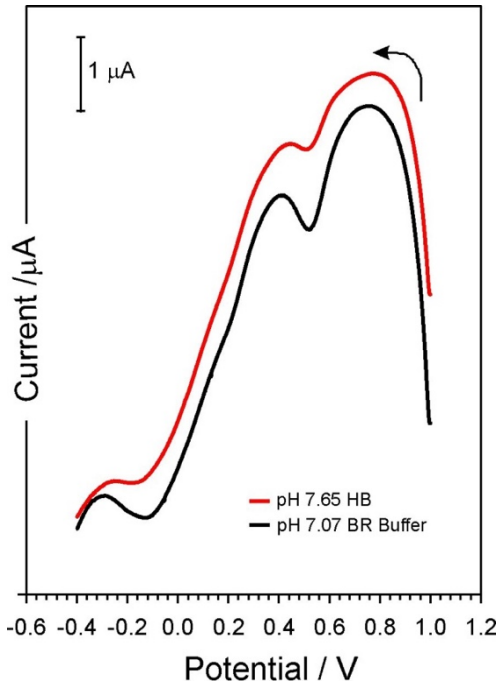

Figure 6.3.14 Square wave voltammogram detailing the response of the Nafion® coated SPE response towards a sample of defibrinated horse blood and pH 7 BR buffer solution.

As previously described in section 6.3.2, in order to minimise the impact of interferents present in the complex media of defibrinated horse blood, the peak position of the reduction process of the SA dimer was selected to determine pH. As highlighted in **Figure 6.3.14**, a distinct peak process towards the defibrinated horse blood sample can be clearly seen at 0.504 V. In comparison to the response towards the pH 7 buffer solution, there is only a minor difference of 8 mV in the

corresponding peak position which is simply due to the difference of pH of the two samples (pH 7.65 and pH 7.07).

A total of three separate electrodes were calibrated using a select pH range (pH 3 – 8) then placed in 10 mL of defibrinated horse blood. A standard commercial pH probe was used to determine the actual pH of the sample and used as a comparison for the calculated pH value, as detailed in **Table 6.3.**

Table 6.3 Peak positions obtained from the Nafion® coated dimer modified SPE response towards defibrinated horse blood and their calculated pH. E= Electrode

	Actual pH	**Calculated pH**	**Calibration Equation**	**R^2**
E1	7.65	7.65	Epa=-0.037pH + 0.8145	0.995
E2	7.74	7.76	Epa=-0.041pH + 0.8395	0.994
E3	7.61	7.60	Epa=-0.042pH + 0.8591	0.993

The values highlighted in **Table 6.3** were calculated by taking the average peak position of three scans of each electrode in the sample of defibrinated horse blood then applying to the respective calibration equation. Each electrode expressed a linear, sub Nernstian response during calibration of the pH range, as detailed in **Table 6.3**, which resulted a maximum deviation of 0.02 pH against the standard pH probe. It is important to note the range of 0.13 pH units recorded between three samples of defibrinated horse blood. This highlights the ambiguity of blood pH and the importance of being able to monitor minor pH fluctuations in each individual sample.

To determine the shelf life of the modified electrode, a two-day time study was conducted to ensure that factors such as air oxidation would not dampen the electrode response in sensing pH. In a similar manner to previous experiments, a Nafion® modified SPE was calibrated in a pH range from 3 to 8, and then immediately tested in a sample of defibrinated horse blood. Taking the peak position recording of the defibrinated horse blood sample, the pH was extrapolated

using the calibration line graph. This value was then compared against the pH reported from the commercial pH probe.

Table 6.4 Peak positions obtained from the Nafion® coated SPE response towards defibrinated horse blood over a 2 day period and their calculated pH. DHB = Defibrinated Horse blood

pH	Day 1	Day 2
3.6	0.676	0.680
5.44	0.596	0.591
7.07	0.534	0.535
7.95	0.509	0.503
DHB pH	7.65	7.74
Calculated pH	7.65	7.76

The peak potential over the subsequent two days was found to vary linearly with pH over the clinically relevant pH range 3-8, as detailed in **Table 6.4**. This resulted in an exact and near exact pH response for the first two days.

6.4 Conclusions

Initially a pressed carbon fibre mesh electrode was employed to electrochemically investigate three different substrates (tyramine, resorcinol and salicylic acid) that express basic, neutral and acidic properties. Particular attention was paid to the electrochemical oxidation of the salicylic acid, which resulted in the adsorption of the electrogenerated dimer byproduct onto the electrode surface. To determine the applicability of this dimer modified electrode response towards pH, square wave voltammetry and cyclic voltammetry techniques were employed. This resulted in the formation of a redox process that expressed an ideal Nernstian response towards a clinically relevant pH range (**Figure 6.3.6**).

The next step involved an investigation into the CF electrode response to electrochemically active interferences typically present in biological samples, i.e. UA and AA. It was found that the presence of both UA and AA in a solution of pH 7 buffer had minimal impact on the peak position (**Figure 6.3.7**). The stability of the anodised SPE was also assessed intra and interspecifically, via consecutive pH

ranges, it resulted in minor deviation and drift in the peak position, demonstrating the robustness of the electrode towards repetitive scanning in varying pH environments.

Based on these preliminary investigations the same approach was conducted using an anodised SPE. Although this provided a similar response to the CF electrode, there was however a minor discrepancy in the line of best fit (R^2=0.987, **Figure 6.3.9**). This less than ideal response was believed to be attributed to the SA leaching back into the solution. Therefore, to entrap the dimer at the electrode surface, a coating of Nafion® was applied to act as a porous membrane. This resulted in an improved electrode response towards pH (**Figure 6.3.11**).

The next step was to determine the stability of the Nafion® /dimer modified SPE, towards repetitive measurements. Therefore, three electrodes were subjected to a series of four consecutive pH ranges (three scans per pH; N=4), which resulted in each electrode being scanned a total of 48 times. This resulted in minor variations in peak positions which would equate to a potential variation 0.002 pH units (**Figure 6.3.13**). Finally, the dimer modified SPE was subjected to testing in a biologically relevant solution, defibrinated horse blood, which resulted a maximum deviation of 0.02 pH against the standard pH probe (**Figure 6.3.14**).

Overall, the Nafion®/dimer modified SPE demonstrated that it can provide an unambiguous and pH sensitive response in a simplistic and cost effective method. However, one thing to be noted with this approach is that it required electrode calibration for each new solution. A 10-minute time delay was necessary prior to any measurement, to allow for the solution to diffuse through the porous Nafion® membrane and reach the electrode surface. Although this may not seem an unreasonable time delay, the cumulative delay associated with calibrating the electrode prior to testing would be too time consuming in terms of mass production.

Chapter 7

Investigating the Use of an Engineered Poly Flavin on Carbon Screen Printed Electrodes as the Foundations of a pH Sensor for Wound Monitoring

Abstract

A custom Flavin derivative bearing a pendant phenol substituent was electropolymerised onto both a pre-anodised carbon polyethylene film and a carbon-based screen printed electrode, their electrochemical properties were then investigated. Initial investigations focused on the carbon polyethylene film as the sensing base substrate, however, due to the ease of fabrication and low costs associated with the screen-printed electrode, it was selected for further investigation. The novel aspects of this work focus on the reversible flavin electrochemistry that was retained and it was found that the peak position shifted by 63 mV/pH over a pH range covering pH 2.75 to 9.2. The stability of the resulting composite has been evaluated and the analytical applicability towards the voltammetric measurement of pH in defibrinated horse blood was critically assessed.

7.1 Introduction

Voltammetric pH sensing using screen printed electrodes (SPEs) was previously discussed in Chapter 6, whereby the anodised SPE was modified by the electrogenerated by-product of the salicylate oxidation. This resulted in a reasonable response to pH, however, the necessary ten-minute delay for electrode calibration meant that it was impractical as a point of care sensor within a clinical setting. The principal aim of this chapter is to develop a SPE capable of monitoring the pH of a wound in a more timely manner. It should also be noted that the fabrication of the salicylate dimer based sensor was procedurally cumbersome. Therefore, it was necessary to consider another alternative redox system which would allow easier construction and facilitate faster and more robust measurements.

Initially, a polyethylene film doped with carbon particles (C-PE), was selected as an alternative substrate to confer electrical conductivity. The carbon-polymer composite film was originally a commercial variant designed as an electromagnetic screening film (Jin, *et al.*, 2013). In some respects it is similar in format to the carbon fibre mesh electrode (Phair, *et al.*, 2013) in that it should be mechanically flexible and therefore conform to the morphology of the wound. The main advantages over the previous approach is that the film is polymeric in nature and thus avoids issues with fragmentation of the fibre. As it is produced from polyethylene, it could also be expected that it would be more amendable to mass manufacture using conventional polymer processing methodologies. The main limitation however relates to the relatively poor conductivity of the substrate when considering its use as a sensing substrate.

It was envisaged however that the outermost polymer layer could be removed to expose a greater proportion of the interfacial carbon resulting in an improvement in the electroanalytical sensing performance (J Phair, Benson, *et al.*, 2014). A mesh design was proposed whereby laser processing was employed to etch tracks onto the film at a level insufficient to penetrate through the film. It could be anticipated

that where the tracks rastered across the X and Y planes, a hole would be created where the tracks intersected and thereby effectively creating a porous mesh like structure as shown in **Figure 7.1.1**.

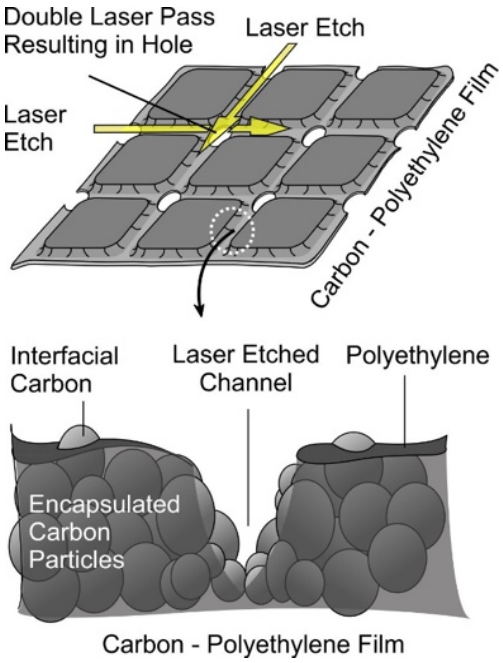

Figure 7.1.1. Laser processing procedure for the preparation of a conductive polyethylene mesh film.

While it would be expected that this modification alone would provide a conductive and mouldable film, it has been previously reported that the underlying carbon would fail to possess any inherent analytical selectivity (J Phair, Joshi, *et al.*, 2014). Given that the principal aim was to develop a mesh capable of monitoring the pH of bodily fluids, it was therefore necessary to consider a further modification to the base system.

In recent years, there has also been a steady interest in the use of voltammetric approaches where the peak positions arising from either the oxidation or reduction of indicator molecules bearing quinoid (Streeter, *et al.*, 2004; Lafitte, *et al.*, 2008) or nitro functionality (Xiong, Batchelor-McAuley, *et al.*, 2011) as an indirect measure of the local pH. In this instance, the modification of anodised carbon particles with a novel Flavin type molecular species (**Figure 7.1.2,** Structure I) was investigated. Flavins are known to exhibit near reversible electrochemical behaviour (Valipour, *et al.*, 2017) which, by virtue of the intrinsic acid-base functionality of the core

structure, will be pH dependent – this is analogous to the processes observed with the salicylate dimer in the previous chapter. The key challenge in the proposed design however relates to anchoring the redox system to the exposed carbon particles. In the case of the salicylate dimer – adsorption was the prime method of attachment but this led to the gradual leaching of the pH sensitive component and was a significant limitation when considering periodic measurements. The custom flavin detailed in **Figure 7.1.2**. however, possess an electropolymerisable phenol group which, it was envisaged, after electro-oxidation would lead to film formation and thereby trap the pH sensitive redox group directly at the electrode. A key assumption made was that the electropolymerisation process would not result in damage to the Flavin center. The key molecular transitions are highlighted in **Figure 7.1.2**.

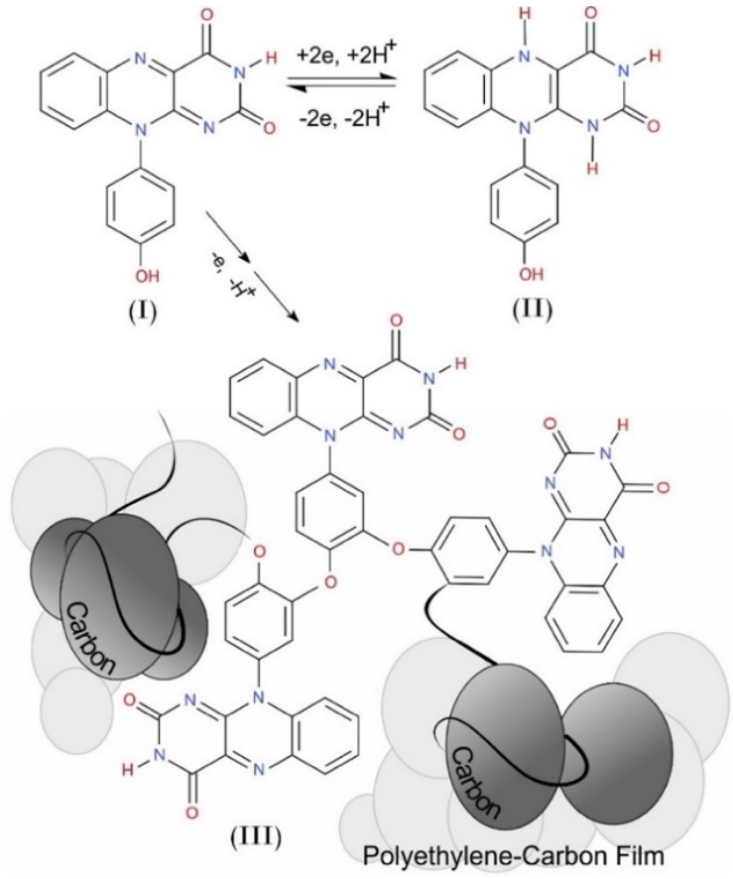

Figure 7.1.2. Redox transition of the flavin unit (**I->II**) and the electro-oxidation of the phenolic substituent leading to the production of a polyphenylene oxide polymer (**I->III**) on exposed carbon surfaces at the film interface.

The preparation of the composite C-PE mesh and its subsequent modification with the poly flavin film was therefore investigated and its potential for use as a pH sensing film was critically assessed by examining the response in defibrinated horse blood. In addition, the same process was also applied to the screen printed electrodes and further investigated as detailed in **Section 7.3.2**.

7.2 Experimental Details

7.2.1 Materials

All chemicals were obtained from Sigma-Aldrich, at the highest grade available and were used without further purification. A three-electrode configuration consisting of a glassy carbon electrode as the working electrode, a platinum wire counter and a 3 M KCl Ag | AgCl half-cell reference electrode (BAS Technicol, UK) was used in the initial investigations. Subsequent investigations involved the exact same configuration except for the replacement of the glassy carbon electrode for a carbon SPE or a C-PE mesh film. Details of the fabrication of the carbon SPEs is previously described in Section 6.2.3.

The analytical capability of the carbon SPE was assessed using defibrinated horse blood as the test matrix principally to determine the robustness of the material and to assess the possibility of surface passivation from either matrix components or the by-products from the electrode process. The defibrinated horse blood was obtained from Fisher Scientific (Loughborough, UK).

Laser patterning of the C-PE mesh film was achieved by using a 30W CO_2 air-cooled computer controlled laser-cutter (FB400 series CadCam Technology Ltd, Nottingham, UK). Directional control over the laser, raster/vector speed and output power was by means of the proprietary software (ApS-Ethos) with a spatial resolution of 25 microns. The laser was rastered across the x and y directions with a spacing of 2 mm between each pass.

Electrochemical analysis was carried out using a VSP-300 Multichannel Potentiostat / Galvanostat / EIS (Bio-Logic Science Instruments, EC-Lab Ltd) with a standard three-electrode configuration with either a glassy carbon or a carbon SPE as the working electrode. Platinum wire served as the counter electrode and a conventional silver/silver chloride (3M NaCl, BAS Technicol UK) reference electrode. All measurements were conducted at 22^{o}C ± 2^{o}C.

7.2.2 Sensor Design and Modification

In order to create a comparative investigation of the film properties, the C-PE film was sectioned and mounted in a laminate casing with a 4 mm square window and thermally sealed (Phair, *et al.*, 2013; Anderson, *et al.*, 2014; J Phair, Benson, *et al.*, 2014).The carbon screen-printed electrodes (SPEs) were fabricated through the same process previously described in **Section 6.2.3.** It is relatively common to electrochemically anodise carbon composite electrodes to elicit an improved electrochemical behaviour (Anderson, *et al.*, 2014; J Phair, Benson, *et al.*, 2014). The electro-oxidation process (+2 V, 0.1 M NaOH) typically exfoliates the carbon particles, thereby, generating more edge plane sites and an increased number of various oxygen functional groups (Anderson, *et al.*, 2014; J Phair, Benson, *et al.*, 2014). This process was also instituted here because it has previously been found that the unmodified screen printed electrodes typically exhibit poor electrochemical behaviour which require a large overpotential to obtain any significant analytical responses (J Phair, Benson, *et al.*, 2014).

7.2.3 Flavin Electro-Polymerisation

Riboflavin was obtained from commercial sources whereas the flavin-phenol derivative was custom synthesized and were a gift courtesy of Dr. Rob Smith, from the Chemistry Department of the University of Central Lancashire. The synthesis of the 10-(4-hydroxyphenyl)benzo[g]pteridine-2,4(3H,10H)-dione was accomplished via modifications to previous methods (Mallesham Bejugam, *et al.*, 2007; Roushani, *et al.*, 2014) by collaborators at the University of Central Lancashire. The reaction

summary is highlighted in **Scheme 7.1**. In summary, p-anisidine (**1**) was reacted with 2-fluoro-1-nitrobenezne (**2**) in the presence of potassium carbonate to yield 4-methoxy-2-nitrodiphenylamine (**3**) which was isolated at the pump in 78% yield. The crude material (**3**) was reduced using zinc dust under acidic conditions, and subsequently treated with alloxan monohydrate (**4**) in the presence of boric acid to yield the 10-(4-methoxyphenyl)benzo[g]pteridine-2,4(3H,10H)-dione intermediate in 93% yield which was demethylated using hydrobromic acid you yield the final derivative (**5**) in 98% yield.

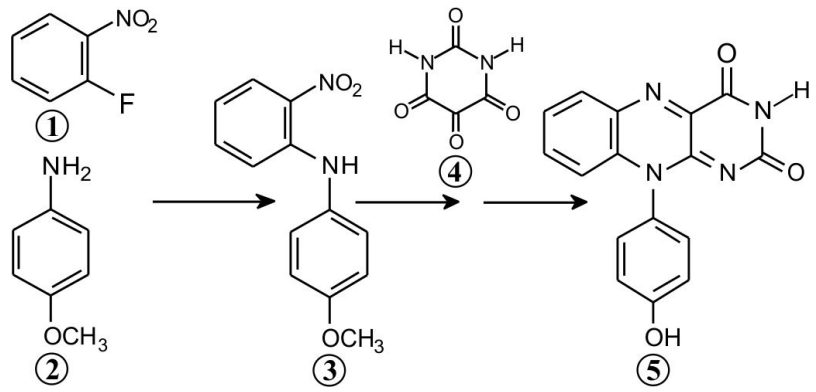

Scheme 7.1. Preparation of the phenolic flavin derivative.

Electropolymerisation was achieved through placing the electrode (glassy carbon or carbon SPE, C-PE mesh film) into an aqueous solution containing the phenol derivative (150 μM, pH 7). Repetitive scan cyclic voltammetry (+0.2 V -> -0.8 V -> +1 V, 50 mV/s) was used to initiate the electropolymerisation process. Solutions were generally degassed with nitrogen prior to commencing the experiments and run under a nitrogen blanket.

7.3 Results and Discussion

7.3.1 Flavin Phenol Electrochemical Properties

The electrochemical properties of the phenolic Flavin derivative were initially investigated using the industry gold standard - glassy carbon electrode and cyclic voltammograms detailing the response are shown in **Figure 7.3.1**. The reduction

and oxidation peaks associated with the Flavin component (**I > II** and **II > I**) can be seen at -0.386 V and -0.362 V respectively. This initial behaviour is consistent with the response observed by others when examining riboflavin (Roushani, *et al.*, 2014; Valipour, *et al.*, 2017) at carbon based electrodes. However, the voltammetric profile changes significantly upon scanning towards more positive potentials. The oxidation of the phenolic component (**I > III**) can be seen at +0.81 V and decreases with consecutive scans, which is consistent with the behaviour expected of mono phenolic species.

It was envisaged that the oxidation of the phenol functionality leads to the formation of oligomeric and polymeric deposits as indicated in **Figure 7.1.2.** When the scan direction is reversed and the potential is swept back towards the Flavin reduction region however, the magnitude of both Flavin peak processes is significantly increased. In separate studies involving the phenolic compound, repetitively scanning the Flavin region without inducing the oxidation of the phenol did not lead to any change in the peak magnitudes. Thus, the increase in the peak height observed on the second and subsequent scans shown in **Figure 7.3.1** can therefore be attributed to the formation of the polymeric deposit on the electrode surface and the accumulation of the material at the interface as anticipated in **Figure 7.1.2.**

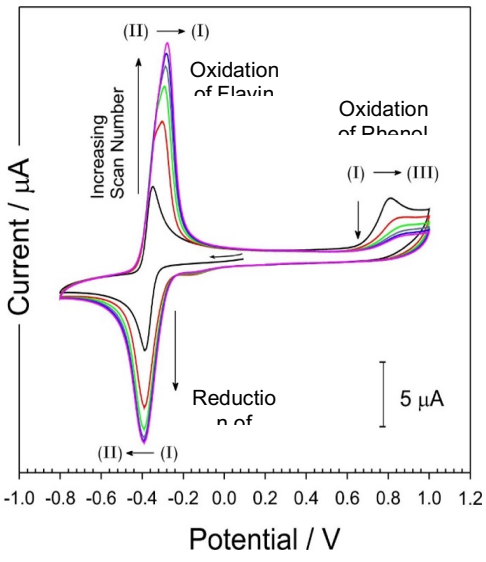

Figure 7.3.1. Five consecutive cyclic voltammograms detailing the response of a glassy carbon electrode towards the Flavin-phenol derivative in pH 7 buffer. Scan rate: 50 mV/s. N_s=5

Further examination of the Flavin voltammetric profile highlights the fact that the initial increase in peak height observed on the second scan, slows after a few cycles and then eventually stops. This can be expected where the passive nature of the polyphenylene oxide film prevents further growth of the film once the available electrode surface has been coated. Further evidence that the phenolic Flavin derivative has indeed formed a polymeric deposit on the electrode surface was obtained through rinsing the electrode and placing it in fresh buffer solution (devoid of the monomer) and examining the voltammetric profiles. As expected, the Flavin redox processes were retained and were found to be stable to repetitive scanning. Cyclic voltammograms detailing the response of the Flavin modified glassy carbon electrode towards pH are detailed in **Figure 7.3.2**. There is little change in the peak height of the Flavin group with varying pH and, again, serves to corroborate the formation of the polymeric material. The peak position was to shift by 60 mV / pH (E/V = 0.0603 pH + 0.1222; N = 7; R^2 = 0.99) and is consistent with a $2H^+$ / 2e process.

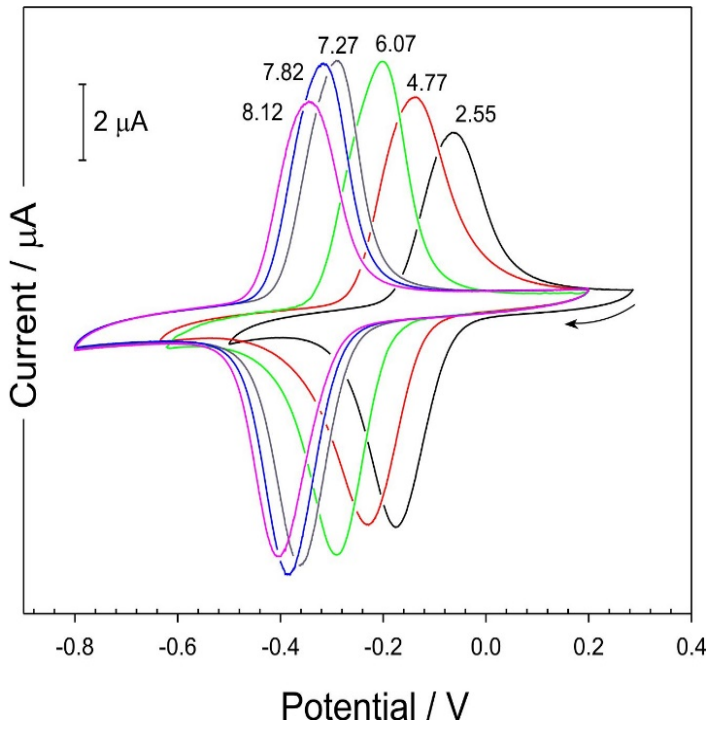

Figure 7.3.2. Cyclic voltammograms detailing the response of a poly Flavin modified glassy carbon electrode in buffers of varying pH. Scan rate: 50 mV/s. N_s=3, N_{pH}=6

7.3.2 Carbon-Polyethylene Mesh Fabrication

The surface profile and etch depths of the C-PE film were initially characterised using a DEKTAK XT Stylus Profiler (Bruker) system with a single pass accounting for a depth of 60 micron. The surface profile is highlighted in **Figure 7.3.3** along with an inset photograph detailing the lasered film. Visual inspection of the film easily highlights the porous mesh like structure of the film and stands in marked contrast to the initial impermeable film. The pores are due to the intersection of perpendicular laser tracks and can be attributed to the fact that, while one pass alone can etch to a depth of 60 micron, a portion of track receiving a second pass (at the intersection) has the potential to etch a further 60 micron and will therefore effectively burn through the 80 micron film.

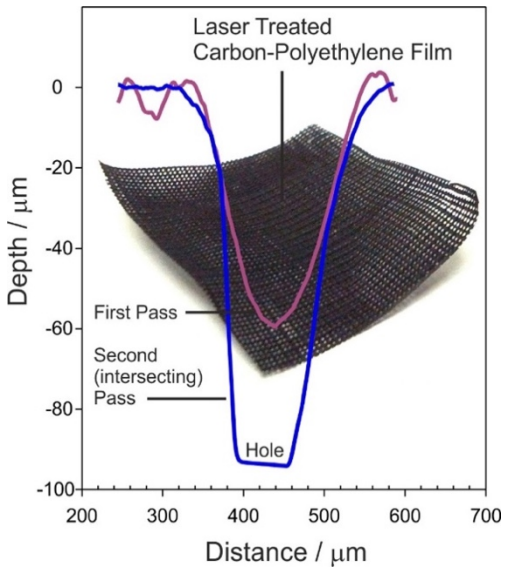

Figure 7.3.3. DekTak surface profile of the lasered film highlighting the typical depth profile of areas receiving a single and double pass. Insert: photograph of the C-PE film after laser treatment.

The laser modification of the film was characterised by a scanning electron microscope and representative images of the resulting mesh are shown in **Figure 7.3.4A-C**. Examination of the laser tracks reveal a highly porous structure that can be attributed to the ablation of the polyethylene, leaving behind residual carbon (**Figure 7.3.4.B**). This is further exemplified in **Figure 7.3.4.C** where the structure of the pore interface (having received 2 laser passes) is shown. The untreated film

(**Figure 7.3.4.B**), in contrast, has a relatively featureless morphology in which isolated aggregations of carbon particles can be seen to penetrate the film surface (as previously postulated in **Figure 7.1.1**). Clearly, the laser treatment greatly increases the exposure of the carbon particles and thus should, along the tracks, increase the interfacial electrochemical properties.

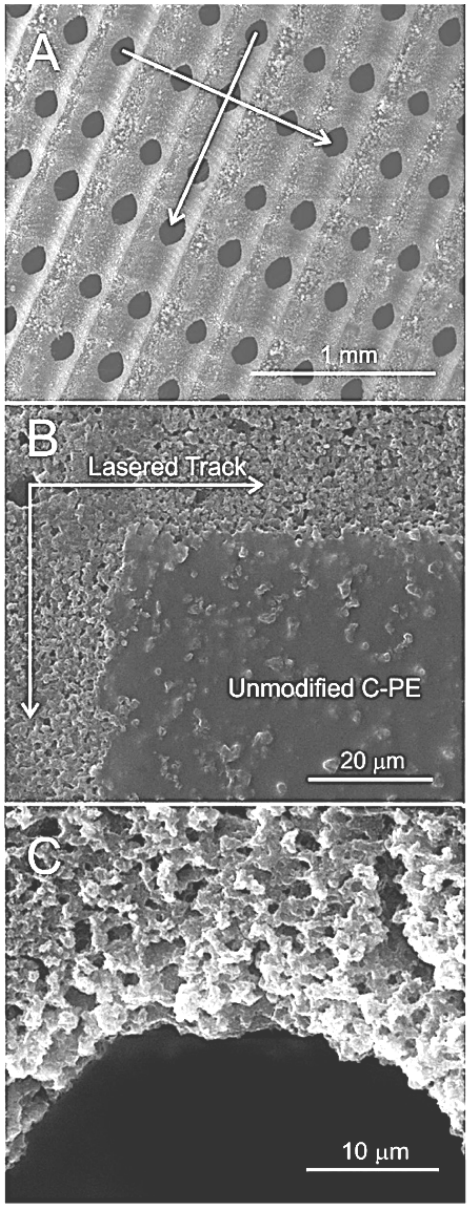

Figure 7.3.4. Scanning electron micrographs of the carbon-polyethylene mesh after laser processing. A) low magnification highlighting the direction of the laser raster and creation of holes within the film. B) Comparison of the laser etched track and unmodified film. C) Removal of the polyethylene at the pore edge as a consequence of laser double pass.

7.3.3 Carbon-Polyethylene Mesh Electrochemistry

Given the apparent stability of the redox processes shown in **Figure 7.3.2**, the next step was to determine if the Flavin film could be transferred to the carbon-polyethylene mesh electrode. Due to the composite nature of the carbon-polyethylene mesh. It was anticipated that the electrochemical properties would be inferior to those exhibited by the glassy carbon. It has been previously shown in **Figure 7.3.4B** that the bare, unmodified carbon-polyethylene film, has a relatively low population of exposed carbon sites through which to induce electroanalytical activity, however, the laser modification of the film should substantially improve the performance. This would still leave the carbon as largely graphitic/basal plane structures and therefore the pre-anodisation through electrochemical oxidation in NaOH should lead to the exfoliation of the former, providing a greater number of edge plane sites that should enhance electron transfer.

The procedure used to form the Flavin on the glassy carbon electrode was again employed for the carbon-polyethylene mesh, as detailed in **Figure 7.3.5.** A similar voltammetric profile to the glassy carbon electrode was observed (**Figure 7.3.1**). However, minor differences were observed in comparison to the glassy carbon electrode, which included a greater peak separation and a less defined peak process. These differences could be attributed to the composite nature of the mesh, however it is important to note that the three processes are still clearly recognisable.

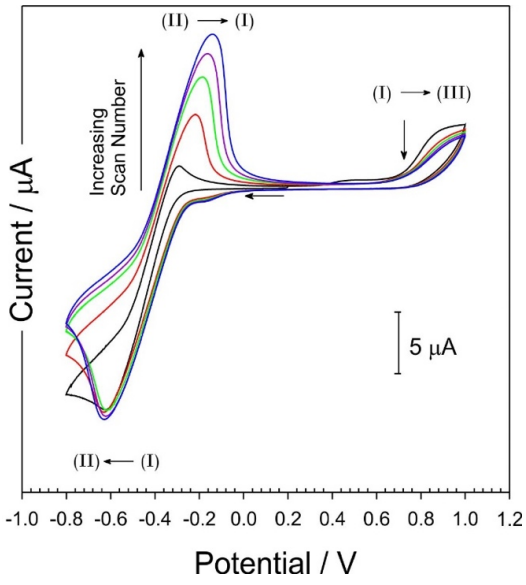

Figure 7.3.5. Five consecutive cyclic voltammograms detailing the response of the carbon-polyethylene mesh electrode towards the Flavin-phenol derivative in pH 7 buffer. Scan rate: 50 mV/s. N_s=5

The electrode was removed, rinsed and placed in fresh buffer. Rather than use cyclic voltammetry to assess the response to pH and perform the measurements under nitrogen, square wave voltammetry was employed to enhance the peak profile without any prior degassing of the solution. Subsequent voltammograms obtained at the Flavin modified mesh are detailed in **Figure 7.3.6**. The position of the oxidation peak was found to vary with pH in an analogous manner to that observed with the glassy carbon electrode with a 60 mV/pH shift (E / V = 0.060 pH + 0.0972; N = 7; R^2 = 0.998). A critical factor here is that although the peak potentials are located within a negative potential region, the response is unaffected by the presence of oxygen.

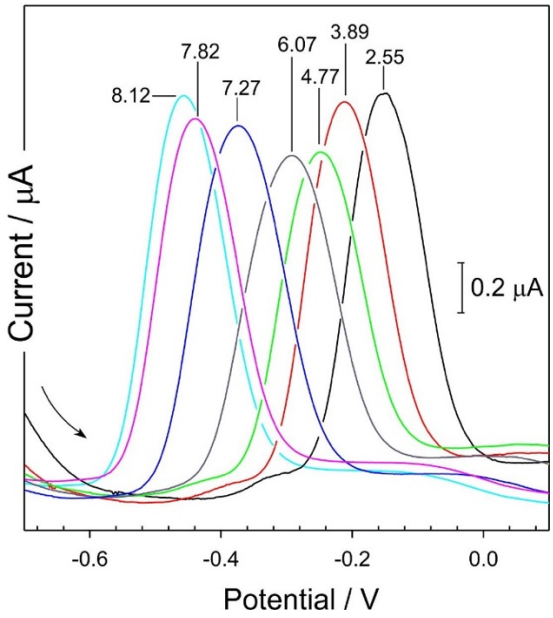

Figure 7.3.6. Square wave voltammograms detailing the response of a poly Flavin modified carbon-polyethylene mesh electrode in buffers of varying pH. N_s=3, N_{pH}=7

The ability of the film to repeatedly monitor pH was determined by scanning the C-PE/Flavin film through a sequence of varying buffer solutions (pH 2.55 to pH 8.12) that covered a physiologically relevant range. After one pH series, had been completed the measurement series was then repeated a further two times. This was to confirm that the pH was reversible and to also assess the degree of drift. Each pH buffer was scanned three times resulting in a total of 63 scans over the entire three series. The variation of peak position with pH for each run is highlighted in **Figure 7.3.7.A**. It should be noted that each point is the average of three measurements and although error bars are included within the figure – the variation (typically less than 2 mV) is so small that they are barely discernible from the actual marker.

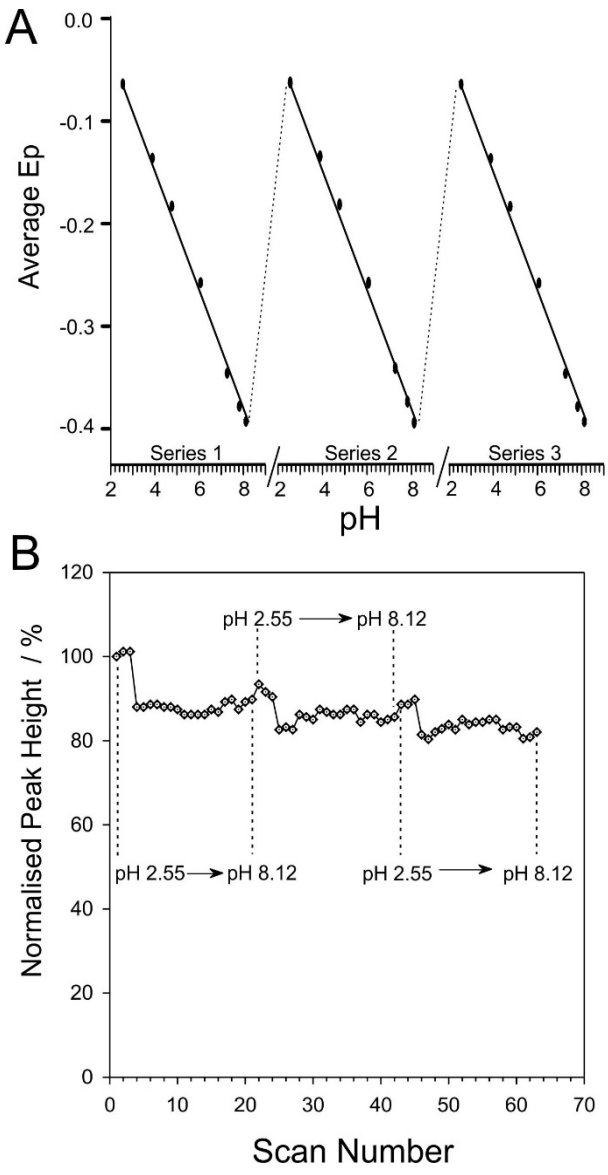

Figure 7.3.7. A) Variation of peak potential with pH over three consecutive pH series recorded at the Flavin modified carbon-polyethylene mesh. B) Influence of repetitive cycling and pH on the peak magnitude of the Flavin modified carbon-polyethylene mesh. N_s=63, N_{pH}=7

The impact of the repetitively scanning on the peak height can provide an indication of the stability of the Flavin film. The normalised peak height, that is based on the magnitude of the first scan, as a function of scan number is highlighted in **Figure 7.3.7.B**. Over 63 repetitive scans (and over 3 entire pH scan series), the oxidation peak associated with the Flavin decreases by less than 20%. This is a vital factor given that the original intention was to engineer a film that could periodically monitor the pH of a biofluid within a wound dressing that may not be changed for up to seven days (Purser, 2010).

7.3.4 Screen Printed Electrodes

The flexible nature of the C-PE mesh makes it a promising candidate for a sensing layer that could conform to a variety of wound morphologies. However, it was of interest to investigate whether a SPE could yield a similar electroanalytical response as this approach would require less processing i.e. laser ablation, and therefore, would be a more economically viable than the C-PE mesh. Based on the multitude of studies published previously involving the commercially available DropSens SPE (Fanjul-Bolado, *et al.*, 2008; Kadara, *et al.*, 2009; Rodríguez, *et al.*, 2018), they were initially considered for investigation. However due to the brittle nature of the ceramic base it would not be applicable for incorporating into a conventional wound dressing. Therefore, as before, the in-house manufactured SPE were selected for further investigation.

In a similar approach to that employed earlier for both the glassy carbon electrode and the C-PE mesh, the SPE was cycled five times in the Flavin-phenol derivative in pH 7 buffer solution, and the response was recorded, as detailed in **Figure 7.3.8.** In a similar process as described before, the SPE electrode was removed, rinsed and placed in fresh buffer for subsequent square wave voltammograms. Representative voltammograms obtained at the Flavin modified SPE are detailed in **Figure 7.3.9** The position of the oxidation peak was found to vary with pH in an analogous manner to that observed with the glassy carbon electrode with a 63 mV/pH shift ($E/V = 0.063\ pH + 0.0924$; $R^2 = 0.990$; $N_s=3$, $N_{pH}=7$).

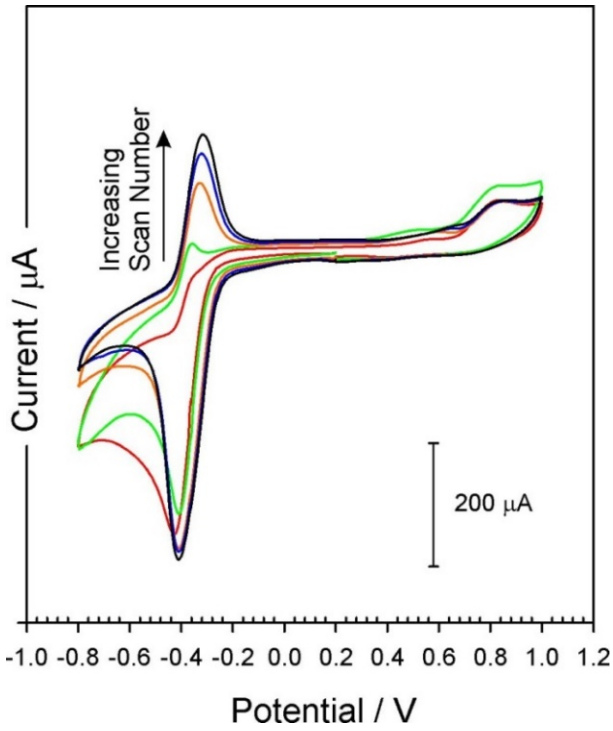

Figure 7.3.8. Five consecutive cyclic voltammograms detailing the response of a SPE towards the flavin-phenol derivative in pH 7 buffer. Scan rate: 50 mV/s. N_s=5

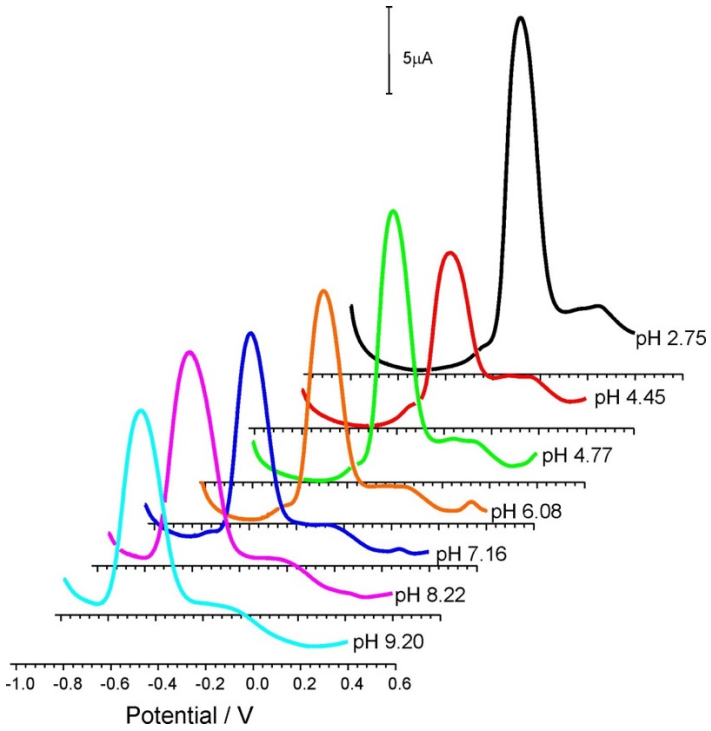

Figure 7.3.9. Square wave voltammograms detailing the response of a poly Flavin modified SPE electrode in buffers of varying pH. N_s=3, N_{pH}=7

Unlike the previous chapter in which the dimer/Nafion® modified SPE required a time delay of 10 minutes to allow for the electrode to calibrate, this was not the

case for the Flavin modified SPE. With a minor peak position variation of 2 mV during a 10-minute period, this signified that a time delay is not necessary for accurate results. The ability of the film to repeatedly monitor pH was determined by running the Flavin modified SPE through a sequence of buffer solutions that covered a physiologically relevant range (pH 2.64 - pH 9.2). This was to confirm that the pH was reversible and to assess the degree of drift the electrode experienced over time.

A total of four different electrodes were tested to determine the inter and intra electrode response towards a pH range over a maximum of 5 days, as detailed in **Table 7.1**. The first electrode (E1) was scanned three times in each pH buffer solution at approximately the same time each day of the time study. Upon each subsequent day, until day four, an additional electrode was added for testing. On day five, no new electrodes were added for testing, this resulted in a total of four electrodes (E1 –E4) within the five-day period, all of which had varying time durations from 2 to a maximum of 5 days of testing.

A plot of the average peak position measurement recorded for the first electrode (E1), which was subjected to 60 measurements over a select pH range over a period of 5 days, is presented in **Figure 7.3.10**. It should be noted that each point is the average of three measurements and although error bars are included within the figure – the variation (typically less than 2 mV) is so small that they are barely discernible from the actual marker.

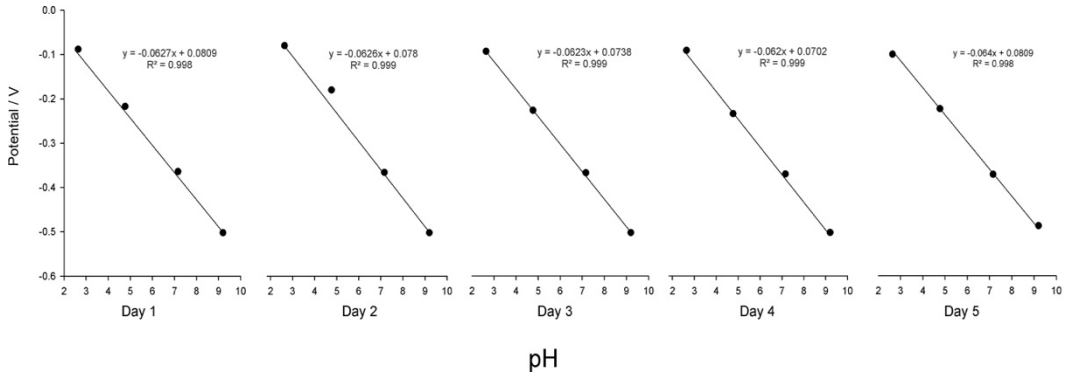

Figure 7.3.10 Peak potential response of Flavin modified SPE to a pH range over a period of five consecutive days. N_s=3, N_{pH}=4

The electrode response over the period of five days yielded a consistent response, demonstrating the stability of the electrode over time. However, it was of particular interest to determine if this single electrode response was consistent with the response of a number of different electrodes. Therefore, the inter electrode response toward pH was compared, as highlighted in **Table 7.1**, which resulted in only a small deviation from the overall average peak position for each pH. This indicates that the production of the electrodes is of a consistently high standard, thus making it reproducible and suitable for mass manufacturing.

Table 7.1 Flavin modified SPE average peak position response over duration of up to 5 days. E= Electrode

	Mean Peak Position / V (Intra)				**Mean / V (Inter)**	**Standard Deviation**
pH	E1	E2	E3	E4		
2.64	-0.093	-0.09	-0.094	-0.091	-0.092	0.002
4.77	-0.224	-0.217	-0.223	-0.236	-0.225	0.008
7.16	-0.368	-0.364	-0.368	-0.347	-0.362	0.010
9.2	-0.499	-0.492	-0.483	-0.437	-0.478	0.028
Number of days	5	4	3	2		

7.3.5 Analytical Applicability in Defibrinated Horse Blood

The analytical accuracy of the Flavin modified SPE was further assessed by comparing its response to defibrinated horse blood against a conventional glass pH probe (Hanna Instruments, Bedfordshire, UK). The Flavin SPE was immersed in the defibrinated horse blood sample and three square wave voltammograms were recorded analogous to the process used previously in **Figure 7.3.11**. A representative voltammogram of the Flavin SPE in defibrinated horse blood highlights the unambiguous identification of the Flavin oxidation peak. A second, slight peak process can be seen to emerge as the potential is swept to more positive potentials and this could be attributed to the oxidation of another low

weight species such as urate or ascorbate. The advantage of utilising the Flavin group is that the peak is in a region where there are no competing processes. However, a minor discrepancy in peak positions was reported between the pH 7 buffer solution (-0.351 V) and the defibrinated horse blood sample (-0.378 V), which is attributed to the difference in pH.

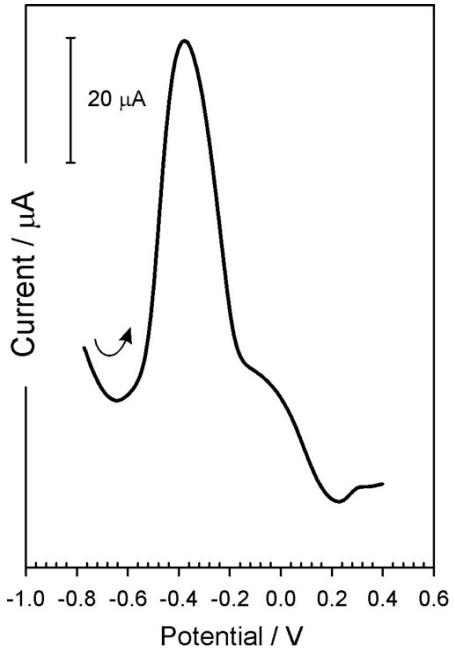

Figure 7.3.11. Square wave voltammogram detailing the response of a poly flavin modified SPE electrode in defibrinated horse blood.

The peak position from each of the defibrinated horse blood were extracted and the calibration data detailed in **Figure 7.3.9** (E/V = 0.063 pH + 0.0924; N = 7; R^2 = 0.990) was used to determine the pH. The results from the three samples are compared with the standard technique in **Table 7.2**

Table 7.2. Analysis of the peaks obtained from the poly Flavin modified SPE electrode response in defibrinated horse blood. E= Electrode

	Mean pH (Intra)	**Standard Deviation**
E1	7.61	0.001
E2	7.61	0.000
E3	7.54	0.002
Mean pH (Inter)	7.59	
Standard Deviation	0.043	

The pH of the defibrinated horse blood was measured using a hand-held pH meter (Eutech Instruments) and produced an average pH of 7.51. The response of the Flavin modified SPE towards defibrinated horse blood is within 0.2 pH unit of the standard system. The fact that the Flavin redox centre can be probed at very low potentials avoids the possibility of oxidising matrix components such as tyrosine and L-tryptophan whose products are known to passivate electrode surfaces (J Phair, Benson, *et al.*, 2014). The peak position is vital in determining the pH, therefore it is vital that the peak positions remain constant upon repetitive scanning. The repeatability of the electrode was assessed through consecutive scanning in horse blood (pH 7.5). A total of ten scans were recorded and the variation of the peak position is detailed on **Table 7.3**.

Table 7.3. Variation of the peak position from respectively scanning (10 scans) three Flavin modified SPE electrodes in defibrinated horse blood. E= Electrode

	Mean	**Standard Deviation**
E 1	-0.358	0.001
E 2	-0.363	0.002
E3	-0.371	0.001
Inter variation	-0.364	0.006

The inter variation of the mean peak positions between the electrodes resulted in a slight variation which resulted in a minor error with a %RSD = 1.76%. While the

intra variation of the electrodes response towards repetitive scanning in defibrinated horse blood showed minor deviation (%RSD =0.28% - 0.59%; N_s=10) in the peak position. The maximum intra variation of the peak position for the three electrodes response towards was found to be 6 mV. This level of error was calculated using each of the individual calibration graphs, it resulted in an error ranging from 0.09 – 0.21 pH units. Although the electrode response towards repetitive scanning towards pH buffer solutions provided promising results, unfortunately the electrode reliability was challenged by repetitive scanning in the defibrinated horse blood. The instant succession of each of the ten scans may have attributed to electrode fouling which is an issue that would need to be addressed in the future.

7.4 Conclusions

The Flavin redox film has been shown to be robust to repetitive scanning in buffer solutions and can provide an accurate measure of pH in defibrinated horse blood**.** The system is free from common interferences found in biofluids by virtue of the cathodic potentials necessary to interrogate the Flavin redox centre and, critically, the measurement of the oxidation potential can be achieved without the need for degassing. The modified screen printed electrode exhibited Nernstian behaviour across the range of pH 2.75 to pH 9.2 (63 mV/pH, **Figure 7.3.9**), which greatly exceeds the clinically relevant remit. The stability of the electrode was assessed over a period of five days and resulted in a minor deviation of the peak position (**Figure 7.3.10**).

The modified screen printed electrode response towards defibrinated horse blood was also investigated (**Figure 7.3.11**). A sharp discernible peak was still obtained in the complex media and accurate intra pH measurements were recorded when compared to the hand-held pH meter, even after numerous scans. However, the complex nature of the defibrinated horse blood did prove to be a challenge for the sensor in terms of reproducibility. The intra variations between the individual electrodes resulted in a maximum potential error of 0.09 – 0.21 pH units (**Table**

7.2). The acceptable level of error is <0.2 pH units, signifies that further electrode standardisation is still required prior to being considered as a simple pH indicator for chronic wounds.

Chapter 8

Conclusions and Recommendations for Future Work

8.1 Conclusions

The treatment of chronic wounds, particularly those associated with diabetic complications, is a perennial problem for modern healthcare services that affects an ever-increasing portion of society. This is particularly worrisome given that the diabetic population and associated costs are expected to double in size within the next 25 years. A critical factor that needs to be considered when dealing with chronic wounds is infection. This can have a huge impact on healing time and could inevitably lead to further discomfort of the patient and ultimately life threatening complications. Most chronic wounds (>74%) are treated within the community and as such there can be a delay in the patient seeking medical attention, which can result in a deterioration of the wound condition which potentially could lead to limb amputation. In addition, the status of the wound is not fully revealed until the dressing is removed and assessed by the clinician. Therefore, there is a pressing demand to develop an *in-situ* sensor that could routinely provide the clinician with information on the status of the wound in regards to healing and the presence of infection.

Over recent years, a number of biomarkers, such as, temperature, bacterial metabolites, and inflammatory mediators, have been identified and investigated to determine their applicability as a key indicator to the healing status of the wound. However, in this research project the focus was predominately on wound pH, which has long been clinical recognised as an important diagnostic. Unfortunately, there has been no significant technological advancement in the development of a clinical point of care system or even a community based system for monitoring wound pH. Therefore, the aim of this investigation was to develop a novel approach that could provide a solution to these issues. Rather than rely on the subjective visual cues of the assessor, an electrochemical sensor could provide a quantitative value for the pH of the wound but, equally as important, the methodology could lay the foundation for the development of an integrated smart dressing capable of monitoring the wound in a routinely and decentralised manner.

A commercially available palladium film was selected as the base substrate to potentiometrically measure pH. The results detailed in Chapter 4 demonstrate that the initial response of the Pd film towards pH was highly variable. Although metallic Pd is pH sensitive, it's been reported that the sensing mechanism of PdO is markedly different, which could have attributed to the poor electrode response. Therefore, in an attempt to enhance the electrodes sensitivity towards pH, the electrode surface was modified with a self-assembly monolayer using the amino acid, L-cysteine. A sub Nernstian response was observed over a clinically relevant pH regime from (pH 3 – 8, **Figure 4.3.7**). However, upon three consecutive pH ranges a significant drift in signal was reported, resulting in substantial deterioration of the electrode response (**Figure 4.3.8**). This poor response is believed to be attributed to air oxidation, and hence the formation of PdO, that would make this system unsuitable for continuous and reproducible monitoring of pH. In addition, a degree of variability in terms of potential drift was reported while using the potentiometric technique (**Figure 4.3.8**), which ultimately led to the transition to voltammetric methodologies. Ultimately, the high cost of the palladium, meant that it was not economically viable as a sensing substrate for a disposable sensor. However, the findings from this chapter helped build the foundation for subsequent chapters.

Chapter 5 describes the development of a composite electrode which employed a carbon fibre mesh as the base substrate and poly-L-tryptophan as the modifying polymer. The detection rationale exploited the pH sensitivity of the quinoid functionalities produced from the electro-oxidation of L-tryptophan's indole substituent. The oxidation of the resulting polymer locked quinone components was found to obey the Nernstian behavior over a pH range from pH 3 – 8 (**Figure 5.3.12**). However, beyond pH 8 a sub Nernstian response was observed which could be attributed to the system moving towards a 2 electron, 1 proton regime brought about by the lack of proton availability under alkaline conditions. Typically, the pH of blood is around pH 7.4, therefore it could be anticipated that the majority of the recorded measurements of chronic wounds would lie within an alkaline region and therefore greater sensitivity would be required. The composite electrode response

towards pH was further challenged in a simulated wound environment, using defibrinated horse blood (**Figure 5.3.13**). A sharp quinoid peak was observed, however a minor discrepancy between the recorded pH was reported when compared to the hand-held pH meter. In addition, the brittle nature of the carbon fibre substrate means that it is not flexible enough for the high degree of morphological variability encountered within diabetic foot ulcers.

Carbon based screen printed electrodes were selected as the base substrate in Chapter 6 due to their low manufacturing costs. In addition, it could potentially be envisioned that the electrode design could be directly printed onto the surface of a conventional dressing, therefore making it more applicable to a wider variety of wound morphologies. The detection rationale employed in this chapter exploited the pH sensitivity of the quinone dimer that was generated from the electrochemical oxidation of salicylate and adsorbed onto the electrode surface (**Figure 6.3.5**). The initial response of the dimer modified SPE exhibited a sub Nernstian behaviour across a pH range covering pH 3 - 8 (**Figure 6.3.9**). However, minor deviations from the line of best fit were observed as the pH increased. In alkaline conditions, this deviation is believed to be attributed to the de-absorption of the dimer into the bulk solution and the loss of interaction between the dimer and the carbon interface. To prevent this, the electrode surface was then coated with a layer of Nafion® to entrap the generated dimer. This modification resulted in the electro-oxidation of the dimer bound at the electrode surface providing a pH dependent response that exhibited a sub Nernstian response (51 mV/pH) over a pH range (pH 3 – pH 8) (**Figure 6.3.12**). The stability of the modified SPE was assessed over four consecutive pH ranges (**Figure 6.3.14**) which exhibited only minor variations that translated to a reported error of 0.002 pH units. However, a ten-minute delay before recording the scan for each new solution was necessary for the electrode to calibrate to its new environment. The analytical performance and stability of the dimer modified screen-printed electrode was assessed using defibrinated horse blood as a simulated wound environment and accurate pH measurements were recorded when compared to the hand-held pH meter (**Figure 6.3.15**).

The sensing rationale in Chapter 7 focused on the reversible nature of an engineered Flavin derivative bearing a pendant phenol derivative that was electropolymerised onto an anodised carbon screen printed electrode. The electrode's response exhibited a super Nernstian response (63 mV/pH) across a pH range 2.75 to 9.20,(**Figure 7.3.9**) and unlike the previous system in Chapter 6, it did not require a ten-minute calibration. Assessment within defibrinated horse blood proved that the electrode could provide a relatively accurate response to pH in comparison to the hand-held pH meter (**Table 7.2**). A crucial advantage of the system relates to the fact that the analytical signal is acquired in a region free from the interferences (ascorbate, urate) typically encountered in wound fluid. However, variations between the different electrodes were reported (**Table 7.3**), as such, this sensor would be best suited to monitor the fluctuations in pH at this stage, rather than record the exact pH.

8.2 Recommendations for Future Work

The system described here focuses primarily on one biomarker – pH, however based upon the carbon screen printed electrode response towards ferrocyanide, it can be anticipated that it could also be employed for other wound biomarkers. These biomarkers could include uric acid, glucose and the process of oxygen sensing through secondary processing, (via enzyme attachment). Therefore, the strategy presented here could provide the foundation for future investigations into the development of a multi-parametric smart bandage.

The main end application of this research was focused on chronic wounds, in particular diabetic foot ulcers. However, the simplistic nature of the design and manufacture of the sensing element, means it could be envisioned that this pH sensor could be integrated into other medical products, such as ostomy wafers. This system could therefore be applicable to a variety of different scenarios from hospitals to elderly care homes, even to tumultuous environments such as the battlefield where medical assistance can be scarce. Therefore, the ability to autonomously and periodically monitor the status of the wound environment could

alert the clinician and/or patient to potential infection thereby enabling a much more robust wound management system.

An aspect of this system that was not discussed in this piece of research was the development of a portable potentiostat. Often, the major emphasis is on the development of the sensing layer and the material science behind it, rather than the actual integration and communication between the sample analyser. In this research project the core remit did not extend to the development and integration of the sensor with a portable potentiostat. However, it is imperative for the future development of this system that this key area is explored. Considering the recent advances in the development of electronics and battery research, it could be anticipated that a miniaturised and integrated prototype device could be produced in the near future.

Surface fouling is a perennial issue for devices dealing with biological fluid samples and, as such, it can significantly hinder the accuracy and lifetime of the device. In regards to the development of a smart bandage, the sensing system would be expected to have the same lifetime expectancy as the conventional dressing it is integrated into. This would ensure that the wound environment is not compromised through unnecessary re-dressing of the wound. A potential future refinement to the sensing layer would be the introduction of a polymeric coating such as polyurethane and cellulose acetate. This could have the potential to provide a layer of protection to the sensing layer through size exclusion, by blocking access of larger proteins while still allowing smaller molecules to permeate through. Based on this refinement, it may be speculated that the lifetime of the sensing elements could be increased. In addition, the sensitivity and clarity of the measurement in a complex wound environment could also be improved.

Further evaluation of the relationship observed between pH and infection within clinical samples is imperative for future development of the approaches taken in this work. Nonetheless, the materials investigated and design rationales have been assessed in simulated fluids. The use of defibrinated horse blood is worthy of note

as it provides a complex environment which mimics that which would be found within a wound environment – albeit without the presence of fibroblast activity. In the last three result chapters, the applicability of the selected material for pH monitoring has been demonstrated. It is evident that the sensing systems presented here could provide an invaluable foundation for the future development of sensors that could ultimately garner clinical merit. The issue of manufacturing viability has been at the forefront of the approaches employed here as, with an ever-cost conscious healthcare system, there needs to be a clear cost benefit in implementing new technologies. Therefore, the materials employed in this research were inexpensive and could readily be adapted for mass manufacturing. The ability to measure the pH of the wound within a clinical setting has become an area of substantial research interest in recent years, yet despite the considerable advances in technology, the strategies developed here remain at the forefront of novel research and clinical applicability.

References

Amjad, S., Carachi, R. and Edward, M. (2007) 'Keratinocyte regulation of TGF-BETA and connective tissue growth factor expression: A role in suppression of scar tissue formation', *Wound Repair and Regeneration*, 15(5), pp. 748–755.

Anderson, A., *et al.* (2014) 'Investigating the use of endogenous quinoid moieties on carbon fibre as means of developing micro pH sensors', *Materials Science and Engineering: C*. Elsevier B.V., 43, pp. 533–537.

Angel, D. E., *et al.* (2011) 'The clinical efficacy of two semi-quantitative wound-swabbing techniques in identifying the causative organism(s) in infected cutaneous wounds', *International Wound Journal*, 8(2), pp. 176–185.

Armstrong, D. and Lipsky, B. (2004) 'Diabetic foot infections: stepwise medical and surgical management', *International Wound Journal*, 1(2), pp. 123–132.

Assal, J. P., *et al.* (2002) 'On your feet! Workshop on the diabetic foot.', *Journal of diabetes and its complications*, 16(2), pp. 183–94.

Augustin, M., *et al.* (2014) 'Cost-of-illness of leg ulcers in the community.', *International wound journal*, 11(3), pp. 283–92.

Bakker, K., Apelqvist, J. and Schaper, N. C. (2011) 'Practical guidelines on the management and prevention of the diabetic foot 2011.', *Diabetes/metabolism research and reviews*, 28(1), pp. 225–231.

Banks, C. E. and Compton, R. G. (2005) 'Exploring the electrocatalytic sites of carbon nanotubes for NADH detection: an edge plane pyrolytic graphite electrode study', *The Analyst*, 130(9), p. 1232.

Banks, C. E. and Compton, R. G. (2006) 'New electrodes for old: from carbon nanotubes to edge plane pyrolytic graphite.', *The Analyst*, 131, pp. 15–21.

Bard, A. J. and Faulkner, L. R. (2001) *Electrochemical Methods: Fundamentals and Applications*. New Jersey, USA: John Wiley & Sons, Inc.

Barillo, D. J. and Marx, D. E. (2014) 'Silver in Medicine: A Brief History BC 335 to present', *Burns*. Elsevier Ltd and International Society of Burns Injuries, 40, pp. S3–S8.

Barnea, Y. and Weiss Eyal Gur, J. (2010) 'Therapeutics and Clinical Risk Management A review of the applications of the hydrofiber dressing with silver (Aquacel Ag ®) in wound care', *Therapeutics and Clinical Risk Management*, 6(1), pp. 21–21.

Beitollahi, H., Taher, M. A. and Hosseini, A. (2014) 'Fabrication of a nanostructure-based electrochemical sensor for simultaneous determination of epinephrine and tryptophan', *Measurement*, 51, pp. 156–163.

Boateng, J. and Catanzano, O. (2015) 'Advanced Therapeutic Dressings for Effective Wound Healing-A Review.', *Journal of pharmaceutical sciences*, 104(11), pp. 3653–80.

Boonkaew, B., *et al.* (2014) 'Cytotoxicity testing of silver-containing burn treatments

using primary and immortal skin cells', *Burns*. Elsevier, 40(8), pp. 1562–1569.

Bouter, K. P., *et al.* (1993) 'The diabetic foot in Dutch hospitals: epidemiological features and clinical outcome.', *The European journal of medicine*, 2(4), pp. 215–218.

Bowler, P. G., Duerden, B. I. and Armstrong, D. G. (2001) 'Wound microbiology and associated approaches to wound management.', *Clinical Microbiology Reviews*. American Society for Microbiology, 14(2), pp. 244–69.

Brem, H. and Tomic-Canic, M. (2007) 'Cellular and molecular basis of wound healing in diabetes.', *The Journal of clinical investigation*. American Society for Clinical Investigation, 117(5), pp. 1219–22.

Broadbent, J., Walsh, T. and Upton, Z. (2010) 'Proteomics in chronic wound research: Potentials in healing and health', *Proteomics - Clinical Applications*, 4(2), pp. 204–214.

Brook, I. (1996) 'Aerobic and Anaerobic Microbiology of Necrotizing Fasciitis in Children', *Pediatric Dermatology*, 13(4), pp. 281–284.

Byrne, R. and Diamond, D. (2006) 'Chemo/bio-sensor networks', *Nature Materials*, 5(6), pp. 421–424.

Cao, Y., *et al.* (2011) 'A peptidomimetic inhibitor of matrix metalloproteinases containing a tetherable linker group', *Journal of Biomedical Materials Research Part A*. Wiley Subscription Services, Inc., A Wiley Company, 96A(4), pp. 663–672.

Cerkoney, K. A. and Hart, L. K. (1980) 'The relationship between the health belief model and compliance of persons with diabetes mellitus.', *Diabetes Care*. American Diabetes Association, 3(5), pp. 594–8.

Chen, J., *et al.* (2017) 'Poly(-cyclodextrin)/carbon quantum dots modified glassy carbon electrode: Preparation, characterization and simultaneous electrochemical determination of dopamine, uric acid and tryptophan', *Sensors and Actuators B*, 252, pp. 9–16.

Chen, S., *et al.* (2007) 'Amperometric third-generation hydrogen peroxide biosensor based on the immobilization of hemoglobin on multiwall carbon nanotubes and gold colloidal nanoparticles', *Biosensors and Bioelectronics*, 22, pp. 1268–1274.

Cherchour, N., *et al.* (2011) 'pH sensing in aqueous solutions using a MnO2 thin film electrodeposited on a glassy carbon electrode', *Electrochimica Acta*. Elsevier Ltd, 56(27), pp. 9746–9755.

Chrzescijanska, E., *et al.* (2014) 'Study of acetylsalicylic acid electroreduction behavior at platinum electrode', *Journal of Electroanalytical Chemistry*. Elsevier, 713, pp. 17–21.

Chu, J., *et al.* (2015) 'An Integrated Solid-State pH Microelectrode Prepared Using Microfabrication', *Electrochimica Acta*. Pergamon, 152, pp. 6–12.

Ciani, I., *et al.* (2012) 'Development of immunosensors for direct detection of three

wound infection biomarkers at point of care using electrochemical impedance spectroscopy', *Biosensors and Bioelectronics*, 31, pp. 413–418.

Clark, R., *et al.* (1998) 'Platelet isoforms of platelet-derived growth factor stimulate fibroblasts to contract collagen matrices.', *Journal of Clinical Investiagtion*, 84(3), pp. 1036–1040.

Clark, R. (1998) *The Molecular and Cellular Biology of Wound Repair*. 2nd edn. New York: Plenum Press.

Comninellis, C. and Pulgarin, C. (1991) 'Anodic oxidation of phenol for waste water treatment', *Journal of Applied Electrochemistry*. Kluwer Academic Publishers, 21(8), pp. 703–708.

Compton, R. G. and Banks, C. E. (2011) *Understanding Voltammetry*. Imperial College Press.

Consortium, Y. H. E. (2011) *NHS spending on diabetes 'to reach £16.9 billion by 2035' | Diabetes UK*, *Diabetes Uk*. Available at: https://www.diabetes.org.uk/about_us/news_landing_page/nhs-spending-on-diabetes-to-reach-169-billion-by-2035 (Accessed: 12 February 2018).

Cortese-Krott, M. M., *et al.* (2009) 'Silver ions induce oxidative stress and intracellular zinc release in human skin fibroblasts', *Free Radical Biology and Medicine*. Pergamon, 47(11), pp. 1570–1577.

Dai, C., *et al.* (2015) 'A novel sensor based on electropolymerized substituted-phenols for pH detection in unbuffered systems', *RSC Advances*. The Royal Society of Chemistry, 5(126), pp. 104048–104053.

Dargaville, T. R., *et al.* (2013) 'Sensors and imaging for wound healing: A review.', *Biosensors and Bioelectronics.*, 41, pp. 30–42.

Davies, T. J. and Compton, R. G. (2005) 'The cyclic and linear sweep voltammetry of regular and random arrays of microdisc electrodes: Theory', *Journal of Electroanalytical Chemistry*. Elsevier, 585(1), pp. 63–82.

Davis, J., *et al.* (2013) 'Plasma-polyplumbagin-modified microfiber probes: A functional material approach to monitoring vascular access line contamination', *ACS Applied Materials and Interfaces*, 5(19), pp. 9367–9371.

Davis, J., *et al.* (2016) *Smart Bandage technologies : Design and Application*. 1st edn. Academic Press.

Dehdashtian, S., Shamsipur, M. and Gholivand, M. B. (2016) 'Fabrication of a novel electrochemical sensor based on an electrosynthesized indolyldihydroxyquinone as a bio-based modifier for sensitive and selective direct electrochemical determination of tryptophan', *Journal of Electroanalytical Chemistry*, 780, pp. 119–125.

Di, J. and Zhang, F. (2003) 'Voltammetry determination of trace manganese with pretreatment glassy carbon electrode by linear sweep voltammetry', *Talanta*. Elsevier, 60(1), pp. 31–36.

Diabetes UK (2011) *Putting feet first: national minimum skills framework The national minimum skills framework for commissioning of footcare services for people with diabetes*.

Dissemond, J., *et al.* (2003) 'pH values in chronic wounds. Evaluation during modern wound therapy', *Hautarzt*, 54(10), pp. 959–965.

Dovi, J. V, Szpaderska, A. M. and DiPietro, L. A. (2004) 'Neutrophil function in the healing wound: adding insult to injury?', *Thrombosis and Haemostasis*. Burn and Shock Trauma Institute, USA., 92(2), pp. 275–280.

Dowsett, C., Bielby, A. and Searle, R. (2014) 'Reconciling increasing wound care demands with available resources.', *Journal of Wound Care*, 23(11), p. 552, 554, 556–8 passim.

Dutt, J., *et al.* (2005) 'Diagnostic implications of uric acid in electroanalytical measurements.', *Electroanalysis*, 17(14), pp. 1233–1243.

Edmonds, M. (2005) 'Infection in the neuroischemic foot.', *The International Journal of Lower Extremity Wounds*. Diabetic Foot Unit, London, UK., 4(3), pp. 145–153.

Enache, T. A. and Brett, O. (2011) 'Pathways of Electrochemical Oxidation of Indolic Compounds', *Electroanalysis*, 23(6), p. 1337.

Evans, R. C., *et al.* (2006) 'A Novel Luminescence-Based Colorimetric Oxygen Sensor with a "Traffic Light" Response', *Journal of Fluorescence*. Springer US, 16(2), pp. 201–206.

Falanga, V. (2005) 'Wound healing and its impairment in the diabetic foot.', *Lancet*. Elsevier, 366(9498), pp. 1736–43.

Fanjul-Bolado, P., *et al.* (2008) 'Electrochemical characterization of screen-printed and conventional carbon paste electrodes', *Electrochimica Acta*. Pergamon, 53(10), pp. 3635–3642.

Feliciano-Ramos, I., *et al.* (2010) 'Self-assembled monolayers of l-cysteine on palladium electrodes', *Journal of Electroanalytical Chemistry*. Elsevier, 650(1), pp. 98–104.

Ferreira, A. V., *et al.* (2016) 'Detection of human neutrophil elastase (HNE) on wound dressings as marker of inflammation', *Applied Microbiology and Biotechnology*. Applied Microbiology and Biotechnology, pp. 1–12.

Fischer, L. M., *et al.* (2009) 'Gold cleaning methods for electrochemical detection applications', *Microelectronic Engineering*, 86, pp. 1282–1285.

Fisher, A. C. (1996) *Electrode dynamics*. Oxford University Press.

Frith, K. and Limson, J. (2010) 'Reprint of pH tuning of Nafion® for selective detection of tryptophan', *Electrochimica Acta*, 55, pp. 4281–4286.

Frykberg, R. G. and Banks, J. (2015) 'Challenges in the Treatment of Chronic Wounds.', *Advances in Wound Care*, 4(9), pp. 560–582.

Fylling, C. P. and Knighton, D. R. (1989) 'Amputation in the diabetic population: incidence, causes, cost, treatment, and prevention.', *Journal of Enterostomal Therapy*, 16(6), pp. 247–255.

Gerhardt, G. A. and Hoffman, A. F. (2001) 'Effects of recording media composition on the responses of Nafion-coated carbon fiber microelectrodes measured using high-speed chronoamperometry', *Journal of Neuroscience Methods*, 109, pp. 13–21.

Gethin, G. (2007) 'The significance of surface pH in chronic wounds', *Wounds UK*, 3(3), pp. 52–56.

Gethin, G., *et al.* (2018) 'Monitoring of pH and temperature of neuropathic diabetic and non-diabetic foot ulcers for 12-weeks: an observational study', *Wound Repair and Regeneration*. Wiley/Blackwell (10.1111).

Ghanassia, E., *et al.* (2008) 'Long-term outcome and disability of diabetic patients hospitalized for diabetic foot ulcers: a 6.5-year follow-up study.', *Diabetes Care*. American Diabetes Association, 31(7), pp. 1288–92.

Gibbons, G., *et al.* (1995) *Management of Diabetic Foot Problems.* 2nd edn. Philadelphia.

Gogol, E. V., *et al.* (2000) 'Amperometric biosensors based on nafion coated screen-printed electrodes for the determination of cholinesterase inhibitors', *Talanta*. Elsevier, 53(2), pp. 379–389.

González-Sánchez, M. I., *et al.* (2015) 'In situ detection of salicylate in Ocimum basilicum plant leaves via reverse iontophoresis.', *Chemical Communications*, 51(92), pp. 16534–6.

Grdeń, M., *et al.* (2008) 'Electrochemical behaviour of palladium electrode: Oxidation, electrodissolution and ionic adsorption', *Electrochimica Acta*. Pergamon, 53(26), pp. 7583–7598.

Greener, B., *et al.* (2005) 'Proteases and pH in chronic wounds.', *Journal of Wound Care*. York, UK., 14(2), pp. 59–61.

Greer, N., *et al.* (2012) *Advanced Wound Care Therapies for Non-Healing Diabetic, Venous, and Arterial Ulcers: A Systematic Review*, *Advanced Wound Care Therapies for Non-Healing Diabetic, Venous, and Arterial Ulcers: A Systematic Review*. Department of Veterans Affairs (US).

Grubb, W. T. and King, L. H. (1980) 'Palladium-palladium oxide pH electrodes', *Analytical Chemistry*. American Chemical Society, 52(2), pp. 270–273.

Guinovart, T., *et al.* (2014) 'Bandage-Based Wearable Potentiometric Sensor for Monitoring Wound pH', *Electroanalysis*, 26(6), pp. 1345–1353.

Harding, K. (2007) *Diagnostics and Wounds. A Consensus Document.*, *Principals of Best Practice*. London.

Hehenberger, K., *et al.* (1998) 'Inhibited proliferation of fibroblasts derived from

chronic diabetic wounds and normal dermal fibroblasts treated with high glucose is associated with increased formation of L-lactate', *Wound Repair and Regeneration*. Blackwell Science, 6(2), pp. 135–141.

Heitner-Wirguin, C. (1996) 'Recent advances in perfluorinated ionomer membranes: structure, properties and applications', *Journal of Membrane Science*. Elsevier, 120(1), pp. 1–33.

Hemmink, G. J. M., *et al.* (2010) 'Ambulatory oesophageal pH monitoring: a comparison between antimony, ISFET, and glass pH electrodes', *European Journal of Gastroenterology & Hepatology*, 22(5), pp. 572–577.

Herber, O. R., Schnepp, W. and Rieger, M. A. (2007) 'A systematic review on the impact of leg ulceration on patients' quality of life.', *Health and quality of life outcomes*. BioMed Central, 5, p. 44.

Herlem, G., *et al.* (2010) 'One-pot electrosynthesis of polyglycine-like thin film on platinum electrodes as transducer for solid state pH measurements', *Talanta*, 82(1), pp. 417–421.

Hizawa, T., *et al.* (2006) 'Fabrication of a two-dimensional pH image sensor using a charge transfer technique', *Sensors and Actuators B: Chemical*. Elsevier, 117(2), pp. 509–515.

Holman, N., Young, R. J. and Jeffcoate, W. J. (2012) 'Variation in the incidence of amputation in the lower limb in England', *Diabetologia*, 55, pp. 1919–25.

Horwat, D., *et al.* (2011) 'Chemistry, phase formation, and catalytic activity of thin palladium-containing oxide films synthesized by plasma-assisted physical vapor deposition', *Surface and Coatings Technology*, 205, pp. 171–177.

Huang, E. S., *et al.* (2009) 'Projecting the Future Diabetes Population Size and Related Costs for the U.S', *Diabetes Care*, 32(12), pp. 2225–2229.

Hunt, T. K. (1981) 'Surgical wound infections: An overview', *The American Journal of Medicine*. Elsevier, 70(3), pp. 712–718.

Hussain, M., *et al.* (2014) 'Effect of anions on the morphology of Co3O4 nanostructures grown by hydrothermal method and their pH sensing application', *Journal of Electroanalytical Chemistry*. Elsevier, 717–718, pp. 78–82.

Inoue, T., Baba, T. and Yuchi, A. (2011) 'Responses of Metalloporphyrin-Based Ion-Selective Electrodes to pH', *Electroanalysis*, 23(2), pp. 536–542.

James, T. J., *et al.* (2003) 'Evidence of oxidative stress in chronic venous ulcers', *Wound Repair and Regeneration*. Blackwell Science Inc, 11(3), pp. 172–176.

Jeffcoate, W. J. and Harding, K. G. (2003) 'Diabetic foot ulcers.', *Lancet (London, England)*. Elsevier, 361(9368), pp. 1545–51.

Jerónimo, P. C. A., Araújo, A. N. and Conceição B.S.M. Montenegro, M. (2007) 'Optical sensors and biosensors based on sol–gel films', *Talanta*. Elsevier, 72(1), pp. 13–27.

Jin, J., *et al.* (2013) 'Enhancing the electrical conductivity of polymer composites', *European Polymer Journal*. Pergamon, 49(5), pp. 1066–1072.

Kadara, R. O., Jenkinson, N. and Banks, C. E. (2009) 'Characterisation of commercially available electrochemical sensing platforms', *Sensors and Actuators B: Chemical*. Elsevier, 138(2), pp. 556–562.

Kaempgen, M. and Roth, S. (2006) 'Transparent and flexible carbon nanotube/polyaniline pH sensors', *Journal of Electroanalytical Chemistry*. Elsevier, 586(1), pp. 72–76.

Kaimori, S., *et al.* (2006) 'Structural development of a minimally invasive sensor chip for blood glucose monitoring', *Analytica Chimica Acta*. Elsevier, 573–574, pp. 104–109.

Kanyong, P., Rawlinson, S. and Davis, J. (2016) 'Fabrication and electrochemical characterization of polydopamine redox polymer modified screen-printed carbon electrode for the detection of guanine', *Sensors and Actuators B: Chemical*. Elsevier, 233, pp. 528–534.

Kassal, P., *et al.* (2015) 'Smart bandage with wireless connectivity for uric acid biosensing as an indicator of wound status', *Electrochemistry Communications*, 56, pp. 6–10.

Kerr, M. (2012) *Foot Care for People with Diabetes: The Economic Case for Change*.

Kim, T. Y. and Yang, S. (2014) 'Fabrication method and characterization of electrodeposited and heat-treated iridium oxide films for pH sensing', *Sensors and Actuators B: Chemical*. Elsevier, 196, pp. 31–38.

Kinoshita, E., *et al.* (1986) 'An examination of the palladium/palladium oxide system and its utility for pH-sensing electrodes', *Electrochimica Acta*. Pergamon, 31(1), pp. 29–38.

Konda, S. K. and Chen, A. (2016) 'Palladium based nanomaterials for enhanced hydrogen spillover and storage', *Materials Today*. Elsevier, 19(2), pp. 100–108.

Kong, Q., *et al.* (2016) 'Hydrogen absorption/desorption properties of porous hollow palladium spheres prepared by templating method', *Journal of Alloys and Compounds*. Elsevier, 664, pp. 188–192.

Korostynska, O., *et al.* (2008) 'Review Paper: Materials and Techniques for In Vivo pH Monitoring', *IEEE Sensors Journal*, 8(1), pp. 20–28.

Kotkar, R. M., Desai, P. B. and Srivastava, A. K. (2007) 'Behavior of riboflavin on plain carbon paste and aza macrocycles based chemically modified electrodes', *Sensors and Actuators B*, 124, pp. 90–98.

Kreider, K. G., Tarlov, M. J. and Cline, J. P. (1995) 'Sputtered thin-film pH electrodes of platinum, palladium, ruthenium, and iridium oxides', *Sensors and Actuators B: Chemical*. Elsevier, 28(3), pp. 167–172.

Kreuer, K. D., *et al.* (2000) 'Proton and water transport in nano-separated polymer

membranes', *Le Journal de Physique IV*. EDP Sciences, 10(7), pp. 279–281.

Kruanetr, S., *et al.* (2014) 'Electrochemical Oxidation of Acetyl Salicylic Acid and its voltammetric sensing in real samples at a sensitive edge plane Pyrolytic Graphite Electrode modified with Graphene', *Int. J. Electrochem. Sci*, 9, pp. 5699–5711.

Lafitte, V. G. H., *et al.* (2008) 'Anthraquinone–ferrocene film electrodes: Utility in pH and oxygen sensing', *Electrochemistry Communications*. Elsevier, 10(12), pp. 1831–1834.

Lanzafame, R. J. (2007) '"Business"', *Photomedicine and Laser Surgery*, 25(5), pp. 371–372.

Larsson, J. and Apelqvist, J. (1995) 'Towards less amputations in diabetic patients. Incidence, causes, cost, treatment, and prevention--a review.', *Acta orthopaedica Scandinavica*, 66(2), pp. 181–192.

Lavery, L., *et al.* (2003) 'Diabetic foot syndrome: evaluating the prevalence and incidence of foot pathology in Mexican Americans and non-Hispanic whites from a diabetes disease management cohort.', *Diabetes Care*, 26(5), pp. 1435–1438.

Lawrence, J., Robinson, K. L. and Lawrence, N. S. (2007) 'Electrochemical Determination of Sulfide at Various Carbon Substrates: A Comparative Study', *Analytical Sciences*, 23(6), pp. 673–676.

Lawrence, N. S., *et al.* (2002) 'Advances in the Voltammetric Analysis of Small Biologically Relevant Compounds', *Analytical Biochemistry*. Academic Press, 303(1), pp. 1–16.

Lazarus, G. S., *et al.* (1994) 'Definitions and guidelines for assessment of wounds and evaluation of healing', *Wound Repair and Regeneration*. Blackwell Science, 2(3), pp. 165–170.

Lee, D. and Cui, T. (2012) 'Carbon nanotube thin film pH electrode for potentiometric enzymatic acetylcholine biosensing', *Microelectronic Engineering*. Elsevier B.V., 93, pp. 39–42.

Levin, M., Neal, L. and Bowker, J. (1993) *The Diabetic Foot*. 5th edn. St. Louis: Mosby Year Book.

Lewis, F. (1967) *The Palladium/ Hydrogen System*. London, UK: Academic Press.

Li, M., *et al.* (2014) 'Nanostructuring carbon fibre probes for use in central venous catheters', *Analytica Chimica Acta*. Elsevier B.V., 812(July), pp. 1–5.

Li, Q., *et al.* (2011) 'A novel pH potentiometric sensor based on electrochemically synthesized polybisphenol A films at an ITO electrode', *Sensors and Actuators, B: Chemical*. Elsevier B.V., 155(2), pp. 730–736.

Li, X., Wan, Y. and Sun, C. (2004) 'Covalent modification of a glassy carbon surface by electrochemical oxidation of r-aminobenzene sulfonic acid in aqueous solution'.

Lin, J., *et al.* (2008) 'Factors affecting therapeutic compliance: A review from the patient's perspective', *Therapeutics and Clinical Risk Management*, 4(1), pp. 269–

286.

Lin, X.-Q. and Jin, G.-P. (2005) 'Monolayer modification of glassy carbon electrode by using propionylcholine for selective detection of uric acid', *Electrochimica Acta*, 50, pp. 3210–3216.

Lindfors, T., Ervelä, S. and Ivaska, A. (2003) 'Polyaniline as pH-sensitive component in plasticized PVC membranes', *Journal of Electroanalytical Chemistry*. Elsevier, 560(1), pp. 69–78.

Lipsky, B. A., *et al.* (1990) 'Outpatient Management of Uncomplicated Lower-Extremity Infections in Diabetic Patients', *Archives of Internal Medicine*. American Medical Association, 150(4), p. 790.

Lipsky, B. A. and Hoey, C. (2009) 'Topical Antimicrobial Therapy for Treating Chronic Wounds', *Clinical Infectious Diseases*. Oxford University Press, 49(10), pp. 1541–1549.

Liu, X., *et al.* (2017) 'Graphene-like carbon nitride nanosheet as a novel sensing platform for electrochemical determination of tryptophan'.

Liu, Y., *et al.* (2009) 'Increased matrix metalloproteinase-9 predicts poor wound healing in diabetic foot ulcers: Response to Muller et al.', *Diabetes Care*, 32(11), p. e137.

Loffler, M. W., *et al.* (2013) 'Wound Fluid in Diabetic Foot Ulceration: More Than Just an Undefined Soup?', *The International Journal of Lower Extremity Wounds*, 12(2), pp. 113–129.

Long, C. L., *et al.* (2003) 'Ascorbic acid dynamics in the seriously ill and injured.', *The Journal of Surgical Research*, 109(2), pp. 144–8.

Love, C., *et al.* (2003) 'Formation and Structure of Self-Assembled Monolayers of Alkanethiolates on Palladium', *American Chemical Society*. American Chemical Society, 125(90A), pp. 2597–2609.

Ma, B., *et al.* (2007) 'Randomized, multicenter, double-blind, and placebo-controlled trial using topical recombinant human acidic fibroblast growth factor for deep partial-thickness burns and skin graft donor site.', *Wound repair and regeneration : official publication of the Wound Healing Society [and] the European Tissue Repair Society*, 15(6), pp. 795–799.

MacMillan, B. G. (1980) 'Infections following burn injury.', *The Surgical Clinics of North America*, 60(1), pp. 185–96.

Mallesham Bejugam, *et al.* (2007) 'Trisubstituted Isoalloxazines as a New Class of G-Quadruplex Binding Ligands: Small Molecule Regulation of c-kit Oncogene Expression', *American Chemical Society*. American Chemical Society, 129(43), pp. 12926–12927.

Margolisa, D. J., *et al.* (2002) 'Venous leg ulcer: Incidence and prevalence in the elderly', *Journal of the American Academy of Dermatology*. Mosby, 46(3), pp. 381–386.

Matzeu, G., Florea, L. and Diamond, D. (2015) 'Advances in wearable chemical sensor design for monitoring biological fluids', *Sensors and Actuators B: Chemical*. Elsevier, 211, pp. 403–418.

Mayet, N., *et al.* (2014) 'A Comprehensive Review of Advanced Biopolymeric Wound Healing Systems', *J. Pharm. Sci.*, 103(8), pp. 2211–2230.

McGrath, M. H. (1990) 'Peptide growth factors and wound healing.', *Clinics in Plastic Surgery*, 17(3), pp. 421–432.

McLister, A., *et al.* (2014) 'Electrochemical approaches to the development of smart bandages: A mini-review', *Electrochemistry Communications*. Elsevier B.V., 40, pp. 96–99.

McLister, A., Lowry, N., *et al.* (2015) 'Novel pH sensing redox wire based on a polyamide homopolymer of L-tryptophan', *Fibers and Polymers*, 16(10), pp. 2294–2297.

McLister, A., *et al.* (2016) 'New Developments in Smart Bandage Technologies for Wound Diagnostics.', *Advanced materials (Deerfield Beach, Fla.)*.

McLister, A. and Davis, J. (2015a) 'Developing a pH Responsive Mesh as a Smart Skin Wafer in Ostomy Appliances', *IFMBE Proceedings : World Congress on Medical Physics and Biomedical Engineering*, 51, pp. 1265–1268.

McLister, A. and Davis, J. (2015b) 'Molecular Wiring in Smart Dressings: Opening a New Route to Monitoring Wound pH', *Healthcare*, 3(3), pp. 466–477.

McLister, A., Mathur, A. and Davis, J. (2017) 'Wound diagnostics: Deploying electroanalytical strategies for point of care sensors and smart dressings', *Current Opinion in Electrochemistry*. Elsevier, 3(1), pp. 40–45.

McNeely, M. J., *et al.* (1995) 'The independent contributions of diabetic neuropathy and vasculopathy in foot ulceration. How great are the risks?', *Diabetes Care*, 18(2), pp. 216–219.

Mehmood, N., *et al.* (2014) 'Applications of modern sensors and wireless technology in effective wound management', *Journal of Biomedical Materials Research - Part B Applied Biomaterials*, 102, pp. 885–895.

Menendez-Botet, C. J. (2003) 'Practices of Point-of-Care Testing.', *Clinical Chemistry*. Clinical Chemistry, 49(8), pp. 1424–1425.

Metters, J. P., Tan, F. and Banks, C. E. (2013) 'Screen-printed palladium electroanalytical sensors', *Journal of Solid State Electrochemistry*. Springer-Verlag, 17(6), pp. 1553–1562.

Mirza-Aghayan, M., Molaee Tavana, M. and Boukherroub, R. (2015) 'Palladium nanoparticles supported on reduced graphene oxide as an efficient catalyst for the reduction of benzyl alcohol compounds', *Catalysis Communications*. Elsevier, 69, pp. 97–103.

Mohr, G. J., *et al.* (2008) 'Design of acidochromic dyes for facile preparation of pH

sensor layers.', *Analytical and Bioanalytical Chemistry*, 392, pp. 1411–1418.

Mohr, G. J. and Müller, H. (2015) 'Tailoring colour changes of optical sensor materials by combining indicator and inert dyes and their use in sensor layers, textiles and non-wovens', *Sensors and Actuators B: Chemical*. Elsevier, 206, pp. 788–793.

Moore, R. R., Banks, C. E. and Compton, R. G. (2004) 'Electrocatalytic detection of thiols using an edge plane pyrolytic graphite electrode', *The Analyst*, 129(8), p. 755.

Morrin, A., *et al.* (2004) 'Electrocatalytic sensor devices: (I) cyclopentadienylnickel(II) thiolato Schiff base monolayer self-assembled on gold', *Talanta*. Elsevier, 64(1), pp. 30–38.

Most, R. S. and Sinnock, P. (1983) 'The epidemiology of lower extremity amputations in diabetic individuals.', *Diabetes care*, 6(1), pp. 87–91.

Moulin, V. (1995) 'Growth factors in skin wound healing.', *European Journal of Cell Biology*. Laboratoire de Recherche des Grands Brulés, 68(1), pp. 1–7.

Moulin, V., *et al.* (1998) 'Platelet releasate treatment improves skin healing in diabetic rats through endogenous growth factor secretion.', *Cellular and Molecular Biology*, 44(6), pp. 961–71.

Moura, L., *et al.* (2013) 'Recent advances on the development of wound dressings for diabetic foot ulcer treatment—A review', *Acta Biomaterialia*, 9(7), pp. 7093–7114.

Muller, M., *et al.* (2008) 'Matrix metalloproteinases and diabetic foot ulcers: the ratio of MMP-1 to TIMP-1 is a predictor of wound healing.', *Diabetic Medicine : a Journal of the British Diabetic Association*, 25(4), pp. 419–26.

Murc, S. J., Krishnara, S. and Saxena, P. K. (2000) 'Tryptophan is a precursor for melatonin and serotonin biosynthesis in in vitro regenerated St. John's wort (Hypericum perforatum L. cv. Anthos) plants', *Plant Cell Reports*, 19, pp. 698–704.

Musa, A. E., *et al.* (2011) 'Disposable miniaturized screen-printed pH and reference electrodes for potentiometric systems', *Electroanalysis*, 23(1), pp. 115–121.

Naga Mahesh, K., Balaji, R. and Dhathathreyan, K. S. (2016) 'Palladium nanoparticles as hydrogen evolution reaction (HER) electrocatalyst in electrochemical methanol reformer', *International Journal of Hydrogen Energy*. Pergamon, 41(1), pp. 46–51.

Nagy, G., *et al.* (1985) 'Ion exchange and transport of neurotransmitters in nation films on conventional and microelectrode surfaces', *Journal of Electroanalytical Chemistry and Interfacial Electrochemistry*. Elsevier, 188(1–2), pp. 85–94.

Nations, T. U. (2010) 'Chronic Wounds and Their Management and Prevention is a Significiant Public Health Issue', *International Wound Journal*, 7(3), pp. 125–126.

Nguyen, C. M., *et al.* (2014) 'Micro pH Sensors Based on Iridium Oxide Nanotubes', *IEEE Transactions on Nanotechnology*, 13(5), pp. 945–953.

O'Donnell, T. F., *et al.* (1977) 'The socioeconomic effects of an iliofemoral venous

thrombosis.', *The Journal of Surgical Research*, 22(5), pp. 483–8.

Ono, S., *et al.* (2014) 'Increased wound pH as an indicator of local wound infection in second degree burns', *Burns*. Elsevier Ltd and International Society of Burns Injuries, pp. 6–7.

Paixão, T. R. L. ., Kosminsky, L. and Bertotti, M. (2002) 'Use of electrochemically pretreated glassy carbon electrodes as pH sensors in potentiometric titrations', *Sensors and Actuators B: Chemical*. Elsevier, 87(1), pp. 41–46.

Park, J. and Eun, C. (2016) 'Electrochemical Behavior and Determination of Salicylic Acid at Carbon-fiber Electrodes', *Electrochimica Acta*. Pergamon, 194, pp. 346–356.

Park, K., *et al.* (2004) 'Preparation and Characterization of Self-Assembled Nanoparticles of Heparin-Deoxycholic Acid Conjugates', *Langmuir*. American Chemical Society, 20(26), pp. 11726–11731.

Park, W. and Kim, S. (2013) 'Triggerable single-component two-electrode voltammetric pH sensors using dyad molecules', *Electrochemistry Communications*. Elsevier B.V., 26(1), pp. 109–112.

Patel, N., Labropoulos, N. and Pappas, P. (2006) 'Current management of venous ulceration', *Plast Reconstr Surg*, 117, p. 254S–60S.

Patil, S. M., *et al.* (2014) 'Electrochemical Behavior of Graphene-Based Sensors on the Redox Mechanism of Aspirin', *Electroanalysis*. WILEY-VCH Verlag, 26(4), pp. 831–839.

Pecoraro, R. E., Reiber, G. E. and Burgess, E. M. (1990) 'Pathways to diabetic limb amputation. Basis for prevention.', *Diabetes care*, 13(5), pp. 513–521.

Pedrosa, V. A., *et al.* (2007) 'Studies on the electrochemical behavior of a cystine self-assembled monolayer modified electrode using ferrocyanide as a probe', *Journal of Electroanalytical Chemistry*, 602, pp. 149–155.

Phair, J., *et al.* (2011) 'A disposable sensor for point of care wound pH monitoring.', *Analyst*, 136(22), pp. 4692–4695.

Phair, J., *et al.* (2013) 'Atmospheric pressure plasma treated carbon fibre weave: A flexible approach to wound monitoring', *Electrochemistry Communications*. Elsevier B.V., 33, pp. 99–101.

Phair, J., Benson, J., *et al.* (2014) 'Butyl grafted polyethylene films doped with carbon black: A foundation for the development of smart bandages', *Sensors and Actuators, B: Chemical*. Elsevier B.V., 193, pp. 764–769.

Phair, J., Joshi, M., *et al.* (2014) 'Laser patterned carbon–polyethylene mesh electrodes for wound diagnostics', *Materials Chemistry and Physics*. Elsevier, 143(3), pp. 991–995.

Phillips, T., *et al.* (1994) 'A study of the impact of leg ulcers on quality of life: Financial, social, and psychologic implications', *Journal of the American Academy of Dermatology*. Elsevier, 31(1), pp. 49–53.

Pletcher, D. (1982) *Industrial electrochemistry*. London, UK: Chapman and Hall Ltd.

Pletcher, D. (2009) *A first course in electrode process*. 2nd edn. Cambridge, UK: The Royal Society of Chemistry.

Poon, V. K. M. and Burd, A. (2004) 'In vitro cytotoxity of silver: implication for clinical wound care', *Burns*. Elsevier, 30(2), pp. 140–147.

Posnett, J. and Franks, P. J. (2010) 'The burden of chronic wounds in the UK.', *Nursing Times*, 104(3), pp. 44–45.

Practice, I. (2008) 'BEST PRACTICE A World Union of Wound Healing Societies ' Initiative Diagnostics and wounds', *World*.

Practice, I. B. (2014) 'Best Practice Guidelines : Wound Management in', *Wounds International*, 5(2), p. 27.

Purser, K. (2010) *Wound Dressing Guidelines*, *NHS Trust Wound Dressing Guidelines*.

Qin, Y., *et al.* (2016) 'Low-temperature solution processing of palladium/palladium oxide films and their pH sensing performance', *Talanta*. Elsevier, 146, pp. 517–524.

Qingwen, L., *et al.* (2001) 'Studies on Self-Assembly Monolayers of Cysteine on Gold by XPS, QCM, and Electrochemical Techniques', *Electroanalysis*. VCH Verlagsgesellschaft mbH, 13(16), pp. 1342–1346.

Ramsey, S. D., *et al.* (1999) 'Incidence, outcomes, and cost of foot ulcers in patients with diabetes.', *Diabetes Care*. American Diabetes Association, 22(3), pp. 382–7.

Rao, C. N., *et al.* (1995) 'α1-Antitrypsin Is Degraded and Non-Functional in Chronic Wounds But Intact and Functional in Acute Wounds: The Inhibitor Protects Fibronectin from Degradation by Chronic Wound Fluid Enzymes', *Journal of Investigative Dermatology*. Elsevier, 105(4), pp. 572–578.

Rathur, H. M. and Boulton, A. J. M. (2007) 'The diabetic foot', *Clinics in Dermatology*, 25, pp. 109–120.

Rawlinson, S., *et al.* (2017) 'Rapid determination of salicylic acid at screen printed electrodes', *Microchemical Journal*, 137, pp. 71–77.

Raza, W. and Ahmad, K. (2018) 'A highly selective Fe@ZnO modified disposable screen printed electrode based non-enzymatic glucose sensor (SPE/Fe@ZnO)', *Materials Letters*. North-Holland, 212, pp. 231–234.

Rodríguez, J., Castañeda, G. and Lizcano, I. (2018) 'Electrochemical sensor for leukemia drug imatinib determination in urine by adsorptive striping square wave voltammetry using modified screen-printed electrodes', *Electrochimica Acta*. Pergamon, 269, pp. 668–675.

Roushani, M. and Abdi, Z. (2014) 'Novel electrochemical sensor based on graphene quantum dots/riboflavin nanocomposite for the detection of persulfate', *Sensors and Actuators B: Chemical*. Elsevier, 201, pp. 503–510.

Santos, E., *et al.* (2007) 'L-Cysteine films on Ag investigated by electrochemical and

nonlinear optical methods', *Chemical Physics*, 342, pp. 236–244.

Sardarinejad, A., Maurya, D. K. and Alameh, K. (2014) 'The effects of sensing electrode thickness on ruthenium oxide thin-film pH sensor', *Sensors and Actuators A: Physical*. Elsevier, 214, pp. 15–19.

Sawada, K., *et al.* (2005) 'A novel fused sensor for photo- and ion-sensing', *Sensors and Actuators B: Chemical*. Elsevier, 106(2), pp. 614–618.

Schmidtchen, A. (2000) 'Degradation of antiproteinases, complement and fibronectin in chronic leg ulcers.', *Acta Dermato-Venereologica*, 80(3), pp. 179–84.

Schneider, L., *et al.* (2007) 'Influence of pH on wound-healing: A new perspective for wound-therapy?', *Archives of Dermatological Research*, 298(9), pp. 413–420.

Schreml, S., *et al.* (2011) '2D luminescence imaging of physiological wound oxygenation', *Experimental Dermatology*. Blackwell Publishing Ltd, 20(7), pp. 550–554.

Schreml, S., *et al.* (2014) 'Luminescent Dual Sensors Reveal Extracellular pH-Gradients and Hypoxia on Chronic Wounds That Disrupt Epidermal Repair', *Theranostics*, 4(7), pp. 721–735.

Sen, C. K., *et al.* (2009) 'Human Skin Wounds: A Major and Snowballing Threat to Public Health and the Economy', *Wound Repair and Regeneration*, 17(6), pp. 763–771.

Sharp, D., Forsythe, S. and Davis, J. (2008) 'Carbon fibre composites: integrated electrochemical sensors for wound management.', *The Journal of Biochemistry.*, 144, pp. 87–93.

Shukla, V. K., *et al.* (2007) 'Evaluation of pH measurement as a method of wound assessment', *Journal of Wound Care*. MA Healthcare London , 16(7), pp. 291–294.

Siddiqui, A. R. and Bernstein, J. M. (2010) 'Chronic wound infection: Facts and controversies', *Controversies in Dermatology: Part III*, 28(5), pp. 519–526.

Da Silva, A., Navarro, M. F. and Batalheiro, J. (1992) 'The importance of chronic venous insufficiency. Various preliminary data on its medico-social consequences', *Phlebologie*, 45(4), pp. 439–43.

Singh, N., Armstrong, D. G. and Lipsky, B. A. (2005) 'Preventing foot ulcers in patients with diabetes.', *JAMA*, 293(2), pp. 217–28.

Slavin, J. (1999) 'The role of cytokines in wound healing.', *Journal of Pathology*, 178(1), pp. 5–10.

Steenfos, H. (1994) 'Growth Factors and wound healing', *Journal of plastic, reconstructive surgery and hand surgery*, 28, pp. 95–105.

Steinberg, I. M. and Steinberg, M. D. (2009) 'Radio-frequency tag with optoelectronic interface for distributed wireless chemical and biological sensor applications', *Sensors and Actuators B: Chemical*. Elsevier, 138(1), pp. 120–125.

Stradins, J. and Hasanli, B. (1993) 'Anodic voltammetry of phenol and benzenethiol derivatives.: Part 1. Influence of pH on electro-oxidation potentials of substituted phenols and evaluation of pKa from anodic voltammetry data', *Journal of Electroanalytical Chemistry*. Elsevier, 353(1–2), pp. 57–69.

Streeter, I., *et al.* (2004) 'A sensitive reagentless pH probe with a ca. 120 mV/pH unit response', *Journal of Solid State Electrochemistry*. Springer-Verlag, 8(10), pp. 718–721.

Sun, J., *et al.* (2012) 'Anodization of Pd in H2SO4 Solutions: Influence of Potential, Polarization Time, and Electrolyte Concentration', *ACS Applied Materials and Interfaces*, 4(11), pp. 6038–6045.

Supalkova, V., *et al.* (2006) 'Electrochemical Sensors for Detection of Acetylsalicylic Acid', *Sensors*. Molecular Diversity Preservation International, 6(11), pp. 1483–1497.

Szunerits, S., *et al.* (2010) 'Preparation of boron-doped diamond nanowires and their application for sensitive electrochemical detection of tryptophan', *Electrochemistry Communications*, 12, pp. 438–441.

Tao, Y., *et al.* (2007) 'Tris(2,2 -bipyridyl)ruthenium(II) electrochemiluminescence sensor based on carbon nanotube/organically modified silicate films', *Analytica Chimica Acta*, 594, pp. 169–174.

Taouil, A., *et al.* (2010) 'Effects of polypyrrole modified electrode functionalization on potentiometric pH responses', *Synthetic Metals*. Elsevier B.V., 160(9–10), pp. 1073–1080.

Thomas, O. (2012) 'Superficial Wound Swabbing : A novel method of sampling and processing', 35(11), pp. 2113–2120.

Thomas, S. (2006) 'Cost of managing chronic wounds in the U.K., with particular emphasis on maggot debridement therapy.', *Journal of wound care*, 15(10), pp. 465–9.

Thorn, J. J., *et al.* (2004) 'Autologous fibrin glue with growth factors in reconstructive maxillofacial surgery.', *International journal of oral and maxillofacial surgery*, 33(1), pp. 95–100.

Toray (2017) *Toray Carbon Fiber Paper 'TGP-H'*. Available at: http://www.fuelcellsetc.com/store/DS/Toray-Paper-TGP-H-Datasheet.pdf.

Tortora, G. and Derrickson, B. (2008) *Principles of Anatomy and Physiology.* 12th edn. Princeton, NJ: Wiley & Sons.

Trengove, N. J., Langton, S. R. and Stacey, M. C. (1996) 'Biochemical analysis of wound fluid from nonhealing and healing chronic leg ulcers', *Wound Repair and Regeneration*. Blackwell Science, 4(2), pp. 234–239.

Trupp, S., *et al.* (2010) 'Development of pH-sensitive indicator dyes for the preparation of mirco-patterned optical sensor layers.', *Sensors and Actuators B*, 150, pp. 206–210.

Valipour, A. and Roushani, M. (2017) 'Using silver nanoparticle and thiol graphene quantum dots nanocomposite as a substratum to load antibody for detection of hepatitis C virus core antigen: Electrochemical oxidation of riboflavin was used as redox probe', *Biosensors and Bioelectronics*. Elsevier, 89, pp. 946–951.

Varghese, M. C., *et al.* (1986) 'Local environment of chronic wounds under synthetic dressings.', *Archives of dermatology*, 122(1), pp. 52–7.

Wagner, S., *et al.* (2003) 'Comparison of inflammatory and systemic sources of growth factors in acute and chronic human wounds', *Wound Repair and Regeneration*. Blackwell Science Inc, 11(4), pp. 253–260.

Wang, H.-S., Ju, H.-X. and Chen, H.-Y. (2002) 'Simultaneous determination of guanine and adenine in DNA using an electrochemically pretreated glassy carbon electrode', *Analytica Chimica Acta*, 461, pp. 243–250.

Wang, H., *et al.* (2000a) 'Adsorptive stripping voltammetric determination of erythromycin at a pretreated glassy carbon electrode', *Microchemical Journal*, 64.

Wang, H., *et al.* (2000b) 'Adsorptive stripping voltammetric determination of erythromycin at a pretreated glassy carbon electrode', *Microchemical Journal*. Elsevier, 64(1), pp. 67–71.

Wang, X., *et al.* (2008) 'Reversible Optical Sensor Strip for Oxygen', *Angewandte Chemie*. WILEY-VCH Verlag, 120(39), pp. 7560–7563.

Wang, Z., Ai, F., *et al.* (2010) 'Electrocatalytic activity of salicylic acid on the platinum nanoparticles modified electrode by electrochemical deposition', *Colloids and Surfaces B: Biointerfaces*. Elsevier, 76(1), pp. 370–374.

Wang, Z., Wei, F., *et al.* (2010) 'Electrocatalytic oxidation of phytohormone salicylic acid at copper nanoparticles-modified gold electrode and its detection in oilseed rape infected with fungal pathogen Sclerotinia sclerotiorum.', *Talanta*, 80(3), pp. 1277–1281.

Werner, S. and Grose, R. (2003) 'Regulation of wound healing by growth factors and cytokines.', *Physiological Reviews*, 83(3), pp. 835–870.

Weyrich, A. S. and Zimmerman, G. A. (2004) 'Platelets: signaling cells in the immune continuum.', *Trends in immunology*, 25(9), pp. 489–495.

Wightman, R. M. (1988) 'Voltammetry with Microscopic Electrodes in New Domains', *Science*, 240(4851), pp. 415–420.

Winter, G. D. (1962) 'Formation of the scab and the rate of epithelisation of superficial wounds in the skin of the young domestic pig.', *Nature.*, 193, pp. 293–294.

Witte, M. B. and Barbul, A. (1997) 'General principles of wound healing.', *The Surgical Cinics of North America*, 77(3), pp. 509–528.

Wolfe, D. B., *et al.* (2002) 'Fabrication of palladium-based microelectronic devices by microcontact printing', *Applied Physics Letters*. American Institute of Physics,

80(12), pp. 2222–2224.

World Union of Wound Healing Societies (2008) *Principles of best practice: Wound infection in clinical practice. An international consensus*. London: Medical Education Partnership.

Xiong, L., Batchelor-Mcauley, C. and Compton, R. G. (2011) 'Calibrationless pH sensors based on nitrosophenyl and ferrocenyl co-modified screen printed electrodes', *Sensors and Actuators, B: Chemical*. Elsevier B.V., 159(1), pp. 251–255.

Xiong, L., Batchelor-McAuley, C. and Compton, R. G. (2011) 'Calibrationless pH sensors based on nitrosophenyl and ferrocenyl co-modified screen printed electrodes', *Sensors and Actuators B: Chemical*. Elsevier, 159(1), pp. 251–255.

Yagati, A. K., *et al.* (2016) 'Label-free and direct detection of C-reactive protein using reduced graphene oxide-nanoparticle hybrid impedimetric sensor', *Bioelectrochemistry*. Elsevier B.V., 107, pp. 37–44.

Yin, K., *et al.* (2018) 'Palladium – silicon nanocomposites as a stable electrocatalyst for hydrogen evolution reaction', *Journal of Colloid and Interface Science*. Academic Press, 522, pp. 242–248.

Zampolli, S., *et al.* (2008) 'Ultra-low-power components for an RFID Tag with physical and chemical sensors', *Microsystem Technologies*. Springer-Verlag, 14(4–5), pp. 581–588.

Zhang, F.-F., *et al.* (2005) 'Simultaneous monitoring of glucose, lactate, l-glutamate and hypoxanthine levels in rat striatum by a flow-injection enzyme electrode array system with in vivo microdialysis sampling', *Journal of Electroanalytical Chemistry*. Elsevier, 575(1), pp. 1–7.

Zhang, L., *et al.* (2016) 'Recent advances in palladium-based electrocatalysts for fuel cell reactions and hydrogen evolution reaction', *Nano Energy*. Elsevier, 29, pp. 198–219.

Zhao, R., *et al.* (2010) 'A pH sensor based on the TiO2 nanotube array modified Ti electrode', *Electrochimica Acta*. Elsevier Ltd, 55(20), pp. 5647–5651.

Zhong, W. (2015) 'Efficacy and toxicity of antibacterial agents used in wound dressings', *Cutaneous and Ocular Toxicology*, 34(1), pp. 61–67.

Zhou, J., *et al.* (2011) 'Development of a prototype wound dressing technology which can detect and report colonization by pathogenic bacteria.', *Biosensors and Bioelectronics.*, 30, pp. 67–72.

Publications Resulting from this Research Work

Book release by Elsevier

Smart Bandage Technologies : Design and Application. Editor: Maria Convey Release date July 2016. Elsevier, ISBN 978-0-12-803762-1.

In peer reviewed journals

Rawlinson, S., **McLister, A**., Kanyong, P. and Davis, J. (2018) 'Rapid determination of salicylic acid at screen printed electrodes', *Microchemical Journal*, 137, pp. 71-77.

Morelli, F., Anderson, A., **McLister, A**., Fearon, J.-J. and Davis, J. (2017) 'Electrochemically driven reagent release from an electronic suture', *Electrochemistry Communications*, 81, pp. 70 -73.

McLister, A., Mathur, A. and Davis, J. (2017) 'Wound diagnostics: Deploying electroanalytical strategies for point of care sensors and smart dressings', *Current Opinion in Electrochemistry*, 3(1), pp. 40–45.

Martin, A., McConville, A., Anderson, A., **McLister, A**. and Davis, J. (2017) 'Microneedle Manufacture: Assessing Hazards and Control Measures', *Safety*, 3(4), p. 25.

McLister A, McHugh J, Cundell J, Davis J. (2016) New Developments in Smart Bandage Technologies for Wound Diagnostics. *Advanced. Materials.* 28(27), pp. 5732 – 5737.

McLister, A. and Davis, J. (2015) 'Molecular Wiring in Smart Dressings: Opening a New Route to Monitoring Wound pH', *Healthcare*, 3(3), pp. 466–477.

McLister, A., Lowry, N., Anderson, A., McHugh, J. and Davis, J. (2015) 'Novel pH sensing redox wire based on a polyamide homopolymer of L-tryptophan', *Fibers and Polymers*, 16(10), pp. 2294 -2297.

Lowry, N., **McLister, A**., McCreadie, K. and Davis, J. (2015) 'An Electronic Approach to Minimising Moisture-Associated Skin Damage in Ostomy Patients', *Medical Hypotheses*, 85(2), pp. 192-196.

In peer reviewed conferences

McLister, A. & Davis, J., 2015. Developing a pH responsive mesh as a smart skin wafer in ostomy appliances. IFMBE Proceedings: World Congress on Medical Physics and Biomedical Engineering, June 7-12, 2015, Toronto, Canada. 51, pp. 1265-1268.